

ANALYTICA CHIMICA ACTA

An international journal devoted to all branches of analytical chemistry

EDITORS

HARRY L. PARDUE (West Lafayette, IN, U.S.A.)

ALAN TOWNSHEND (Hull, Great Britain)

J.T. CLERC (Berne, Switzerland)

WILLEM E. VAN DER LINDEN (Enschede, The Netherlands)

PAUL J. WORSFOLD (Plymouth, Great Britain)

Editorial Advisers

F.C. Adams, Antwerp
M. Aizawa, Yokohama
J.F. Alder, Manchester
C.M.G. van den Berg, Liverpool
A.M. Bond, Bundoora, Vic.
S.D. Brown, Newark, DE
J. Buffle, Geneva
P.R. Coulet, Lyon
S.R. Crouch, East Lansing, MI
R. Dams, Ghent
L. de Galan, Vlaardingen
M.L. Gross, Lincoln, NE
W. Heineman, Cincinnati, OH
G.M. Hieftje, Bloomington, IN
G. Horvai, Budapest
T. Imasaka, Fukuoka
D. Jagner, Gothenburg
G. Johansson, Lund
D.C. Johnson, Ames, IA
A.M.G. Macdonald, Birmingham
D.L. Massart, Brussels
P.C. Meier, Schaffhausen
M.E. Meyerhoff, Ann Arbor, MI

J.N. Miller, Loughborough
H.A. Mottola, Stillwater, OK
M.E. Munk, Tempe, AZ
M. Otto, Freiberg
D. Pérez-Bendito, Córdoba
C.F. Poole, Detroit, MI
S.C. Rutan, Richmond, VA
J. Ruzicka, Seattle, WA
A. Sanz-Medel, Oviedo
S. Sasaki, Toyohashi
T. Sawada, Tokyo
K. Schügerl, Hannover
M.R. Smyth, Dublin
M. Thompson, Toronto
G. Tölg, Dortmund
Y. Umezawa, Tokyo
E. Wang, Changchun
J. Wang, Las Cruces, NM
H.W. Werner, Eindhoven
O.S. Wolfbeis, Graz
Yu.A. Zolotov, Moscow
J. Zupan, Ljubljana

ANALYTICA CHIMICA ACTA

Scope. *Analytica Chimica Acta* publishes original papers, preliminary communications and reviews dealing with every aspect of modern analytical chemistry. Reviews are normally written by invitation of the editors, who welcome suggestions for subjects. Preliminary communications of important urgent work can be printed within four months of submission, if the authors are prepared to forego proofs.

Submission of Papers

Americas

Prof. Harry L. Pardue
Department of Chemistry
1393 BRWN Bldg, Purdue University
West Lafayette, IN 47907-1393
USA
Tel: (+1-317) 494 5320
Fax: (+1-317) 496 1200

Computer Techniques

Prof. J.T. Clerc
Universität Bern
Pharmazeutisches Institut
Baltzerstrasse 5, CH-3012 Bern
Switzerland
Tel: (+41-31) 654171
Fax: (+41-31) 654198

Other Papers

Prof. Alan Townshend
Department of Chemistry
The University
Hull HU6 7RX
Great Britain

Tel: (+44-482) 465027
Fax: (+44-482) 466410

Prof. Willem E. van der Linden
Laboratory for Chemical Analysis
Department of Chemical Technology
Twente University of Technology
P.O. Box 217, 7500 AE Enschede
The Netherlands
Tel: (+31-53) 892629
Fax: (+31-53) 356024

Prof. Paul Worsfold
Dept. of Environmental Sciences
University of Plymouth
Plymouth PL4 8AA
Great Britain

Tel: (+44-752) 233006
Fax: (+44-752) 233009

Submission of an article is understood to imply that the article is original and unpublished and is not being considered for publication elsewhere. *Anal. Chim. Acta* accepts papers in English only. There are no page charges. Manuscripts should conform in layout and style to the papers published in this issue. See inside back cover for "Information for Authors".

Publication. *Analytica Chimica Acta* appears in 14 volumes in 1993. The subscription price for 1993 (Vols. 267-280) is Dfl 4214.00 plus Dfl. 462.00 (p.p.h.) (total approx. US\$ 2816.75). *Vibrational Spectroscopy* appears in 2 volumes in 1993. The subscription price for *Vibrational Spectroscopy* (Vols. 4 and 5) is Dfl. 700.00 plus Dfl. 66.00 (p.p.h.) (total approx US\$ 461.50). The price of a combined subscription (*Anal. Chim. Acta* and *Vib. Spectrosc.*) is Dfl. 4592.00 plus Dfl. 528.00 (p.p.h.) (total approx. US\$ 3084.25). All earlier volumes (Vols. 1-266) except Vols. 23 and 28 are available at Dfl. 259.50 (US\$ 156.25), plus Dfl. 18.00 (US\$ 10.75) p.p.h., per volume. The Dutch guilder price is definitive. The U.S. dollar price is subject to exchange-rate fluctuations and is given only as a guide. Subscriptions are accepted on a prepaid basis only, unless different terms have been previously agreed upon.

Our p.p.h. (postage, packing and handling) charge includes surface delivery of all issues, except to subscribers in the U.S.A. Canada, Australia, New Zealand, China, India, Israel, South Africa, Malaysia, Thailand, Singapore, South Korea, Taiwan, Pakistan, Hong Kong, Brazil, Argentina and Mexico, who receive all issues by air delivery (S.A.L. - Surface Air Lifted) at no extra cost. For Japan, air delivery requires 25% additional charge of the normal postage and handling charge; for all other countries airmail and S.A.L. charges are available upon request.

Subscription orders. Subscription orders can be entered only by calendar year and should be sent to: Elsevier Science Publishers B.V., Journals Department, P.O. Box 211, 1000 AE Amsterdam, The Netherlands. Tel: (+31-20) 5803 642, Telex 18582, Telefax: (+31-20) 5803598, to which requests for sample copies can also be sent. Claims for issues not received should be made within six months of publication of the issues. If not they cannot be honoured free of charge. Readers in the U.S.A. and Canada can contact the following address: Elsevier Science Publishing Co. Inc., Journal Information Center, 655 Avenue of the Americas, New York, NY 10010, U.S.A. Tel: (+1-212) 633 3750, Telefax: (+1-212) 633 3990, for further information, or a free sample copy of this or any other Elsevier Science Publishers journal.

Advertisements. Advertisement rates are available from the publisher on request.

Detailed "Instructions to Authors" for *Analytica Chimica Acta* was published in Volume 256, No. 2, pp. 373-376. Free reprints of the "Instructions to Authors" of *Analytica Chimica Acta* and *Vibrational Spectroscopy* are available from the Editors or from: Elsevier Science Publishers B.V., P.O. Box 330, 1000 AH Amsterdam, The Netherlands. Telefax: (+31-20) 5862 845.

US mailing notice - *Analytica Chimica Acta* (ISSN 0003-2670) is published biweekly by Elsevier Science Publishers (Molenwerf 1, Postbus 211, 1000 AE Amsterdam). Annual subscription price in the USA US\$ 2816.75 (subject to change), including air speed delivery. Second class postage paid at Jamaica, NY 11431. **USA Postmasters:** Send address changes to *Anal. Chim. Acta*, Publications Expediting, Inc., 200 Meacham Av., Elmont, NY 11003. Airfreight and mailing in the USA by Publication Expediting.

ANALYTICA CHIMICA ACTA

An international journal devoted to all branches of analytical chemistry

(Full texts are incorporated in CJELSEVIER, a file in the Chemical Journals Online database available on STN International; Abstracted, indexed in: Aluminum Abstracts; Anal. Abstr.; Biol. Abstr.; BIOSIS; Chem. Abstr.; Curr. Contents Phys. Chem. Earth Sci.; Engineered Materials Abstracts; Excerpta Medica; Index Med.; Life Sci.; Mass Spectrom. Bull.; Material Business Alerts; Metals Abstracts; Sci. Citation Index)

VOL. 271 NO. 2

CONTENTS

JANUARY 18, 1993

Environmental Analysis

- Limitations of XAD resins for the isolation of the non-colloidal humic fraction in soil extracts and aquatic samples
R.M. Town and H.K.J. Powell (Christchurch, New Zealand) 195

Electroanalytical Chemistry and Sensors

- Methylotrophic yeast microbiosensor based on ion-sensitive field effect transistors for methanol and ethanol determination
Y.I. Korpan, A.P. Soldatkin, N.F. Starodub, A.V. El'skaya (Kiev, Ukraine), M.V. Gonchar, A.A. Sibirny (L'vov, Ukraine) and A.A. Shul'ga (Kiev, Ukraine) 203
- Adsorptive preconcentration for voltammetric measurements of trace levels of vanadium in the presence of copper
P.A.M. Farias, A.K. Ohara, I. Takase (Rio de Janeiro, Brazil), S.L.C. Ferreira (Salvador, Brazil) and J.S. Gold (Santa Clara, CA, USA) 209
- Determination of 4-nitrobiphenyl by adsorptive stripping square-wave polarography
P. Hernández, F. Galan-Estella and L. Hernández (Madrid, Spain) 217

Enzyme Determinations

- Zeptomole detection limit for alkaline phosphatase using 4-aminophenylphosphate, amperometric detection, and an optimal buffer system
R.Q. Thompson, M. Porter, C. Stuver (Oberlin, OH, USA), H.B. Halsall, W.R. Heineman (Cincinnati, OH, USA), E. Buckley and M.R. Smyth (Dublin, Ireland) 223
- Determination of L-glutamate and L-glutamine by flow-injection analysis and chemiluminescence detection: comparison of an enzyme column and enzyme membrane sensor
G. Blankenstein (Jülich, Germany), F. Preuschoff, U. Spohn, K.-H. Mohr (Halle, Germany) and M.-R. Kula (Jülich, Germany) 231

Flow Analysis

- Simultaneous determination of sucrose and reducing sugars using indirect flow-injection biamperometry
J. Michałowski, A. Kojto (Białystok, Poland), M. Trojanowicz, B. Szostek (Warsaw, Poland) and E.A.G. Zagatto (Piracicaba, Brazil) 239
- Spectrofluorimetric flow-injection determination of calcium using Calcein
N. Chimpalee, D. Chimpalee, R. Jarungpattananon, S. Lawratchavee (Nakorn Pathom, Thailand) and D.T. Burns (Belfast, UK) 247

Chemometrics

- Multicriteria target vector optimization of analytical procedures using a genetic algorithm. Part II. Polyoptimization of the photometric calibration graph of dry glucose sensors for quantitative clinical analysis
D. Wienke, C. Lucasius (Nijmegen, Netherlands), M. Ehrlich (Dresden, Germany) and G. Kateman (Nijmegen, Netherlands) 253
- Application of informational analysis of variance in analytical chemistry
C. Sârbu (Cluj-Napoca, Romania) 269
- Design of experiments and data treatment in the study of mixed-ligand complexes
M. Zelić (Zagreb, Croatia) 275

(Continued overleaf)

ห้องสมุดมหาวิทยาลัยเทคโนโลยีพระจอมเกล้าธนบุรี

15 11.10.2536

Contents (continued)

Expert system for interpretation of x-ray diffraction spectra B. Adler, P. Schütze and J. Will (Schkopau, Germany)	287
Triacylglycerol determination based on fatty acid composition using chemometrics J. García Pulido and R. Aparicio López (Seville, Spain)	293
<i>Separations</i>	
Systematic investigation of multi-element preconcentration from copper alloys by carbamate precipitation before atomic absorption spectrometric analysis Ch. Frigge and E. Jackwerth (Bochum, Germany)	299
Polyfunctionality of resin carboxyl sites in ion exchange with alkali metal ions H. Tamura, M. Kudo and R. Furuichi (Sapporo, Japan)	305
<i>Spectrophotometry</i>	
Determination of nonionic surfactants by spectrophotometry after extraction with potassium triiodide A.A. Boyd-Boland and J.M. Eckert (Sydney, Australia)	311
Improved spectrophotometric method for the determination of low levels of bromide D.R. Jones (North Ryde, Australia)	315
Modified acid–base behaviour of resin-bound pH indicators S. Motellier and P. Toulhoat (Fontenay-aux-Roses, France)	323
<i>Book Reviews</i>	331
<i>Author Index</i>	337

Limitations of XAD resins for the isolation of the non-colloidal humic fraction in soil extracts and aquatic samples

Raewyn M. Town¹ and H. Kipton J. Powell

Department of Chemistry, University of Canterbury, Private Bag, Christchurch (New Zealand)

(Received 31st January 1992; revised manuscript received 23rd September 1992)

Abstract

XAD resins are widely used to isolate aquatic humic substances. In this work the molecular adsorption and subsequent desorption of a soil humic acid on XAD-2, 4, -7 and -8 was studied. Gel permeation chromatography established that size-exclusion effects were operative; large humic molecules (MW > 30 000) were not significantly adsorbed by these XAD resins. These results highlight the operational definition of humic substances isolated via XAD resins.

Keywords: Gel permeation chromatography; Extraction; Humic substances; Soils; Waters; XAD resins

The use of XAD resins for the isolation of fulvic and humic acids from aquatic sources is a well established technique [1–5]. They have also been used to isolate fulvic acids from soil extracts [6]. Indeed, this method has been used by the International Humic Substances Society (IHSS) for the isolation of standard aquatic humic substance samples [4] and for the isolation of the IHSS reference Summit Hill soil fulvic acid [7].

Any method proposed for the isolation of humic substances should ideally allow a “representative” sample of the humic material to be obtained. This may not result from the use of XAD resins due to specific interactions with some moieties in humic substances or to the rejection of hydrophilic components of humic substances [8]. Although the series of XAD resins exhibit a range of properties, some species known to inter-

act strongly with one or more of the XAD resins include hydrophobic moieties [9], aromatic species [10,11] and metal ions [12–14]. Humic substances will contain some or all of these components as indicated by elemental analysis, ¹³C NMR and surface tension measurements [15].

In addition, some irreversible aggregation of humic moieties may occur in the pores of the resins at low pH, resulting in physical trapping of adsorbed material [6]. The concentration of humic substances on the resin matrix is much greater than that in solution. At high concentrations (> 1 g l⁻¹) humic materials may strongly and irreversibly aggregate and dehydrate [16]. Further, interactions may occur between molecules bound on adjacent sites on XAD resins [17].

XAD resins also exhibit size-exclusion effects. It is reported that the capacity of XAD-4 for molecules of MW 5000 is only one third of that of XAD-2, while XAD-4 has no capacity for a polyacrylic acid of MW 90 000 [2]. In the absence of size exclusion, the retention efficiencies of XAD-2

Correspondence to: R.M. Town, Department of Analytical Chemistry, University of Geneva, Sciences II, 30 Quai E. Ansermet, CH-1211 Geneva 4 (Switzerland) (present address).

and XAD-7 have been reported to increase with increasing molecular weight for a homologous series [18,19].

Fulvic acids are quantitatively adsorbed (at pH 2.0) and desorbed (at pH 7.0) from XAD-7 and XAD-8; however, release of humic acid from these resins has involved the use of strongly alkaline conditions (pH 13). More recently, questions have been raised about the reliability of this XAD resin extraction procedure for humic acids [8].

In this work, the molecular adsorption and desorption characteristics of soil humic substances on XAD resins were studied. Filtered samples of 0.025 μm were used to minimize the colloidal fraction. The process studied is distinct from colloid/particulate trapping followed by desorption and dissolution by NaOH, which contributes to the isolation of fulvic and humic acids from aquatic sources [1–5].

EXPERIMENTAL

Humic substances

Humic acid (HA) was the Summit Hill IHSS reference soil humic acid. The ash content was 1.15%.

Fulvic acid was sample FA4, extracted from IHSS peat by the acid pyrophosphate–XAD-7 method [6]. The ash content was 0.2%.

XAD resins

Amberlite XAD-7, XAD-2 and XAD-4 resins (20–60 mesh) were obtained from Aldrich and XAD-8 (20–60 mesh) from Sigma. Monomers and impurities were removed by hot Soxhlet extraction with AnalaR-grade methanol (BDH) until no detectable loss of monomers was observed by ^1H NMR on concentrated extracts (at least 2 h). Clean resin was stored in AnalaR-grade methanol and washed thoroughly with triply distilled water before use.

Equilibration of soil humic substances with XAD resins

All uptake experiments were done with soil-derived HA, unless stated otherwise.

The uptake of humic acid on XAD-2, XAD-4 and XAD-8 was studied as a function of pH. The concentration of dissolved HA equilibrated with the resins was within the range 0.24–0.30 mg ml^{-1} . The ratio of mg HA per gram of resin was within the range 2–7. This is realistic in terms of the isolation of humic acids from soil extracts; it is lower than that used successfully for the concentration and isolation of fulvic acids from 0.025- μm filtered soil extracts [6]. It is significantly higher than that involved in the isolation of dissolved (and colloidal) humic acids from aquatic samples. However, it was well below the reported capacity of the resins for retention of (partially colloidal, not filtered) humic acids [2].

Batch experiments were performed in which HA in 0.01 mol l^{-1} KNO_3 (pH 7.0, 0.025- μm membrane filtered) was equilibrated with clean XAD resin in a titration cell; dissolved oxygen was removed by purging with oxygen-free nitrogen. Both adsorption and desorption processes were studied. To effect adsorption the solution was acidified from pH 7.0 to pH 2.5–3.0 by stepwise addition of HNO_3 (vapour distilled). The minimum pH of 2.5 was chosen to minimize precipitation of HA [20]. To desorb the humic acid, the pH was raised stepwise to 11–13 by addition of KOH.

The resin was allowed to equilibrate with the HA solution for at least 1 h at each pH value; equilibrium was attained within 30 min. The concentration of HA in solution at each pH and its molecular size distribution were determined by UV–visible spectrophotometry and gel permeation chromatography (GPC), respectively. For GPC, each sample (ca. 1 ml) was filtered (0.025 μm) before being applied to the gel column. Details of the GPC procedure have been reported [21].

Isolation of aquatic humic substances

The humic water sample was from surface water draining a podzolized soil with original vegetation at Larry's Creek Forestry Site (West Coast, South Island, New Zealand). The concentration of humic substances was 24.8 mg l^{-1} (determined spectrophotometrically against FA standards). The 500-ml sample was filtered (0.45 μm)

at natural pH (3.6), then acidified to pH 2.0 (HCl). The humic substances were concentrated by passing the solution at pH 2.0 through a column of XAD-8 resin (containing 14 g of resin); 87% of the coloured material was adsorbed. The amount of humic substances passed through the column was well below the adsorption capacity of the resin. The flow-rate did not exceed 1 ml min⁻¹. Humic substances were desorbed with 0.1 mol l⁻¹ AnalaR-grade NaOH; the humic/fulvic acid separation was then effected by acidifying this solution to pH 1.0. After 24 h the precipitated humic acid was collected on a 0.025- μ m membrane filter, washed with dilute HCl to remove ash, then with Milli-Q-deionized water until free from chloride. This sample was not cation exchanged. The fulvic acid remaining in solution at pH 1.0 was re-adsorbed on XAD-8, washed with Milli-Q-deionized water to remove chloride, then eluted with 0.1 mol l⁻¹ NaOH. The fulvic acid was cation exchanged on Dowex 50W-8X (H⁺ form) and isolated by freeze-drying.

RESULTS

Equilibration of soil humic acid with XAD-4

The adsorption of HA on XAD-4 is illustrated in Fig. 1. A pH 7.0 HA solution was initially equilibrated with the resin; the pH was then lowered to effect adsorption. At pH 3.0 only 24% of the HA was adsorbed. The molecular size distributions for these solution samples were not measured.

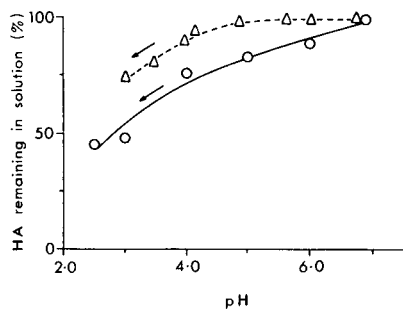


Fig. 1. Adsorption of humic acid on XAD resins. Δ = XAD-4; \circ = XAD-8.

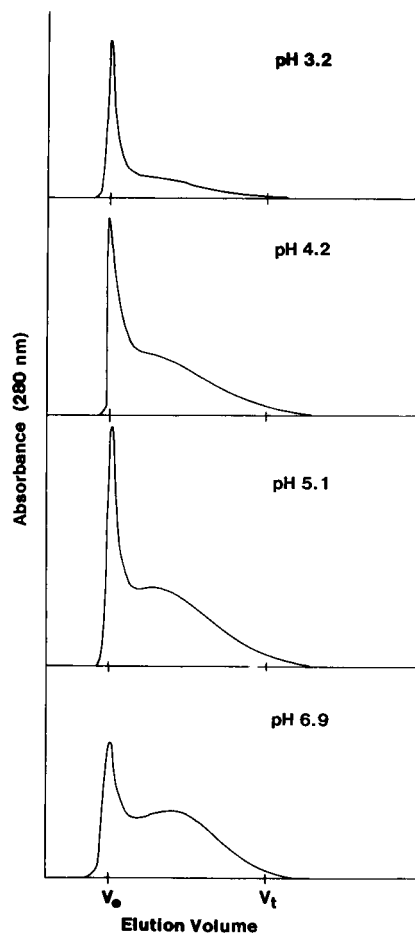


Fig. 2. Molecular size distributions for humic acid remaining in solution in the presence of XAD-2. GPC eluent, 0.01 mol l⁻¹ borax + 0.001 mol l⁻¹ Na₄P₂O₇; pH = 9.18.

Equilibration of soil humic acid with XAD-2

Only 10% of the HA was adsorbed on XAD-2 following acidification to pH 3.0. The molecular size distributions for the HA remaining in solution at selected pH (as determined by GPC) are shown in Fig. 2. The ratio of “large” to “small” molecules remaining in solution (based on GPC peak areas) was 1:0.48 (pH 6.9), 1:0.40 (pH 6.2), 1:0.34 (pH 5.1), 1:0.31 (pH 4.2) and 1:0.14 (pH 3.2), where “large” molecules are defined as those eluting at V_0 and “small” molecules at ca. $V_t/2$ [21].

The material adsorbed from a 0.025- μ m filtered HA solution could not be desorbed quanti-

tatively from the resin when the pH was raised, even after standing at pH 11 overnight (data not shown). The resin was then Soxhlet extracted with AnalaR-grade methanol for 6 h in an attempt to release the strongly adsorbed molecules. The molecular size distribution in this methanol extract indicated the presence of both large and small molecules.

Equilibration of soil humic acid with XAD-8

An HA solution at pH 7.0 was initially equilibrated with the resin; on lowering the pH to 2.5, 55% of the humic acid was adsorbed on the resin (Fig. 1). Subsequent raising of the pH resulted in 10% of the adsorbed material being retained even after the resin had been stood at pH 11 overnight (not shown). In contrast, soil fulvic acid was 90% adsorbed at pH 2.0 and 100% desorbed at pH 7.0 (data not shown).

The molecular size distribution of the humic acid remaining in solution (0.025- μm filtered) at each pH is given in Fig. 3. The ratio of “large” to “small” molecules was 1:0.43 (pH 6.9), 1:0.57

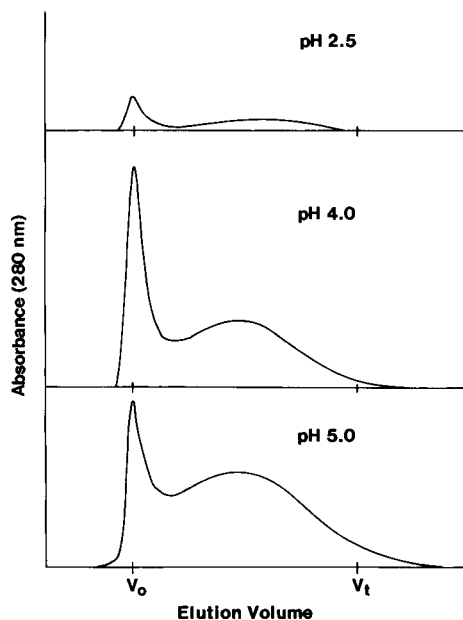


Fig. 3. Molecular size distributions for humic acid remaining in solution in the presence of XAD-8. GPC eluent, 0.01 mol l⁻¹ borax + 0.001 mol l⁻¹ Na₄P₂O₇; pH = 9.18.

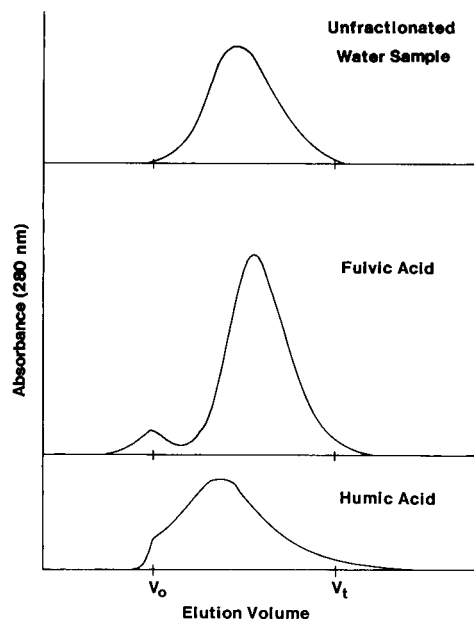


Fig. 4. Molecular size distributions for humic substances from river water. GPC eluent, 0.01 mol l⁻¹ borax + 0.001 mol l⁻¹ Na₄P₂O₇; pH = 9.18.

(pH 5.0), 1:0.32 (pH 4.0), 1:0.28 (pH 3.0) and 1:0.24 (pH 2.5).

Samples of XAD resin equilibrated with HA at pH 2.5 and at pH 7.0 were hot Soxhlet extracted with AnalaR-grade methanol. For the resin sample equilibrated at pH 2.5 only small molecules were released by methanol extraction; both large and small molecules were released from the resin at pH 7.0.

Gel permeation chromatography of aquatic humic substances

The molecular size distributions for the unfractionated water sample and for the isolated humic and fulvic acids, as determined by GPC, are shown in Fig. 4.

DISCUSSION

Properties of XAD resins

XAD-2 and XAD-4 are non-polar, hydrophobic, styrene-divinylbenzene copolymers; XAD-7

and XAD-8 are polar, cross-linked polymers of methyl methacrylate. Their characteristics have been reported elsewhere [2].

As supplied, these resins contain monomers and other impurities which must be removed before use. Various cleaning protocols have been reported [2,22,23]. In this work, XAD resins were cleaned by Soxhlet extraction with AnalaR-grade methanol for at least 2 h. Following this initial procedure the resin was further extracted with a fresh volume of AnalaR-grade methanol for ca. 1 h; no involatile impurities were detected in the ^1H NMR of this methanol extract (after concentration).

Equilibration of soil humic acid with XAD resins

The amount of humic acid equilibrated with XAD resins was always below the reported capacities of these adsorbents for fulvic acid [2]. The minimum pH for adsorption of HA was set at 2.5–3.0. During isolation of humic substances from natural waters the sample is acidified to pH 2.0 to maximize the hydrophobicity of the humic material and hence optimize its potential to adsorb on XAD resins. However, previous work [20] has shown that the solubility of soil HA at pH 2.0 is very low (ca. 0.01 mg l^{-1}). Hence the minimum pH of 2.5 used in work was chosen to minimize the contribution from precipitation and redissolution processes so that molecular adsorption of HA on XAD resins could be probed.

It was observed that fulvic acid was 80% adsorbed on XAD-8 at pH 2.5 and 100% of this desorbed at pH 7.0. In contrast, only 55% of an HA sample could be adsorbed on XAD-8 at pH 2.5.

In this work, using filtered ($0.025\text{-}\mu\text{m}$) humic acid solutions, equilibrium at each pH was attained within 30 min. This is in contrast to equilibration times of the order of 8 h reported by Aiken et al. [2]. The slow uptake could be due to the presence of particulate or colloidal material.

Interactions between soil humic acid and XAD resins

Under the experimental conditions used, soil humic acid was neither quantitatively adsorbed nor desorbed by any of the XAD resins studied

(Fig. 1). when the XAD resins were initially equilibrated with a HA solution at pH 7, no measurable amount was adsorbed. However, after the solution had been acidified to effect adsorption, ca. 10% of the total HA sample remained irreversibly bound when the pH was raised to ca. 11. Specifically, following adsorption on XAD-2 at pH 3.0 and subsequent raising of the pH to 7.0, no small molecules were detected in solution.

If a simple adsorption–desorption mechanism is in effect then the humic molecules should be completely desorbed by pH 10–13. Incomplete desorption of humic molecules at this pH has been reported by other workers [3,18,24]. These observations indicate a very strong interaction between some of the humic acid moieties and the XAD resin matrix and/or that some components become permanently occluded within the pores of the resin.

Although the humic acid solutions initially contained only soluble material (having been $0.025\text{-}\mu\text{m}$ filtered at pH 7.0), colloidal material will have formed in solution as the pH was lowered [20]. Colloids that are protonated and adsorbed on XAD resin at pH 3.0 may precipitate within the resin pores. For such material, alkali dissolution from inside the pores may not be effective.

In an attempt to release the humic molecules that were not desorbed by alkali, the XAD resins were Soxhlet extracted with methanol. GPC of these extracts exhibited peaks for both large and small humic molecules. Changing the solvent, especially changing between aqueous and organic phases, causes swelling and shrinking of XAD adsorbents, which may rupture a proportion of the resin beads [22]. Therefore, the small proportion of humic moieties released by methanol extraction may have arisen from precipitated matter physically trapped in the resin pores.

Size fractionation of humic acid

The observation that HA was not quantitatively adsorbed or desorbed by XAD resins would not be an insurmountable problem provided that the isolated fraction of humic acid was representative of the entire sample. This was not the case. This work established that size-exclusion effects

are operative, with the smaller molecules being selectively adsorbed at all pH values (Figs. 2 and 3). This effect was more pronounced for the smaller pore sized XAD-2 than for XAD-8, and was particularly marked at pH ca. 3.0.

Implications for the structure of humic and fulvic acids

Previous work [20] established that selective precipitation of large humic acid molecules occurs as the solution pH is decreased, with no measurable amount of this fraction remaining in solution below pH 4. However, in the presence of XAD resins there was a dramatic enhancement of the relative solubility of these larger components (Figs. 2 and 3). This may indicate that the presence of both large and small molecules is a prerequisite for aggregation of humic acid.

The size exclusion observed with XAD-8 (mean pore diameter 0.025 μm) indicates that humic acid structures with apparent dimensions greater than 0.025 μm exist in aqueous solution (even though the humic solutions were 0.025- μm filtered prior to equilibration). Small-angle x-ray scattering has established that the radius of gyration (a measure of molecular size) of humic acid in aqueous solution at pH 5 is 0.00136–0.00206- μm [25]. This may imply that some exclusion of the humic molecules from the XAD matrix occurs on the basis of polarity.

The more hydrophilic resins (XAD-7 and XAD-8) are reported to be more efficient for the concentration of fulvic acid than are the more hydrophobic XAD-2 and XAD-4 [1,2,26]. The opposite trend has been reported for aquatic humic acids [18], but this was not observed in this work. For soil HA the adsorbed species were predominantly of smaller molecular size. The observation that these small HA molecules could not be completely desorbed from the resin suggests that they are distinctly different from fulvic acid moieties. That is, the small "humic acid" molecules are *not* merely "fulvic acid" which was coprecipitated during the extraction procedure. For example, they may be of much lower solubility or more hydrophobic and/or more aromatic and/or more phenolic in character. On the basis of GPC, Blondeau [27] also proposed that fulvic acids are dis-

tinct chemical entities that cannot be regarded simply as a lower molecular weight fraction of humic acid.

Implications for the isolation of soil humic substances

The IHSS humic acid used in this work was extracted from soil with 0.1 mol l⁻¹ NaOH. The above results indicate that none of the XAD resins studied could isolate a sample of the soil-derived humic acid which is comparable to the product precipitated following NaOH extraction. It is important to note that the limited solubility of HA (in contrast to FA) severely restricts the application of XAD resins to its isolation from soil extracts.

Comparison of soil and aquatic humic substances

Humic substances can only be defined operationally. Isolation methods involving the least aggressive chemical conditions are to be favoured. For both aquatic and soil-derived humic substances, the distinction between humic and fulvic acids is based on solubility at pH 1.0. Aquatic humic acid is further limited to that fraction of the organic carbon which is retained on a XAD resin at pH 2 and released at pH 13.

Aquatic humic substances have different physico-chemical characteristics from those derived from soil [28]. In particular, aquatic humic substances have lower molecular weight [29,30] and are predominantly aliphatic [31]. According to Visser [32], aquatic humic and fulvic acids have more characteristics in common than do those derived from soil. It is possible that these observations are an artifact of the isolation procedures.

Some differences between aquatic and soil-derived humic substances may be caused by the choice of extraction procedure. However, the proportion of aquatic humic substances in rivers and lakes which originate from soil can be significant (in some instances greater than 50%) [33].

In previous work on the solubility of humic acid [20], it was established that only small molecules are dissolved in weakly acidic solutions. Therefore, if a significant proportion of aquatic humic acid arises from leaching of soil at

pH 3–5, then comparatively few large molecules found in the water will be soil derived. It was observed that the smaller molecules which are preferentially solubilized in this pH range [20] were concentrated by XAD resins.

As used in this work, XAD resins did not provide any advantages over the conventional NaOH extraction procedure for the isolation of humic acid from soil extracts; they may actually be disadvantageous.

Isolation of aquatic humic substances

To investigate whether any molecular size fractionation occurs on isolation of aquatic humic substances by XAD-8 resin, humic and fulvic acids were isolated from a humic water using the procedure which has been used by the IHSS [4]. Most of the humic substances in the sample arose from leaching of surrounding podzolized yellow-brown earths.

In this isolation procedure, a sample that had been 0.45- μm filtered at natural pH was acidified to pH 2.0, then passed through an XAD-8 column. It was of interest to establish whether or not significant precipitation occurred on acidification of a natural water sample, as it had been shown that the solubility of soil HA decreases very markedly in weakly acidic solutions [20].

UV-visible spectrophotometry of the sample solutions at natural pH (3.6) and at pH 2.0 (both 0.025- μm filtered) established that 60% of the coloured material had precipitated on acidification. This material was inferred to be humic acid. It is likely that retention of this material by XAD resins did not involve normal processes of molecular adsorption, but rather occlusion and redissolution.

The isolated humic acid contained a significant amount of large molecules, whereas none were detected in the whole water sample (Fig. 4). It is possible that these large molecular units arose from aggregation of (or with) smaller moieties by precipitation at pH 1.0 or during preconcentration on XAD [6] (the isolated humic acid was concentrated ca. 500-fold on the resin). The apparent molecular size of the smaller humic acid components was greater than that for the unfractionated sample; that for fulvic acid was less.

The aquatic humic acid had a lower proportion of large molecules than did the IHSS soil humic acid. Further, in contrast to the experiments with soil-derived humic acid, no visible coloured material remained on the XAD-8 resin at pH 12 following concentration of the aquatic humic substances (even though this sample was only 0.45- μm filtered). This may indicate that the components of soil humic acid which are strongly adsorbed by XAD-8 are not present in aquatic humic acid and/or are an artifact of the NaOH extraction process.

REFERENCES

- 1 J.A. Leenheer and E.W.D. Huffman, Jr., *J. Res. U.S. Geol. Surv.*, 4 (1976) 737.
- 2 G.R. Aiken, E.M. Thurman, R.L. Malcolm and H.F. Walton, *Anal. Chem.*, 51 (1979) 1799.
- 3 E.M. Thurman and R.L. Malcolm, *U.S. Geol. Surv. Water Supply Pap.*, 1817-G (1979).
- 4 E.M. Thurman and R.L. Malcolm, *Environ. Sci. Technol.*, 15 (1981) 463.
- 5 J.A. Leenheer and T.I. Noyes, *U.S. Geol. Surv. Water Supply Pap.*, 2230 (1984).
- 6 J.E. Gregor and H.K.J. Powell, *J. Soil Sci.*, 37 (1986) 577.
- 7 R.S. Swift, personal communication, 1988.
- 8 S.M. Serkiz and E.M. Perdue, *Water Res.*, 24 (1990) 911.
- 9 R.L. Gustafson and J. Paleos, in S.D. Faust and J.V. Hunter (Eds.), *Organic Compounds in Aquatic Environments*, Dekker, New York, 1971, p. 213.
- 10 G.A. Junk, J.J. Richard, M.D. Grieser, D. Witiak, J.L. Witiak, M.D. Arguello, R. Vick, H.J. Svec, J.S. Fritz and G.V. Calder, *J. Chromatogr.*, 99 (1974) 745.
- 11 G. Chiavari, L. Pastorelli and P. Vitali, *Fresenius' Z. Anal. Chem.*, 317 (1984) 130.
- 12 D.J. Mackey, *J. Chromatogr.*, 236 (1982) 81.
- 13 D.J. Mackey, *J. Chromatogr.*, 242 (1982) 275.
- 14 C-C. Wan, S. Chiang and A. Corsini, *Anal. Chem.*, 57 (1985) 719.
- 15 G.R. Aiken, D.M. McKnight, R.L. Wershaw and P. McCarthy (Eds.), *Humic Substances in Soil, Sediment, and Water. Geochemistry, Isolation, and Characterization*, Wiley-Interscience, New York, 1985.
- 16 G.G. Leppard, J. Buffle and R. Baudat, *Water Res.*, 20 (1986) 185.
- 17 J. Paleos, *J. Colloid Interface Sci.*, 31 (1969) 7.
- 18 R.F.C. Mantoura and J.P. Riley, *Anal. Chim. Acta*, 76 (1975) 97.
- 19 A.K. Burnham, G.V. Calder, J.S. Fritz, G.A. Junk, H.J. Svec and R. Willis, *Anal. Chem.*, 44 (1972) 139.
- 20 H.K.J. Powell and R.M. Town, *Anal. Chim. Acta*, 267 (1992) 47.

- 21 H.K.J. Powell and R.M. Town, *Anal. Chim. Acta*, 256 (1992) 81.
- 22 S.A. Daignault, D.K. Noot, D.T. Williams and P.M. Huck, *Water Res.*, 22 (1988) 803.
- 23 M.W. Tabor and J.C. Loper, *Int. J. Environ. Anal. Chem.*, 19 (1985) 281.
- 24 M. Hiraide, Y. Arima and A. Mizuike, *Anal. Chim. Acta*, 200 (1987) 171.
- 25 R.L. Wershaw and D.J. Pinckney, *J. Res. U.S. Geol. Surv.*, 5 (1977) 571.
- 26 E.M. Thurman, R.L. Malcolm and G.R. Aiken, *Anal. Chem.*, 50 (1978) 775.
- 27 R. Blondeau, *Org. Geochem.*, 9 (1986) 47.
- 28 R.L. Malcolm, *Anal. Chim. Acta*, 232 (1990) 19.
- 29 E.M. Thurman, R.L. Wershaw, R.L. Malcolm and D.J. Pinckney, *Org. Geochem.*, 4 (1982) 27.
- 30 N. Plechanov, *Org. Geochem.*, 5 (1983) 143.
- 31 R.L. Malcolm, in G.R. Aiken, D.M. McKnight, R.L. Wershaw and P. MacCarthy (Eds.), *Humic Substances in Soil, Sediment, and Water. Geochemistry, Isolation, and Characterization*, Wiley-Interscience, New York, 1985, p. 181.
- 32 S.A. Visser, *Water Res.*, 17 (1983) 1393.
- 33 J. Buffle, *Complexation Reactions in Aquatic Systems*, Horwood, Chichester, 1988.

Methylotrophic yeast microbiosensor based on ion-sensitive field effect transistors for methanol and ethanol determination

Y.I. Korpan, A.P. Soldatkin, N.F. Starodub and A.V. El'skaya

Institute of Molecular Biology and Genetics of the Ukrainian Academy of Science, Kiev (Ukraine)

M.V. Gonchar and A.A. Sibirny

L'vov Branch of A.V. Palladin Institute of Biochemistry of the Ukrainian Academy of Science, L'vov (Ukraine)

A.A. Shul'ga

Semiconductor Physics Department, Kiev State University, 64 Vladimirska, Kiev 252017 (Ukraine)

(Received 21st April 1992; revised manuscript received 14th September 1992)

Abstract

Bioassays for methanol and ethanol based on disposable biosensors were developed using mutant cells of methylotrophic yeasts *Hansenula polymorpha* 34-19 and *Pichia pinus* 2468, respectively. Cells were immobilized in calcium alginate gel on the gate of pH-sensitive field effect transistors and the local acidification of the medium due to specific consumption of alcohols was recorded. The assay time was a few minutes. As the washing time exceeded 1 h, after a single use of the biosensor a new membrane was formed on the transducer or another biosensor was used. Both developed assays showed in unbuffered medium a detection limit near to 0.5 mM and linear calibration graphs over the alcohol concentration range 5–100 mM. Specificity studies showed no cross-sensitivity and no response to similar alcohols such as propanols and butanols, although a response to formaldehyde was observed in both instances. The effects of the cell contents in the membrane, buffer concentration and sample pH on the response of the biosensors were studied.

Keywords: Biosensors; Ethanol; Ion-sensitive field effect transistors; Methanol; Yeasts

The determination of alcohols is very important in toxicological studies and in the biotechnological and food industries. Numerous assays have been developed including enzyme-based chromogenic methods [1–3] and electrode [4–7] and fibre-optic [8] biosensors.

Whereas in the approaches mentioned above isolated enzymes were used, natural multi-enzyme systems such as intact cells can also be used for analytical purposes. For example, a biosensor based on acetic acid bacteria and a membrane-bound alcohol dehydrogenase complex immobilized on the gate of an ion-sensitive field effect transistor (ISFET) has been used for alcohol determination [9,10]. Attractive features of cell biocatalysts are the ability to use nature-optimized

Correspondence to: Y.I. Korpan, Institute of Molecular Biology and Genetics of the Ukrainian Academy of Science, Kiev (Ukraine).

multi-enzyme systems, the ability to use biocatalytic activity not available in the form of an isolated enzyme and the increased storage and/or performance stability of the biocatalytic system that is maintained in its natural environment that could be obtained [11,12].

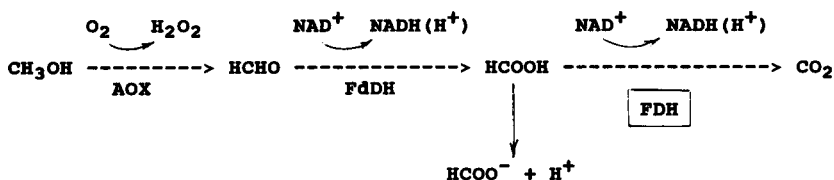
Potential advantages of ISFETs as transducers for biosensors include the possibility of miniaturization, compatibility with integrated circuit technology and inter alia suitability for large-scale production at low unit cost and high sensitivity [13].

Gonchar et al. [14] described the phenomenon of methanol-induced acidification of the extracellular medium by the methylotrophic yeasts *Hansenula polymorpha* and *Pichia pinus* and a high correlation between the phenomenon of acidification and methylotrophic metabolism was established. It was shown that genetic damage of the methanol metabolic system changes the acidification process and allows the use of these yeasts as highly specific biocatalysts in bioassays and biosensors.

To impart specificity to different alcohols to yeast cells, some modifications of their metabolic enzymatic pathways were introduced by mutations. The mutant *Hansenula polymorpha* 34-19 secretes the acidic metabolic product in the extracellular medium in the presence of methanol because of the damage introduced in the formate dehydrogenase. The specific reaction with ethanol of the mutant *Pichia pinus* 2468 is due to suppression of the acetyl-CoA synthetase activity (Fig. 1). The specific rate of proton secretion lies in the range 10–20 nmol H^+ min^{-1} per 1 mg of cell depending on their physiological state.

This paper describes biological assays for methanol and ethanol based on disposable cell biosensors. The biosensors used incorporate cells of the mutant methylotrophic yeasts *H. polymorpha* and *P. pinus*, respectively, immobilized on the gate insulator of pH-sensitive ISFETs. The performance characteristics of the biosensors and their dependence on the biomembrane and the sample solution composition were studied and are discussed.

A. *Hansenula polymorpha* 34-19



B. *Pichia pinus* 2468

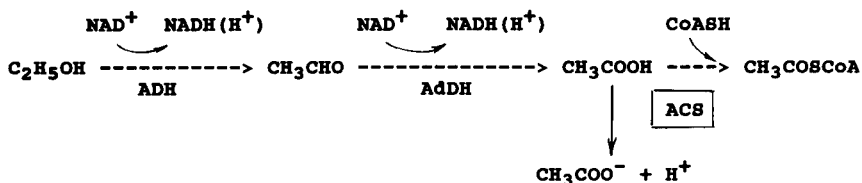


Fig. 1. Ethanol and methanol oxidation scheme and genetic blocks for methylotrophic yeasts. AOX = alcohol oxidase; FdDH = formaldehyde dehydrogenase; FDH = formate dehydrogenase; ADH = alcohol dehydrogenase; AddH = acetaldehyde dehydrogenase; ACS = acetyl-S-CoA synthetase; boxes = enzyme genetic block.

EXPERIMENTAL

Reagents

Yeast extract and bacto-peptone were purchased from Difco Laboratories (USA) and sodium alginate from Chemicals Co. (UK). All other reagents were obtained commercially and were used as received.

Culture and immobilization procedure

Mutant cells of the methylotrophic yeasts *Hansenula polymorpha* 34-19 (met 9-2 ftd) [15] were used for methanol assay. The microorganisms were cultured at 30°C in a medium containing 5 g l⁻¹ yeast extract, 5 g l⁻¹ bacto-peptone, 20 mg l⁻¹ methionine and 1% (v/v) methanol to the exponential phase of growth.

The strain of the methylotrophic yeast *Pichia pinus* 2468 (ade2 arg1 acs2) [16] was used for ethanol assay. The microorganisms were cultivated at 30°C in a medium containing 0.5 g l⁻¹ yeast extract, 10 g l⁻¹ glucose, 50 mg l⁻¹ adenine and arginine until the cell concentration reached 1 mg dry weight ml⁻¹. Subsequently the cells were washed by centrifugation. For the induction of enzyme synthesis, cells were transferred into the medium with ethanol and were incubated on a shaker (200 rpm) at 30°C for 8–10 h, then washed.

A mixture of 10 μg of wet washed cells and 1 μl of 2% sodium alginate solution was deposited by the drop method on the surface of one ISFET. On the surface of the other ISFET only 1 μl of 2% sodium alginate solution was deposited. Subsequently the chip was immersed in 0.1 M CaCl₂ solution for 5 min to complete the biomembrane formation process.

Apparatus

A sensor chip with dimensions 2 mm × 4 mm consisted of two *n*-channel working in the depletion mode pH-sensitive ISFETs with silicon nitride as the pH-sensitive material [13]. One of the ISFETs on the chip was covered with the biomembrane containing cells (measuring ISFET) and the other with the cell-free membrane (reference ISFET). The output signal of the biosensor was measured as the difference between the out-

puts of the measuring and reference ISFETs. Measurements were made in daylight and at room temperature.

Procedures for measurement of alcohol concentration

Measurements were made in a glass cell having a volume of about 4 ml and filled with distilled water or buffer mixture [17]. The yeast-ISFET biosensors were immersed in vigorously stirred sample solution. After stabilization of the output signal of the sensor a portion of the analyte was added to the cell. The change in the differential output voltage of the biosensor was continuously recorded and the maximum rate of the voltage change was plotted as a function of analyte concentration.

RESULTS AND DISCUSSION

When methanol or ethanol is added to the sample solution alcohol molecules diffuse into the biomembrane covering the measuring ISFET and are oxidized by immobilized yeast cells to formic or acetic acid, respectively. Subsequent local acidification of the medium results in variation of the measuring ISFET gate voltage and this is recorded by the chart recorder. A typical dependence of the sensor output on time after addition of alcohols to the measurement cell is shown in Fig. 2. The baseline was measured in the absence of alcohol.

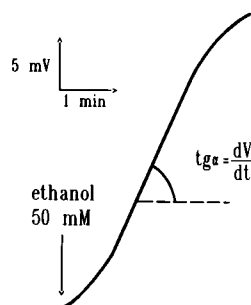


Fig. 2. Typical response curve of the cell ISFET ethanol biosensor in distilled water at a cell concentration in the membrane of 10 mg ml⁻¹.

Experiments have shown that although the cell kinetics in the biomembrane was reversible, the time needed to restore the initial baseline of the sensor's output exceeded 1 h. Therefore, for faster assays, it proved necessary to form a new biomembrane on the transducer after each measurement or to use another biosensor. The deposition technique for the membrane formation appeared to be reproducible and variations of the biosensor response from one de novo formed membrane to another did not exceed 10%.

The kinetics of the sensor response was slow because of the slow cell metabolism and the sensor's response time was about 25 min. The steady-state value of the sensor's output reached after addition of the analyte is determined by the equilibrium established between the rate of proton secretion from the cells and proton flow out of the membrane because of diffusion. Measurements can be made much faster if not the steady-state but the kinetic response is determined, i.e., the maximum rate of the output voltage change (dV_{out}/dt)_{max}. The dependence of the initial rate of the output voltage change (dV_{out}/dt) on the alcohol concentration is plotted in Fig. 3. Each point on this plot was measured for the biosensor having a de novo formed biomembrane. The calibration graph for this biosensor-based bioassay was linear in the range

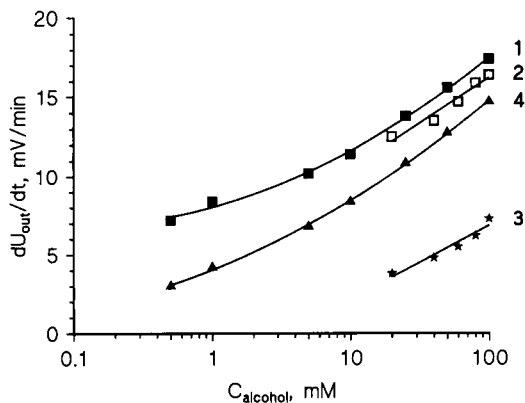


Fig. 3. Calibration graphs for ethanol- (1 = in distilled water; 2 = 0.5 mM per pH unit buffer mixture; 3 = 2.0 mM per pH unit buffer mixture) and methanol- (4 = in distilled water) specific cell ISFETs measured at a cell concentration in the membrane of 8 mg ml^{-1} .

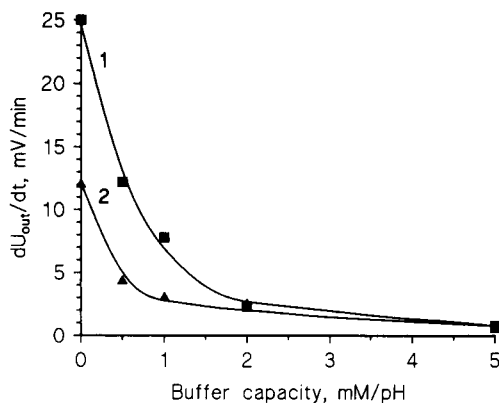


Fig. 4. Dependence of sensor output on buffer capacity of the sample measured in polymix buffer (pH 6.0) with a cell concentration of 10 mg ml^{-1} and an alcohol concentration of 100 mM: 1 = ethanol; 2 = methanol.

of analyte concentrations from 5 to 100 mM for both methanol and ethanol. The detection limit in both instances was about 0.5 mM. As can be seen, the sensor response is strongly affected by the buffer capacity of the sample solution.

The presence of buffer species in the sample solution led to a dramatic decrease in the biosensor output (Fig. 4) because it facilitates diffusion of protons out of the membrane. One way to mitigate partially the decrease in the response is to increase the cell content in the membrane. This is illustrated in Fig. 5, from which one can see a linear dependence of the kinetic sensor

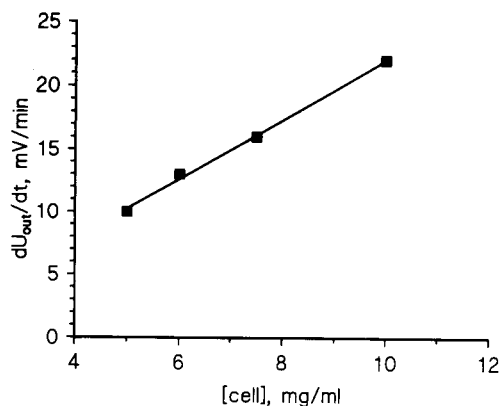


Fig. 5. Dependence of the initial slope of the sensor response on *P. pinus* cell concentration in the membrane measured in distilled water at an ethanol concentration of 50 mM.

response on the cell concentration in the membrane for methanol assay. The observed large suppression of the biosensor response with increasing buffer capacity of the sample forms the major obstacle to the wider application of this type of potentiometric cell biosensor. For cell biocatalysts this problem seems even more severe than for enzymes because the slow kinetics of the cell metabolism can hardly compete with the fast kinetics of the “facilitated transport” of protons out of the membrane by the buffer species present.

To study the pH dependence of the biosensor output, mixed buffer solutions with different pH values were used. The characteristic feature of the multi-component buffer solution is that it has a nearly constant buffer capacity in the pH range 4–9. The use of a buffer with constant buffer capacity permits the true pH dependence of the sensor to be determined. Otherwise a different buffer capacity of the sample at different pH may result in different response values even if the rate of metabolism in the cells does not change. The pH dependence of the methanol and ethanol biosensor output is shown in Fig. 6. The signal for 100 mM alcohol concentration was measured in buffer solution having a buffer capacity of 1 mM

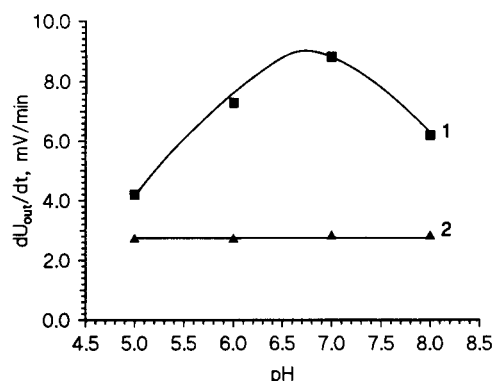


Fig. 6. pH dependence of the biosensor response in buffer mixture (buffer capacity 1 mM, cell concentration 10 mg ml⁻¹, alcohol concentration 100 mM). 1 = Ethanol; 2 = methanol.

per pH unit. For the ethanol biosensor the observed pH dependence has a bell shape with optimum pH near 7, whereas for the methanol sensor the output does not depend on pH in the range 5–8.

Because for many applications specificity of the analyte detection is important, this selectivity of the developed biosensors was tested. No cross-sensitivity was observed: the methanol biosensor did not respond to ethanol and vice

TABLE 1

Results of the specificity test of the ethanol and methanol cell ISFETs compared with the results from the literature

Analyte	Enzyme sensor AOX electrode ^a [9]	<i>Acetobacter aceti</i> FET sensor [9]	<i>H. Polymorpha</i> FET sensor	<i>P. pinus</i> FET sensor
Methanol	+	–	+	–
Ethanol	+	+	–	+
Propan-1-ol	+	+	–	–
Propan-2-ol	–	–	–	–
Butan-1-ol	+	+	–	–
Butan-2-ol	–	–	–	–
Allyl alcohol	+	+	–	–
Other primary alcohols	+	(C ₂ –C ₆) +	–	–
Formaldehyde	+	ND	+	+
Formate	+	ND	–	–
Acetate	+	–	–	–
Lactate	+	–	–	–
Glucose	–	–	–	–

^a AOX = alcohol oxidase.

versa. Also, both biosensors showed no response to propanols, butanols, pentanols and some other chemically similar compounds. However, a response to formaldehyde was observed in both instances. A survey of the specificity test is presented in Table 1. It can be seen that with regard to specificity the biosensors developed are much superior to those based on the use of *Acetobacter acetii* AM 1801 or alcohol oxidase [9]. The results of this specificity test demonstrate the potential of the cell biocatalysts for the development of highly specific biological assays with adjusted specificity.

Conclusion

Disposable cell ISFET biosensors specific to methanol and ethanol were developed using mutant cells of methylotrophic yeasts *Hansenula polymorpha* and *Pichia pinus*, respectively, immobilized in calcium alginate gel. Calibration graphs for the biosensor-based assays developed were linear in the concentration range 5–100 mM for both alcohols. The assay time was a few minutes and the detection limit of the biosensors in unbuffered medium was near 0.5 mM for both methanol and ethanol. Specificity tests showed characteristics superior to those of other biosensors for alcohols. Practical application of the developed biosensors in different fields seems possible provided that the assay conditions permit the buffer capacity of the samples to be controlled.

Further developments will include fabrication of a cell ISFET biosensor specific to formaldehyde on the basis of a double mutant of meth-

ylotrophic yeast A3-11 with suppressed activity of formate dehydrogenase and alcohol oxidase.

REFERENCES

- 1 C. Verduyn, J.P. van Dijken and W.A. Scheffers, *J. Microbiol. Methods*, 2 (1984) 15.
- 2 J. Kocar, J. Schneider, L. Skursky and H. Dubsky, *Anal. Biochem.*, 137 (1984) 74.
- 3 M.V. Gonchar, Y.I. Korpan and A.A. Sibirny, *Ukr. Biokhim. Zh. (USSR)*, 63 (1991) 62.
- 4 J. Kulis, V. Laurinavichus, M. Pesliakienė and V. Gureviciene, *Biotechnol. Appl. Biochem.*, 11 (1989) 149.
- 5 K. Matsumoto, H. Matsubara, H. Hamada, H. Ukeda and Y. Osajima, *J. Biotechnol.*, 14 (1990) 115.
- 6 Y. Kitagawa, K. Kitabatake, I. Kubo, E. Tamiya and I. Karube, *Anal. Chim. Acta*, 218 (1989) 61.
- 7 F. Vargo, W.M. Ledingham and F.G.L. Lima, *Agric. Biol. Technol.*, 33 (1989) 286.
- 8 S. Gautier, L.J. Blum and P.R. Coulet, *J. Biolumin. Chemilumin.*, 5 (1990) 57.
- 9 Y. Kitagawa, E. Tamiya and I. Karube, *Anal. Lett.*, 20 (1987) 81.
- 10 E. Tamiya, I. Karube, Y. Kitagawa, M. Ameyama and K. Nakashima, *Anal. Chim. Acta*, 207 (1988) 77.
- 11 D.M. Rawson, *Int. Ind. Biotechnol.*, 8 (1988) 18.
- 12 M.A. Arnold and M.E. Meyerhoff, *CRC Crit. Rev. Anal. Chem.*, 20 (1988) 149.
- 13 A.V. El'skaya and V.I. Strikha, *Stud. Biophys.*, 132 (1989) 83.
- 14 M.V. Gonchar, V.I. Titorenko, N.M. Hladerevska and A.A. Sibirny, *Biokhimiya (USSR)*, 55 (1990) 2148.
- 15 A.A. Sibirny, V.M. Ubiyovok, M.V. Gonchar, V.I. Titorenko, A.Y. Voronovsky, Y.G. Kapultsevich and K.M. Bliznik, *Arch. Microbiol.*, 154 (1990) 566.
- 16 I.I. Tolstorukov, B.D. Efremov, S.V. Benevolensky, V.I. Titorenko and A.A. Sibirny, *Yeast*, 5 (1989) 179.
- 17 B. Olsson, *Anal. Chim. Acta*, 209 (1988) 123.

Adsorptive preconcentration for voltammetric measurements of trace levels of vanadium in the presence of copper

Pércio A.M. Farias, Aniy K. Ohara and Iracema Takase

Department of Chemistry, Pontificia Universidade Católica, 22453-900 Rio de Janeiro (Brazil)

Sergio L.C. Ferreira

Institute of Chemistry, Universidade Federal da Bahia, Salvador (Brazil)

Jon S. Gold

Department of Chemistry, Santa Clara University, Santa Clara, CA 95053 (USA)

(Received 1st June 1992; revised manuscript received 12th August 1992)

Abstract

An electrochemical stripping procedure for trace measurements of vanadium is described in which preconcentration is achieved by the adsorption of a vanadium–2-(2'-thiazolylazo)-*p*-cresol complex on a static mercury drop electrode. Cyclic voltammetry was used to characterize the interfacial and redox behavior. Optimum experimental conditions were found to be the use of a stirred acetate buffer (pH 4.2) solution with a 2-(2'-thiazolylazo)-*p*-cresol concentration of 1.0×10^{-5} M, a preconcentration potential of 0.00 V, a scan rate of 100 mV s^{-1} and a linear scan mode. The response is linear over the concentration range 5–30 $\mu\text{g V}^{5+} \text{ l}^{-1}$. For a 5-min preconcentration time, the detection limit is 3.9 nM. Possible interferences by anions and other trace metals were investigated. Sequential determination of copper with vanadium is possible. The method was applied to the analysis of mineral water.

Keywords: Stripping voltammetry; Voltammetry; Adsorption; Copper; Preconcentration; Vanadium; Waters

Vanadium at ng ml^{-1} levels is an essential trace element, possessing specific physiological functions, but it can be toxic when present at $\mu\text{g ml}^{-1}$ concentrations. In environmental chemistry, vanadium is one of the most important elements, acting as a tracer in the evaluation of air pollution caused by fossil fuel combustion.

Vanadium in environmental samples has gen-

erally been determined by conventional [1] or catalytic [2] spectrophotometry, atomic absorption spectrometry [3,4], emission spectrometry [5], x-ray fluorescence spectrometry [6], neutron activation analysis [7] and reversed-phase liquid chromatography [8]. However, electrochemical methods such as catalytic polarography have been shown to be the most sensitive [9]. Alternatively, cathodic adsorptive stripping voltammetric measurements based on complexing V(V) with catechol [10], Solochrome Violet RS [11] or 5-Br-PADAP [12] can be used for determining this ion.

Correspondence to: P.A.M. Farias, Department of Chemistry, Pontificia Universidade Católica, 22453-900 Rio de Janeiro (Brazil).

The method presented here is demonstrated to be advantageous in terms of high sensitivity (with a high degree of freedom from commonly interfering species) and to be useful for the sequential determination of copper.

Copper is also an important trace metal in many biological and environmental systems [13] and many methods suitable for the determination of copper in these media have been reported. Anodic stripping voltammetry (ASV) is a conventional electrochemical method for determining trace levels of copper [14]. In adsorptive stripping voltammetry, several ligands such as catechol [15], quinolin-8-ol [16], imidazole [17] and 1,10-phenanthroline [18] have been used for the determination of copper. Each of these complexing ligands has its own peculiarities and is subject to interference from other potential complexing agents that may be present in any given analysis. This laboratory has been involved with studies of new ligands that display greater stability and form complexes that allow analyses with maximum freedom from interfering species.

This paper describes an adsorptive voltammetric method for trace measurements of V(V). The method is based on the effective interfacial accumulation of the V(V) complex with 2-(2'-thiazolylazo)-*p*-cresol on the surface of a static mercury drop electrode (SMDE) with the subsequent reduction of the complex. The influence of copper in these media was also studied. In addition, the effect of a wide range of potentially interfering species such as anions, cations and organic surfactants was examined. The method was utilized for the determination of traces of vanadium in a commercial mineral water. Similar azo compound-based adsorption voltammetric methods for trace measurements of uranyl [19,20], copper [21] and iron [22] have been reported previously.

EXPERIMENTAL

Apparatus and reagents

The PAR 264-A voltammetric analyser with a PAR 303 static mercury drop electrode used here has been described in detail previously [19,20]. Purified water, produced in a Milli-Q water pu-

rification system (Millipore), was used for all dilutions and to prepare solutions. All chemicals were of analytical-reagent grade.

A 1000 $\mu\text{g ml}^{-1}$ stock solution of V(V) was prepared by dissolving an appropriate amount of NH_4VO_3 (J.T. Baker) in NaOH solution (2 g l^{-1}). A 2×10^{-3} M stock solution of 2-(2'-thiazolylazo)-*p*-cresol (TAC) was prepared in ethanol. The supporting electrolyte was a 1 M acetate buffer (pH 4.2). The mineral waters subsequently analyzed (Ibirá, São Paulo), were obtained commercially and from of the spring.

Procedure

A 10-ml volume of supporting electrolyte solution (9.5 ml of purified water + 0.5 ml of acetate buffer) containing 1×10^{-5} M TAC was pipetted into the cell and purged with nitrogen for 8 min. The preconcentration potential, measured versus an Ag/AgCl reference electrode (usually 0.00 V), was applied to a fresh mercury drop while the solution was stirred. Following the accumulation period (usually 60 s) the stirring was stopped and, after a 15-s equilibration time, the voltammogram was recorded using a linear scan of decreasing voltage (100 mV s^{-1}), terminated at -0.60 V . When the background stripping voltammogram had been obtained, aliquots of vanadium standard solution were introduced. The solution was then deaerated and stirred for 2 min to allow chelate formation. All data were obtained at $23 \pm 1^\circ\text{C}$.

RESULTS AND DISCUSSION

Parameters affecting the adsorptive stripping behavior

Figure 1 shows the effect of pH on the linear scan stripping peak currents (B) and potentials (A) for copper- and vanadium-TAC complexes. The solution pH from 3.3 to 5.4 has a pronounced effect on the magnitude of the peak current. In addition, the potential of the peaks becomes sharply more negative with increasing pH. The largest copper peak current was observed at pH 3.6 for the copper-TAC complex (B, curve a) and

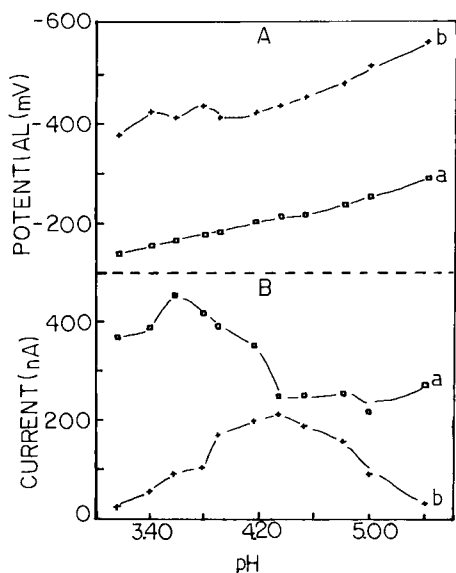


Fig. 1. Effects of pH on the linear scan adsorptive stripping peak current (B) and potential (A) for copper-TAC and vanadium-TAC complexes. Electrolyte, 0.05 M acetate buffer containing 1.0×10^{-5} M TAC and $20 \mu\text{g l}^{-1}$ of (b) vanadium and (a) copper; accumulation time, 60 s at 0.00 V; scan rate, 50 mV s^{-1} ; equilibrium time, 30 s; filter, 0.1 s; medium drop size (area 0.016 cm^2).

4.2–4.6 for the vanadium-TAC complex (B, curve b).

The influence of acetate concentration (0.02–0.20 M) was examined at pH 4.2. The vanadium-TAC complex peak current depends strongly of the acetate concentration; the peak current decreases with increasing buffer concentration. In contrast, acetate concentration over the range 0.020–0.20 M had no effect on the copper-TAC complex peak current response. Hence 0.05 M acetate buffer (pH 4.20) was used for all further work.

Previously a method for the determination of copper using various heterocyclic azo compounds was reported [21]. Figure 2 shows the cyclic voltammograms (first scan, 1.5×10^{-5} M ligand, $24.6 \mu\text{g l}^{-1}$ vanadium) of the various ligands and vanadium-ligand complexes. Voltammograms A, B, C and D are those obtained from the ligands TAC, 4-(2-thiazolylazo)resorcinol (TAR), 2-(2-thiazolylazo)-5-dimethylaminophenol (TAM) and 1-(2-thiazolylazo)-2-naphthol (TAN), respectively.

The TAC ligand (curve A) is seen to exhibit the best sensitivity and resolution as determined by the separation of the free ligand and complex reduction peaks and by the narrow half-width of the reduction peak of the complex. Cyclic voltammograms obtained for the vanadium complexes without preconcentration showed no significant differences, but yielded a significantly lower sensitivity.

Repetitive voltammograms were obtained at various pH values. Figure 3 shows repetitive cyclic voltammograms for 1×10^{-5} M TAC (A) recorded in the presence of $40 \mu\text{g l}^{-1}$ vanadium (C) and $20 \mu\text{g l}^{-1}$ copper (B) in unstirred 0.05 M acetate buffer (pH 5.0) solution. The cathodic peak currents of the vanadium-TAC complex (peak C), from -0.53 to -0.45 V, and the copper-TAC complex (peak B), at -0.26 V, gradually increase with repetitive scans while the current of the free ligand TAC (peak A) at -0.20 V simultaneously decreases until it almost returns to the baseline. In the pH range 4.8–5.4 the vanadium-TAC complex and free TAC showed this behavior, but at lower pH this effect disappeared (pH range studied = 3.2–4.8). This effect is not observed at pH 5.0 if the final potential used is lower than -0.90 V. For copper this effect appears in the pH range studied. The peak current with the adsorbed complexes at saturation is several times greater than that of the solution species alone (estimated from the first scan, designated 1). Four poorly resolved peaks are observed in the anodic branch. The peak designated A' appears to be two overlapping peaks corresponding to the cathodic peaks A and B. This overlap yielded a curve that can be interpreted by considering the peak at a more negative potential to decrease while the more positive side increases slightly with repetitive scans. The overlapping peaks designated C' may be interpreted as corresponding to the cathodic peak C.

The effect of the accumulation potential on the peak current of the complexes was evaluated over the range 0.05 to -0.40 V (Fig. 4). The largest peak current of the vanadium-TAC complex (curve b) was observed for accumulation in the range 0.00 to -0.05 V and for the copper-TAC complex (curve a) from 0.05 to -0.10 V.

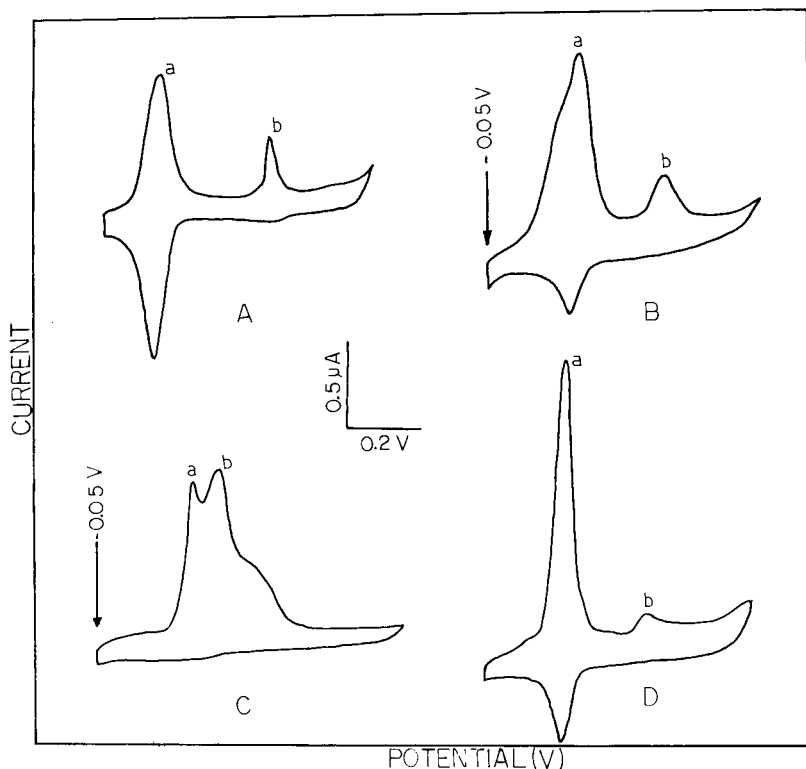


Fig. 2. Cyclic voltammograms for (a) 1×10^{-5} M of (A) TAC, (B) TAR, (C) TAM and (D) TAN complexed with (b) $24.6 \mu\text{g l}^{-1}$ of vanadium in a stirred 0.05 M acetate buffer (pH 4.20) solution. Scan rate, 100 mV s^{-1} ; accumulation time, 60 s at -0.05 V; equilibrium time, 30 s; filter, 0.1 s; large drop size.

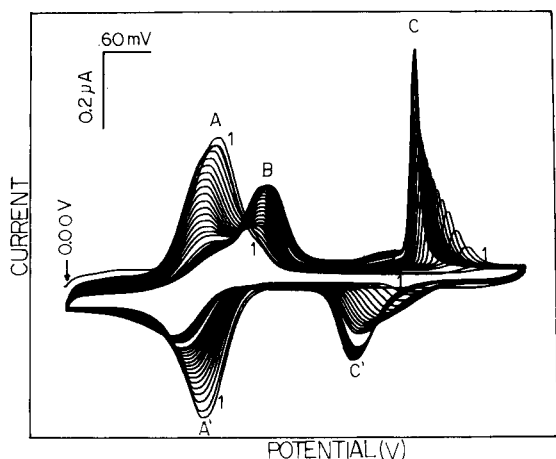


Fig. 3. Repetitive cyclic voltammograms for (A) 1×10^{-5} M TAC with (B) $20 \mu\text{g l}^{-1}$ of copper and (C) $40 \mu\text{g l}^{-1}$ of vanadium in unstirred 0.05 M acetate buffer (pH 5.0) solution. Scan rate, 50 mV s^{-1} ; equilibrium time, 30 s; filter, 0.1 s. The first scan is indicated by 1.

The complexes are stable for at least 3 h in the deaerated acetate buffer medium (pH 4.2).

Other experimental variables affecting the adsorptive stripping response were evaluated and optimized. For example, Fig. 5 shows the effect of

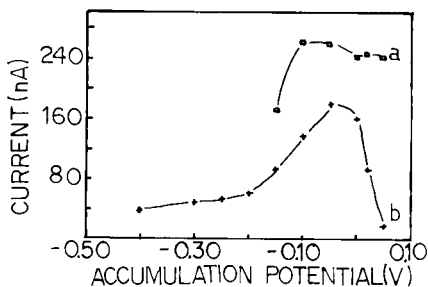


Fig. 4. Dependences of stripping peak current on the accumulation potential for (b) vanadium-TAC and (a) copper-TAC complexes. Acetate buffer, 0.05 M (pH 4.20); large drop size; scan rate, 100 mV s^{-1} . Other conditions as in Fig. 1.

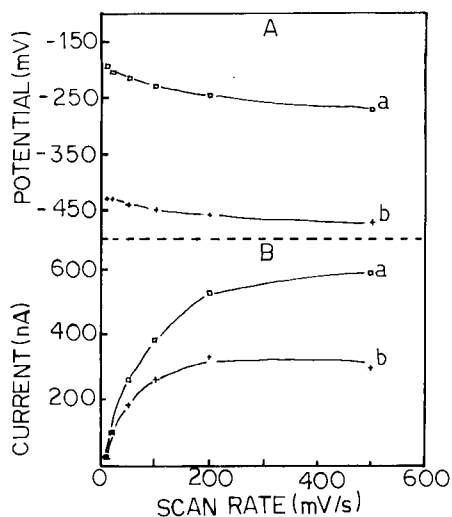


Fig. 5. Dependences of (B) peak current and (A) potential on the scan rate for (b) vanadium-TAC and (a) copper-TAC complexes. Other conditions as in Fig. 1.

potential scan rate on the peak currents (B) and potentials (A) of the vanadium-TAC (b) and copper-TAC (a) complexes. As expected, the complex peak currents depend strongly on the scan rate. The peak current increases with increasing scan rate until it levels off at 200 mV s^{-1} . The peak potential shifted negatively, from -425 to -460 mV for the vanadium-TAC complex and from -200 to -255 mV for the copper-TAC complex, on increasing the scan rate

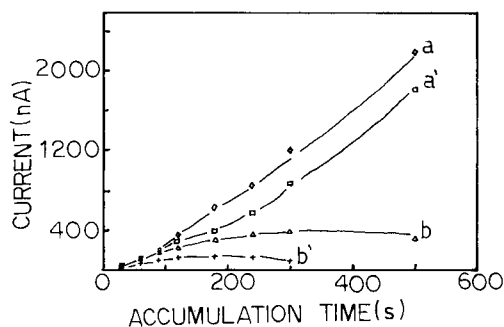


Fig. 6. Effect of accumulation time on the current of the stripping peaks of the vanadium and copper complexes with TAC. Curves a and a' are the resulting currents for solutions containing $20 \mu\text{g l}^{-1}$ of copper and a mixture of $20 \mu\text{g l}^{-1}$ of copper and $10 \mu\text{g l}^{-1}$ of vanadium, respectively. Curves b and b' are the resulting currents for solutions containing $10 \mu\text{g l}^{-1}$ of vanadium and a mixture of $10 \mu\text{g l}^{-1}$ of vanadium and $20 \mu\text{g l}^{-1}$ of copper, respectively. Supporting electrolyte, 0.05 M acetate buffer (pH 4.20) containing $1 \times 10^{-5} \text{ M}$ TAC; scan rate, 100 mV s^{-1} . Other conditions as in Fig. 1.

from 10 to 500 mV s^{-1} . Hence 100 mV s^{-1} was used in all subsequent scans as this rate yields optimum results with respect to both sensitivity and resolution.

A comparison between linear-scan and differential-pulse stripping voltammograms was made. Both stripping modes exhibited significant peak current enhancement compared with direct voltammetric measurements. The low-pass filter and equilibrium times were fixed at 0.1 and 15 s ,

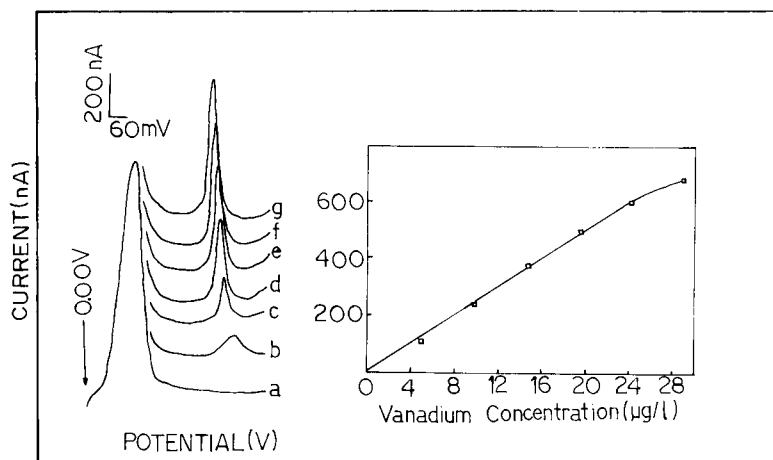


Fig. 7. Stripping voltammograms obtained for solutions of increasing vanadium concentration from 5 to $28 \mu\text{g l}^{-1}$ (b–g). Electrolyte, 0.05 M acetate buffer (pH 4.20) containing $1.0 \times 10^{-5} \text{ M}$ TAC (a); large drop size (area 0.032 cm^2); accumulation time, 60 s . Other conditions as in Fig. 6. Also shown are the resulting calibration graphs.

respectively. The linear scan mode was used throughout this study, however, as it offers greater speed.

Figure 6 shows the dependence of the adsorptive stripping peak currents with varying accumulation times for vanadium–TAC (b) and copper–TAC (a) complexes. The presence of copper in the vanadium–TAC complex (curve b') and of vanadium in the copper–TAC complex (curve a') resulted in lower currents. This effect is even more pronounced with longer accumulation times. Hence, for further quantitative work a relatively short accumulation time (60 s) was generally used.

Quantitative utility

Figure 7 shows voltammograms for solutions of increasing vanadium concentration ($5\text{--}28\ \mu\text{g l}^{-1}$) after 60 s (large drop size) of accumulation. Well defined current stripping peaks were observed over this concentration range. The resulting calibration graphs are also shown in Fig. 7. The stripping peak current increases linearly with increasing concentration. A positive shift in the potential of the peaks was observed on changing the concentration from 5 to $28\ \mu\text{g l}^{-1}$. The ligands TAR, TAM and TAN were also tested to verify the linear relationship between current and vanadium concentration ($5\text{--}25\ \mu\text{g V}^{5+}\ \text{l}^{-1}$). Both TAR and TAN yielded a linear increase in peak current whereas TAM did not. However, TAC remains the ligand of choice owing to its superior sensitivity and resolution, as discussed above.

The sequential determination of vanadium and copper using the ligand TAC was studied over the concentration range $10\text{--}70\ \mu\text{g l}^{-1}$ (the same conditions as described for Fig. 7). The determination of copper is possible in the presence of vanadium ($10\ \mu\text{g l}^{-1}$), but only after masking the copper ($70\ \mu\text{g l}^{-1}$) with 1,2-cyclohexanediaminetetraacetic acid (CDTA) ($2 \times 10^{-6}\ \text{M}$). Both calibrations were observed to be linear up to $40\ \mu\text{g l}^{-1}$ with an accumulation time of 60 s.

The effective preconcentration associated with the adsorption process results in a significantly decrease in the detection limit compared with the corresponding solution measurements. Detection limits of 3.9×10^{-9} and $8.1 \times 10^{-10}\ \text{M}$ for vanadium and copper, respectively, were observed.

The accumulation time used was 5 min for vanadium and 10 min for copper.

The adsorptive stripping response of vanadium and copper in simultaneous measurements are highly reproducible. Eleven successive measurements yielded a relative standard deviation of 1.7% for copper and 3.6% for vanadium. Such behavior is attributed to the reproducibility of the adsorption process and to the use of a new drop of reproducible area in each run.

The major sources of interferences are likely to be co-existing metal ions and organic surfactants. These species could result in either new reduction peaks or overlap with existing peaks of the TAC complex, thus obscuring the measurement. The effect of various ions that could interfere was studied for both complexes. Measurements of $25\ \mu\text{g l}^{-1}$ vanadium and copper were not affected by the addition of up to $2.5\ \text{mg l}^{-1}$ of Br^- , Cl^- , SO_4^{2-} , CN^- , $\text{S}_2\text{O}_3^{2-}$, $\text{B}_4\text{O}_7^{2-}$, CO_3^{2-} , F^- , tartrate, Al^{3+} , Mg^{2+} , Ba^{2+} , Mn^{2+} , Ca^{2+} , Sr^{2+} , La^{2+} , Th^{4+} , UO_2^{2+} , Cd^{2+} , Hg^{2+} , Zn^{2+} , Ag^+ and Pb^{2+} , $0.25\ \text{mg l}^{-1}$ of Cr^{3+} , Mo^{6+} , Ti^{4+} , Fe^{2+} , Fe^{3+} and Ni^{2+} and $25\ \mu\text{g l}^{-1}$ of V^{4+} , Co^{2+} , Nb^{5+} , Bi^{3+} , Sn^{2+} , I^- and WO_4^{2-} . All data were obtained using the same conditions as in Fig. 7.

The suitability of this method for the determination of vanadium in environmental samples was verified. The samples chosen were obtained from the spring Ibirá (São Paulo) as this spring is known to yield water with especially high levels of vanadium. Five successive standard additions to commercially obtained samples of this water resulted in well defined adsorptive stripping peaks. The vanadium peak current in the original sample can thus be quantified based on the resulting standard addition plots. Three consecutive analyses yielded an average value of $96 \pm 3\ \mu\text{g l}^{-1}$, with a 95% confidence limit. This value is similar to results obtained by graphite furnace atomic absorption spectrometry $97 \pm 4\ \mu\text{g l}^{-1}$ with the same confidence limit.

The sequential determination of vanadium and copper is demonstrated on a similar sample of Ibirá water obtained directly from the source. The sample was filtered (Millipore, $0.045\ \mu\text{m}$), acidified (pH 2.3) and stored in a polyethylene



Fig. 8. Sequential determination of copper and vanadium in mineral water (Adhemar de Barros spring, Ibirá, São Paulo) by the standard addition method. Conditions: 5 ml of mineral water + 0.5 ml of 1 M acetate buffer (pH 4.20) containing 0.5×10^{-5} M TAC for A and an additional 0.5×10^{-5} M for B + 4.5 ml of purified water. Accumulation time, 180 s for copper and 30 s for vanadium. Other conditions as in Fig. 7. Standards added for (A) copper = (a) 0, (b) 1.2, (c) 2.5 and (d) $3.7 \mu\text{g Cu}^{2+} \text{ l}^{-1}$ and for (B) vanadium = (a) 0, (b) 4.9, (c) 9.9 and (d) $14.7 \mu\text{g V}^{5+} \text{ l}^{-1}$.

bottle. Figure 8 shows the results of the determination. A linear response was obtained for copper and vanadium (with correlation coefficients of 0.99998 and 0.99967, respectively), by the standard addition method with a preconcentration time of 180 s for copper and 30 s for vanadium. For the initial determination of copper a TAC concentration of 0.5×10^{-5} M was used. Following the determination of copper, more ligand was added to the cell to achieve a final concentration of 1.0×10^{-5} M for the determination of vanadium (owing to the low concentration of copper, the masking agent CDTA was not used). Three consecutive analyses yielded an average value of $55 \pm 6 \mu\text{g l}^{-1}$ for vanadium and $1.7 \pm 0.6 \mu\text{g l}^{-1}$ for copper.

Conclusion

An effective means for the determination of trace levels of vanadium has been described. The use of TAC for adsorptive stripping measurements of vanadium offers an attractive alternative

to catechol and Solochrome Violet RS. It gives similar detection limits but with reduced interferences from several cations and anions and a well defined peak current shape. The sequential determination with copper also offers a great advantage. Further studies involving simultaneous and sequential measurements of trace metals with different ligands are in progress.

Support of this research by SCT/PR and CNPq of the Brazilian Government is gratefully acknowledged.

REFERENCES

- 1 T. Fukasawa, S. Miyata and S. Matsunaga, *Anal. Chim. Acta*, 130 (1981) 353.
- 2 M.J. Fishman and M.W. Skougstad, *Anal. Chem.*, 36 (1964) 1643.
- 3 M. Taminaga, K. Bansho and Y. Umezaki, *Anal. Chim. Acta*, 169 (1985) 171.
- 4 P.B. Barrera, E.B. Gonzalez and A.B. Barrera, *Anal. Chim. Acta*, 236 (1990) 475.
- 5 A. Sugimac, *Anal. Chim. Acta*, 121 (1980) 331.
- 6 P.C. Cole, J.M. Eckert and K.L. Williams, *Anal. Chim. Acta*, 153 (1983) 61.
- 7 R.R. Greenberg and H.M. Kingston, *Anal. Chem.*, 55 (1983) 1160.
- 8 J. Miura, H. Hoshino and T. Yotsuyanagi, *Anal. Chim. Acta*, 233 (1990) 121.
- 9 G. Svehla and G. Tölg, *Talanta*, 23 (1976) 755.
- 10 C.M.G. Van den Berg and Z.Q. Huang, *Anal. Chem.*, 56 (1984) 2383.
- 11 P.A.M. Farias and I. Takase, *Electroanalysis*, in press.
- 12 J. Lu, W. Jin and S. Wang, *Anal. Chim. Acta*, 238 (1990) 375.
- 13 R.G. Petersdorf, R.D. Adams, E. Braunwald, K.J. Isselbacher, J.B. Martin and J.D. Wilson (Eds.), *Harrison's Principles of Internal Medicine*, McGraw-Hill, New York, 1983, pp. 471, 531.
- 14 J. Wang, *Stripping Analysis. Principles, Instrumentation and Applications*, VCH, New York, 1985.
- 15 C.M.G. Van den Berg, *Anal. Lett.*, 17 (1984) 2141.
- 16 C.M.G. Van den Berg, *J. Electroanal. Chem.*, 215 (1986) 111.
- 17 S. Lin and N. Hu, *Beijing Shifan Daxue Xuebao*, 4 (1987) 60; *Chem. Abstr.*, 109 (1988) 47483u.
- 18 F. Quentel and C. Madec, *Anal. Chim. Acta*, 230 (1990) 83.
- 19 P.A.M. Farias and A.K. Ohara, *Electroanalysis*, 3 (1991) 985.
- 20 P.A.M. Farias and A.K. Ohara, *Fresenius' J. Anal. Chem.*, 342 (1992) 87.
- 21 P.A.M. Farias, S.L.C. Ferreira, A.K. Ohara, M.B. Bastos and M.S. Goulart, *Talanta*, 39 (1992) 1245.
- 22 P.A.M. Farias, A.K. Ohara and S.L.C. Ferreira, *Anal. Lett.*, in press.

Determination of 4-nitrobiphenyl by adsorptive stripping square-wave polarography

P. Hernández, F. Galan-Estella and L. Hernández

Departamento de Química Analítica y Análisis Instrumental, Universidad Autónoma de Madrid, 28049 Madrid (Spain)

(Received 29th January 1992; revised manuscript received 16th June 1992)

Abstract

The adsorption conditions on a hanging mercury drop electrode for 4-nitrobiphenyl in aqueous solution with Britton–Robinson buffer was reconsidered. The best adsorption conditions found were pH = 3, an accumulation potential of -10 mV [vs. Ag/AgCl (3 M)] and an accumulation time of 100 s. Under these conditions, an adsorptive stripping square-wave polarographic (SWP) and a differential-pulse polarographic (DPP) procedure for the determination of 4-nitrobiphenyl were developed. These methods gave linear ranges from 0.06 to 0.5 ng ml⁻¹ and determination limits of 80 pg ml⁻¹ for DPP and 120 pg ml⁻¹ for SWP.

Keywords: Polarography; Stripping voltammetry; Nitrobiphenyl

One of the substances recognized by the International Agency for Research on Cancer as potentially carcinogenic is 4-nitrobiphenyl (4-NBP), a substance to which the population is exposed daily as it originates from industrial engines, diesel vehicles and heating systems. It is also present in the work place environment where aluminium electrodes are manufactured according to Joderberg's method.

The carcinogenic potential of 4-NBP is based on its enzymatic reduction to 4-aminobiphenyl (4-ABP), which is a known carcinogen [1]. Therefore, it is necessary to determine the existing levels in the environment, especially in densely populated areas, in the neighbourhood of power stations and in industrial areas.

The levels of 4-NBP existing in the atmosphere are $\mu\text{g ml}^{-1}$ or ng ml^{-1} (ultra-trace levels), hence it is necessary to use highly sensitive techniques

for its determination. The most often utilized technique has been gas chromatography with electron-capture detection (GC-ECD) and mass spectrometry (GC-MS), combined with an initial separation from other composite materials by means of liquid chromatography. Determination by GC-ECD or GC-MS shows detection ranges from 10 to 200 pg m⁻³ [2].

Barek et al. [3] carried out an electrochemical performance study in ethanol–water (1:1) using controlled-potential coulometry and differential-pulse polarography (DPP) of 4-NBP and 4-ABP with a glassy carbon working electrode, and determined 10 $\mu\text{mol l}^{-1}$ by means of d.c. voltammetry and 1 $\mu\text{mol l}^{-1}$ by differential-pulse voltammetry. The same group [4] succeeded in lowering the detection limits to 2×10^{-9} – 10×10^{-9} mmol l⁻¹ using adsorptive stripping pulse voltammetry with accumulation times varying from 3 to 9 min.

To determine 4-NBP concentration levels in rain water, it was tried to reproduce the results obtained by Barek et al., but no reproducible

Correspondence to: L. Hernández, Departamento de Química Analítica y Análisis Instrumental, Universidad Autónoma de Madrid, 28049 Madrid (Spain).

results were obtained with aqueous solutions containing the compounds at concentrations similar to those which they used. For that reason, a new study was carried out considering the adsorption conditions in detail. It was intended to evaluate the different parameters of the adsorption isotherm and at the same time lower the determination limit using adsorptive stripping with square-wave voltammetry (SWV), a technique which gives, theoretically, a four times better sensitivity [5]. To achieve the proposed goals, cyclic voltammetry (CV), DPP and SWV were used.

EXPERIMENTAL

Apparatus and reagents

A Model 384B polarograph (Princeton Applied Research) connected to a PAR 303A polarographic stand with an Ag/AgCl (3 M) reference electrode was used.

A 350 $\mu\text{g ml}^{-1}$ stock standard solution of 4-nitrobiphenyl (Sigma) was prepared. Working standard solutions were obtained by appropriate dilution with water.

The reagents used were of analytical-reagent grade. Throughout the procedure deionized water obtained with a Milli-Q Milli-RO system (Waters) and triply distilled mercury were used.

Procedure

A stream of nitrogen is passed through the polarographic cell containing 4-NBP and the supporting electrolyte for 300 s. After this time, an accumulation step is applied by imposing on the hanging mercury drop electrode (HMDE) a fixed potential, prior to the reduction of the mixture, for fixed period, keeping the solution stirred at 500 rpm.

Thereafter, stirring is stopped, maintaining the accumulation potential for 5 s, followed by the measuring stage using CV, SWV and DPP.

RESULTS AND DISCUSSION

The 4-NBP adsorption is clearly illustrated by making reduction measurements with and with-

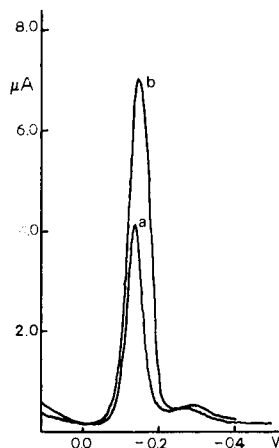


Fig. 1. Differential-pulse polarograms of 0.70 $\mu\text{g ml}^{-1}$ 4-NBP with $E_{ac} = 10$ mV, (a) without accumulation and (b) with an accumulation period of 30 s.

out accumulation (Fig. 1). The occurrence of adsorption is verified by the electrocapillary curve obtained in Britton–Robinson buffer. A clear adsorption is observed for potentials between +10 and -50 mV, which can be attributed to the interaction between the NO_2 group and mercury or through one of the negatively charged mesomeric species in the 4-NBP equilibrium (Fig. 2).

In order to improve the accumulation conditions, the effect of the medium and accumulation potential (E_{ac}) were studied at a fixed accumulation time of 30 s, varying E_{ac} and the pH.

The instrumental variables were as follows. In CV a scan rate of 100 mV s^{-1} was used, whereas in SWV a frequency of 50 Hz and a staircase step height of 2 mV, which gives a scan rate of 100 mV s^{-1} and a pulse amplitude (ΔE) of 50 mV, were employed. In DPP an identical amplitude was used and a scan rate of 10 mV s^{-1} was adopted.

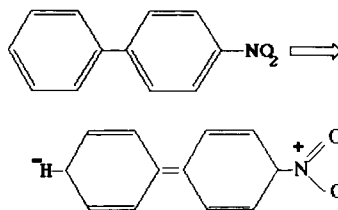


Fig. 2. Mesomeric forms of 4-NBP.

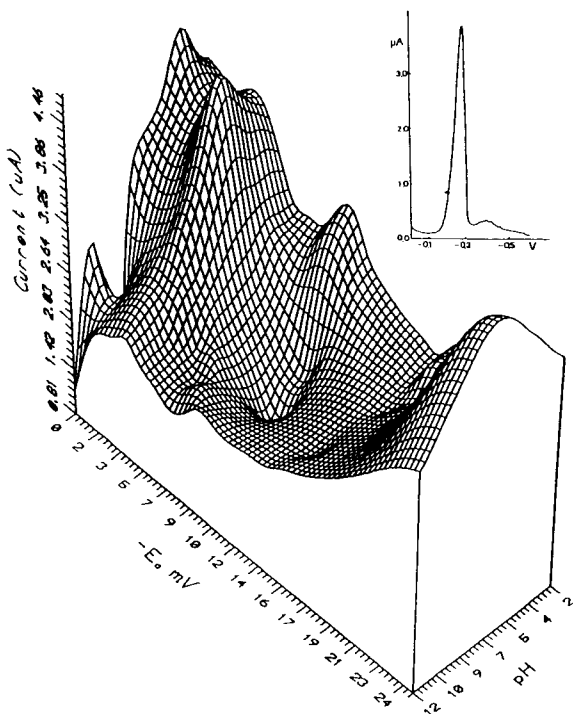


Fig. 3. Variation of I_p in SWV with pH and accumulation potential ($t_{ac} = 30$ s) and response voltammogram after accumulation under better conditions. 4-NBP concentration = $0.70 \mu\text{g ml}^{-1}$.

4-NBP solutions of $0.7 \mu\text{g ml}^{-1}$ in 0.04 M Britton–Robinson buffer in aqueous medium with variation of the pH using sodium hydroxide gave the results presented in Fig. 3. The results coincide for the three techniques. The highest I_p was obtained for E_{ac} between -5 and -15 mV in solutions of pH 3. The value of the accumulation potential is in agreement with the electrocapillary curve results.

By plotting the values obtained for the peak potential (E_p) versus pH, a linear relationship (Fig. 4) with a slope of 47 mV per pH unit was obtained for all three techniques; this value is far away from the theoretical value, assuming that in the reduction of the NO_2 group 4 H^+ and 4 e^- are involved, leading to the production of $-\text{NHOH}$ groups. This deviation may be due to the total irreversibility of the electron transfer process. This is clearly shown in the cyclic voltam-

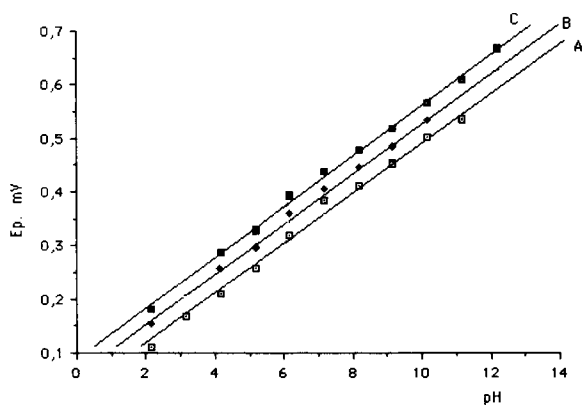


Fig. 4. Influence of pH on E_p . (A) DPP; (B) SWV; (C) CV.

mograms obtained, where a high cathodic peak but no anodic peak is observed (Fig. 5).

Using the best conditions for maximum I_p (pH = 3, $E_{ac} = -10 \text{ mV}$ and accumulation time = 30 s) and fixing the other instrumental parameters, in CV the scanning rate and in SWV the frequency were changed. A linear relationship was found between I_p and the scanning rate and frequency, whereas a logarithmic relationship between E_p and the same parameters was observed: $I_{p \text{ CV}} (\mu\text{A}) = 0.536 + 0.02 v (\text{mV s}^{-1})$ ($r = 0.999$); $I_{p \text{ SWV}} (\mu\text{A}) = 0.166 + 0.100 X(\text{Hz})$ ($r = 0.998$);

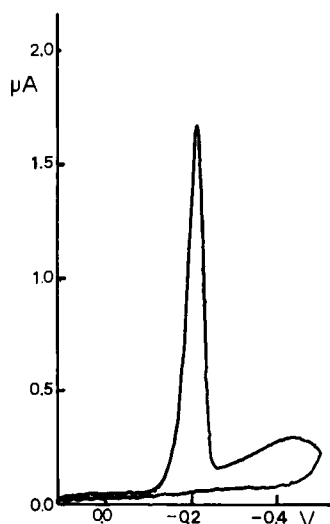


Fig. 5. Cyclic voltammogram of $0.70 \mu\text{g ml}^{-1}$ 4-NBP. For other conditions, see text.

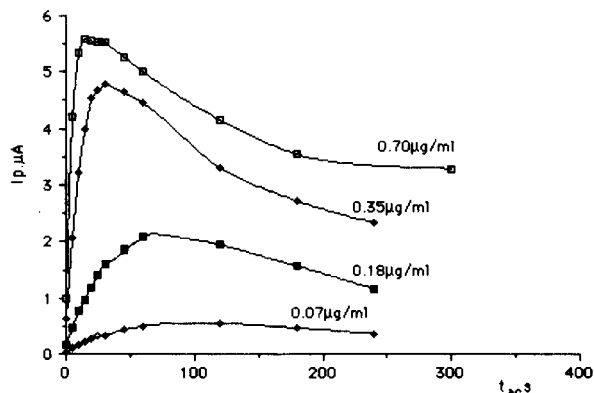


Fig. 6. Dependence of current on accumulation time at different concentrations.

$E_{p,CV}$ (V) = $0.157 + 0.051 \log v$ ($mV s^{-1}$) ($r = 0.997$); and $E_{p,SWV}$ (V) = $0.130 + 0.061 \log X$ (Hz) ($r = 0.999$). This behaviour was also found by other workers [6] for compounds containing a benzodiazepine electroactive group (midazolam). They concluded that the electrochemical process is produced by adsorption controlled by diffusion.

In order to confirm this hypothesis, a study was made keeping all the parameters constant and changing only the concentration and accumulation time (Fig. 6). It appears that for concentrations between 0.70 and $0.18 \mu g ml^{-1}$, the accumulation process is very rapid, reaching a maximum I_p and followed by a decrease with time. For concentrations below $0.07 \mu g ml^{-1}$, I_p remains constant after 100 s.

A detailed analysis of the experimental I_p versus $ct_{ac}^{1/2}$ curves (Fig. 7) shows an apparent maximum. The ascending and descending parts can be considered to be linear, and are represented by the equations

$$y = 0.0061x - 0.004; r = 0.981 \quad (0.7 \mu g ml^{-1})$$

$$y = 0.027x + 0.016; r = 0.976 \quad (0.35 \mu g ml^{-1})$$

$$y = 0.082x + 0.568; r = 0.988 \quad (0.07 \mu g ml^{-1})$$

for the ascending portion and

$$y = 0.012x + 0.311; r = 0.958 \quad (0.7 \mu g ml^{-1})$$

$$y = 0.027x + 6.45; r = 0.989 \quad (0.35 \mu g ml^{-1})$$

for the descending portions for the levels of concentration represented. The values close to the I_p maximum correspond to the saturation zone. In this situation no reliable results are obtained which would allow a precise evaluation of the surface coverage (Γ) and diffusion coefficient (D). However, a possible adsorption mechanism can be proposed together with the results obtained in SWV (variations of I_p and E_p with frequency).

The molecule reaches the vicinity of the electrode by diffusion and is adsorbed on its surface according to a Langmuir isotherm. Once saturation has been reached, desorption of the 4-BNP on the electrode may occur. This mechanism can explain the experimentally observed behaviour of the variation of I_p with t_{ac} .

The use of other supporting electrolytes at pH 3 (phosphate and acetate buffers) does not improve the results obtained when using the Britton–Robinson buffer.

The variations of the instrumental variables which are inherent to each technique suggest the following modifications to be made with respect to I_p and in E_p in the nitrobiphenyl voltammetric waves previously adsorbed on the mercury electrode: when the pulse amplitude is modified a linear increase in I_p up to 80 mV in DPP and up to 50 mV in SWV is produced; and when the scan rate is modified in DPP a linear increase in I_p up to 60 $mV s^{-1}$ is produced. There is no change in the I_p value when the scan rate is raised further.

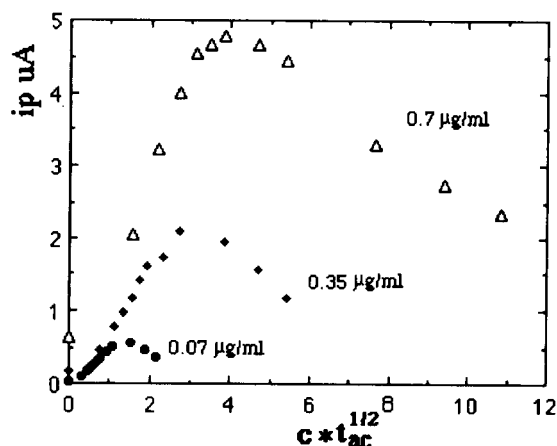


Fig. 7. Variation of I_p in SWV with $ct_{ac}^{-1/2}$.

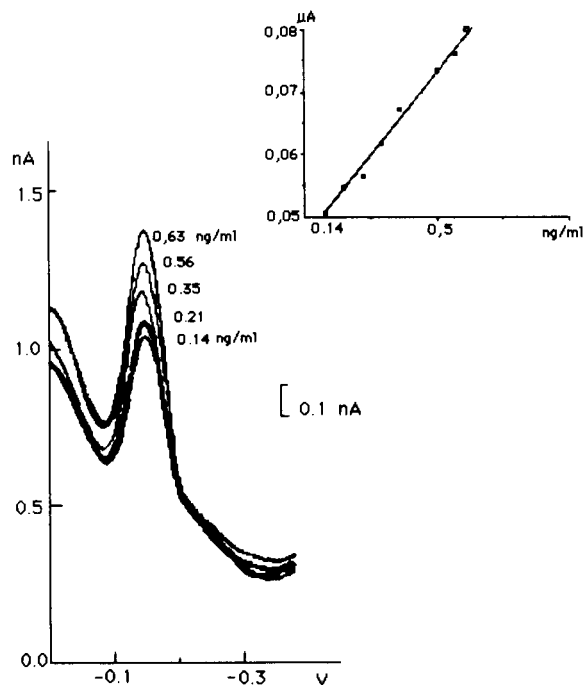


Fig. 8. Calibration graph for different concentrations of 4-NBP using the DPP conditions described in the text.

In SWV, as already noted, there is a linear relationship between I_p and frequency (Table 1). A stepwise increment of the square wave produces a notable increase in the peak half-width.

Using the optimum conditions obtained for the different methodological and instrumental variables for the accumulation of 4-NBP and subsequent reduction, a study was made of the relationship between I_p and concentration (Fig. 8). There is a linear response of these parameters between 0.06 and 0.5 ng ml⁻¹. The straight lines are represented by the following equations:

$$y(\mu A) = 0.3 + 0.286x \text{ (ng ml}^{-1}\text{)}; r = 0.997$$

in SWV and

$$y(\mu A) = 0.046 + 0.55x \text{ (ng ml}^{-1}\text{)}; r = 0.998$$

in DPP.

The method has a relative error of 4.5% and a relative standard deviation of 7.0% based on ten different solutions of each of the concentrations 0.1, 0.3 and 0.8 ng ml⁻¹ and with five independent measurements on each solution. The determination limits were 80 pg ml⁻¹ in DPP and 120 pg ml⁻¹ in SWV, corresponding to 10 σ (σ being the relative standard deviation of the background noise).

The method was applied to the determination of 4-NBP in rain water in an area located near Madrid, where a possible emission source of gas-oil engine combustion is present. A 500-ml sample of rain water was used. A single 50-ml extract with diethyl ether was concentrated to 5 ml by evaporating the solvent and the analysis was performed using gas chromatographic methods with electron-capture, flame ionization and MS detection. No 4-NBP was detected, but by means of the electrochemical method it could be detected although the signal is below the determination limit (currents are ca. 8 nA). Its presence was also confirmed by the standard addition method.

The authors thank Cristina Martín Dominguez for her contribution to the experimental work and the DGICYT for financial support of the project (grant PB-89-152).

REFERENCES

- 1 Suspected Carcinogens. A Subfile of the NIOSH Toxic Substances List. US DHEW Publication No. (NIOSH) 75-188, Rockville, MD, 1975.
- 2 M. Ochme, S. Mano and S. Stray, *J. High Resolut. Chromatogr. Chromatogr. Commun.*, 5 (1982) 418.
- 3 J. Barek, A. Derk, M. Müller and J. Zima, *Collect. Czech. Chem. Commun.*, 50 (1985) 2853.
- 4 J. Barek, G. Malic and J. Zima, *Collect. Czech. Chem. Commun.*, 55 (1990) 2904.
- 5 J. Osteryoung and J. O'Dea, in A.J. Bard (Ed.), *Electroanalytical Chemistry*, Vol. 14, Square-Wave Voltammetry, Marcel Dekker, New York, 1986, p. 209.
- 6 A.J. Ribes and J. Osteryoung, *Anal. Chem.*, 23 (1990) 2632.

Zeptomole detection limit for alkaline phosphatase using 4-aminophenylphosphate, amperometric detection, and an optimal buffer system

Robert Q. Thompson, Margaret Porter and Cameron Stuver

Chemistry Department, Oberlin College, Oberlin, OH 44074 (USA)

H. Brian Halsall and William R. Heineman

Biomedical Chemistry Research Center and Department of Chemistry, University of Cincinnati, Cincinnati, OH 45221 (USA)

Eileen Buckley and Malcolm R. Smyth

Dublin City University, Dublin 9 (Ireland)

(Received 31st July 1992; revised manuscript received 2nd September 1992)

Abstract

Trace detection of bovine alkaline phosphatase was studied using the substrate, 4-aminophenylphosphate, and amperometric detection of the product, 4-aminophenol. Six aminoethanol buffers were compared with respect to their abilities to stabilize the product and to promote enzyme activity. In ethanolamine and 2-(methylamino)ethanol buffers, progress curves were linear from zero time to at least 60 min, while progress curves in the other buffers became non-linear in a short time due to product decomposition. The highest reaction rate at pH 10.0 was found in the 2-(methylamino)ethanol buffer, while the highest pseudo-rate constant, V_{\max}/K_m , was found in tris(hydroxymethyl)aminomethane. Higher buffer concentration and the addition of magnesium ion enhanced enzyme activity, while the addition of zinc ion decreased enzyme activity.

In 1.0 F, pH 10.0, 2-(methylamino)ethanol buffer and in the presence of $1 \text{ mg ml}^{-1} \text{ MgCl}_2$, the detection limit for aqueous mouse IgG-alkaline phosphatase conjugate was 25 amol ml^{-1} or 500 zeptomoles (10^{-21} mol). The reaction time was 60 min. Under similar conditions, the detection limit for IgG-alkaline phosphatase adsorbed onto a microtiter plate was 4 attomoles.

Keywords: Amperometry; Cyclic voltammetry; Immunoassay; Alkaline phosphatase; Aminoethanol buffers; Detection limit

Immunoassay has become a standard analytical technique over the past decade with ever-decreasing detection limits, and alkaline phosphatase is widely used as an enzyme label in such assays [1]. We have advocated the use of the

substrate, 4-aminophenylphosphate, and amperometric measurement of bovine alkaline phosphatase activity for assays that require the lowest detection limits [2,3]. Although there has been increasing interest in 4-aminophenylphosphate since 1988 when it was first used in electrochemical immunoassay [4], no comprehensive study of this enzyme-substrate-product system has been

Correspondence to: R.Q. Thompson, Chemistry Department, Oberlin College, Oberlin, OH 44074 (USA).

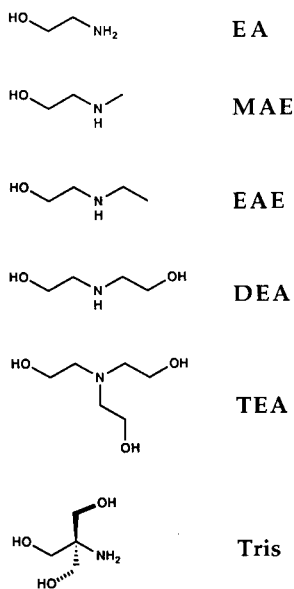


Fig. 1. Structure and abbreviation of each of the buffers used in this study.

reported. In order to attain the highest sensitivity for enzyme immunoassay, the effects of buffer type, pH, buffer concentration, and additives on the activity of alkaline phosphatase and on the detection of the product, 4-aminophenol, were examined. Six buffers were chosen for study: ethanolamine, diethanolamine, 2-(methylamino)ethanol, 2-(ethylamino)ethanol, triethanolamine, and tris(hydroxymethyl)aminomethane. These aminoalcohol buffers were chosen because of their related structures (Fig. 1) and because previously they had been found to promote transphosphorylation of the substrate, 4-nitrophenylphosphate [4]. The buffers were prepared as 0.010–1.0 F solutions and then adjusted to pH 8.0, 9.0, or 10.0, since bovine alkaline phosphatase is most efficient at high pH [4]. The product of the enzyme reaction, 4-aminophenol, is somewhat unstable in aqueous solution, so the effect of buffer on product stability and detector sensitivity was examined. The effects of buffer and added magnesium and zinc ions on the enzyme–substrate reaction progress curves and the enzyme kinetics constants were also studied. Detection limits for an antibody–alkaline phosphatase conjugate in solution and adsorbed on a

microtiter plate were determined in the optimal reaction/detection system.

EXPERIMENTAL

Materials

All chemicals were used without further purification or drying. Alkaline phosphatase from calf intestine was purchased from Boehringer (Mannheim) (No. 567744) as a 10 mg ml⁻¹ solution in triethanolamine buffer, containing 1 mM ZnCl₂ and 0.1 mM MgCl₂. Mouse IgG conjugated to alkaline phosphatase was obtained from Jackson ImmunoResearch (No. 015-050-003) as a 600 μg ml⁻¹ solution. The protein stock solutions were diluted with an aqueous solution, containing 1 g l⁻¹ bovine serum albumin, 1 g l⁻¹ NaCl, and 0.1 g l⁻¹ NaN₃, which acted as a stabilizer and prevented enzyme adsorption to the glass vessels. Microtiter plates from Corning (Easy Wash ELISA plates) were used in the detection limit studies.

Ethanolamine (EA), 2-(methylamino)ethanol (MAE), 2-(ethylamino)ethanol (EAE), diethanolamine (DEA), triethanolamine hydrochloride (TEA), and tris(hydroxymethyl)aminomethane (Tris), all of 99% purity or better, were purchased from Aldrich. All buffers contained 1 mg ml⁻¹ of MgCl₂, an enzyme activator. The MgCl₂ solid was added to the buffer when the pH was less than 10.5 to prevent formation of insoluble Mg(OH)₂. The hydrochloride salt of 4-aminophenol was obtained from Sigma, and the 4-aminophenylphosphate was synthesized from 4-nitrophenylphosphate by hydrogenation [2]. Air-saturated, distilled, deionized water was used to prepare all solutions; the oxygen concentration was not measured.

Flow injection system

A syringe pump (Model 22, Harvard Apparatus) set at 0.50 ml min⁻¹ was used to dispense the carrier solution (buffer), and a peristaltic pump (Model IP-12, Ismatec/Brinkmann) set at 0.40 ml min⁻¹ pulled the samples through the injection valve. The 20-μl slider valve (Chemintert/Milton Roy) was pneumatically actuated and

controlled with a personal computer (Macintosh SE, Apple Computer) equipped with an input/output board (Model ACSE-12, Strawberry Tree Computers). The valve and detector were connected by a 25 cm \times 0.5 mm i.d. PTFE tube. The amperometric detector consisted of a three-electrode 4- μ l flow cell (Bioanalytical Systems; glassy carbon working electrode, Ag/AgCl reference electrode) and a potentiostat (Model LC-3A, Bioanalytical Systems). The signal from the detector was sampled by the computer at 10 Hz with 12-bit resolution, and peak heights were computed automatically from these data.

Cyclic voltammetry

Cyclic voltammograms were obtained on a computer-controlled electrochemical analyzer (Cypress Systems, Model CYSY-1). The scan range was -400 mV to 1200 mV vs. Ag/AgCl, and the scan rate was 100 mV s $^{-1}$. The working electrode was a glassy carbon electrode with a surface area of ca. 0.07 cm 2 .

RESULTS AND DISCUSSION

Electrochemical properties of the buffers, substrate, and product

Cyclic voltammograms of the six buffers at pH 8.0, 9.0, and 10.0 were obtained. The oxidation limit was defined as that applied potential that gave an oxidation current significantly different from baseline (ca. 5 μ A), and these potentials at pH 10.0 are given in Table 1. The oxidation limits increased as the buffering agent changed from tertiary to secondary to primary amine, and within

those designations the limits increased with increasing number of electron-withdrawing groups in the molecule. In other words, Tris, a primary amine with 3 electron-withdrawing groups, had the highest oxidation limit, and TEA, a tertiary amine, had the lowest limit. The limits increased with decreasing pH; the reaction becomes less favorable at lower pH because the oxidation half-reaction has protons as product. The α_0 values (Table 1), the fraction of buffer that had a free (oxidizable) amine group, at pH 10.0 ranged from 0.52 to 0.99.

The substrate, 4-aminophenylphosphate, gave a similar voltammogram in all buffers. The oxidation limit ranged from $+0.35$ V to $+0.50$ V without observable trends. The substrate showed good stability in all buffers as well.

Hydrodynamic voltammograms of the product, 4-aminophenol, were generated over the applied voltage range, -0.10 to $+0.60$ V, in 0.10 V increments. The optimal potential was chosen as the lowest potential that gave a peak height within 90% of the highest recorded peak height in that voltammogram. The optimal values ranged from $+0.20$ V to $+0.50$ V, and two trends were evident. First, as the pH increased the optimal potential fell. Because the oxidation half-reaction has two protons as product, the reaction becomes more favorable at higher pH. Second, the optimal potential increased slightly as the buffering agent changed from primary to secondary to tertiary amine. Perhaps this has something to do with the buffering capacity or the product stability (see below). In any case, an applied potential of $+0.30$ V was chosen for all subsequent studies in order to avoid substrate oxidation current and because

TABLE 1

Oxidation limits, pK_a values, and α_0 values for the buffers at pH 10.0

	Buffer					
	TEA	EAE	MAE	DEA	EA	Tris
Oxidation limit (mV)	600	700	800	850	910	1100
pK_a^a	7.762	9.961	9.88	8.883	9.498	8.073
α_0^b	0.99	0.52	0.57	0.93	0.76	0.98

^a The pK_a values are those at zero ionic strength obtained from Martell and Smith [7]. ^b $\alpha_0 = [R-NH_2]/([R-NH_2] + [R-NH_3^+]) = K_a/([H^+] + K_a)$.

this is close to the optimal product potential for all the buffers. This value also was used in our previous study [2].

Detector sensitivity toward 4-aminophenol

Buffered solutions (0.10 F buffer) of 4-aminophenol were injected into the flow system and the resulting peak heights were measured. The concentration of the phenol ranged from 0.050 μM to 3.0 μM , and the solutions were injected within 5 min to avoid any decomposition. Detector sensitivity was defined as the slope of the calibration line (in $\text{nA } \mu\text{M}^{-1}$). The average sensitivity was 55 $\text{nA } \mu\text{M}^{-1}$ with a range of 43–65 $\text{nA } \mu\text{M}^{-1}$. No clear trend with pH from 7.0 to 10.0 or with buffer type was found. A recent report confirms our pH study [6]. A slight decrease in sensitivity toward 4-aminophenol was found when the buffer concentration was increased. The response with 1.0 F MAE, pH 10.0 buffer was 75% of the response with 0.10 F MAE, pH 10.0 buffer.

Stability of 4-aminophenol

The product, 4-aminophenol, rapidly converts to quinone in aqueous solution, especially at basic pH [1,2]. Therefore, stock solutions of the phenol were prepared in slightly acidic deionized water, dilutions were made in buffer, and the solutions were used immediately. The effect of buffering agent on product stability was studied in 0.10 F, pH 10.0 buffer, since at this pH the product should be most unstable and be most affected by buffer composition. A solution of 5 μM 4-aminophenol was injected into the flow system every 2 min, and the resulting peak current values were measured and plotted versus time (Fig. 2a). At pH 10.0, three distinct buffer types were evident. Type A buffers, MAE and EA, inhibited decomposition of the product. In type B buffers, EAE and DEA, the phenol rapidly decomposed, while in type C buffers, Tris and TEA, the decomposition was even more rapid.

Product stabilization is most likely due to a combination of processes that limit the reaction of oxygen with the product. The buffers could react with dissolved oxygen. If this were the case, then a buffer of low oxidation potential and large

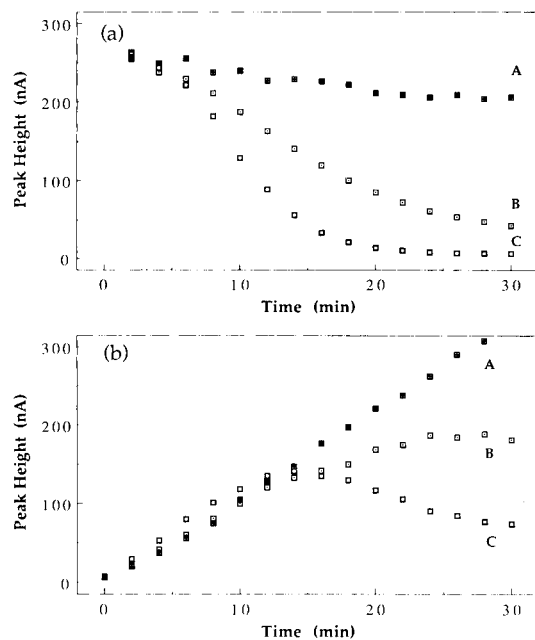


Fig. 2. (a) Stability curves for 5.0 μM 4-aminophenol in the three types of buffers at pH 10.0. (b) Progress curves for the hydrolysis of 0.50 mM 4-aminophenylphosphate catalyzed by alkaline phosphatase in the three types of buffers at pH 10.0. Each point represents the average value of peak height at the specified time for the two buffers of the same type. (A) MAE and EA; (B) EAE and DEA; (C) Tris and TEA.

fraction of free amine should be most stabilizing. Looking at Table 1, it makes some sense that Tris was not very good at stabilizing 4-aminophenol since it has a very high oxidation potential. By this reasoning, however, TEA (low oxidation limit, high α_0) should have been the most stabilizing, but instead it was the worst. The buffers could also prevent decomposition of 4-aminophenol via hydrogen bonding between the electronegative oxygen atom of the phenol and a hydrogen atom of the buffer's amine group. The higher the $\text{p}K_a$ of the buffer and the greater fraction of the amine in protonated form (lower α_0), the stronger would be the hydrogen bonding and the greater would be the stability of the complex. In general, this is what was found (see Table 1). Tertiary and secondary amines, except MAE, may have been too bulky to form stable complexes. This would explain why EAE was a poorer stabilizing buffer than MAE, even though its oxidation potential

was lower and its pK_a was higher. Product stability increased as the buffer concentration was raised, supporting both explanations. In any case, MAE and EA stabilized 4-aminophenol best at pH 10.0.

It is thought that the first step in the decomposition is loss of hydrogen ion from the phenol group. Thus, the stability at pH 9.0 should be much better than at pH 10.0 since the fraction of phenolate ion at pH 9.0 is low. This was the case; even in TEA buffer more than half of the phenol remained after 30 min. The ordering of buffers on the basis of product stability was less clear. MAE, EA, and DEA gave the best stability at pH 9.0, followed closely by the others.

Progress curves for the enzyme-catalyzed hydrolysis of 4-aminophenylphosphate

The substrate, 4-aminophenylphosphate, and 0.10 F, pH 10.0 buffer were mixed in the presence of alkaline phosphatase, and this reaction mixture was injected into the flow system at 2-min intervals. Peak heights were recorded and plotted versus time (Fig. 2b). The buffers fell into the same three groups as before. Type A buffers, MAE and EA, showed linear progress curves past 30 min (out to at least 60 min). Type B buffers, EAE and DEA, gave linear curves for about 15 min, and then the curves reached a constant value at about 20 min. Type C buffers, Tris and TEA, produced linear curves for less than 15 min, and then the product concentration actually decreased with time. These progress curves dramatically display the competition between production of the 4-aminophenol and decomposition

of the phenol in air-saturated buffer, and they correspond exactly with the stability of the phenol as shown in Fig. 2a. Consequently, if longer enzyme-catalyzed hydrolysis reaction times are required to gain higher assay sensitivity, then at pH 10.0 MAE or EA buffer should be chosen. At pH 9.0, MAE or EA was still the best choice, but the choice was not nearly so clear. As reported elsewhere, 0.10 F, pH 9.0 Tris buffer yielded progress curves which were linear to 20 min [2]. Higher buffer concentration also improved the stability of 4-aminophenol and, thereby, lengthened the linear portion of the progress curves. For example, in 1.0 F Tris buffer the signal versus time plot was linear for nearly 30 min, before leveling off and then beginning a slow decline after 50 min.

Kinetics values for alkaline phosphatase

A volume of 100 μl of 40 ng ml^{-1} alkaline phosphatase (AP) was added to 10 ml of a buffered solution containing 4-aminophenylphosphate at time zero. The amount of 4-aminophenol produced between 2 and 10 min was measured amperometrically and was taken to be proportional to the rate of the enzyme-catalyzed reaction. Reaction rates were obtained for substrate concentrations in the range 5–5000 μM , for all buffers at pH 9.0 and 10.0. The data were fit to single-substrate, Michaelis–Menten kinetics by non-linear regression, and the apparent kinetics constants, V_{max} and K_m , were computed (Table 2). The values may be slightly in error because of product decomposition; the data have been left uncorrected since the decomposition reaction and

TABLE 2

Kinetics constants for 4-aminophenylphosphate in 0.10 F buffers ^a

	Buffer					
	Tris	DEA	EAE	EA	TEA	MAE
K_m (μM) at pH 10	260	590	570	400	310	630
V_{max} (nA min^{-1})	17	20	21	20	16	25
V_{max}/K_m	0.07	0.03	0.04	0.05	0.05	0.04
K_m (μM) at pH 9	27	26	24	35	23	45
V_{max} (nA min^{-1})	11	10	8	7	4	7
V_{max}/K_m	0.41	0.38	0.33	0.20	0.17	0.16

^a All values have an uncertainty of $\pm 10\%$.

its rate law are not fully known. At pH 10.0 the MAE buffer stands out with the highest V_{\max} and K_m , while Tris provides the largest pseudo-rate constant, V_{\max}/K_m .

An enzyme is most efficient when it operates at a high rate in the presence of little substrate, i.e. when V_{\max}/K_m is maximal. Tris buffer, of all the buffers tested, provided the most ideal conditions for bovine alkaline phosphatase at both pH 9.0 and 10.0, although the rate constant was much higher at pH 9.0. For studies of this enzyme involving short incubation times Tris buffer may be preferred. The MAE buffer was the worst at supporting enzyme efficiency, but for highest sensitivity in immunoassay saturating substrate conditions and long incubation times are employed. In this case, MAE buffer would be the best choice since it provided the highest V_{\max} . The enzyme-saturating substrate concentration in 0.10 F, pH 10.0 MAE buffer would be ca. 6 mM, which is not too wasteful of substrate. At pH 9.0 reaction rates and K_m values were lower in all the buffers. For MAE the maximal rate was 3 times higher at pH 10.0 compared to pH 9.0. Also, the pK_a value of MAE is closer to 10 than 9 (Table 1), so the buffering is better.

The effects of buffer concentration and added metals on the kinetics constants in pH 10.0, MAE buffer were studied. Buffer concentration was varied from 0.010 to 1.0 F. The kinetics constants increased enormously with increased buffer concentration (Table 3). This makes sense since these buffers are good phosphate acceptors and facilitate the transphosphorylation reaction, and a larger concentration of acceptor would increase the reaction rate. For the highest reaction rate

one should use a large buffer concentration, but the price is increased reagent use, since one would need a ca. 80 mM substrate solution with 1.0 F, pH 10.0 MAE buffer to obtain the maximal rate.

Alkaline phosphatase contains two essential metals, magnesium and zinc. Addition of magnesium ion to the reaction mixture was found to be essential for optimal activity. A concentration of 1 mg $MgCl_2$ per ml of buffer is ideal. In contrast, the addition of zinc ion to the reaction mixture reduced the rate of hydrolysis of 4-aminophenylphosphate. Even as little as 3 μg $ZnCl_2$ per ml of buffer reduced the maximal velocity by a factor of 5, and increased zinc concentration reduced further both the V_{\max} and K_m values. This effect was also noted for the more commonly used substrate, 4-nitrophenylphosphate, in opposition to other reports [5].

Detection limits for aqueous IgG-alkaline phosphatase

To see how little enzyme label could be detected in solution, $pg\ ml^{-1}$ solutions ($20\text{--}480\ amol\ ml^{-1}$) of mouse IgG-alkaline phosphatase conjugate were prepared and tested with the optimized buffer system. The conditions were 1.0 F, pH 10.0 MAE buffer containing 1 mg ml^{-1} $MgCl_2$, 10 mM 4-aminophenylphosphate in the MAE buffer, IgG-alkaline phosphatase solutions in the MAE buffer, and a 60-min reaction time. A volume of 20 μl of each enzyme solution was mixed with 80 μl of the substrate solution in a separate well of a microtiter plate. After an hour, each solution was aspirated and injected into the flow injection/ampereometric system. The 20 points were plotted as nA versus $amol\ ml^{-1}$, and the calibration line was: peak height in nA = $(48 \pm 3)\ nA + (1.26 \pm 0.02)\ nA\ ml\ amol^{-1}$ [IgG], with a standard error of 10.7 nA and a correlation coefficient of 0.997. Taking the detection limit to be the concentration that gives a signal three times the standard error plus the y-intercept, the calculated detection limit was 25 $amol\ ml^{-1}$ (7.5 $pg\ ml^{-1}$) or 500 zeptomoles (10^{-21} mol) of IgG-alkaline phosphatase. This converts to 300 000 molecules. Other trials gave detection limits ranging from 300 to 1000 zeptomoles.

TABLE 3

Kinetics constants for 4-aminophenylphosphate in pH 10.0 MAE buffer ^a

	Buffer concentration (F)			
	0.010	0.10	0.50	1.0
K_m (μM)	210	630	1900	7600
V_{\max} ($nA\ min^{-1}$)	11	25	45	61
V_{\max}/K_m	0.05	0.04	0.02	0.008

^a All values have an uncertainty of $\pm 10\%$.

The concentration of substrate in the reaction mixture, 8 mM, was just slightly larger than the K_m value for the enzyme, so a larger concentration might be warranted. At a substrate concentration of 24 mM the reaction rates were higher, as predicted, but the detection limit was approximately the same (750 zeptomoles) due to the larger blank signal (ca. 200 nA) and slightly more uncertainty. The use of 3 mM substrate yielded significantly higher detection limits. Eight millimolar is a good compromise between assay sensitivity and reagent cost. Likewise, 60 min is a reasonable amount of time for the reaction. Other reagent volumes were tried, including 1 ml substrate per 100 μ l enzyme, 250 μ l substrate per 25 μ l enzyme, and 50 μ l substrate per 5 μ l enzyme. The two larger volume pairs gave approximately equal concentration detection limits (20 amol ml⁻¹), and the smaller two volume pairs gave approximately equal mass detection limits (500 zeptomoles). The choice of 80 μ l substrate per 20 μ l enzyme in the final assay procedure was ultimately a matter of convenience.

Detection limits for adsorbed IgG–alkaline phosphatase

In a sandwich immunoassay the final step would be addition of labeled antibody. To simulate this, 50 μ l of IgG–alkaline phosphatase in acetate buffer (10⁻⁴ F, pH 5.2, 0.05% NaN₃, 0.05% Tween-20) were allowed to stand in a well of the microtiter plate for 15 h. The antibody solution was then aspirated from the well and 150 μ l of the acetate buffer were added. After several minutes the buffer was removed by aspiration. Finally, 60 μ l of 10 mM 4-aminophenylphosphate in 1.0 F, pH 10.0 MAE buffer were added, and

the reaction was allowed to proceed for 60 min. Twenty IgG–alkaline phosphatase standards in the range 20–480 amol ml⁻¹ were tested, giving the regression line: peak height in nA = (58 ± 3) nA + (0.29 ± 0.02) nA ml amol⁻¹ [IgG], with a standard error of 7.5 nA and a correlation coefficient of 0.975. The detection limit was 80 amol ml⁻¹ or 4 attomoles. Other trials gave limits between 2 and 6 attomoles. From these studies it is apparent that the optimal buffer system should provide detection limits in the low attomole range, if not lower, for complete immunoassays and other biochemical tests employing alkaline phosphatase.

Some of the instrumentation was obtained through a grant to R.Q.T from the American Chemical Society Petroleum Research Fund (Grant No. 20262-B7). Support also came from the Howard Hughes Medical Institute under a grant to Oberlin College and from the National Science Foundation under Grant No. CHE-8217045 to the University of Cincinnati.

REFERENCES

- 1 J.P. Gosling, Clin. Chem., 36 (1990) 1408.
- 2 Y. Xu, H.B. Halsall and W.R. Heineman, J. Pharm. Biomed. Anal., 7 (1989) 1301.
- 3 R.Q. Thompson, G.C. Barone, H.B. Halsall and W.R. Heineman, Anal. Biochem., 192 (1991) 90.
- 4 H.T. Tang, C.E. Lunte, H.B. Halsall and W.R. Heineman, Anal. Chim. Acta, 214 (1988) 187.
- 5 R.B. McComb, G.N. Bowers and S. Posen, Alkaline Phosphatase, Plenum Press, New York, 1979.
- 6 I.M. Christie, P.H. Treloar, Z.B. Koochaki, P.M. Vadgama and G.N. Smith, Anal. Chim. Acta, 257 (1992) 21.
- 7 A.E. Martell and R.M. Smith, Critical Stability Constants, Plenum Press, New York, 1974.

Determination of L-glutamate and L-glutamine by flow-injection analysis and chemiluminescence detection: comparison of an enzyme column and enzyme membrane sensor

Gert Blankenstein

Institute of Enzyme Technology, Heinrich Heine University Düsseldorf, P.O. Box 20 50, D(W)-5170 Jülich (Germany)

Frank Preuschoff, Uwe Spohn and Karl-Heinz Mohr

Institut für Biotechnologie 2, Martin-Luther-Universität Halle-Wittenberg, Weinbergweg 16a, D(O)-4020 Halle (Saale) (Germany)

Maria-Regina Kula

Institute of Enzyme Technology, Heinrich Heine University Düsseldorf, P.O. Box 20 50, D(W)-5170 Jülich (Germany)

(Received 7th July 1992)

Abstract

Glutamate and glutamine were determined by luminol chemiluminescence with flow-injection analysis (FIA) based on immobilized L-glutamate oxidase and glutaminase coupled with peroxidase. The laboratory-made flow-through cell of the detector has a measured volume of only 15 μ l. The hydrogen peroxide produced in the first reaction is detected by luminol chemiluminescence catalysed by peroxidase. A membrane sensor and enzyme reactor based on immobilized hydrogen peroxidase are used for the determination of hydrogen peroxide. It was observed that *Arthromyces ramosus* peroxidase produced a 100 times stronger luminescence signal than horseradish peroxidase. By immobilization of the microbial peroxidase on a membrane inside the flow cell, simplification could be achieved with regard to apparatus, reagents and operation. The sensitivity of detection was considerably improved. In addition, the concept of a hydrogen peroxide biosensor was realized. The membrane sensor shows a detection limit of 1×10^{-7} M for L-glutamate and 1×10^{-6} M for L-glutamine. The calibration graphs were approximately linear in the range of 1×10^{-7} – 6×10^{-5} M for L-glutamate and 1×10^{-6} – 2.5×10^{-3} M for L-glutamine. The membrane sensor was stable over a period of 10 weeks (> 1000 analyses).

Keywords: Biosensors; Chemiluminescence; Enzymatic methods; Flow injection; Enzyme reactor; Glutamate; Glutamine

L-Glutamate is an economically important biotechnological product. It is contained in many kinds of foods and contributes to their enhanced flavour. The monitoring of L-glutamate is essen-

tial for food processing and fermentation control. In addition, glutamate levels in blood are determined for clinical diagnosis purposes.

Several methods have been reported for the enzymatic determination of L-glutamate. Yao et al. [1], Yamauchi et al. [2] and Wollenberger et al. [3] proposed amperometric enzyme electrodes with immobilized glutamate oxidase. Riedel and

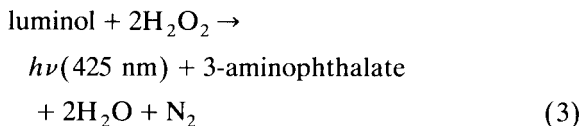
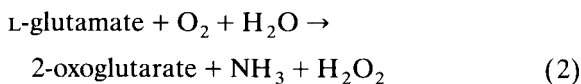
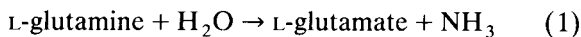
Correspondence to: M.-R. Kula, Institute of Enzyme Technology, Heinrich Heine University Düsseldorf, P.O. Box 20 50, D(W)-5170 Jülich (Germany).

Scheller [4] developed an amperometric microbial sensor for L-glutamate. Puchades et al. [5] described a fluorimetric flow-injection analysis (FIA) method for the determination of L-glutamate dehydrogenase. Procedures with autoanalysers have been published for the enzymatic spectrophotometric determination of L-glutamate [6].

L-Glutamine is applied in medicine and peptide synthesis [7]. Further, the L-glutamine concentration is an important process parameter in animal cell culture. Romette and Cooney [8] used a Clark-type enzyme electrode for the determination of L-glutamine to control mammalian cell cultures. Renneberg et al. [9] proposed a glutamine sensor using co-immobilized glutaminase and glutamate oxidase with amperometric hydrogen peroxide detection. Dullau and Schügerl [10] determined glutamine photometrically in the FIA mode using glutaminase and glutamine dehydrogenase.

The determination of hydrogen peroxide by chemiluminescence offers numerous advantages [11–14] compared with other methods. Light emission can be quantified at levels over a wide linear working range using relatively simple instrumentation. Complexed metal ions and peroxidase are used for catalysis. The peroxidase-catalysed hydrogen peroxide–luminol chemiluminescence has the additional advantage of higher selectivity because pH values less than 9 can be used [15,16]. In this work two different kinetic determinations, based on the ultimate generation

and detection of hydrogen peroxide with luminol and peroxidase are described. L-Glutamine and L-glutamate are enzymatically degraded to yield stoichiometric amounts of hydrogen peroxide as follows:



Glutamate oxidase and glutaminase were co-immobilized on controlled-pore glass (CPG) for the determination of glutamate and glutamine. Peroxidase was either immobilized on CPG or on a preactivated membrane according to Assolant-Vinet and Coulet [17]. The CPG-immobilized enzyme was used in an enzyme column and the membrane was placed in the flow cell of the FIA detector. Both systems were compared with regard to sensitivity and speed of analysis.

EXPERIMENTAL

Reagents

L-Glutamate oxidase was obtained from Yamasa Shoyu (Choshi, Japan) and microbial peroxidase, MP-9 microperoxidase, glutaminase and

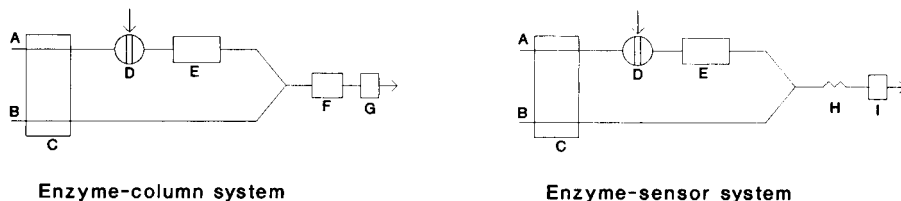


Fig. 1. Set-ups of the flow-injection systems for the chemiluminometric determination of L-glutamine and L-glutamate using peroxidase as catalyst. A = 0.1 M phosphate buffer (pH 7.4 for L-glutamate and pH 6.5 for L-glutamine); B = luminol reagent (for composition, see text); C = pumps (for flow-rates, see text); D = injection valve; E = enzyme reactor (filled with co-immobilized glutaminase/glutamate oxidase for the determination of L-glutamine and filled only with glutamate oxidase for the determination of L-glutamate); F = enzyme reactor filled with immobilized peroxidase; G = flow-through cell; H = mixing coil; I = flow-through peroxidase sensor.

luminol from Sigma (Neu-Ulm, Germany). All other chemicals were of analytical-reagent grade (Merck, Darmstadt, Germany).

Detection of chemiluminescence

The channel of the flow cell is directly faced to the rectangular end of a specially designed fibre-optic bundle (Schöllly, Denzlingen, Germany). The other end of the fibre-optic bundle (diameter 4.4 mm) is faced to the window of an Oriel Model 77348 photomultiplier tube (PMT) (L.O.T., Darmstadt, Germany). The PMT, housed in a Oriel Model 70680 housing, is connected via a current preamplifier (Oriel Model 70710) to a readout system (Oriel Model 70701). The PMT was powered by a high-voltage power supply (Oriel Model 70705). The voltage for the PMT was maintained at 800 V. The output from the readout was recorded on a Synchronic four-channel pen recorder (Metrawatt, Nürnberg, Germany).

Data evaluation in FIA was performed manually by peak-height measurements. Signal values are given in relative units, corrected for the sensitivity range of the detector.

Flow-injection system

A schematic flow diagram is presented in Fig. 1. The FIA system consisted of two piston pumps (Metrohm, Herisau, Switzerland), a low-pressure injection valve (Rheodyne, Cotati, CA), the luminescence detector described above and Teflon tubing (0.8 mm i.d.). The flow of reagent and carrier was continuously controlled by a flow meter (Promochem, Wesel, Germany).

Preparation of the immobilized enzyme reactor

The immobilization of the enzyme was carried out by a modified method described by Yao et al. [1]. The controlled-pore glass (aminopropyl-CPG, pore size 92.8 nm, particle size 130–250 mesh), obtained from Fluka (Neu-Ulm, Germany), was packed into a column (20 mm × 3 mm i.d.). A 2.5% (v/v) solution of glutaraldehyde in potassium phosphate (0.1 M, pH 7.0) was pumped at 1 ml min⁻¹ for 2 h through the column in order to activate the support. After the column had been washed with buffer for 2 h, enzymes were loaded on to the column by recirculating 4 ml of enzyme

solution through the column at 0.5 ml min⁻¹ for 24 h at 4°C. The amounts of enzyme and buffer used for immobilization were as follows: 2 mg of glutamate oxidase (20 U) and 2 mg of glutaminase (15 U) in 4 ml of 0.1 M phosphate buffer (pH 6.5) were used for the glutamine column and 4 mg of glutamate oxidase (40 U) in 4 ml of 0.1 M phosphate buffer (pH 7.4) for the glutamate column. The enzyme column was finally washed with glycine buffer (0.1 M, pH 7.0) for 3 h. The enzyme reactor was stored at 4°C when not in use.

Construction of the flow-through enzyme membrane sensor

The hydrogen peroxide sensor consisted of a flow cell into which a membrane with immobilized peroxidase had been integrated [18]: 7 mg of microbial peroxidase dissolved in 200 μl of buffer solution [phosphate-buffered saline (PBS)] (pH 7.0) containing 137 mM sodium chloride, 2.7 mM potassium chloride, 8 mM disodium hydrogenphosphate and 1.5 mM potassium dihydrogenphosphate, was immobilized on 15 mm² of preactivated membrane (Ultrabind, Gelman Sciences, Ann Arbor, MI) following the manufacturer's instructions. A 2.6 × 3.2 cm strip of the membrane was cut and placed in the laboratory-made luminometric flow cell. The latter was assembled with the enzyme membrane opposite the rectangular end of the fibre-optic bundle as shown in Fig. 2. The cell volume was 15 μl.

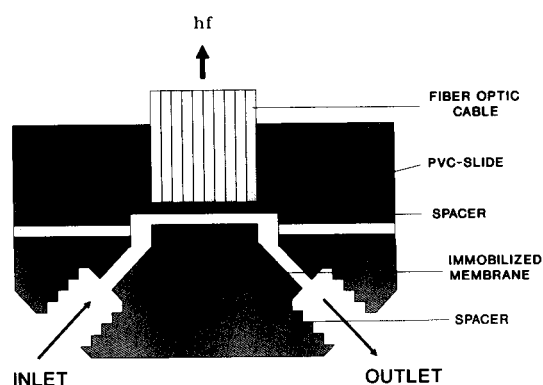


Fig. 2. Design of the flow-through enzyme membrane sensor. The light emission generated during the determination is conducted through the fibre-optic cable to the photomultiplier; hf = photon energy.

The hydrogen peroxide formed by the glutamate oxidase reaction was determined by measuring the light emitted from excited luminol as catalysed by the microbial peroxidase, immobilized on the membrane.

RESULTS AND DISCUSSION

The determination of glutamate and glutamine is based on hydrogen peroxide detection via luminol chemiluminescence. Several peroxidases and hexacyanoferrate(III) were used for hydrogen peroxide determination and compared with respect to sensitivity and reliability. Different catalysts for the hydrogen peroxide determination via luminol chemiluminescence were tested in relation to sensitivity, reproducibility and stability. Subsequently a hydrogen peroxide biosensor was tested with regard to suitability for chemiluminometric glutamate/glutamine determination.

Use of hexacyanoferrate(III) as catalyst for luminol chemiluminometric determination of L-glutamate

The FIA setup is shown in Fig. 3. For the determination of L-glutamate, 200 μ l of glutamate standard solution were injected into a buffer stream (A); the reagent solution contained 10 mM luminol (B) and 0.1 M hexacyanoferrate(III) (C) as catalyst for the chemiluminescence reaction. A high sensitivity (0.001 mM) and a wide linear working range from 0.001 to 1.0 mM L-

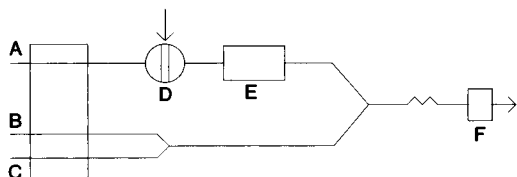


Fig. 3. Set-up of the flow-injection system with chemiluminescence detection for the determination of L-glutamate using hexacyanoferrate(III) as catalyst. A = 0.1 M phosphate buffer (pH 7.5); B = 0.1 M hexacyanoferrate(III); C = reagent (10 mM luminol in 0.1 M carbonate buffer, pH 10.6); D = injection valve; E = enzyme reactor (20 mm \times 0.3 mm i.d.) filled with immobilized glutamate oxidase; F = flow-through cell of detector.

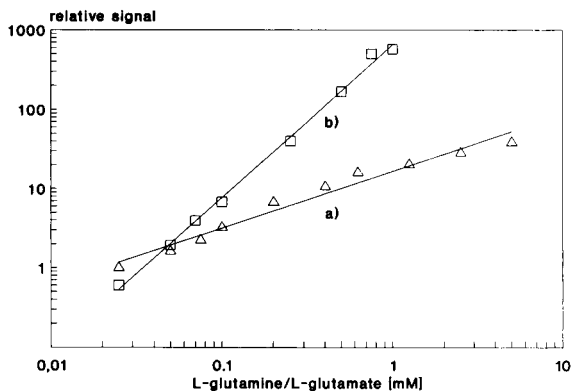


Fig. 4. Calibration graphs for L-glutamate and L-glutamine using the optimized FIA configuration as described in the text. (a) L-Glutamine (stop time 21 s), regression line $y = 0.72x + 2.8079$, $r = 0.987$; (b) L-glutamate (stop time 10 s), regression line $y = 1.702x + 6.1698$, $r = 0.998$.

glutamate were observed. The disadvantages are the high background luminescence and the insufficient selectivity with respect to easily oxidizable substances present in real samples caused by hexacyanoferrate(III) in strongly alkaline solution.

Use of microperoxidase from equine heart as catalyst for the luminol chemiluminescence

L-Glutamate. The FIA setup is shown in Fig. 1. Experiments were first conducted to establish the optimum pH of the enzyme reactors coupled with the optimum pH of the luminol chemiluminescence. It must be taken into account that L-glutamate oxidase is not stable at pH 7.5 and the intensity of the luminol chemiluminescence is considerably diminished at pH < 8.5. This was the reason why the glutamate oxidase reactor had to be integrated into the carrier channel of the flow-injection set-up. The use of 0.1 M phosphate buffer (pH 7.4) as the carrier solution and 2.5 mM luminol in 0.1 M carbonate buffer (pH 10.4) as the reagent solution was selected for FIA. The flow-rates of the carrier and reagent were 0.5 ml min^{-1} . Figure 4 shows a typical calibration with the optimized experimental set-up.

L-Glutamine. The FIA set-up is shown in Fig. 1. The pH of the carrier solution was chosen as 6.0, allowing both glutaminase and glutamate oxidase catalysis. The reagent solution and the

TABLE 1

Effect of stop time on response of the analytical system to an injection of 40 μl of a 0.625 mM L-glutamine standard

Stop time (s)	Relative response (%)
0	1
6	2.80
11	6.23
21	8.37
31	9.80
41	12.09

flow-rates were the same as for L-glutamate, hence the maximum hydrogen peroxide generation could be achieved. The use of the stopped-flow technique as proposed by Ruzicka and Hansen [19] leads to an improvement in sensitivity for the FIA assay, as shown in Table 1. The sample concentration profile is stopped in the glutamine enzyme column. A stop time of 20 s gives sufficient sensitivity and an acceptable sampling rate. Figure 4 shows a typical calibration graph for the determination of L-glutamine. A linear relationship between the increase in hydrogen peroxide and the amount of L-glutamine was observed in the range 0.05–5.0 mM.

*Use of immobilized microbial peroxidase from *Arthromyces ramosus* as catalyst for the detection of hydrogen peroxide*

The peroxidase of *Arthromyces ramosus* was tested. Akimoto et al. [20] found that microbial peroxidase is a potent catalyst for the chemiluminescence reaction of hydrogen peroxide with luminol, the luminescence produced per unit of microbial peroxidase being well over 100 times stronger than that produced by, for example, horseradish peroxidase. Therefore, the influence of different flow-rates on the detector peak height was tested. The configuration of the set-up was the same as shown in Fig. 1. Increasing flow-rates of the carrier and the reagent channel increased the detector signal (Table 2). This can be explained by the fact that the peroxidase reaction is so rapid that the luminescence emission has decreased considerably before reaching the detector cell. Therefore, immobilization of the catalyst within the detector cell should cause much higher

TABLE 2

Effect of flow-rate on signal peak height and time to return to baseline, t_{rb} ^a

Flow-rate (ml min^{-1})	Relative response (%)	t_{rb} (s)
0.6	1	105
0.7	2.9	99
0.8	7.3	81
0.9	7.6	75
1.0	12.1	60
1.2	26.5	45
1.5	59.4	28

^a 40 μl of 1.5 mM hydrogen peroxide solution were injected into the flow-injection system.

sensitivity. This can be realized by the flow-through enzyme membrane sensor as described before.

Determination of L-glutamate and L-glutamine with the hydrogen peroxide biosensor

The microbial peroxidase was immobilized on a pretreated membrane and placed in the flow-through cell of the luminometric detector as shown in Fig. 2. The set-up of the whole system is shown in Fig. 1. Typical calibration graphs for L-glutamate and L-glutamine are presented in Fig. 5. The analytical time for the measurement of one peak was only 30 s for L-glutamate and 40 s for L-glutamine.

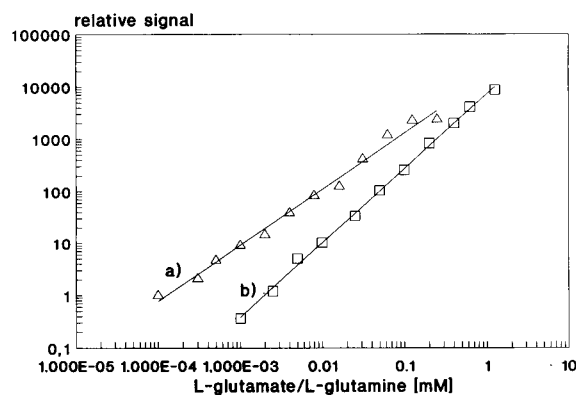


Fig. 5. Calibration graphs for L-glutamate and L-glutamine by using the hydrogen peroxidase biosensor. (a) L-Glutamate, regression line $y = 18528x - 42.56$, $r = 0.996$, calibration range 0.0001–0.30 mM; (b) L-glutamine, regression line $y = 48.4x + 1.0299$, $r = 0.997$, calibration range 0.001–2.5 mM.

TABLE 3

Comparison between enzyme reactor and biosensor in relation to range of sensitivity

Sample	System	Range of linearity (mM)	Reproducibility (R.S.D.) (%)
L-Glutamate	Enzyme reactor ^a	0.025–1.0	2.2
	Enzyme reactor ^b	0.001–1.0	5.0
	Biosensor ^c	0.0001–0.0625	1.9
L-Glutamine	Enzyme reactor ^a	0.05–5.0	2.4
	Biosensor ^c	0.001–2.5	2.1

^a Microperoxidase from equine heart was used as catalyst for the chemiluminescence reaction. ^b 0.1 M hexacyanoferrate(III) was used as catalyst for the chemiluminescence reaction. ^c Microbial peroxidase from *Arthromyces ramosus* was used as catalyst for the chemiluminescence reaction.

Comparison of the chemiluminometric determination of L-glutamate with other detection methods

Table 3 shows a comparison between the L-glutamate and L-glutamine determination using the peroxide biosensor and enzyme reactor method with respect to calibration range, sensitivity and reproducibility. The biosensor configurations for L-glutamate and L-glutamine are more sensitive and the reproducibility is better. The long-term stability of the peroxide biosensor was tested by over 500 injections of a 1.5 mM hydrogen peroxide standard solution at a flow-rate of 1.2 ml min⁻¹ (Fig. 6). The decrease in the detector signal after 500 injections was not significant.

Conclusions

L-Glutamate and L-glutamine can be rapidly determined via FIA chemiluminescence detection of hydrogen peroxide. Immobilized microbial peroxidase is especially suited for the catalytic oxida-

tion of luminol by hydrogen peroxide resulting in chemiluminescence

The use of a hydrogen peroxide membrane sensor with immobilized microbial peroxidase results in a very high sensitivity for glutamate/glutamine determination with the FIA technique.

The flow-through reactors packed with immobilized glutamate oxidase/glutaminase are operating at their optimum pH values and ensure the highest sensitivity. Very wide linear determination ranges can be achieved. The long-term stability of the glutamate oxidase reactor and of the hydrogen peroxide sensor are encouraging for application in bioprocess analytical measurements.

The authors thank Yamasa Shoyu (Japan) for the L-glutamate oxidase. F. Preuschoff and U. Spohn acknowledge financial support from the Federal Ministry of Research and Technology (0319658A).

REFERENCES

- 1 T. Yao, N. Kobayashi and T. Wasa, *Anal. Chim. Acta*, 231 (1990) 121.
- 2 H. Yamauchi, H. Kusakabe, Y. Midorikawa, T. Fujishima and A. Kuninaka, in *Third European Congress on Biotechnology*, Vol. 1, Verlag Chemie, Weinheim, 1984 p. 705.
- 3 U. Wollenberger, F.W. Scheller, A. Böhmer, M. Passarge and H.G. Müller, *Biosensors*, 4 (1989) 381.
- 4 K. Riedel and F. Scheller, *Analyst*, 112 (1987) 341.

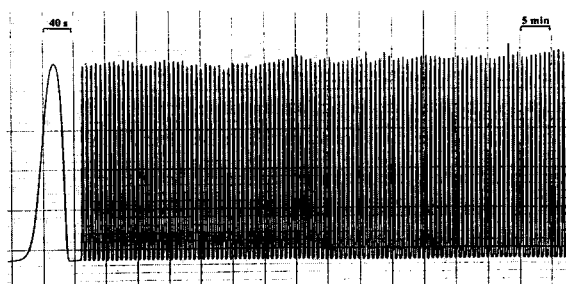


Fig. 6. Long-term stability of the hydrogen peroxide sensor in the flow-injection system: 100 consecutive injections of 0.5 mM hydrogen peroxide sample.

- 5 R. Puchades, L. Lemieux and R.D. Simard, *J. Food Sci.*, (1989) 423.
- 6 H. Kusakabe, Y. Midorikawa and T. Fujishima, *Agric. Biol. Chem.*, 48 (1984) 181.
- 7 G.B. Kline and S.H. Cox, *J. Org. Chem.*, 26 (1961) 1854.
- 8 J. Romette and C.L. Cooney, *Anal. Lett.*, 20 (1987) 1069.
- 9 R. Renneberg, G. Trott-Kriegeskorte, M. Lietz, V. Jäger, M. Pawlowa, G. Kaiser, U. Wollenberger, F. Schubert, R. Wagner, R.D. Schmid and F.W. Scheller, *J. Biotechnol.*, 21 (1991) 173.
- 10 T. Dullau and K. Schügerl, in R.D. Schmid (Ed.), *FIA Based on Enzymes and Antibodies* (GBF Monograph, No. 14), VCH, Weinheim, 1975, p. 27.
- 11 W.R. Seitz, *Methods Enzymol.*, 57 (1978) 445.
- 12 T.P. Whitehead, L.J. Kricka, T.J.N. Carter and G.H.G. Thorpe, *Clin. Chem.*, 25 (1979) 1531.
- 13 D.T. Bostick and D.M. Hercules, *Anal. Lett.*, 7 (1974) 347.
- 14 J.P. Auses, S.L. Cook and J.T. Maloy, *Anal. Chem.*, 47 (1975) 244.
- 15 B. Olsson, *Anal. Chim. Acta*, 136 (1982) 113.
- 16 M.S. Abdel-Latif and G.G. Guilbault, *Anal. Chim. Acta*, 221 (1989) 11.
- 17 C.H. Assolant-Vinet and P.R. Coulet, *Anal. Lett.*, 19 (1986) 875.
- 18 F. Preuschoff, U. Spohn, G. Blankenstein, K.H. Mohr and M.-R. Kula, *Fresenius' J. Anal. Chem.*, submitted for publication.
- 19 J. Ruzicka and E.H. Hansen, *Flow Injection Analysis*, Wiley, New York, 1988.
- 20 K. Akimoto, Y. Shinmen, M. Sumida, T. Amachi, H. Yoshizumi, Y. Saeki, S. Shimizu and H. Yamada, *Anal. Biochem.*, 189 (1990) 182.

Simultaneous determination of sucrose and reducing sugars using indirect flow-injection biamperometry

Jacek Michałowski and Anatol Kojło

Institute of Chemistry, Warsaw University Branch, Białystok (Poland)

Marek Trojanowicz and Bogdan Szostek

Department of Chemistry, University of Warsaw, Pasteura 1, 02-093 Warsaw (Poland)

Elias A.G. Zagatto

Centre for Nuclear Energy and Agriculture, University of São Paulo, Piracicaba (Brazil)

(Received 1st April 1992; revised manuscript received 17th July 1992)

Abstract

The method developed for the determination of sugars is based on reduction of hexacyanoferrate(III) by simple carbohydrates in a strongly alkaline medium at elevated temperature. Changes in hexacyanoferrate(III) concentration are monitored amperometrically with platinum wire electrodes polarized at 200 mV. Sucrose determination requires on-line hydrolysis in hydrochloric acid. The detection sensitivity for different simple sugars and disaccharides and the influence of several interferents were examined. Sucrose and glucose were determined with a sampling rate of 40 h^{-1} in natural samples from a sugar production process spiked with glucose.

Keywords: Amperometry; Flow injection; Glucose; Sucrose; Sugars; Reducing sugars

Numerous flow-injection methods have already been reported for the determination of sugars in foods, biological materials and physiological fluids [1–16]. Although in routine analysis, especially for the simultaneous determination of several species, liquid chromatographic methods predominate, in many instances those methods can be replaced by fast flow-injection procedures for the determination of one or two components.

In reported flow-injection procedures for the determination of sugars, electrochemical detec-

tion methods are most frequently used, although owing to the relatively low electrochemical activity of sugars, they are mostly determined indirectly. In the potentiometric determination of simple sugars platinum [1] and metallic copper [2] electrodes have been used. Indirect amperometric detection of simple carbohydrates at platinum electrodes in alkaline solutions has been performed by application of a triple-pulse potential waveform [3], although indirect amperometric detection has also been reported [1].

There has been rapid progress recently in enzymatic flow-injection methods for the determination of simple sugars and disaccharides with amperometric detection. For this purpose either

Correspondence to: M. Trojanowicz, Department of Chemistry, University of Warsaw, Pasteura 1, 02-093 Warsaw (Poland).

oxidases [4,5] or dehydrogenases [6,7] of simple sugars are utilized. In systems with regeneration and recycling of coenzyme and enzyme, a repetitive enzymatic determination can be carried out [8]. In multi-enzyme systems the determination of sucrose in the presence of glucose [9] and the simultaneous determination of sucrose and glucose [10] have been performed. Spectrophotometric [11–14] and chemiluminescence [15,16] detection have also been employed in the flow-injection determination of sugars.

The aim of this study was to develop a flow-injection method for the determination of sugars using biamperometric detection with two polarized electrodes using a hexacyanoferrate(III)–hexacyanoferrate(II) indicating system. In previous applications of flow-injection biamperometry mostly an I_2-I^- indicating system has been employed [17–19].

The reduction of hexacyanoferrate(III) by carbohydrate aldehyde groups has already been applied to flow-injection determinations with potentiometric [1,20,21], amperometric with one polarized working electrode [1] and spectrophotometric [14] detection. In this study, a univariate optimization of the manifold and operating conditions was performed for biamperometric detection of sugars with hexacyanoferrate(III)–hexacyanoferrate(II) indicating system.

EXPERIMENTAL

Apparatus

The measuring system consisted of a multi-channel pump (MS Reglo; Ismatec, Zurich), a laboratory-made rotary injection valve and a flow cell connected to an a.c.–d.c. polarograph (PLP 225C; Zalmed, Warsaw), which was in turn connected to a potentiometric strip-chart recorder (TZ 4620; Laboratorní Přstroje, Prague).

The flow-through cell used was the same as described previously [17]; the platinum wire electrodes were 0.6 mm in diameter and 13 mm long. A constant polarizing voltage of 200 mV was applied from the polarograph.

The system used is shown in Fig. 1. The manifold was made of polypropylene tubing (0.7 mm

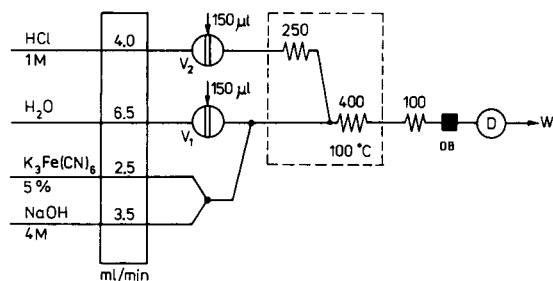


Fig. 1. Schematic diagram of the optimized flow-injection system used for the simultaneous determination of sucrose and reducing sugars with biamperometric detection. D = flow-through amperometric detector; DB = debubbler; V_1 , V_2 = injection valves.

i.d.) with laboratory-made Perspex connectors. The heating coils, made of PTFE tubing (0.7 mm i.d., wall thickness 0.2 mm), were immersed in boiling water under reflux; for this purpose a heating mantle with a 1-l round-bottomed flask and a 50-cm reflux condenser were used. The standard Technicon fitting B0 from an AAII AutoAnalyzer was used as a debubbler. The manifold is equipped with two injection valves, V_1 and V_2 . The sample solution injected with valve V_1 reacts with hexacyanoferrate(III) and after cooling in a 100-cm delay loop and debubbling in DB it is transported to the detector. When injected with valve V_2 , first the sample compounds are hydrolysed in a 250-cm coil and then react with hexacyanoferrate(III), and the resulting hexacyanoferrate(II) is detected.

Polarimetric reference measurements were carried out using a Polamet-S polarimeter (Carl Zeiss, Jena).

Reagents

D-(+)-Glucose was obtained from Polfa (Kraków) and D-(–)-fructose from Ubichem (Eastlight). All other reagents used were of analytical-reagent grade from POCh (Gliwice).

Stock standard solutions of normal and invert sucrose, D-(–)-fructose and D-(+)-glucose were prepared as described previously [13] and stored in a refrigerator. All solutions were prepared in triply distilled water. Working standard solutions in the 50–300 mg l⁻¹ invert sucrose range were

freshly prepared by dilution of the stock standard solution with water.

White-beet juices and syrups from various stages of sugar production were provided by the ŁAPY sugar factory.

Procedure for determination of sucrose and glucose in natural samples

Determinations were made using the flow system shown in Fig. 1, where two 150- μ l portions of sample were injected with valves V_1 and V_2 with a time delay of 30 s. Calibration graphs were obtained for both parts of the manifold with and without a hydrolysis step based on injections of 100, 150, 200, 250 and 300 μ g ml⁻¹ invert sugar solutions.

Fresh juice and thin syrup after filtration were diluted 1000-fold and thick syrup 4000-fold with distilled water and then injected into the system. Results obtained in the part of the manifold involving hydrolysis were subtracted from those obtained without hydrolysis.

RESULTS AND DISCUSSION

Optimization of the flow-injection system

The sensitivity of detection for different simple sugars using the proposed system with indirect biamperometric detection depends substantially on the reaction time of hexacyanoferrate(III) reduction, temperature and the concentrations of reagents used. Other essential contributions to the detection sensitivity come from the conditions of biamperometric detection such as the geometry

of the flow-through cell, the area of the indicating electrodes and the magnitude of the polarizing voltage applied. The choice of the geometry of the flow cell and the area of the indicator electrodes was based on previous work [17–19], whereas other factors were optimized during this study.

The effect of temperature on hexacyanoferrate(III) reduction was studied using the system shown in Fig. 1, but without the HCl line and injection valve V_2 used for sucrose hydrolysis. Samples of 150 μ l of 100 mg l⁻¹ glucose solutions were injected into the stream of water pumped at a flow-rate of 5.5 ml min⁻¹ and merged with streams of 1% hexacyanoferrate(III) (4.3 ml min⁻¹) and 2 M NaOH (3.2 ml min⁻¹). A significant increase in signal magnitude with increase in temperature was observed over the whole range of temperature examined (Fig. 2). In the flow system without the debubbler an increase in temperature also had a strong adverse effect on the precision of measurements. The use of the debubbler improved the precision 5–6-fold, whereas there was only a slight increase in the total dispersion in the system (about 3%). At 100°C the relative standard deviation (R.S.D.) of measurements with multiple ($n = 5$) injections of 100 mg l⁻¹ glucose solution was 0.5–0.6%. This temperature was found to be the optimum, consistent with previous observations [14], and was used in subsequent studies.

The determination of sucrose with biamperometric detection requires its preliminary hydrolysis to simple carbohydrates. According to previous findings [14], this was done in hydrochloric

TABLE 1

Optimization of experimental conditions for on-line hydrolysis of sucrose in the flow-injection system ^a

Length of reaction coil (cm)	Peak height for different HCl concentrations (μ A)				Sampling rate (h ⁻¹)
	0.5 M		1.0 M		
	Sucrose	Invert sucrose	Sucrose	Invert sucrose	
200	5.2	5.6	5.1	5.5	45
250	5.3	5.5	5.3	5.3	40
300	5.4	5.4	5.2	5.2	33

^a Injected: 100 mg l⁻¹ sucrose or invert sucrose with valve V_2 (Fig. 1).

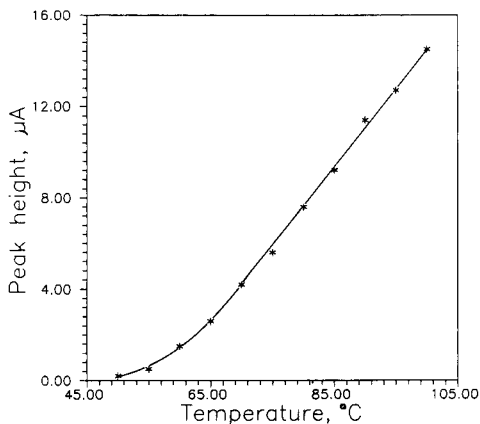


Fig. 2. Effect of temperature on flow-injection response for the injection of 150 μl of 100 mg l^{-1} glucose solution in the system with biampometric detection. See text for details.

acid solution. Table 1 shows the influence of the length of the reaction coil and the HCl concentration on the efficiency of hydrolysis in the flow system shown in Fig. 1. In this study the results obtained under different conditions for sucrose and invert sucrose solutions of the same concen-

tration injected with valve V_2 were compared. A 250-cm long reaction coil and a 1 M concentration of hydrochloric acid for hydrolysis at 100°C were found to be the optimum conditions. Although under these conditions a slightly smaller signal was obtained than with a 300-cm reaction coil, the sampling rate was higher. With higher HCl concentrations a decrease in the signal magnitude was observed, and the risk of sugar caramelization must also be taken into account.

The same measuring set-up was also employed for the optimization of the concentration of hexacyanoferrate(III) and sodium hydroxide solutions for the detection of simple sugars. The system with one injection valve and splitting the sample prior to the reaction coils was replaced with the system with two independent injection valves because of unfavourable reproducibility of results. The optimization was done using 150- μl injections of 100 mg l^{-1} glucose and fructose standard solutions injected with both valves V_1 and V_2 . The results obtained are given in Table 2. The first peak corresponds to the injection with valve V_1 and the second peak, which is smaller owing

TABLE 2

Effect of concentration of reagents on flow-injection response obtained for injections of 100 mg l^{-1} glucose and fructose in the system with two injection valves shown in Fig. 1

NaOH concentration (M)	$\text{K}_3\text{Fe}(\text{CN})_6$ concentration (%)	Peak height, mm			
		Glucose		Fructose	
		1st peak	2nd peak	1st peak	2nd peak
3	0.5	11.2	3.9	13.0	6.5
	1	11.0	4.6	12.5	5.7
	2	11.2	4.9	12.9	5.9
	3	11.5	5.2	13.0	6.2
	4	11.1	4.8	12.5	5.9
4	0.5	11.5	4.7	12.5	5.6
	1	12.0	4.7	13.1	5.4
	2	12.5	5.0	13.5	5.4
	3	12.3	5.1	13.3	5.4
	4	13.5	5.5	14.0	6.0
5	0.5	12.8	5.8	13.0	6.0
	1	13.5	6.4	13.5	6.5
	2	13.9	4.2	12.3	5.0
	3	14.0	4.2	12.4	5.1
	4	14.5	4.3	12.6	5.0
	0.5	14.0	4.2	12.4	5.2
	1	14.2	4.3	12.4	5.2
	2	14.2	4.5	12.6	5.5
	3	14.2	4.5	12.6	5.5
	4	14.2	4.5	12.6	5.5

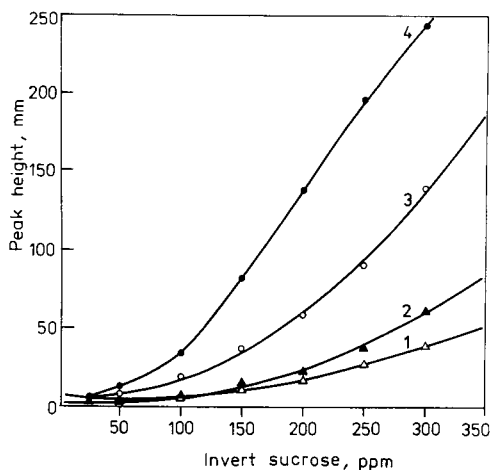


Fig. 3. Calibration graphs obtained for invert sucrose at polarizing voltages of (1) 50, (2) 100, (3) 150 and (4) 200 mV. Injected: 150 μl of invert sucrose solution with valve V_1 .

to the larger dispersion of the injected sample solution, corresponds to the injection with valve V_2 . The optimum conditions were considered to be those for which signals corresponding to the injections of glucose or fructose solution were identical with injection with either valve V_1 or V_2 . This was observed with 5% hexacyanoferrate(III) and 4 M NaOH at flow-rates of 2.5 and 3.5 ml min^{-1} , respectively.

For the optimized manifold and dimensions of the indicating electrodes mentioned under Experimental, the effect of the polarizing voltage in the range 50–200 mV on the signal magnitude observed for invert sucrose concentrations ranging from 25 to 300 mg l^{-1} was examined (Fig. 3). The change in the polarizing voltage affects both the signal magnitude and the extent of the linear response range. The optimum polarizing voltage was taken as 200 mV, at which a linear response was observed in the range 100–300 mg l^{-1} invert sucrose injected with valve V_2 and for 100–250 mg l^{-1} invert sucrose injected with valve V_1 . With such a system the R.S.D. obtained for multiple ($n = 5$) injections of sample containing 10.5% (w/w) sucrose and 17% (w/w) glucose was 0.63% for injection with valve V_1 and 0.77% for injection with valve V_2 .

The sensitivity of detection for different sugars was also examined under the same conditions

TABLE 3

Relative sensitivity of the flow-injection response obtained in the optimized measuring system with biamperometric detection for 100 mg l^{-1} solutions of different carbohydrates

Injected species	Relative sensitivity	
	Biamperometric detection	Spectrophotometric detection [14]
Glucose	1.000	1.000
Fructose	1.007	1.004
Xylose	1.166	1.052
Ribose	0.890	0.892
Galactose	0.903	0.879
Sucrose	0.097	1.035 ^a
Maltose	0.421	0.398 ^a
Lactose	0.655	0.675 ^a

^a After hydrolysis.

(Table 3). All results reported in Table 3 from this study were obtained for injection into the manifold without a hydrolysis step. Those results which were obtained under similar conditions were virtually identical with those observed previously for flow-injection analysis with spectrophotometric detection [14]. Simple carbohydrates other than glucose and fructose exhibit some differences in signal magnitude up to 16% sensitivity for glucose, but their content in the natural samples examined is negligible. Similarly to the previous studies, disaccharides showed also a response; the smallest signal was observed for sucrose.

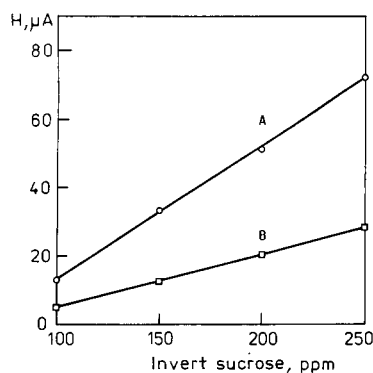


Fig. 4. Calibration graphs obtained for 150 μl of invert sucrose solutions injected with valve (A) V_1 and (B) V_2 in the flow-injection system with biamperometric detection at a polarizing voltage of 200 mV.

TABLE 4

Tolerance levels of the presence of metal ions causing an error not exceeding 2% in flow-injection determination of 100 mg l⁻¹ glucose using indirect biampometric detection

Metal	Tolerance level (mg l ⁻¹)
Co, Ni, Mn(II)	1.2
Fe(II)	1.5
Fe(III), Cu, Ca, Mg	15

Interferences

Interference with the proposed indirect biampometric detection with the hexacyanoferrate(III)–hexacyanoferrate(II) indicating system can be produced by the presence of species that bind any of the reagents used or influence the

equilibrium of the indicating redox couple. Therefore, the effect of the presence of several transition and alkaline earth metal ions was investigated (Table 4). In spite of the different type of detection applied in this study in comparison with that in previous papers, the tolerance level of metal cations examined was similar to that one observed with spectrophotometric detection [14].

Because of the reductive effect also found for sucrose (Table 3), the influence of sucrose on glucose determination was examined. Solutions of 100 mg l⁻¹ glucose were spiked with different amounts of sucrose and injected with valve V₁. A positive error of about 2% was observed with a 170 mg l⁻¹ sucrose level in the injected glucose solutions. This level, however, is much larger than observed in the real samples reported on below.

TABLE 5

Results of biampometric flow-injection determination of sucrose and glucose in natural samples from sugar production spiked with known amounts of glucose

Sample	Sucrose (% w/w)				Glucose (% w/w)			
	Found by polarimetry	Found by FIA	Error (%)	r ²	Added	Found by FIA	Error (%)	r ²
Fresh white-beet juice ^a	14.1	14.0	-0.7	0.958	10.0	10.5	+5.0	0.999
	13.9	14.0	+0.7		10.0	9.8	-2.0	
	14.5	14.6	+0.7		10.0	9.9	-1.0	
	12.5	13.0	+4.0		10.0	10.2	+2.0	
	14.1	14.3	+1.4		15.0	14.5	-3.3	
	13.9	13.7	-1.4		15.0	15.1	+0.7	
	14.5	14.8	+2.1		15.0	15.6	+4.0	
	12.5	12.0	-4.0		15.0	15.0	0	
Thin syrup ^a	13.5	13.9	+3.0	0.993	10.0	10.7	+7.0	0.999
	13.8	13.9	+0.7		10.0	9.7	-3.0	
	13.6	13.1	-3.7		10.0	9.9	-1.0	
	11.2	11.1	-0.9		10.0	9.9	-1.0	
	13.5	13.4	-0.7		13.0	13.5	+3.8	
	13.8	13.4	-2.9		13.0	13.1	+0.8	
	13.6	13.1	-3.7		13.0	12.8	-1.5	
	11.2	10.9	-2.7		13.0	12.9	-0.8	
Thick syrup ^b	57.7	57.0	-1.2	0.943	40.0	42.0	+5.0	0.999
	61.0	58.3	-4.4		40.0	41.0	+2.5	
	64.2	63.9	-0.5		40.0	39.1	-2.3	
	52.0	52.9	+1.7		40.0	40.0	0	
	57.7	53.9	-6.6		60.0	62.1	-0.3	
	61.0	62.1	+1.8		60.0	59.8	-0.3	
	64.2	64.8	+0.9		60.0	59.2	-1.3	
	52.0	51.9	-0.2		60.0	61.1	+1.8	

^a Diluted 1:1000 prior to injection. ^b Diluted 1:4000 prior to injection.

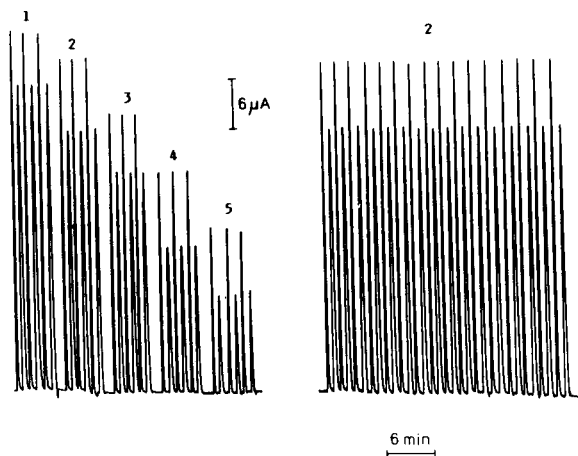


Fig. 5. Flow-injection response recorded for multiple injections of five thick syrup samples with added known amounts of glucose: 1 = 12.4% sucrose, 18% (w/w) glucose; 2 = 17.2% sucrose, 9.8% glucose; 3 = 15.4% sucrose, 8.7% glucose; 4 = 14.6% sucrose, 3.7% glucose; 5 = 11.8% sucrose, 3.2% glucose.

Determination of sucrose and glucose in natural samples

The method was applied to the analysis of fresh white-beet juice samples and syrups from different stages of sugar production. Because of the very low natural content of reducing sugars in these samples (in contrast to similar samples from sugar-cane processing [14]), they were spiked with known amounts of glucose.

Calibration of the measuring system was done using the same 150- μ l volumes of the invert sucrose solutions injected with both valves. The analytical signal obtained for injection with valve V_1 corresponds to the content of reducing sugars in the injected standard or sample solution (first peak). The signal corresponding to injection with valve V_2 is related to the total content of reducing sugars present in the raw sample and formed from the hydrolysis of sucrose. Figure 4 shows the calibration graphs obtained and Fig. 5 presents an example of the flow-injection response recorded for multiple injections of several real samples.

The results obtained were correlated with sucrose determination by polarimetry and with the known amounts of added glucose (Table 5). The

correlation coefficients showed satisfactory agreement. In order to obtain a baseline separation of the two peaks resulting from injections with valves V_1 and V_2 , injection with valve V_2 was made 30 s after injection with valve V_1 , and then after a further 60 s the next solution was injected with valve V_1 . Such a procedure leads to a sampling frequency 40 h⁻¹.

Conclusions

The flow-injection biamperometric method developed here is an alternative for the rapid, simultaneous determination of sugars to the spectrophotometric procedure reported previously [14]. The chemical conditions are similar. The replacement of optical detection with simple amperometric detection with two polarized metallic electrodes should be advantageous in routine applications in the sugar industry when control of sucrose together with reducing sugars is needed. From an instrumental point of view, the signal magnitude is in a convenient range of microamps, and the detector cell with two platinum wire electrodes does not require frequent maintenance.

REFERENCES

- 1 K. Brunt, *Analyst*, 107 (1982) 1261.
- 2 P.W. Alexander, P.R. Haddad and M. Trojanowicz, *Anal. Lett.*, 18 (1985) 1953.
- 3 S. Hughes and D.C. Johnson, *Anal. Chim. Acta*, 132 (1981) 11.
- 4 H. Lundback and B. Olsson, *Anal. Lett.*, 18 (1985) 871.
- 5 W. Matuszewski, M. Trojanowicz and L. Ilcheva, *Electroanalysis*, 2 (1990) 147.
- 6 G. Marko-Varga, R. Appleqvist and L. Gorton *Anal. Chim. Acta*, 179 (1986) 371.
- 7 K. Matsumoto, O. Hamada, H. Ukeda and Y. Osajima, *Anal. Chem.*, 58 (1986) 2732.
- 8 P. Roehring, C.M. Wolff and J.P. Schwing, *Anal. Chim. Acta*, 153 (1983) 181.
- 9 B. Olsson, B. Stalbon and G. Johansson, *Anal. Chim. Acta*, 179 (1986) 203.
- 10 M. Masoom and A. Townshend, *Anal. Chim. Acta*, 171 (1985) 185.
- 11 J. Toei and N. Baba, *Bunseki Kagaku*, 35 (1985) 411.
- 12 M.J. Medina, J. Bartroli, J. Alonso, M. Blanco and J. Fuentes, *Anal. Lett.*, B17 (1984) 385.
- 13 E.A.G. Zagatto, I.L. Mattos and A.O. Jacintho, *Anal. Chim. Acta*, 204 (1988) 259.

- 14 I.L. Mattos, E.A.G. Zagatto and A.O. Jacintho, *Anal. Chim. Acta*, 214 (1988) 247.
- 15 C.A. Koerner and T.A. Nieman, *Anal. Chem.*, 58 (1986) 116.
- 16 M. Maeda and A. Tsuji, *Anal. Sci.*, 2 (1986) 183.
- 17 M. Trojanowicz, A. Hulanicki, W. Matuszewski, M. Palys, A. Fuksiewicz, T. Hulanicka-Michalak, S. Raszewski, J. Szyller and W. Augustyniak, *Anal. Chim. Acta*, 188 (1986) 165.
- 18 W. Matuszewski, A. Hulanicki and M. Trojanowicz, *Anal. Chim. Acta*, 194 (1987) 269.
- 19 M. Trojanowicz, W. Matuszewski, B. Szostek and J. Michalowski, *Anal. Chim. Acta*, 261 (1992) 391.
- 20 H. Ohura, T. Imato, Y. Asamo, S. Yamasaki and N. Ishibashi, *Bunseki Kagaku*, 35 (1986) 807.
- 21 H. Ohura, T. Imato, S. Yamasaki and N. Ishibashi, *Anal. Sci.*, 3 (1987) 453.

Spectrofluorimetric flow-injection determination of calcium using Calcein

N. Chimpalee, D. Chimpalee, R. Jarungpattananon and S. Lawratchavee

Department of Chemistry, Faculty of Science, Silpakorn University, Nakorn Pathom 73000 (Thailand)

D. Thorburn Burns

Department of Analytical Chemistry, The Queen's University of Belfast, Belfast BT9 5AG (UK)

(Received 9th June 1992)

Abstract

Calcium can be determined spectrofluorimetrically ($\lambda_{em} = 520$ nm, $\lambda_{ex} = 365$ nm) based on its reaction with Calcein in strongly alkaline solution in a flow-injection system. The carrier stream was deionised water and the reagent streams were 0.6 M potassium hydroxide and $60 \mu\text{g ml}^{-1}$ Calcein. The injection rate was 50 h^{-1} . The calibration graph was sigmoid, but, however, linear between 3.0 and $7.0 \mu\text{g ml}^{-1}$ Ca based on injection volumes of $250 \mu\text{l}$. The relative standard deviation ($n = 10$) was 0.23% for $4 \mu\text{g ml}^{-1}$ Ca. The system has been applied to the determination of calcium in certified reference mineral samples.

Keywords: Flow injection; Flow system; Fluorimetry; Spectrophotometry; Calcein; Calcium

Numerous reagents are available for the spectrophotometric determination of calcium directly or indirectly, via, for example, ligand-exchange reactions [1,2]. Many of these reactions have been adapted for use in flow-injection systems [3,4], for example those using cresolphthalein complexone [5,6], glyoxalbis(2-hydroxyanil) [7] and zinc (EDTA) + 4-(2-pyridylazo)resorcinol, monosodium salt hydrate (PAR) [8].

In contrast few reagents exist for the fluorimetric determination of calcium [1,2]; those available include 4-methylumbelliferone-8-methyliminodiacetic acid (Calcein Blue) [9], fluorescein-2'-7'-bismethyliminodiacetic acid, sodium salt (Calcein) [10–12], 8-[bis(carboxymethyl)aminomethyl]-

7-hydroxy-2-methylisoflavone (Isocein) [13], 1,5-[bis(carboxymethyl)aminomethyl]naphthalene-2,6-diol (BDDN) [14], 8-hydroxyquin aldehyde 8-quinolyldiazine [15] and 2-[(2-amino-5-methylphenoxy)-methyl]-6-methoxy-8-aminoquinoline-*N,N,N',N'*-tetraacetic acid ("Quin-2") [16]. Of these, only the last has been used in flow-injection analysis. We now report on the first use of the readily available reagent, Calcein, for the spectrofluorimetric flow-injection determination of calcium.

EXPERIMENTAL

Apparatus

Fluorescence intensities were measured at 520 nm (excitation wavelength 365 nm) with a Shimadzu RF-540 spectrofluorimeter fitted with a

Correspondence to: D.T. Burns, Department of Analytical Chemistry, The Queen's University of Belfast, Belfast BT9 5AG (UK).

25- μ l, 1.5-mm, Quartz, Suprasil I, flow cell (Hellma) and recorded with a Shimadzu DR-3 Data recorder. Solutions were pumped using a variable-speed peristaltic pump (MS-Reglo, Ismatec.) fitted with Viton pump tubes for the Calcein and potassium hydroxide solutions and a Tygon pump tube for the deionised water. Samples were injected using an Omnifit four-way valve fitted with a by-pass coil. Flow lines were PTFE tubing (0.8 mm i.d.). Omnifit three-way connectors (“Hex”) were used for mixing the solutions. A diagram of the flow system is shown in Fig. 1.

Reagents and chemicals

Calcein stock solution. A stock solution of 1000 $\mu\text{g ml}^{-1}$ Calcein was prepared by dissolving 0.25 g of Calcein (Fluka, puriss) in 250 ml of 0.6 M potassium hydroxide. This solution was stored in a plastic bottle and kept in a refrigerator.

Calcein working solution. The reagent working solution of 60 $\mu\text{g ml}^{-1}$ was prepared daily, as required, by dilution of 15 ml of Calcein stock solution to 250 ml with 0.6 M potassium hydroxide.

Calcium standard solution. A solution of 1000 $\mu\text{g ml}^{-1}$ Ca^{2+} as nitrate (BDH, SpectrosoL).

All other reagents were of analytical grade and deionised water was used.

General procedure. Sample and standard solution were examined using the flow system and conditions given in Fig. 1. Typical peaks and calibration graph are shown in Fig. 2.

Mineral sample preparation procedure. Accurately weighed samples (0.1000 g) were dissolved in 4 ml of aqua regia. After boiling the solution was cooled, diluted to 10 ml and filtered through a Whatman No. 1 filter paper into a 100-ml volumetric flask and made up to volume with water. Diluted further as necessary with water to achieve the suitable calcium concentration for measurement.

Examination of the main experimental variables

The experimental variables were examined in a univariate manner.

Effect of reagent concentrations. With the concentration of the potassium hydroxide solution fixed at 0.6 M the Calcein concentration was varied from 20 to 100 $\mu\text{g ml}^{-1}$ which produced a series of sigmoid calibration graphs over the range 0–10 $\mu\text{g ml}^{-1}$ Ca. A Calcein concentration of 60 $\mu\text{g ml}^{-1}$ gave the greatest slope and range of linearity and was thus used thereafter.

With the concentration of Calcein fixed at 60 $\mu\text{g ml}^{-1}$, the potassium hydroxide concentration was varied from 0.2 to 1.0 M. The slopes of the sigmoid calibration graphs only changed slightly with increase in potassium hydroxide concentration over the range 0.2–1.0 M (relative peak height at 10 $\mu\text{g ml}^{-1}$ Ca: 0.2 M KOH, 88 mm; 0.4 M KOH, 85 mm; 0.6 M KOH, 80 mm; and at 1.0 M KOH, 79 mm). A potassium hydroxide concentration of 0.6 M was selected for further work.

Effect of operating variables. The effect of flow-rate, reaction coil length, mixing coil length

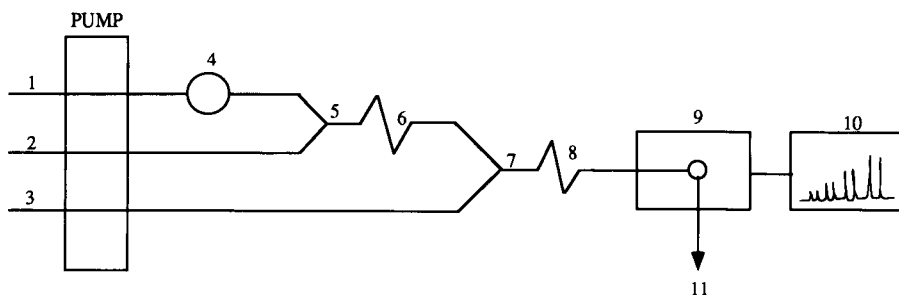


Fig. 1. Schematic diagram of the flow-injection system: (1) deionised water at 1.20 ml min^{-1} ; (2) 0.6 M potassium hydroxide solution at 1.0 ml min^{-1} ; (3) 60 $\mu\text{g ml}^{-1}$ Calcein solution at 0.80 ml min^{-1} ; (4) sample injector (250 μl); (5,7) mixing points (Omnifit three-way connector, “Hex”); (6) mixing coil (200 $\text{cm} \times 0.8$ mm i.d.); (8) reaction coil (100 $\text{cm} \times 0.8$ mm i.d.); (9) spectrofluorimeter; (10) recorder; (11) waste.

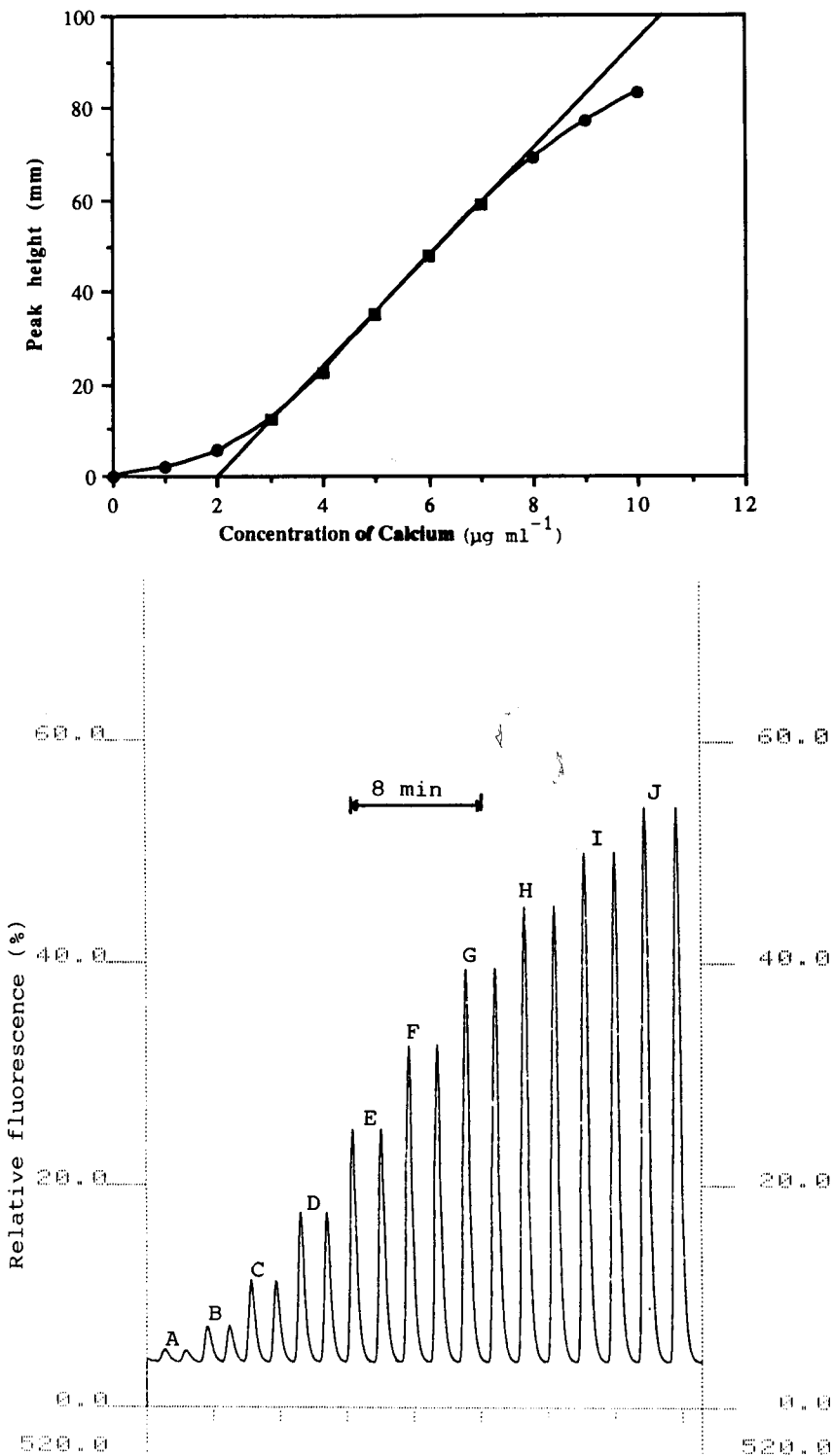


Fig. 2. Signals and calibration graph obtained in the determination of calcium. Sample size: 250 µl; calcium content: (A) 1.0; (B) 2.0; (C) 3.0; (D) 4.0; (E) 5.0; (F) 6.0; (G) 7.0; (H) 8.0; (I) 9.0 and (J) 10.0 µg ml⁻¹.

and sample injection volume were each studied under the above optimised reagent conditions.

The total flow-rate was varied from 1.30 to 3.70 ml min⁻¹. The peak heights decreased with increase in flow-rate whilst the peak widths became narrower. A flow-rate of 3.0 ml min⁻¹ was selected as a compromise between sampling rate and sensitivity.

When the length of the mixing coil was fixed at 200 cm the peak heights were found to decrease slightly (ca. 3%) with increase in reaction coil length from 100 to 400 cm. A 100-cm (0.8 mm i.d.) reaction coil was therefore selected. When the length of the reaction coil was fixed at 100 cm the peak heights were found to vary slightly (18% over the calibration range 0–10 µg ml⁻¹ Ca) with increase in mixing coil length from 100 to 400 cm. A mixing coil length of 200 cm was therefore adopted.

The volume of sample injected was varied from 100 to 1000 µl by changing the length of the injection loop in the injection valve. The peak heights increased non-linearly with increasing sample volume and the peak widths became broader. A volume of 250 µl was a compromise between sensitivity and sample injection rate.

Effect of sample acidity. The effect of nitric acid concentration in 4 µg ml⁻¹ Ca sample solutions was examined over the range 0–5% (v/v). Peak heights were constant up to 1% (v/v) nitric acid and increased slowly, almost linearly, with increase in acid concentration up to 5% (v/v) (2.5% increase in peak height per 1% increase in acid). In subsequent work the acid concentration of sample solutions was kept below 1% (v/v).

RESULTS AND DISCUSSION

The sigmoid-shaped calibration graphs and the effects of variation in Calcein concentration were similar to those observed earlier by Robinson and Weatherell using a conventional manual procedure [12]. The concentration-dependent curvature at low concentrations is probably due to incomplete formation of the absorbing/emitting species whilst that at higher concentrations is due to quenching. The advantages of using flow injection

TABLE 1

Determination of calcium in mineral samples

Sample	Nominal CaO (wt.%)	Found ^a CaO (wt.%)
BCS-CRM 368 Dolomite	30.8	31.35 ± 0.10
BCS-CRM 393 Limestone	55.4	55.50 ± 0.20
NIST-SRM 120 _c Phosphate rock (Florida)	48.02	47.91 ± 0.14

^a Mean ± standard deviation for 5 replicates.

tion for the present and similar reactions are in the control of time-dependent instability of calcium reagent solutions [12], improved standard deviations attained and sample throughput.

Under the conditions described a linear calibration region was obtained for 3–7 µg ml⁻¹ Ca ($R = 0.999$ $n = 5$). The relative standard deviation for the determination of 4 µg ml⁻¹ Ca was 0.23% (10 replicates).

The effects of possible interferences in the determination was examined for 4 µg ml⁻¹ Ca sample solutions. Nitrate, sulphate and chloride were without effect at 100-fold weight excess over calcium, as were aluminium and magnesium at 25-fold excess and iron(III), zinc and copper at 1:1 weight ratios.

The results obtained for the determination of calcium in mineral samples were in acceptable agreement with the certified values (see Table 1). The method is simple to operate and is more rapid (50 injections per hour) than when using the method in a manual format.

REFERENCES

- 1 F.D. Snell, *Photometric and Fluorometric Methods of Analysis. Metals Part 2*, Wiley, New York, 1978.
- 2 H. Onishi, *Photometric Determination of Traces of Metals. Part IIA. Individual Metals Aluminium to Lithium*, Wiley, New York, 4th edn., 1986.
- 3 J. Ruzicka and E.H. Hansen, *Flow Injection Analysis*, Wiley-Interscience, New York, 2nd edn. 1988.
- 4 M. Valcarcel and M.D. Luque de Castro, *Flow-Injection Analysis, Principles and Applications*, Ellis Horwood, Chichester, 1987.

- 5 W.D. Basson and J.F. van Staden, *Analyst*, 103 (1978) 296.
- 6 J.F. van Staden and A. van Rensburg, *Analyst*, 115 (1990) 605.
- 7 A.O. Janintho, E.A.G. Zagatto, B.F. Reis, L.C.R. Pessenda and F.J. Krug, *Anal. Chim. Acta*, 130 (1981) 361.
- 8 G. Nakagawa, H. Wada and C. Wei, *Anal. Chim. Acta*, 145 (1983) 135.
- 9 K.A. Matsoukas and M.A. Demertzis, *Analyst*, 113 (1988) 251.
- 10 D.F.H. Wallach, D.M. Surgenor, J. Soderberg and E. Delana, *Anal. Chem.*, 31 (1959) 456.
- 11 B.L. Kepner and D.M. Hercules, *Anal. Chem.*, 35 (1963) 1238.
- 12 C. Robinson and J.A. Weatherell, *Analyst*, 93 (1968) 722.
- 13 G.M. Huitink, *Anal. Chim. Acta*, 70 (1974) 311.
- 14 B. Budesínský and T.S. West, *Talanta*, 16 (1969) 399.
- 15 E.A. Boizhevol'nov, L.F. Fedorova, I.A. Krasavin and V.M. Dziomko, *Zh. Anal. Khim.*, 24 (1969) 531.
- 16 H. Wada, H. Atsumi and G. Nakagawa, *Chem. Express*, 4 (1989) 483.

Multicriteria target vector optimization of analytical procedures using a genetic algorithm

Part II. Polyoptimization of the photometric calibration graph of dry glucose sensors for quantitative clinical analysis

D. Wienke and C. Lucasius

Laboratory for Analytical Chemistry, Catholic University of Nijmegen, Toernooiveld 1, 6525 ED Nijmegen (Netherlands)

M. Ehrlich

Medizinische Akademie "Carl Gustav Carus" Dresden, Institut für Biochemie, Karl-Marx-Strasse 3, D(O)-8080 Dresden (Germany)

G. Kateman

Laboratory for Analytical Chemistry, Catholic University of Nijmegen, Toernooiveld 1, 6525 ED Nijmegen (Netherlands)

(Received 1st June 1992; revised manuscript received 10th September 1992)

Abstract

The target vector criterion as the vector distance between a set of desired responses and a set of really obtained responses of a multivariate function was combined with the genetic algorithm to improve simultaneously six properties of a biochemical test strip for human blood glucose determination as a function of twelve chemical and technological parameters. The advantage of the genetic algorithm in comparison with other search techniques became obvious for the search in this twelve-dimensional variables space with up to seven bit resolution, i.e., up to 1.93^{25} search positions. The results obtained by target vector optimization on the basis of the genetic search technique were critically compared with the results obtained by a prediction with classical and non-linear partial least-squares regression and realized in laboratory and industrial verification experiments. In this way advantages and disadvantages of deductive and inductive polyoptimization strategies could be discussed theoretically and with respect to experimental results.

Keywords: Optimization methods; UV-Visible spectrophotometry; Biosensors; Blood; Calibration; Genetic algorithm; Glucose; Multicriteria target vector optimization; Reagent strips

Multicriterial or polyoptimization means the simultaneous search of the desired values $\mathbf{y}(d) = [y_1(d), y_2(d), \dots, y_m(d)]$ for a multivariate function f of the type

$$(\mathbf{y}_1, \mathbf{y}_2, \dots, \mathbf{y}_m) = f(\mathbf{x}_1, \mathbf{x}_2, \dots, \mathbf{x}_k) \quad (1)$$

concerning m \mathbf{y} variables (responses or criteria), which depend on k independent \mathbf{x} variables.

One example of a multicriterial optimization problem in analytical chemistry is the optimization of $i = 1, \dots, m$ distances between chromatographic peaks as a function f of $j = 1, \dots, k$ chromatographic conditions (mobile phase composition, pH value, etc.) [1–12]. Another example is the simultaneous optimization of the intensities of $i = 1, \dots, m$ emission lines in atomic spectrom-

Correspondence to: D. Wienke, Laboratory for Analytical Chemistry, Catholic University of Nijmegen, Toernooiveld 1, 6525 ED Nijmegen (Netherlands).

etry of a mixture as function f of the $j = 1, \dots, k$ excitation conditions for a given spectrometer type [13–24].

One method to approach the desired response vector $\mathbf{y}(d)$ is multicriterial target vector optimization [24], also known as goal programming [25] or the optative vector method [26,27]. Multicriterial target vector optimization means, in principle, the minimization of the vector distance $D = \mathbf{y}(d) - \mathbf{y}(a)$ of the (by the user) specified $\mathbf{y}(d)$ to the actually reached vector $\mathbf{y}(a)$ in the m -dimensional space of the response variables. This is done by searching in the k -dimensional x -space. Among other measures for D , the Euclidian distance is a possibility for describing the closeness between $\mathbf{y}(d)$ and $\mathbf{y}(a)$ [24–27], for example.

Thus the multicriterial target vector optimization allows the simultaneous minimization and/or maximization and/or the search for target values different from extremes of single variables within the total set of m responses via a maximization of the similarity of response vectors. In other words, multicriterial target vector optimization is a more general polyoptimization strategy in contrast to techniques that are dealing only with pure simultaneous maximization or with pure simultaneous minimization of all response variables. It should only be remarked that the correct weighting of the responses also determines the size of the distance D .

As stated in part I [24], not only the distance measure as a special optimization criterion but further the mathematical constraints, the means of obtaining the function f and the search technique used influence the success and the quality of a polyoptimization result. Especially the choice of the search technique is important for reaching the global or local optimum and if the k -dimensional search space can be checked representatively.

A newer search technique is the genetic algorithm (GA), developed by Holland [28,29] and recently also introduced into chemometrics. Kateman [30] placed the GA in general into the whole range of techniques using principles of natural evolution and parallel information processing such as learning expert systems and artificial neural networks (ANN).

Lucasius and co-workers [25–33] reported applications of the GA to optimize the fit between the structure of DNA molecules and their corresponding NMR spectra and also for wavelength selection problems in spectrometry. Bos and Weber [34] described the optimization of numerical parameters of an ANN with a GA and Fontain [35] discussed the use of GA for distance optimization of molecules in computer-aided synthesis design.

The use of the GA for multicriterial optimization of excitation parameters in atomic emission spectrometry was discussed in Part I [24]. It was found that the GA has a higher chance of reaching global optima at difficult structured response surfaces than classical search techniques.

The second important property of the GA, that of handling high-dimensional search spaces, will be discussed in this paper for the practical case of optimization of analytical procedures with m responses. High-dimensional search spaces exist when the number k of independent variables increases or/and if the resolution per variable increases. Then the search space size grows exponentially in k .

The target vector criterion was combined with a search technique based on a genetic algorithm for multicriterial optimization of the photometric calibration graph of a biochemical test strip for the determination of glucose in human blood. Attempts were made to optimize twelve chemical and technological parameters of the strip preparation to obtain simultaneously the desired sizes of six optical properties (responses) of the test strip.

This so-called indirect optimization via variation of the k independent variables was then compared with a direct multicriterial prediction on the basis of a classical and a non-linear partial least-squares (PLS) regression.

THEORY

The theory of multicriterial target vector optimization with different types of distance measures was discussed in detail in Part I [24]. The theory and practice of the genetic algorithm for

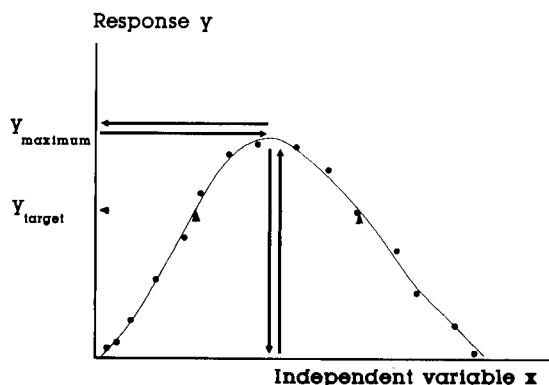


Fig. 1. A biunique solution for the (global) extremum (bold straight lines). For the target optimization problem (dotted lines) a non-biunique solution is obtained.

its use in multicriterial optimization was also outlined there. In this theoretical part, attention is focused more on the relationships, advantages and disadvantages of direct and indirect multicriterial optimization strategies.

From the univariate optimization problem in Fig. 1 it can be seen that for the exact (global) optimum no difference in the solutions between direct (deductive) and indirect (inductive) optimization strategy occurs (bold lines). According to the maximum, both projections behave bi-uniquely. However, if so-called target values are desired as optima other than from the extrema of the response function f , it becomes more difficult. Such a case is shown by the dotted lines in Fig. 1. A projection from x on to y via response function f yields in every case one solution. Sometimes it can be the same. A reverse projection from y on to x via f can yield for the given example two solutions. The situation is not longer biunique.

In the multiple case with $m = 1$ response variable y (Fig. 2) but $k > 1$ independent variables (x_1, \dots, x_k), a biunique projection for the global maximum can be found again. However, the number of possible target solutions can rise to infinity, obtained by the total number of all projections of the dotted curve on to the x_1 – x_2 plane. The number of target solutions is commonly also larger for a univariate or a multiple case with more than one optimum. Even for the case of

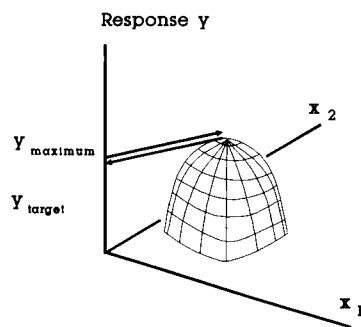


Fig. 2. Direct (deductive) optimization versus indirect (inductive) optimization of a multiple function $y = f(x_1, x_2, \dots, x_k)$. As in Fig. 1 the deductive strategy yields a non-biunique solution again in comparison with the inductive method.

unlimited periodic functions such as sine or cosine functions with an unlimited number of global optima, the number of target solutions is usually larger than the number of extremes.

Further generalization to $m > 1$ responses (multicriterial case) yields new problems: the individual optima of the m response variables can differ from each other according to their position in the X space (Fig. 3). As in the multiple case (Fig. 2), all of them can be obtained by an individual biunique projection. For the multicriterial global compromise maximum y_{\max} sometimes a biunique projection between the X and Y spaces can also exist. This depends on the overlaid

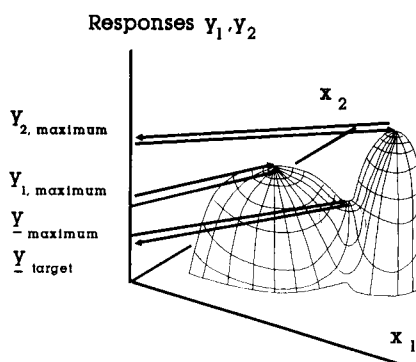


Fig. 3. Direct (deductive) optimization versus indirect (inductive) optimization of a multicriterial function (y_1, y_2, \dots, y_m) $= f(x_1, x_2, \dots, x_k)$. As in Figs. 1 and 2 the deductive strategy yields a non-biunique solution again in contrast to the indirect optimization, which gives a biunique (global) maximum y_{\max} .

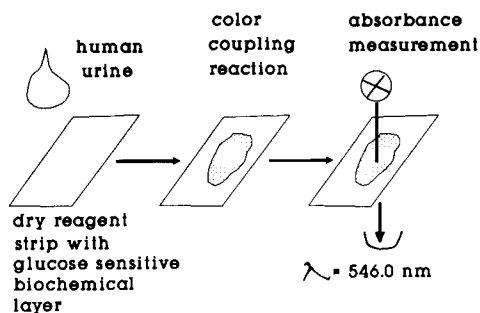


Fig. 4. The principle of the multicriterial optimized dry reagent test strip for the determination of human glucose in clinical analysis (see text for details).

functions y_1, y_2, \dots, y_m . In contrast to y_{\max} for the multicriterial compromise target vector optimum y_{target} , in most instances no biunique projection exists (Fig. 3, projection of the dotted curves on to the x_1 - x_2 plane).

Summarizing the theoretical considerations, it could be shown that the case of the target vector optimization problem is characterized much more often by a situation with disturbed biuniques between the two variables spaces than the case of the determination of classical optima, e.g., pure extrema. One way to overcome this problem is the so-called analytical solution. The extremes of

a multicriterial function (Eqn. 1) can sometimes be found by looking for the roots of the first derivative of f . One can try to find desired target values different from the pure extremes by filling the desired values $y(d)$ into f and trying to find the corresponding values $x(d)$. Thus the analytical solution is the most straightforward deductive strategy. However, if there is no way to invert f the optimization problem can be solved by the inductive strategy: stepwise variation of the x variables using an efficient and save search technique, predicting $y(a)$ for every actual search step $x(a)$ on basis of f and minimizing $D = y(d) - y(a)$.

EXPERIMENTAL

As a chemical example, the optimization of the slope and the shape of the photometric calibration graph for a biochemical dry reagent test strip for glucose determination in human urine was chosen (Fig. 4). The test strip consists of a polymer layer coated with a thin gelatine film containing a glucose-sensitive combination of different biochemical reagents [36]. The concentrations of these reagents and the chemical process parame-

TABLE 1

Names and ranges of experimentally varied chemical and process parameters (x -variables) and corresponding measured properties of the glucose strip (y -variables)

Name of x -variable	Abbreviation	Experimentally varied range	Name of y -variable	Experimentally measured range
Chromium acetate solution (5%)	CrAc	1.5–3.0 ml ^a	A5/4 ^c	0.175–0.321
Glucose oxidase	GOD	522–20 880 units ^a	A15/4 ^c	0.330–0.670
Peroxidase	POD	378–9450 units ^a	A25/4 ^c	0.385–0.930
Developer	Dev	120–480 mg ^a	A5/35 ^c	0.155–0.250
Ethylene glycol	EthGly	0–2475 ml ^a	A15/35 ^c	0.320–0.560
pH of the casting medium	pH-C	6.7–8.0	A25/35 ^c	0.360–0.820
pH of the dry film surface	pH-F	6.94–7.85		
Water absorption after 1 min	H ₂ O	0.88–2.49 mg cm ⁻¹		
Layer thickness	Thick	5.8–8.7 μm		
Support layer (1 = cellulose acetate, 2 = polyester)	Supp	1 or 2 ^b		
Conditions of drying (1 = slow, 2 = fast)	Dry	1 or 2 ^b		
Sodium sulphite	NaS	80–230 mg ^a		

^a The figures refer to 100 ml of casting medium in each cast. ^b 1 and 2 are used for processing nominal data. ^c A15/4 means the absorbance of 15 mmol l⁻¹ glucose at 546 nm after 6 weeks of keeping at 4°C.

ters for the preparation of the strips form in total $k = 12$ independent variables (Table 1). Chosen combinations of certain levels of these variables determine the shape and the slope of the calibration graph for a strip in a theoretical unpredictable way. Therefore, it was decided to follow a systematic empirical strategy.

The calibration graph for a given strip was characterized by $m = 6$ y variables: the photometric absorbances for the three glucose concentration levels of 5, 15 and 25 mmol l^{-1} for a constant temperature at 4°C and after artificial ageing (6 weeks at 35°C) for the same three glucose levels again. The aim of the study was now to approach an optimum parameter set $x(d)$ which yields via a function f according to Eqn. 1 a desired non-linear calibration graph $y(d)$ for both the low and high temperature range with absorbance values of

$$y(d) = \begin{pmatrix} y_1(d) \\ y_2(d) \\ y_3(d) \\ y_4(d) \\ y_5(d) \\ y_6(d) \end{pmatrix} = \begin{pmatrix} A5/4 \\ A15/4 \\ A25/4 \\ A5/35 \\ A15/35 \\ A25/35 \end{pmatrix} = \begin{pmatrix} 0.20 \\ 0.45 \\ 0.65 \\ 0.20 \\ 0.45 \\ 0.65 \end{pmatrix}$$

where $A1/2$ means the absorbance at 546.0 nm for a glucose concentration level 1 (mmol l^{-1}) for a constant temperature 2 (°C).

The preparation of the strips was carried out in two experimental steps: casting the films with variation of the presumably influencing parameters (Table 1) and cutting each film to a sufficient number of single strips for all investigations; and keeping two samples of the same film charge (represented by around 100 strips for one charge) for 6 weeks at two different temperatures (4 and 35°C), treatment of every charge with three glucose solutions (5, 15 and 25 mmol l^{-1}) and followed by the determination of the strip absorbance at 546 nm [ten parallel measurements with a Specol 20 spectrophotometer (Carl Zeiss, Jena, Germany)] giving the six y variables for every charge.

Keeping the samples for 6 weeks at 35°C simulates ageing for 1 year at room temperature. This

was done because a second aim of the optimization was that the shape of the calibration graph should be independent of the keeping temperature.

By combination of classical factorial designs with other designs formed on the basis of results of a principal component analysis (so-called multivariate design [36–38]), in total 104 carefully selected experiments were carried out for simultaneous variation of the levels of the $k = 12$ independent variables within the limits given in Table 1. The experimentally varied ranges of the independent variables resulted from experience and from some earlier manual experiments. Further details can be found in [36,39]. These 104 experiments led to two mutually dependent matrices: the data matrix $X_{104,12}$ of varied chemical and technological parameters and the data matrix $Y_{104,6}$ of corresponding measured calibration graphs per dry reagent strip. These two data matrices formed the basis for the following multicriterial optimization studies.

All multivariate calculations (PLS, MLR) were done by the program package MULTIVAR [40,41] on an IBM-PC. Part of the multicriteria optimization was carried out by the program package POLYOPT [42] as an exhaustive grid search on an IBM-PC under MS-DOS. The other part was done with a program formed by the Genetic Algorithms Library Toolbox GATES [43,44] and the evaluation function $1/D$ used on a Sun-Sparc workstation under the UNIX operating system.

RESULTS AND DISCUSSION

Deductive polyoptimization with partial least-squares regression

The application of the classical PLS method as a deductive polyoptimization technique to the data sets $X_{104,12}$ and $Y_{104,6}$ was limited by potentially three critical points: (i) a larger number than $k = 12$ independent variables had to be predicted from a smaller number of $m = 6$ dependent variables; (ii) the relationship f between the two data matrices was expected to be non-linear; and (iii) this seeming multivariate non-linearity can potentially disturb the necessary biunique-

ness between the data sets as outlined in the theoretical section.

The observed difference between the optimum predicted by classical PLS [45] and the experimentally realizable optimum as reported recently [36] seemed to support the individual expectations (i)–(iii). However, a detailed analysis of the eigenvalues and the loading of the estimated classical PLS model showed that the limitations (ii) and (iii) are more important than (i). The square roots of the PLS eigenvalues of the autoscaled data sets are 22.96, 6.02, 5.62, 2.49, 1.77 and 1.09. Hence the importance of the extracted latent PLS variables decreases with a ratio of approximately 4 : 1 : 0.9 : 0.3 : 0.2 : 0.05.

The first and most important pair of latent variables influences all six absorbances of the test strip simultaneously (Fig. 5). The other pairs of latent variables yield special corrections of the absorbances giving the characteristic non-linear shape and the temperature stability of the cali-

bration graphs. This result, that all six y variables are completely controlled by the first three to four latent PLS variables (Fig. 5a), in principle, and that nearly the full variance of the data sets is stored in those first few latent variables allows two backward-oriented conclusions.

The first conclusion is that only those x variables are important for the desired calibration graph which contribute to the first four latent variables. The other remaining x variables have a minor influence on the strip quality. Second, the result means that obviously sets of x variables have a correlated impact on the six response variables (Fig. 5b), despite the fact that they were varied independently from each other using an experimental design.

In the prediction step, such a set of x variables will be predicted together as a set of variables again. In other words, because of the special multivariate correlations within the data sets $X_{104,12}$ and $Y_{104,6}$, it can be concluded that the

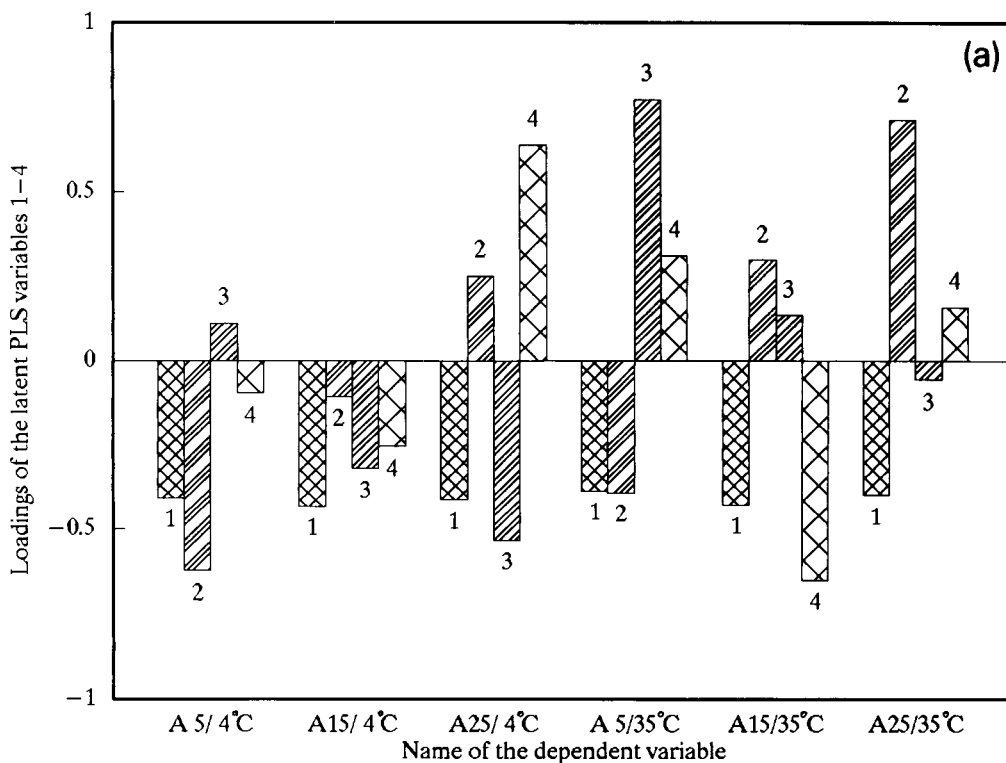


Fig. 5. Loadings of the original (a) six y - and (b) twelve x -variables on the most important four latent variables extracted from the classical PLS model from the data sets $Y_{104,6}$ and $X_{104,12}$.

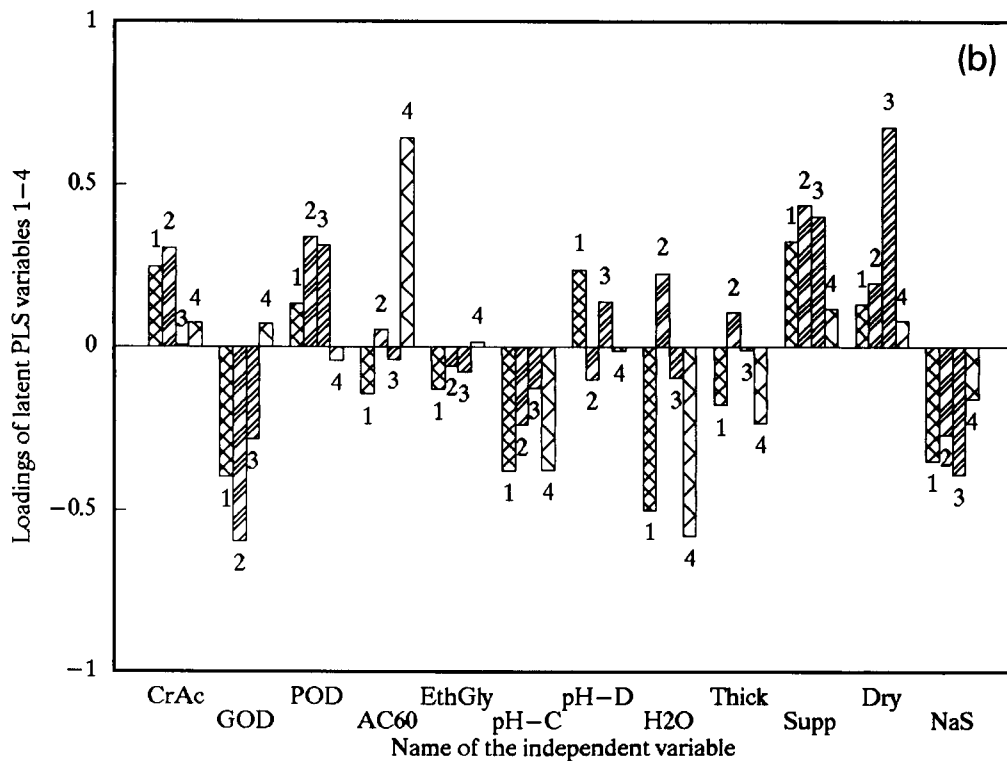


Fig. 5 (continued).

critical point (i), e.g., the prediction of twelve x variables on the basis of six y variables, can be ignored as a problem for those data sets. As an independent numerical security check for this hypothesis, a pseudo-non-linear PLS regression was performed. The data set $Y_{104,6}$ was extended by adding all fifteen binary interaction terms and the six pure squared terms giving in total a data matrix of $m = 27$ dependent variables. This number $m = 27$ now exceeded the number $k = 12$ of independent variables. Further, this introduction of additional second-order polynomial terms into the Y matrix with application of the classical PLS method (called PY-PLS) sometimes promises a more adequate fit to slightly non-linear data sets [46] attacking simultaneously with (i) also the second problem (ii) above.

A comparison of the x conditions used up to the optimization with the predicted optima (Table 2) on the basis of classical PLS, the realizable optimum, and on the basis of this PY-PLS, showed

that the main improvement could be achieved by a drastic decrease in the concentration of the enzyme glucose oxidase (GOD). The recently given biochemical interpretation of this PLS results was that a useless excess of GOD causes early ageing of the strips and in this way a continuous change in the calibration graph for the strip [36,39]. On the other hand, the absolute concentration values of 505 units predicted by classical PLS and of -720 units predicted by PY-PLS for GOD were found intuitively to be too low, i.e., biochemically meaningless.

Thus 1044 units for the GOD concentration were realized as a practically more useful level. All other variables were set in the laboratory verification experiment and in the pilot plant as found by classical PLS (Table 2). In this way test strips with the desired long-term thermal stability and the expected non-linear calibration graphs could be synthesized as reported recently [36]. This means in practice that the polynomial MLR

model (Table 3, Figs. 6 and 7) is more able than the classical PLS to predict the correct levels for the twelve x variables to obtain a temperature-stable calibration graph. As a consequence, an advanced PLS model (PX-PLS) which uses the same modified X matrix as the MLR model was applied to the data sets. Additionally, a further pseudo-non-linear PLS version was implemented by replacing the linear inner relationship with a second-order polynomial [47,48].

The results of pseudo-non-linear PLS with data matrices extended by polynomial terms (PY-PLS, PX-PLS) and with a second-order polynomial for the inner relationship (PP-PLS) show the same tendencies (Table 2) in the predictions as classical PLS: minimize the initial GOD concentration

and the ethylene concentrations, choose the fast drying mode DRY = 2 of the strip, use as the support layer SUPP = 2 (polyester material), etc. However, the absolute values predicted by the three non-linear PLS versions for GOD were found to be too low again and biochemically meaningless.

Summarizing the results of deductive polyoptimization with both classical and the pseudo-non-linear PLS models, it can be seen that the rank problem (i) can be solved and non-linearities (ii) can be treated by adapted PLS versions. The interpolation and the extrapolation of such non-linear models remains a dangerous step in general and should be avoided.

Additionally to this problem is the disturbed

TABLE 2

Comparison of the experimentally realized conditions for glucose test strip preparation before optimization with the predicted conditions after optimization by classical PLS, optimization by classical PLS with additional polynomial terms in the Y -matrix (PY-PLS) and in the X -matrix (PX-PLS) and polynomial PLS with second-order inner relationship (PP-PLS) ^a

	CrAc (ml)	GOD (units)	POD (units)	Dev (mg)	EthGly (ml)	pH-C	pH-D	H ₂ O (mg cm ⁻¹)	Thick (μ m)	Supp	Dry	NaS (mg)
Typical example before optimization	3	10440	1890	240	0.75	7	7.3	1.3–1.6	6.4–7.0	1	2	120
Predicted with PLS	3 ± 0.05	505 ± 1141	4001 ± 580	225 ± 5	0.74 ± 0.06	6.94 ± 0.05	7.5 ± 0.05	1.64 ± 0.05	7.2 ± 0.24	2 ± 0.15	1.6 ± 0.18	101 ± 13
Verification experiments												
Lab charge R ₁	3	1044	3800	225	0.75	7	7.51	1.52	8.0	2	2	100
Lab charge R ₂	3	1044	3800	225	0.75	7	7.61	1.41	7.1	2	2	100
Lab charge R ₃	3	1044	3800	260	0.75	7	7.5	1.34	6.8	2	2	100
Lab charge R ₄	3	1044	3800	225	0.75	7	7.5	1.58	7.8	2	2	100
Lab charge R ₅	3	1044	3500	225	0.75	7	7.66	1.46	7.5	2	2	100
Pilot plant control expt.	3	1566	3800	225	0.75	7	7.5	1.70	8.5	2	2	100
Predicted with PY-PLS	3.1 ± 0.05	-720 ± 1046	4425 ± 530	248 ± 15	0.78 ± 0.07	6.9 ± 0.04	7.5 ± 0.05	1.56 ± 0.04	7.2 ± 0.23	2.2 ± 0.14	2 ± 0.16	92 ± 11
Predicted with PX-PLS	3 ± 0.05	59 ± 1170	4030 ± 585	222 ± 15	0.68 ± 0.06	7 ± 0.05	7.5 ± 0.06	1.66 ± 0.04	7.3 ± 0.24	2 ± 0.15	1.7 ± 0.19	106 ± 13
Predicted with PP-PLS ^b	3 ± 0.05	333 ± 1100	3900 ± 490	220 ± 15	0.75 ± 0.06	6.87 ± 0.05	7.5 ± 0.05	1.65 ± 0.05	7.2 ± 0.23	2 ± 0.14	1.9 ± 0.17	100 ± 0.13

^a The conditions of the verification experiments done after the PLS optimization are also given. The confidence intervals of prediction (\pm) were approximated by cross-validation. ^b Original data sets without any added polynomial terms.

TABLE 3

Polynomial multivariate regression model for the 104 experimental data points, six dependent and twelve independent variables and two squared and four binary interaction terms

y	Intercept	CrAc pH-F GOD · GOD	GOD H ₂ O H ₂ O · Thick	POD Thick pH-C · H ₂ O	Dev Supp GOD · POD	EthGly Dry Dev · CrAc	pH-C NaS POD · POD
A5/4	$2.94552 \cdot 10^{-1}$	$-6.7388 \cdot 10^{-3}$ $1.10951 \cdot 10^{-2}$ $4.39602 \cdot 10^{-3}$ $-2.2682 \cdot 10^{-2}$	$6.42062 \cdot 10^{-2}$ $3.08577 \cdot 10^{-3}$ $-2.4210 \cdot 10^{-2}$	$3.83755 \cdot 10^{-2}$ $1.68062 \cdot 10^{-2}$ $2.43028 \cdot 10^{-2}$	$1.24733 \cdot 10^{-2}$ $1.79498 \cdot 10^{-2}$ $-6.3282 \cdot 10^{-3}$	$1.06748 \cdot 10^{-3}$ $-8.0684 \cdot 10^{-3}$ $4.81782 \cdot 10^{-2}$	$6.49459 \cdot 10^{-3}$ $-3.1011 \cdot 10^{-3}$
A15/4	$5.87667 \cdot 10^{-1}$	$-6.6624 \cdot 10^{-4}$ $2.12030 \cdot 10^{-2}$ $-6.9812 \cdot 10^{-3}$ $-5.1551 \cdot 10^{-2}$	$2.94308 \cdot 10^{-2}$ $-6.2058 \cdot 10^{-3}$ $-5.1977 \cdot 10^{-2}$	$-5.1930 \cdot 10^{-3}$ $8.37106 \cdot 10^{-2}$ $5.58876 \cdot 10^{-2}$	$3.72161 \cdot 10^{-2}$ $3.07169 \cdot 10^{-2}$ $-6.1353 \cdot 10^{-2}$	$9.46608 \cdot 10^{-3}$ $-7.6402 \cdot 10^{-3}$ $5.16195 \cdot 10^{-4}$	$-1.8793 \cdot 10^{-3}$ $3.15741 \cdot 10^{-3}$
A25/4	$7.92998 \cdot 10^{-1}$	$1.22195 \cdot 10^{-2}$ $6.10983 \cdot 10^{-3}$ $-1.1307 \cdot 10^{-2}$ $-1.1525 \cdot 10^{-1}$	$-7.3914 \cdot 10^{-2}$ $-7.1871 \cdot 10^{-3}$ $-1.0268 \cdot 10^{-1}$	$-1.2222 \cdot 10^{-1}$ $1.16627 \cdot 10^{-1}$ $1.04064 \cdot 10^{-1}$	$1.07343 \cdot 10^{-1}$ $3.92732 \cdot 10^{-2}$ $-1.6823 \cdot 10^{-1}$	$1.22244 \cdot 10^{-2}$ $-6.6063 \cdot 10^{-4}$ $-1.2720 \cdot 10^{-1}$	$-1.2799 \cdot 10^{-2}$ $1.57017 \cdot 10^{-2}$
A5/35	$2.57727 \cdot 10^{-1}$	$-6.5504 \cdot 10^{-3}$ $1.88586 \cdot 10^{-3}$ $5.46664 \cdot 10^{-4}$ $-2.4567 \cdot 10^{-2}$	$3.84279 \cdot 10^{-2}$ $-1.2294 \cdot 10^{-3}$ $-2.9051 \cdot 10^{-2}$	$2.79137 \cdot 10^{-2}$ $1.45249 \cdot 10^{-2}$ $1.77412 \cdot 10^{-2}$	$1.89933 \cdot 10^{-2}$ $1.23935 \cdot 10^{-2}$ $2.53629 \cdot 10^{-3}$	$2.53392 \cdot 10^{-3}$ $-3.3727 \cdot 10^{-3}$ $3.15507 \cdot 10^{-2}$	$7.33487 \cdot 10^{-3}$ $1.84913 \cdot 10^{-3}$
A15/35	$4.97370 \cdot 10^{-1}$	$-4.7199 \cdot 10^{-3}$ $-1.0128 \cdot 10^{-2}$ $-3.4816 \cdot 10^{-4}$ $-5.4247 \cdot 10^{-2}$	$3.72093 \cdot 10^{-3}$ $-1.0675 \cdot 10^{-3}$ $-5.8509 \cdot 10^{-2}$	$-3.2711 \cdot 10^{-3}$ $9.83987 \cdot 10^{-2}$ $4.94254 \cdot 10^{-2}$	$2.57522 \cdot 10^{-2}$ $2.24904 \cdot 10^{-2}$ $-4.1943 \cdot 10^{-2}$	$2.18397 \cdot 10^{-3}$ $1.76268 \cdot 10^{-3}$ $-5.7852 \cdot 10^{-3}$	$-1.3629 \cdot 10^{-3}$ $-2.4250 \cdot 10^{-3}$
A25/35	$6.95756 \cdot 10^{-1}$	$2.89603 \cdot 10^{-3}$ $-3.7112 \cdot 10^{-2}$ $-1.1005 \cdot 10^{-3}$ $-1.2553 \cdot 10^{-1}$	$-7.8908 \cdot 10^{-2}$ $-1.3917 \cdot 10^{-3}$ $-1.0694 \cdot 10^{-1}$	$-8.2873 \cdot 10^{-2}$ $1.72733 \cdot 10^{-1}$ $1.08731 \cdot 10^{-1}$	$9.47050 \cdot 10^{-2}$ $3.90166 \cdot 10^{-2}$ $-6.8523 \cdot 10^{-2}$	$-6.8387 \cdot 10^{-3}$ $5.06819 \cdot 10^{-3}$ $-9.1130 \cdot 10^{-2}$	$-6.0565 \cdot 10^{-3}$ $2.09326 \cdot 10^{-2}$

biuniqueness, which cannot simply be rejected by some modifications of the existing PLS theory. The only way to overcome this problem [(iii); see

p. 257] and to overcome the danger of an arbitrary extrapolation is a reverse strategy, i.e., inductive polyoptimization.

TABLE 4

Results of multicriterial target vector optimization with grid search using variables resolution RES = 3 and RES = 5 between the runs but constant variables resolution within the runs^a

RES	Grid size	1/D	CrAc (ml)	GOD (units)	POD (units)	Dev (mg)	EthGly (ml)	pH-C	pH-D	H ₂ O (mg cm ⁻¹)	Thick (μm)	Supp	Dry	NaS (mg)
3	531 441	50.0	3.0	522	4914	120	0.00	6.70	7.40	1.685	8.70	2.0	2.0	155.25
5	244 140 625	89.5	3.0	5611	4914	120	0.00	6.70	7.16	1.685	5.80	2.0	1.0	80.50
Corresponding predicted responses														
			A5/4	A15/4	A25/4	A5/35	A15/35	A25/35						
3			0.2020	0.4531	0.6532	0.1844	0.4404	0.6541						
5			0.2057	0.4555	0.6472	0.1943	0.4462	0.6475						

^a 1/D = reciprocal Euclidian distance of that best member of the whole search population that is the closest to the desired target vector $y(d)$.

Inductive polyoptimization with grid search and genetic algorithm

The verified MLR model (Table 3, Figs. 6a,b and 7a,b) was introduced into the grid search module of POLYOPT [38] together with the inverted Euclidian distance $1/D$ as measure of fitness. Because of the significant size of the higher order terms in the MLR model and their different signs, a response surface with numerous local optima was expected.

Grid searching as an exhaustive technique was applied to obtain a raw overview of the twelve-dimensional hypersurface with the advantage of acquiring all local and the global polyoptima corresponding a chosen resolution, RES.

The only, but major, disadvantage of exhaustive searching is the exploding size of the search

space size S :

$$S = \prod_{j=1}^k (\text{RES})_j \quad (2)$$

as a product of the single resolutions of the k variables. The grid sizes for RES = 3 and RES = 5 (Table 4) yield a large number of search positions. By evaluation of 500 grid positions per minute with POLYOPT on an IBM-PC (Intel 80486, 33 MHz), the case for RES = 5 required 34 days of computing time. This experiment was done also to control the results of GATES.

For GATES the same MLR model (Table 3) was used and also the inverted Euclidian distance as measure of fitness. Further parameter settings of the GA program are given in Table 5.

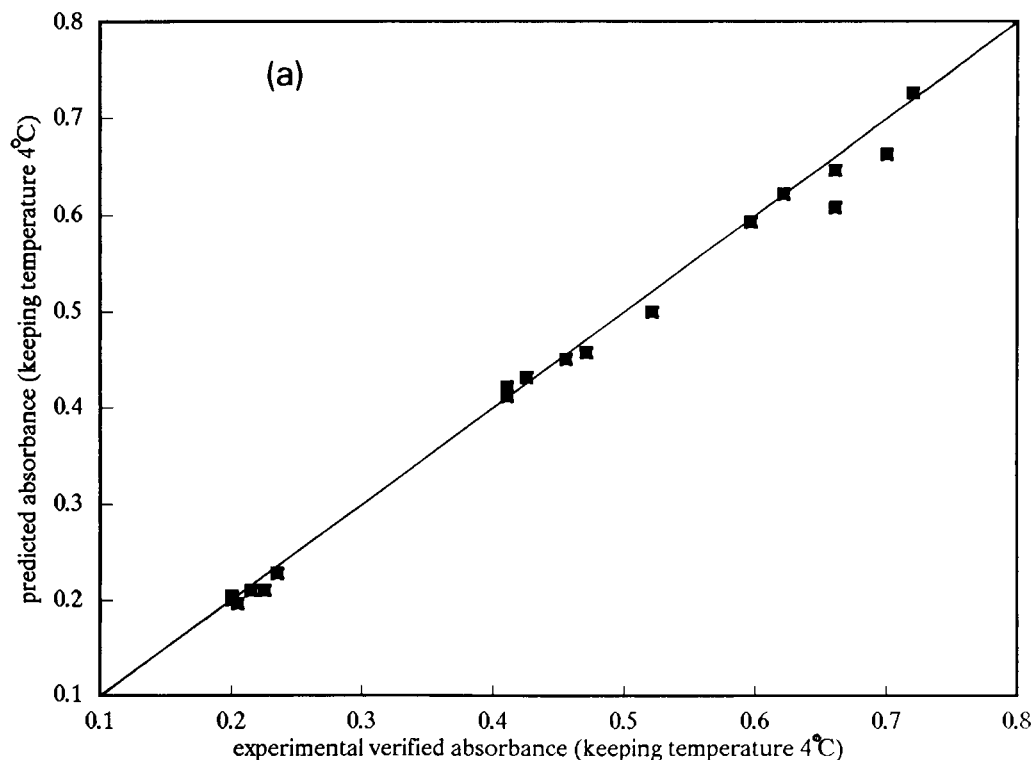


Fig. 6. Independent validation of the predictive power of the developed multivariate polynomial regression model (MLR) by plotting the results for all six response variables simultaneously obtained by five additional control experiments in a laboratory- and one large-scale experiment in a pilot plant (see also Table 4) versus the values for the six response variables predicted by the MLR. The calibration of the model was carried out with 104 designed experiments. Keeping temperature: (a) 4°C; (b) 35°C.

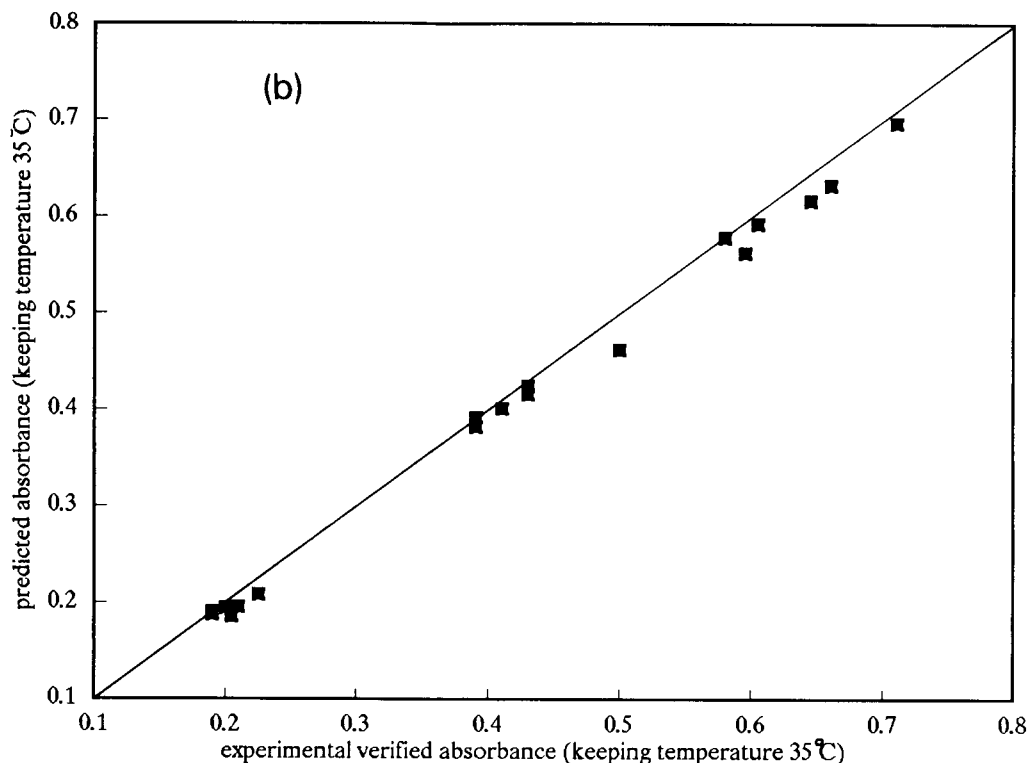


Fig. 6 (continued).

The computation time for the corresponding GA run for RES = 5 at a SunSparc Workstation was a few minutes of real time. A transformation of this time corresponds to approximately 1 h on the personal computer used for POLYOPT. After this hardware correction the gain in computing time by the use of the genetic algorithm in contrast to the grid search was at least 1:800 for RES = 5. This gain in computing time increases exponentially with a linear increase in RES.

For the resolution RES = 5 the same global optimum was detected by GATES as by an exhaustive search with POLYOPT (Tables 4 and 6). A useful graphical expression for the convergence control of the GA is the running measure of fitness $1/D$ (Fig. 8).

The polyoptimum obtained for the poor resolution of RES = 3 (Table 4) already shows a close similarity to the results obtained with the PLS versions (Table 2) using the experimental ranges per variable as a basis for a comparison (Table 1).

Going now from resolution RES = 3 to a higher value RES = 5 (Table 4), larger changes only for the variables GOD, layer thickness, drying conditions and sodium sulphate can be observed. The low variable resolutions of 3 and 5 are not valid yet for a fair competition with the PLS techniques. PLS, in principle, samples the X space continuously. Therefore, the discrete resolution of the search space for the GA was increased up to 7 bits, e.g., $128 + 1$ levels per variable. Such an increase allows nearly continuous sampling of the X space during the search.

On the other hand, this increase in resolution potentially also can increase the number of dangerous local optima rapidly. To overcome this problem partially, all runs of the GA presented in Table 6 were repeated five times independently with different initial parameter settings. Thus the predicted optima (Table 6) came close to the PLS predictions, in general, but the initial GOD concentrations were now predicted also with a low

tendency, i.e., 3728 units, but biochemically much more meaningful than with PLS.

However, as shown experimentally in Part I [20], the GA provides no guarantee of finding the global optimum, but potentially it has a higher chance of reaching global optima than the search techniques known up to now. In addition to the repetition of a run, in practice the possibility exists of choosing an individually adapted search step width per single variable based on physically and chemically reasonable interval sizes and based on the expected individual experimental error of the considered x variable. In this way a drastic reduction of the search space takes place but keeping the important information. The global optima can be reached more easily. The results of such an experiment confirm this hypothesis with rapidly improved measures of fitness (Table 7). All predicted optimum levels of the variables also

came closer to the PLS predictions but the GOD remained at a meaningful level of around 3600 units.

It should further be remarked that all inductive optimization runs with POLYOPT and GATES were performed within the experimentally given individual variables ranges (Table 1), which means an interpolation only during the search via the MLR model (Table 3) as a less dangerous mathematical operation in contrast to an arbitrary extrapolation. Such an extrapolation sometimes happens by application of a deductive strategy such as PLS if this is necessary to reach the desired polyoptimum.

Conclusions

Multicriterial target optimization can in principle be carried out in two ways. First, one can try to project directly a desired vector of the re-

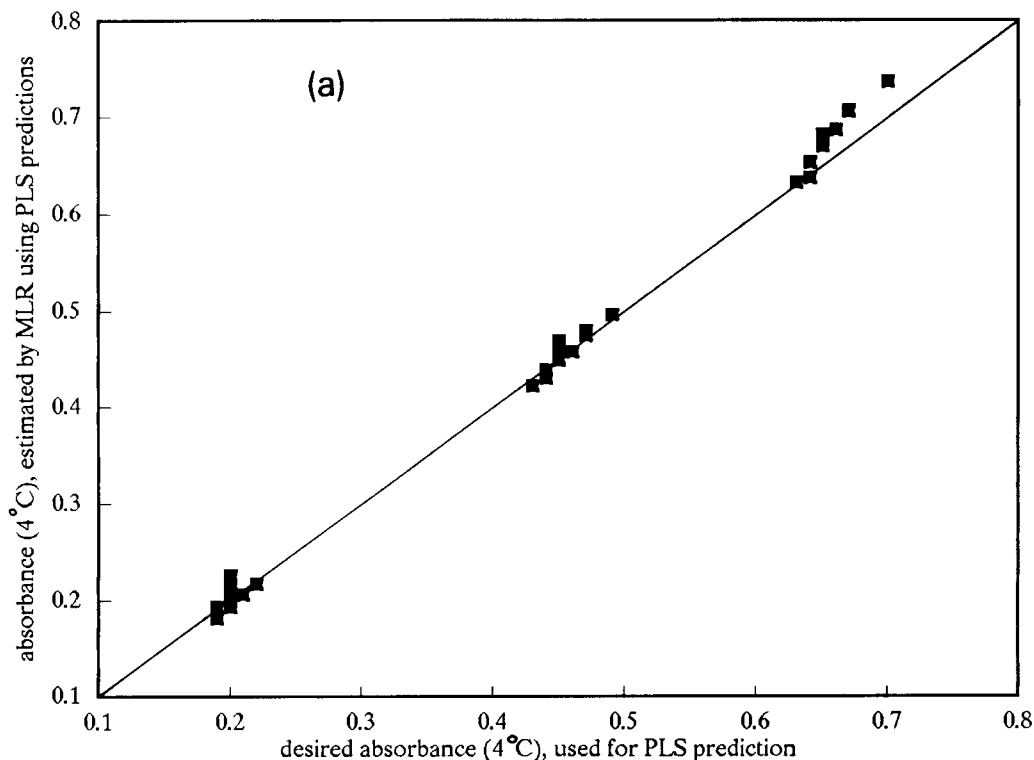


Fig. 7. Comparison of the predictive power of the classical PLS model with that of the multivariate polynomial regression model (MLR) for all six response variables simultaneously for five additional control experiments in a laboratory- and one large-scale experiment in a pilot plant (see also Table 4). The calibration of both models was carried out with 104 designed experiments. Temperature: (a) 4°C; (b) 35°C.

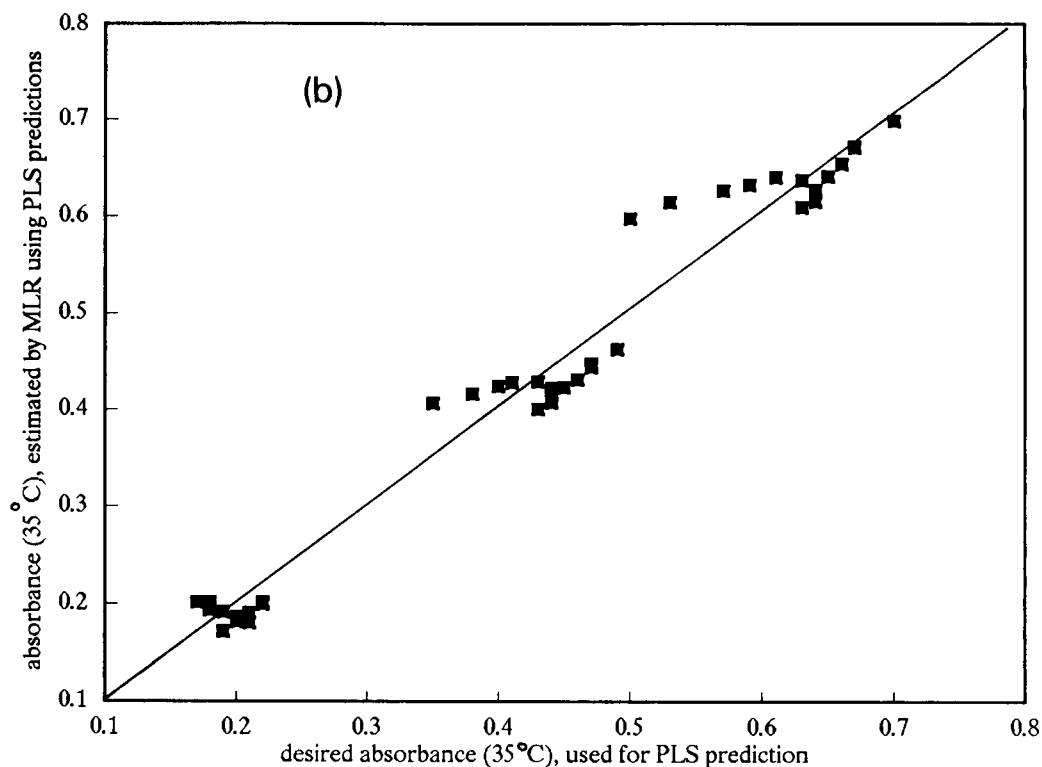


Fig. 7 (continued).

TABLE 5

Set-up parameters and their practical meaning for the genetic algorithm toolbox GATES used for the multicriterial optimization of the glucose data ^a

Algorithmic variable	Setting	Practical meaning
No. of bitstrings	400	Size of the search population
Bitstring format	[0–9,*]; $k \cdot \text{RES}$	k bitstrings with resolution RES, 0–9 bits
Level count	128	Digitization of every variable
Gray coding	Yes	Others: binary, natural coding
Max. number of generations	1500	Optimization search steps
Fitness blow-up	3.0	Dynamic evaluation of fitness quality
Enforced relative best fitness	9.0	
Elitist count	20	Control of selective reproduction
Mutation probability (start/end/rate)	0.01/0.01/0.0	During all generations constant 1% of the strings mutate
Cross swap	Segmented	How the strings exchange their information; alternative: uniform
Cross swap probability (start/end/rate)	0.10/0.10/0.00	Bits are swapped if $P > 1\%$ and with constant probability
Cross mate probability (start/end/rate)	0.95/0.95/0.00	
Sharing feel scope	No share	Population may not split into subpopulations during search
Sharing feel blow-up	2.0	No meaning if no share allowed
Sharing probability	0.5/0.5/0.0	No meaning if no share allowed

^a For further theoretical details see also [28,29].

TABLE 6

Results of multicriterial target vector optimization with the genetic algorithm using increasing variables resolution RES between the runs but constant variables resolution within the runs ^a

RES	1/D	Generations	CrAc (ml)	GOD (units)	POD (units)	Dev (mg)	EthGly (ml)	pH-C	pH-D	H ₂ O (mg cm ⁻¹)	Thick (μm)	Supp	Dry	NaS (mg)
5	89.5	129	3.0	5611	4914	120	0.0	6.7	7.16	1.68	5.8	2.00	1.00	80.5
9	90.4	151	3.0	5611	4914	120	0.0	6.7	7.05	1.68	5.8	2.00	1.00	80.5
17	90.1	707	2.6	4339	5481	120	0.3	6.7	7.73	1.78	6.0	1.93	1.56	80.5
129	107.8	1197	2.5	3728	5236	134	0.0	6.7	7.22	1.79	5.8	1.91	1.91	81.6
Corresponding predicted responses														
			A5/4	A15/4	A25/4			A5/35		A15/35			A25/35	
5			0.2057	0.4555	0.6472			0.1943		0.4462			0.6475	
9			0.2050	0.4571	0.6490			0.1946		0.4465			0.6478	
17			0.2077	0.4558	0.6494			0.1946		0.4493			0.6499	
129			0.2003	0.4548	0.6509			0.1950		0.4442			0.6483	

^a 1/D = reciprocal Euclidian distance of that best member of the whole search population that is the closest to the desired target vector $y(d)$.

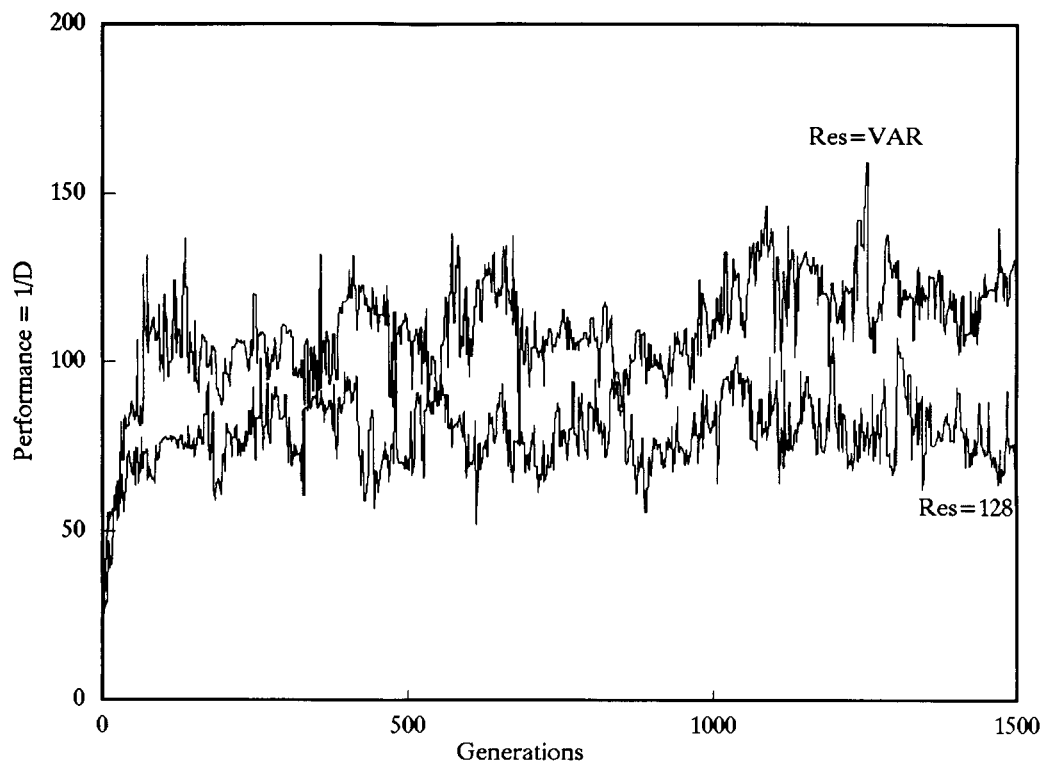


Fig. 8. The inverse Euclidian distance $1/D$ as measure of fitness between the desired response vector $y(d)$ and the best response vector $y(a)$ really reached during the search for an actual search position (a) in the twelve-dimensional x -variables space using the genetic algorithm.

response variables via a response surface model function f on to the space of independent variables. This is called direct or deductive polyoptimization and can be performed in practice with, for example, an inverse multivariate regression technique such as partial least-squares regression. The other possibility is the search in the \mathbf{X} space, predicting the $\mathbf{y}(a)$ vector for the actual search position and comparing it with a desired response vector $\mathbf{y}(d)$, for example, on the basis of a vector distance measure. This search can be carried out by multicriteria target vector optimization with a genetic algorithm as an efficient search method.

The advantage of the first strategy is that it works straightforwardly and that it requires one step for the estimation of the model and one step for the prediction of the optimum vector $\mathbf{x}(o)$ as an approximation of the desired $\mathbf{x}(d)$. A disadvantage of this deductive strategy is that it can only be applied if a biunique relationship between \mathbf{Y} and \mathbf{X} space exists. Another disadvantage is the potential danger of an arbitrary, difficult to control and not allowed extrapolation of the \mathbf{X} space to reach the desired polyoptimum.

If the necessary biuniqueness is disturbed, the

inductive strategy helps to find $\mathbf{x}(o)$. A search in the \mathbf{X} space can always be performed. A further advantage is that interpolation and extrapolation of the \mathbf{X} space can be strictly controlled.

Disadvantages of the inductive polyoptimization strategy are that it requires, like the deductive strategy, only one step also for the estimation of the response model function but numerous repetitions of the prediction step during the optimization search for the comparison of $\mathbf{y}(d)$ and $\mathbf{y}(a)$. Hence the inductive strategy is more time consuming in general. This happens especially if the number of search positions rises with an increase in the number of variables and/or an increase in the resolution of the variables. This disadvantage can be partly compensated by the GA as a parallel and evolutionary search technique, as was shown for the described optimization problem of dry reagent strips. The second problem for the indirect polyoptimization strategy is undesirable local optima. For this situation the GA also offers a practical solution.

Summarizing the results in Part I and this paper, it can be concluded that multicriteria target vector optimization on the basis of a suitable

TABLE 7

Results of five independent repeated runs of the multicriterial target vector optimization with the genetic algorithm using individual variables resolution and different numbers of generations ^a

Run	1/D	Generations	Individual resolution (step width)													
			128	128	64	64	32	128	64	128	64	4	4	64		
			CrAc (ml)	GOD (units)	POD (units)	Dev (mg)	EthGly (ml)	pH-C	pH-D	H ₂ O (mg cm ⁻¹)	Thick (μm)	Supp	Dry	NaS (mg)		
1	138.3	571	2.5	3565	5993	154	0.0	6.7	7.44	1.80	5.9	2.00	2.00	85.2		
2	159.3	1250	2.9	3728	5562	143	0.1	6.7	7.20	1.82	5.8	2.00	2.00	84.0		
3	145.6	998	2.8	3565	5993	149	0.0	6.7	7.30	1.86	5.8	2.00	2.00	81.7		
4	154.9	209	3.0	3565	6424	160	0.0	6.7	7.18	1.86	5.8	2.00	2.00	84.0		
5	154.1	1204	2.7	3565	6139	160	0.0	6.7	7.37	1.84	5.8	2.00	2.00	87.5		
			Corresponding predicted responses													
			A5/4			A15/4			A25/4			A5/35		A15/35		A25/35
1			0.2037			0.4537			0.6496			0.1965		0.4464		0.6504
2			0.2032			0.4531			0.6486			0.1967		0.4475		0.6512
3			0.2025			0.4536			0.6488			0.1953		0.4480		0.6500
4			0.2024			0.4546			0.6495			0.1963		0.4492		0.6504
5			0.2026			0.4528			0.6502			0.1953		0.4478		0.6505

^a The individual variables resolutions were chosen with respect to their importance and impact on the y -variables seen from the size of the PLS loadings. $1/D$ = reciprocal Euclidian distance of that best member of the whole search population that is the closest to the desired target vector $\mathbf{y}(d)$.

similarity measure between desired and actual response vectors and combined with a GA search technique is a powerful tool for optimizing simultaneously a set of responses of an analytical procedure or of a chemical product as discussed on the examples from atomic emission spectrometry and of the photometric calibration graph for a glucose test strip for clinical analysis.

REFERENCES

- S.L. Morgan and S.N. Deming, *J. Chromatogr.*, 112 (1975) 267.
- R.J. Laub and J.H. Purnell, *J. Chromatogr.*, 112 (1975) 71.
- B. Sachok, R.C. Kong and S.N. Deming, *J. Chromatogr.*, 199 (1980) 317.
- J.L. Glajch, J.J. Kirkland, K.M. Squire and J.M. Minor, *J. Chromatogr.*, 199 (1998) 57.
- C.E. Goewie, *J. Liq. Chromatogr.*, 9 (1986) 1431.
- P.J. Schoenmakers, *J. Liq. Chromatogr.*, 10 (1987) 1865.
- D.L. Massart, B.G.M. Vandeginste, S.N. Deming, Y. Michotte and L. Kaufman, *Chemometrics—a Textbook Elsevier*, Amsterdam, 1988.
- P.J. Schoenmakers, *Optimization of Chromatography Selectivity*, Elsevier, Amsterdam, 1986.
- W. Wittkowski and J. Lütke, *Chem. Technol.*, 36 (1984) 117.
- S.N. Deming, *J. Chromatogr.*, 550 (1991) 15.
- H.R. Keller, D.L. Massart and J.P. Brans, *Chemometr. Intell. Lab. Syst.*, 11 (1991) 175.
- B. Bourguignon and D.L. Massart, *J. Chromatogr.*, 586 (1991) 11.
- G.L. Moore, P.J. Humphries-Cuff and A.E. Watson, *Spectrochim. Acta, Part B*, 39 (1984) 915.
- H.A. Spaink, T.T. Lub, G. Kateman and H.C. Smit, *Anal. Chim. Acta*, 184 (1986) 87.
- R.M. Belchamber, D. Betteridge, A.P. Wade, A.J. Cruickshank and P. Davison, *Spectrochim. Acta, Part B*, 41 (1986) 503.
- G.S. Pyen, S. Long and R.F. Browner, *Appl. Spectrosc.*, 40 (1986) 264.
- M.S. Hendrick and R.G. Michel, *Anal. Chim. Acta*, 192 (1987) 183.
- L. Ebdon, P. Norman and S.T. Sparkes, *Spectrochim. Acta, Part B*, 426 (1987) 619.
- P. Werner and H. Friege, *Appl. Spectrosc.*, 41 (1987) 32.
- O.A. Guell and J.A. Holcombe, *Spectrochim. Acta, Part B*, 43 (1987) 459.
- B. Naumann, B. Knull, F. Kerstan and J. Opfermann, *J. Anal. At. Spectrom.*, 3 (1988) 1121.
- S. Greenfield, M.S. Salman, M. Thomson and J. Tyson, *J. Anal. Atom. Spectrom.*, 4 (1989) 55.
- D. Wienke and K. Danzer, *Fresenius' Z. Anal. Chem.*, 342 (1992) 1.
- D. Wienke, C. Lucasius and G. Kateman, *Anal. Chim. Acta*, 265 (1992) 211.
- L.E.S. Khuri and F.U. Conion, *Technometrics*, 23 (1981) 363.
- D. Wienke and K. Danzer, presented at Euroanalysis VII/COBAC V, Vienna, 1990.
- D. Wienke, in J. Havel and M. Meloun (Eds.), *Proc. 2nd Czechoslovakian Conference on Chemometrics*, University of Brno, 1990, p. 34.
- J.H. Holland, *Adaptation in Natural and Artificial Systems*, University of Michigan Press, Ann Arbor, MI, 1975.
- D.E. Goldberg, *Genetic Algorithms in Search, Optimization and Machine Learning*, Addison-Wesley, Reading, MA, 1989.
- G. Kateman, *Analyst*, 115 (1990) 487.
- C.B. Lucasius and G. Kateman, in J.D. Schaffer (Ed.), *Third International Conference on Genetic Algorithms*, Morgan Kaufmann, San Mateo, CA, 1989, p. 170.
- C.B. Lucasius, M.J.J. Blommers, L.M.C. Buydens and G. Kateman, in L. Davis (Ed.), *Handbook of Genetic Algorithms*, Van Nostrand Reinhold, New York, 1991, p. 251.
- C.B. Lucasius and G. Kateman, *Trends Anal. Chem.*, 10 (1991) 254.
- M. Bos and H.T. Weber, *Anal. Chim. Acta*, 247 (1991) 97.
- E. Fontain, *Anal. Chim. Acta*, 265 (1992) 226.
- M. Ehrlich, D. Wienke, K. Danzer and G. Kateman, *Fresenius' J. Anal. Chem.*, 343 (1992) 532.
- S. Wold, M. Sjöström, R. Carlson, T. Lundstedt, S. Hellberg, B. Skagerberg, W. Wikström and J. Ohmann, *Anal. Chim. Acta*, 191 (1986) 17.
- D. Wienke, K. Danzer, M. Gitter, J. Aures, U. Münch, H.G. Byhan and H.J. Pohl, *Anal. Chim. Acta*, 223 (1989) 247.
- M. Ehrlich, PhD Thesis, University of Jena, in preparation.
- D. Wienke, *MULTIVAR*, Software Package for Multivariate Data Analysis, User Documentation, University of Jena, Jena, 1990.
- D. Wienke, PhD Thesis, University of Jena, 1990.
- D. Wienke, *POLYOPT—Program Multicriteria Target Vector Optimization*, User Documentation, 1991 unpublished.
- C.B. Lucasius and G. Kateman, *Comput. Chem.*, submitted for publication.
- C.B. Lucasius, PhD Thesis, University of Nijmegen, in preparation.
- M.A. Sharaf, D.L. Illman and B.R. Kowalski, *Chemometrics*, Wiley, New York, 1986.
- S. Clementi, G. Cruciani, G. Curti and B. Skagerberg, *J. Chemometr.*, 2 (1989) 499.
- S. Wold, N. Kettaneh-Wold and B. Skagerberg, *Chemometr. Intell. Lab. Syst.*, 7 (1989) 53.
- V.M. Taavitsainen and P. Korhonen, *Chemometr. Intell. Lab. Syst.*, 14 (1992) 185.

Application of informational analysis of variance in analytical chemistry

C. Sârbu

Department of Analytical Chemistry, Babeş-Bolyai University, R-3400 Cluj-Napoca (Romania)

(Received 27th February 1992; revised manuscript received 1st June 1992)

Abstract

The fundamentals of informational statistics are explained with regard to their importance for analytical chemistry. Informational statistics, like robust statistical techniques, are resistant against uncertainties concerning the data, such as outliers or divergences from the normal distribution. Using a new informational function, namely informational energy, the null hypothesis was tested to decide whether a certain factor has a significant effect on the results.

Keywords: Analysis of variance; Informational statistics

In any experiment two or more methods (laboratories) yield generally more or less different results, because analytical determinations may be influenced by basic factors (qualitative or quantitative) that control the conditions of experiment and also by random factors.

It is the objective of analysis of variance (ANOVA) to investigate the several kinds of factors, operating simultaneously, and to decide which are important and to estimate their effects. ANOVA assumes the additivity of variances of random variables due to the effects of independent factors. It is used to break down the total variance into its components, i.e., into a sum of several distinct components, each corresponding to a source of variance.

The F -tests that are subsequently made are determined from the ratios of these respective components. The F ratio can then be compared with tabulated F values using the degrees of

freedom corresponding to the numerator and denominator for each F ratio. If the observed F ratio exceeds the tabulated value at the chosen confidence level, then one would conclude statistical significance at this level of confidence. If, on the other hand, the calculated value of the F ratio is smaller than that given in tables, the factor in question does not affect the mean value.

When applying ANOVA one assumes that the overall errors are normally distributed, the errors are statistically independent and the errors have the same variance. Often the homogeneity of variance is not respected and in such instances ANOVA could lead to erroneous conclusions if methods with widely differing precisions are compared.

The analysis of variance can be applied in several distinct forms, according to the structure of the process being investigated. Excellent discussions of this topic were presented by Hirsch [1] and by Massart and co-workers [2,3].

In this work, using a new informational function, namely informational energy, the null hypothesis was tested to decide whether a certain factor has a significant effect on the results.

Correspondence to: C. Sârbu, Department of Analytical Chemistry, Babeş-Bolyai University, R-3400 Cluj-Napoca (Romania).

THEORY

The informational energy (IE) concept and its detailed theoretical study as well as its implications in the field of mathematics called “informational statistics” was introduced by Onicescu [4] and Onicescu and Stănescu [5]. It is well known by chemometricians from information theory that the Shannon entropy may be calculated using the observed frequencies [2–6]:

$$H(A) = - \sum_{i=1}^n f_i \log_2 f_i \quad (1)$$

Onicescu observed that $H(A)$ is the mean value of logarithm to base 2 of all probabilities (frequencies) and he addressed the question of whether the mean value of probabilities (frequencies)

$$E = \sum_{i=1}^n p_i^2 \approx \sum_{i=1}^n f_i^2 \quad (2)$$

could not be a function “with similar characteristics of representation like Shannon’s entropy”. Onicescu named it informational energy (IE). Moreover, for a system having a continuous distribution function, one can write

$$E = \int_{-\infty}^{+\infty} \rho^2(x) dx \quad (3)$$

where

$$\rho(x) = dF(x)/dx \quad (4)$$

is the derivative of the distribution function of information, and hence an exactly particular form of energy [6].

IE describes with the same success as Shannon’s entropy the uniformity or diversity of a system, process or phenomenon. IE is more sensitive in a certain way than the entropy to modifications of the system. Moreover, this informational function permits the calculation of the informational correlation (IC) and the informational correlation coefficient (ICC), parameters of interest in analytical chemistry.

Informational energy and correlation

The IE of a finite set of events or states A_1, A_2, \dots, A_n each having a associated probabil-

ity p_1, p_2, \dots, p_n with $p_i \geq 0$ and $\sum_{i=1}^n p_i = 1$ is given by

$$E_{(p_1, p_2, \dots, p_n)} = \sum_{i=1}^n p_i^2 \quad (5)$$

According to Mihoc’s considerations [7] concerning the estimation of IE, if the probabilities p_i ($i = 1, 2, \dots, n$) of a finite set of states are estimated by relative frequencies f_i of a real experiment, then the empirical IE may be calculated with the following expression:

$$E(f_1, f_2, \dots, f_n) = \sum_{i=1}^n f_i^2 \quad (6)$$

Equations 5 and 6 give information concerning the degree of organization of a system or the mode of partition of its elements. Defined in this way, IE reveals some remarkable properties. First, it reaches its minimum value when all the probabilities are equal ($p_1 = p_2 = \dots = p_n$), i.e., the case of totally unorganized systems:

$$E_{(p_1, p_2, \dots, p_n)} = 1/n \quad (7)$$

If $p_k = 1$ and $p_{i \neq k} = 0$, i.e., the case with well organized systems, then IE is

$$E_{(p_1, p_2, \dots, p_n)} = 1 \quad (8)$$

Hence it results that the possible values for IE are between $1/n$ and 1.

It is also interesting that Cresin [8], applying IE in biology, demonstrated that it is more useful to consider the normalized informational energy, i.e.,

$$E' = \frac{\sum_{i=1}^n f_i^2 - (1/n)}{1 - (1/n)} \quad (9)$$

It is obvious that in this case the possible values of E' are between 0 and 1 and do not depend on n .

In the particular case of a set of two finite systems of events A_1, A_2, \dots, A_n and B_1, B_2, \dots, B_m , each with probability p_1, p_2, \dots, p_n and q_1, q_2, \dots, q_m , respectively, q_{ij} is the conditional probability of the event B given event A , i.e.,

$$q_{ij} = P(B_j | A_i) \quad (10)$$

The *IE* of the system of events B_1, B_2, \dots, B_m conditioned by the occurrence of the integral system of events A_1, A_2, \dots, A_n , the so-called “conditional informational energy” (*CIE*) is defined by

$$E_{(B_1, B_2, \dots, B_m | A_1, A_2, \dots, A_n)} = \sum_{i=1}^n \sum_{j=1}^m p_i^2 q_{ij}^2 \quad (11)$$

When the two systems are independent, the *IE* of the system of events (A_i, B_j) will be

$$E_{(A_i, B_j)} = E_{(A_1, A_2, \dots, A_n)} \times E_{(B_1, B_2, \dots, B_m)} \quad (12)$$

This means that *IE* is multiplicative and not additive as Shannon’s entropy.

The informational correlation (*IC*) between two systems (probabilistic partitions) has the following equation:

$$C_{(p_1, p_2, \dots, p_n; q_1, q_2, \dots, q_n)} = \sum_{i=1}^n p_i q_i \quad (13)$$

The *IC* is always positive, but < 1 , being zero if and only if all $p_i q_i$ are zero, i.e., the two systems are “indifferent”.

By the normation of correlation, similar to the statistical correlation coefficient, an informational correlation coefficient (*ICC*) may be obtained:

$$r_{(p_1, p_2, \dots, p_n; q_1, q_2, \dots, q_n)} = \frac{C_{(p_1, p_2, \dots, p_n; q_1, q_2, \dots, q_n)}}{E_{(p_1, p_2, \dots, p_n)} \times E_{(q_1, q_2, \dots, q_n)}} = \frac{\sum_{i=1}^n p_i q_i}{\sum_{i=1}^n p_i^2 \sum_{i=1}^n q_i^2} \quad (14)$$

It is obvious that the possible values for *ICC* are between 0 and 1, being unity if and only if the probability distributions of the two partitions are the same.

Informational analysis of variance

The majority of ANOVA methods refer to the testing of the null hypothesis $H_0: \mu_1 = \mu_2 = \dots = \mu_q$, where $\mu_i > 0$ ($0 \leq i \leq q$) are means of q statistical populations. If the null hypothesis is

true it results that the q populations have the same mean. This homogeneity concerning the means may be tested also using the informational energy concept [9,10].

The one-way layout. Suppose some factor A which we consider as having some effect on a response variable of interest y has q levels. An experiment is set up in which n measurements are made of the response y at all levels. The levels q are called treatments or controlled factors, there being q controlled factors in the experimental design. Each y_{ij} result can be written as a sum of a constant μ (the general mean), α_i , a term which measures the effect of the factor A at the i th level, and an error term e_{ij} , called the residual error or residual. The linear (or additive) model

$$y_{ij} = \mu + \alpha_i + e_{ij} \quad (15)$$

can be written for the one-way layout. It is necessary now to test the null hypothesis $H_0: \mu_1 = \mu_2 = \dots = \mu_q$.

Let ξ be a new random variable with q values each having an associated probability p_i :

$$p_i = \mu_i / \sum_{i=1}^q \mu_i \quad i = 1, 2, \dots, q \quad (16)$$

Now, it is possible to observe that the null hypothesis H_0 is equivalent to the hypothesis $H^*: p_1 = p_2 = \dots = p_q = 1/q$. The H^* hypothesis is true when $E_{(\xi)} = 1/q$, i.e., when the informational energy of the random variable ξ is minimal.

If we define μ_i as

$$\mu_i = \sum_{j=1}^n y_{ij} / n \quad i = 1, 2, \dots, q \quad (17)$$

and substitute Eqn. 17 into Eqn. 16, we obtain

$$p_i = \frac{\frac{1}{n} \sum_{j=1}^n y_{ij}}{\frac{1}{n} \sum_{i=1}^q \sum_{j=1}^n y_{ij}} = \frac{\sum_{j=1}^n y_{ij}}{\sum_{i=1}^q \sum_{j=1}^n y_{ij}} \quad (18)$$

Substituting Eqn. 18 into Eqn. 5, the empirical

informational energy of random variable ξ is given by the following expression:

$$\tilde{E}_{(\xi)} = \sum_{i=1}^q p_i^2 = \sum_{i=1}^q \frac{\left(\sum_{j=1}^n y_{ij} \right)^2}{\left(\sum_{i=1}^q \sum_{j=1}^n y_{ij} \right)^2}$$

or

$$\tilde{E}_{(\xi)} = \frac{\sum_{i=1}^q \left(\sum_{j=1}^n y_{ij} \right)^2}{\left(\sum_{i=1}^q \sum_{j=1}^n y_{ij} \right)^2} \quad (19)$$

As the numerator of the expression for $\tilde{E}_{(\xi)}$ contains a sum of squares of the random variables, it is possible using the theorems of classical repartition to construct a criterion for testing the hypothesis $H^* : E_{(\xi)} = 1/q$ [7].

If $E_{(\xi)} = \tilde{E}_{(\xi)}$ the null hypothesis is accepted, and on the other hand, if $E_{(\xi)} \neq \tilde{E}_{(\xi)}$ the null hypothesis is rejected, hence the effect of factor A is taken as significant.

The two-way layout. Let us consider the case in which an experiment must be set up to study the effects of two factors A and B on a response variable y . Factor A has q levels whereas factor B has m levels. For each combination of levels, we measure the response y_{ij} by carrying out n observations. In cases with no replications and if we assume that there is no interaction between the two factors, one may adopt a linear model:

$$y_{ij} = \mu + \alpha_i + \beta_j + e_{ij} \quad (20)$$

The hypothesis $H_0(\alpha_i = 0)$, i.e., the factor A has no significant effect, is equivalent to the hypothesis

$$H^* : p_1 = p_2 = \dots = p_q$$

This is equivalent to $H_1^* : E_{(\xi)} = 1/q$.

The estimated informational energy, $\tilde{E}_{(\xi)}$, concerning the probabilities p_i is given by Eqn. 19. The null hypothesis is then accepted when $E_{(\xi)} = \tilde{E}_{(\xi)}$, hence all α_i values are equal to zero; the effect of factor A is not significant.

The hypothesis $\beta_j = 0$ ($j = 1, 2, \dots, m$), i.e., the factor has no significant effect, is equivalent to the hypothesis

$$H^* : p'_1 = p'_2 = \dots = p'_m$$

where

$$p'_j = \frac{y_{.j}}{\sum_{j=1}^m y_{.j}} \quad (21)$$

and which is equivalent to the hypothesis

$$H_1^* : E_{(\xi')} = 1/m$$

The estimated informational energy concerning the probabilities p'_j is given by

$$\tilde{E}_{(\xi')} = \sum_{j=1}^m p_j'^2 = \frac{\sum_{j=1}^m y_{.j}^2}{\left(\sum_{j=1}^m y_{.j} \right)^2} \quad (22)$$

If $E_{(\xi')} \neq \tilde{E}_{(\xi')}$ the null hypothesis is rejected, hence the effect of factor B is significant.

RESULTS AND DISCUSSION

Two relevant cases discussed by Massart and co-workers [2,3] using classical ANOVA methods are considered for comparing the advantages of informational analysis of variance.

The one-way layout

Seven laboratories were asked to determine aflatoxin M_1 in milk using the same method. A portion of a well-homogenized milk sample was given to each of the seven laboratories and each was asked to perform five independent determinations. The aim of the study was to investigate whether there is a effect of the laboratory (between-laboratory precision) on the results. The results obtained (ng g^{-1}) are given in Table 1.

The null hypothesis $\alpha_i = 0$ ($i = 1, 2, \dots, 7$) is equivalent to the hypothesis

$$H^* : p_1 = p_2 = \dots = p_7$$

The probabilities p are calculated with Eqn. 16.

TABLE 1

Determination of aflatoxin M (ng g⁻¹) in seven laboratories (from [3])

	Laboratory						
	a	b	c	d	e	f	g
	1.6	4.6	1.2	1.5	6.0	6.2	3.3
	2.9	2.8	1.9	2.7	3.9	3.8	3.8
	3.5	3.0	2.9	3.4	4.3	5.5	5.5
	1.8	4.5	1.1	2.0	5.8	4.2	4.9
	2.2	3.1	2.9	3.4	4.0	5.3	4.5
Mean:	2.4	3.6	2.0	2.6	4.8	5.0	4.4

This is equivalent to the hypothesis $H^* : E_{(\xi)} = 1/q$ or $E_{(\xi)} = 1/7 = 0.1428$.

The empirical informational energy associated with the probabilities p_i is given by

$$\tilde{E}_{(\xi)} = \sum_{i=1}^7 p_i^2 = \frac{\sum_{i=1}^7 y_i^2}{\left(\sum_{i=1}^7 y_i\right)^2} = \frac{96.88}{615.04} = 0.1575$$

As $E_{(\xi)} \neq \tilde{E}_{(\xi)}$, the difference between laboratories is significant and it is concluded that there is an important laboratory effect, which means that one or more laboratories show a bias. For identifying extreme values one may perform pair-wise comparisons of the group means using the same algorithm.

By applying classical ANOVA one obtained the same results because the calculated F value (9.33) is higher than the tabulated value $F_{6,24}^{0.05}$ (2.45).

TABLE 2

Two-way layout table for the clinical laboratory problem

	Day												
	1	2	3	4	5	6	7	8	9	10	11	12	13
Position 1	138	137	137	136	137	136	140	139	137	135	132	136	138
Position 2	140	137	136	139	138	137	139	138	139	135	136	137	142
	Day												
	14	15	16	17	18	19	20	21	22	23	24	25	
Position 1	141	137	136	137	138	138	138	136	140	139	140	138	
Position 2	139	137	139	137	138	138	138	139	140	141	141	139	

The two-way layout

The work discussed by Amenta [11] was concerned with quality control in clinical laboratories and involved the analysis of 50 samples from the same pool, two per day at different places in the run of the routine determinations carried out during that day for 25 consecutive days. The following questions were asked: is there a significant contribution to the total variance from day-to-day variations?; and is there a significant effect due to the position in the run? (See Table 2.)

Using ANOVA at the 5% confidence level, both null hypotheses are rejected, which means that there is a significant contribution to the total variance due to variation between days and between positions [3].

At the 1% confidence level [2], the first null hypothesis is rejected because the calculated F value (3.72) is higher than the tabulated value $F_{24,24}^{0.01}$ (2.66), which means that there is a significant contribution to the total variance due to variations between days. The second hypothesis is accepted because the calculate F value (6.12) is smaller than the tabulated value $F_{1,24}^{0.01}$ (7.82), which means that there is no significant contribution to the total variance due to variations between positions. However, this result is a paradox because $s_{\text{day}}^2 < s_{\text{position}}^2$ (5.36 < 8.82).

Considering the informational analysis of variance, the hypothesis $\alpha_i = 0$ ($i = 1, 2, \dots, 25$) is equivalent to the hypothesis

$$H^* : p_1 = p_2 = \dots = p_{25}$$

This is equivalent to $H_1^* : E_{(\xi)} = 1/25 = 0.0400$.

The empirical informational energy associated with the probabilities p_i is given by

$$E_{(\xi)} = \sum_{i=1}^{25} p_i^2 = \frac{\sum_{i=1}^{25} y_i^2}{\left(\sum_{i=1}^{25} y_i\right)^2} = \frac{475\,198.75}{11\,878\,362} = 0.0400$$

As $E_{(\xi)} = \tilde{E}_{(\xi)}$, there is not a significant contribution to the total variance from day-to-day variations.

The hypothesis $\beta_j = 0$ ($j = 1, 2$) is equivalent to the hypothesis

$$H^* : p'_1 = p'_2$$

This is equivalent to $H_1^* : E_{(\xi')} = 1/2 = 0.5000$.

The estimated informational energy concerning the probabilities p'_j is given by

$$E_{(\xi')} = \sum_{j=1}^2 p_j'^2 = \frac{\sum_{j=1}^2 y_{.j}^2}{\left(\sum_{j=1}^2 y_{.j}\right)^2} = \frac{38\,011.112}{76\,021.518}$$

$$= 0.5000$$

As $E_{(\xi')} = \tilde{E}_{(\xi')}$, there is not a significant effect due to the position in the run. Hence both null hypotheses are accepted. These results illustrate the efficiency of the informational analysis of variance in comparison with classical ANOVA.

Conclusions

The problem of analysis of variance has been dealt with in a mathematically simpler way using the informational energy concept. The informa-

tional analysis of variance (IANOVA) can be more efficient than the usual ANOVA methods because, like robust statistical techniques, it is resistant against uncertainties concerning the data, such as outliers or divergences from the normal distribution. An additional advantage of this method is that it is simple to carry out. However, it should be noted that, although the theory is conceptually simple, it has a very firm mathematical foundation and that in some instances the mathematics can become complex [12].

REFERENCES

- 1 R.F. Hirsch, *Anal. Chem.*, 49 (1977) 691 A.
- 2 D.L. Massart, A. Dijkstra and L. Kaufman, *Evaluation and Optimization of Laboratory Methods and Analytical Procedures*, Elsevier, Amsterdam, 1978.
- 3 D.L. Massart, B.G.M. Vandeginste, S.N. Deming, Y. Michotte and L. Kaufman, *Chemometrics: a Textbook*, Elsevier, Amsterdam, 1988.
- 4 O. Onicescu, *C.R. Acad. Sci., Ser. A*, 263 (1966) 841.
- 5 O. Onicescu and V. Ștefănescu, *Informational Statistics*, Editura Tehnică, Bucharest, 1979.
- 6 O. Onicescu, *Rev. Statist.*, 11 (1966) 4.
- 7 V. Ștefănescu, *Applications of Informational Energy and Correlation*, Editura Academiei, Bucharest, 1979, Anexa 2.
- 8 R. Cresin, *Rev. Statist.*, 12 (1966) 17.
- 9 C. Sârbu and H. Nașcu, *Rev. Chim. (Bucharest)*, 41 (1990) 276.
- 10 I. Văduva, *The Analysis of Variance*, Editura Tehnică, Bucharest, 1970.
- 11 J.S.A. Amenta, *Am. J. Clin. Pathol.*, 49 (1968) 842.
- 12 I. Petrică and V. Ștefănescu, *New Aspects of the Theory of Information*, Editura Academiei, Bucharest, 1982.

Design of experiments and data treatment in the study of mixed-ligand complexes

Marina Zelić

Center for Marine Research Zagreb, Rudjer Bošković Institute, P.O.B. 1016, 41001 Zagreb (Croatia)

(Received 12th March 1992; revised manuscript received 11th August 1992)

Abstract

The problems of the design of experiments and data presentation in the study of mixed-ligand complexes are discussed and illustrated by means of already published polarographic and voltammetric results. Recommendations for design of experiments and data treatment are given. It is indicated that the increased half-wave potential shift (in comparison with the situation in a mixture of binary complexes), caused by the presence of ternary species, depends on the number of electrons exchanged in the electrode reaction and the concentration ratio between mixed and simple complexes.

Keywords: Experimental design; Polarography; Voltammetry; Mixed-ligand complexes

Mixed-ligand complexes have been studied since the 1950s [1]. The increased interest in these compounds is connected with the recognition of their role in real multi-ligand systems such as natural and polluted waters or body fluids [2]. Different experimental methods [3–8] for the characterization of ternary species have been developed but most of them could give only a joint and not a specific response. Hence evidence for mixed-ligand complex formation is generally obtained from a model that fits experimental results.

The existing theoretical treatment [9–14] is mainly focused on systems consisting of one metal ion and two complexants, although three or four different ligands can be included in the same coordination species. It should be stressed that mixed-ligand complexes (MA_aB_b) generally constitute a significant fraction of the total dissolved

metal in a narrow ligand concentration range only. This is important for understanding of the effects of pollution and the occurrence of poisoning because the concentration of the “second” ligand can reach the level at which, together with one of the existing complexants, it will transform a significant fraction of dissolved metal into ternary species. In other words, even studies that include seemingly unrealistic combinations of one common and one unusual, i.e., synthetic, ligand are not without meaning.

Although the conditions under which one or all mixed-ligand complexes are expected to constitute a high fraction of the total dissolved metal can be predicted, appropriate experimental design is only exceptionally performed [7]. However, because of poorly chosen ligand concentrations mixed species can be easily overlooked or studied in solutions where they constitute only a minor fraction of the total metal. Taking into account that for a maximum coordination number $N > 2$ several series of measurements should be performed [7] in order to determine all stability

Correspondence to: M. Zelić, Center for Marine Research Zagreb, Rudjer Bošković Institute, P.O.B. 1016, 41001 Zagreb (Croatia).

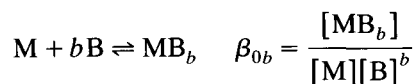
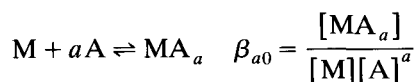
constants, it is obvious that an uncritical choice of ligand concentrations can lead to more experiments than really necessary, because some results are useless. This is especially important during studies that include some expensive ligands or chemicals that are not available in large amounts.

Because the instrumental methods usually give only a cumulative response, an illustrative (graphical) presentation of the experimental results, which indicates the “contribution” of mixed-ligand complexes, would be welcome.

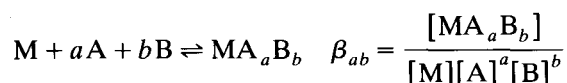
For these reasons, the problems of experimental design and data presentation will be treated here in more detail. Some principles will be discussed with already published polarographic and voltammetric measurements as examples but conclusions obtained in this way are of wider importance.

THE EQUILIBRIA

It is assumed that the metal ion of interest (M) can form more than one simple complex species with each of the ligands A and B.



Additionally, one or more mixed-ligand species can also be formed:



Usually, experiments are performed at a gradually increasing concentration of one ligand (A) and a constant level of the other (B) which gives the weaker complexes. When both complexants are of comparable strength, each of them can be tested in both roles. Constant values of ionic strength (I) and total metal concentration ($[M]_t$) are assumed.

From known stability constants of simple binary complexes, statistically expected values of

β_{ab} can be calculated [9,10] because

$$\log \beta_{ab} = \log S + (a/V) \log \beta_{V0} + (b/V) \log \beta_{0V}$$

where $S = V! / a!b!$ and $V = a + b$.

In polarographic and voltammetric methods, based on the measurement of the half-wave or peak potential shift ($\Delta E_{1/2}$ or ΔE_p), in dependence on the ligand concentration, additional assumptions are made: kinetic lability of all the complexes (simple and mixed), i.e., reversibility of the electrode reaction; large excess of both complexants over total metal concentration, i.e., $[A]_t \gg [M]_t$ and $[B]_t \gg [M]_t$; absence of polynuclear species; and absence of pronounced surface activity of ligands and/or complexes. Under such conditions, the following mass-balance equation:

$$[M]_t = [M] + \sum_{a=1}^N [MA_a] + \sum_{b=1}^N [MB_b] + \sum_{a+b=2}^N [MA_aB_b]$$

where N denotes the highest possible coordination number, should be valid (obviously neither a nor b can be equal to zero in the last sum that reflects the presence of the ternary species).

Because both complexants are present in large excess, total and free ligand concentrations can be taken as equal, assuming that HA and HB are strong acids. If not, free concentrations at a chosen pH value should be calculated using corresponding protonation constants.

RESULTS AND DISCUSSION

Experimental design

Maximum coordination number $N = 2$. If the highest possible coordination number is $N = 2$, the experimental conditions under which the only mixed-ligand species constitutes a large fraction of the total dissolved metal should be found. According to Schaap and McMasters [7], the highest relative concentration of MAB will be reached if

$$\beta_{01}[B] = \beta_{10}[A] \quad (1)$$

or

$$\beta_{02}[\text{B}]^2 = \beta_{20}[\text{A}]^2 \quad (2)$$

but the origin of the given expressions is not clear. In a recent paper [14] a different relationship:

$$1 + \beta_{01}[\text{B}] + \beta_{02}[\text{B}]^2 = \beta_{20}[\text{A}]^2 \quad (3)$$

was derived. It is obvious that for very high [B] values, i.e., low levels of MB complex and “free” dissolved metal, Eqns. 2 and 3 should give the same results. Their connection with Eqn. 1 is hardly possible because at low levels of the constant ligand

$$1 + \beta_{01}[\text{B}] \approx \beta_{20}[\text{A}]^2 \quad (4)$$

or

$$\beta_{01}[\text{B}] \approx \beta_{20}[\text{A}]^2 \quad (5)$$

The curves calculated from Eqns. 1–3 for the Cu^{2+} –ethylenediamine–oxalate system at $I = 1 \text{ mol l}^{-1}$ [7] are given in Fig. 1. Comparing the three values of [A] (i.e., [en]) that correspond to a given [B] (i.e., [ox]), it was confirmed that the third equation is better than the others. For a chosen [B] it gives the same value of [A] at the maximum concentration of MAB as a completely

independent calculation of species distribution, performed using known β_{a0} and β_{0b} together with statistically expected β_{11} constant (Fig. 1B).

It is useful to construct a $\log [\text{B}]$ vs. $\log [\text{A}]$ diagram at the beginning of each complex formation study when a ternary species is expected. Such a plot reflects the fact that the percentage of the total metal in the form of the mixed-ligand complex is primarily governed by the concentration level of the constant ligand. In other words, from this type of curve one can easily read the concentration of the “second” ligand that should be taken in order to obtain the highest possible ratio $[\text{MAB}]/[\text{M}]_t$ at a given [B]. The point is that, according to Eqn. 3, the relationship between the two concentrations ([A] and [B]) does not depend on the formation constant of the only mixed-ligand species.

Figure 1A gives the optimum pairs of ligand concentrations but does not indicate the maximum possible percentage (P_m) of the total copper(II) in the form of $\text{Cu}(\text{en})\text{ox}$ that will be obtained under such conditions. For that reason, another diagram that gives P_m as a function of [B] should be constructed. In a log–linear presentation it will generally be an S-shaped curve. For a proper design of the experiment, this curve can

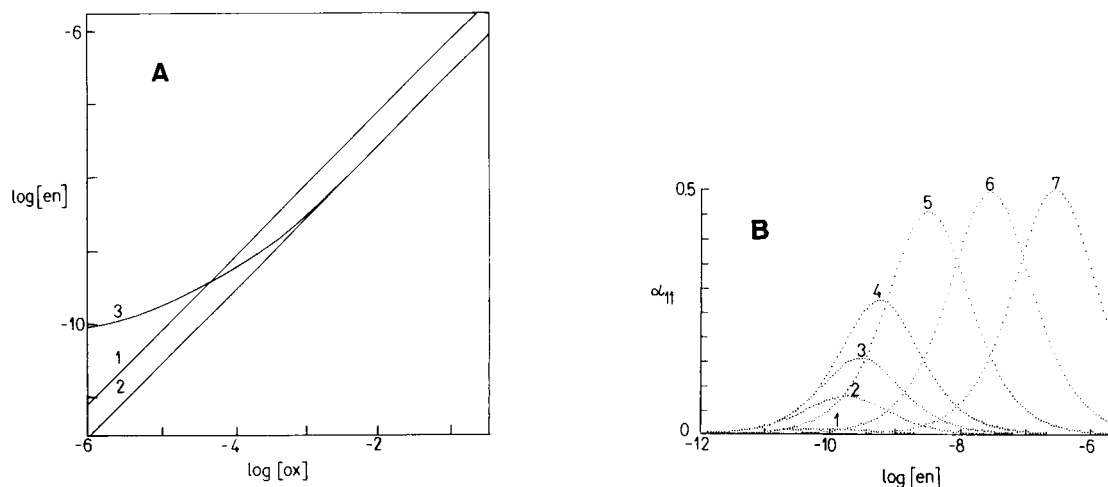


Fig. 1. (A) Relationship between the concentrations of free oxalate (ox) and ethylenediamine (en) at which the highest possible percentage of $\text{Cu}(\text{en})\text{ox}$ is expected at $I = 1 \text{ mol l}^{-1}$. The curves were calculated using (1) Eqn. 1, (2) Eqn. 2 and (3) Eqn. 3. $\log \beta_{10} = 10.8$, $\log \beta_{20} = 20.3$, $\log \beta_{01} = 5.7$, $\log \beta_{02} = 9.2$ [7]. (B) Expected fraction (α_{11}) of the total Cu(II) bound in $\text{Cu}(\text{en})\text{ox}$ as a function of [en] at a constant [ox] of (1) 10^{-6} , (2) 10^{-5} , (3) 3×10^{-5} , (4) 1×10^{-4} , (5) 1×10^{-3} , (6) 0.01 and (7) 0.1 mol l^{-1} , calculated assuming $\log \beta_{11} = 15.05$.

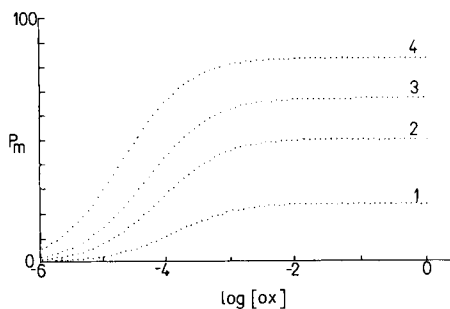


Fig. 2. Highest possible percentage of total copper(II) in the form of $\text{Cu}(\text{en})\text{ox}$ at a given level of $[\text{ox}]$ and the optimum concentration of $[\text{en}]$. Assumed values of $\log \beta_{11}$ are (1) 14.55, (2) 15.05, (3) 15.35 and (4) 15.75.

be calculated using the statistically expected β_{11} (Fig. 2, curve 2). Such a plot should be interpreted in the following way: at a chosen level of the ligand of constant concentration the highest possible relative concentration of MAB is read on the y-axis but this value can be reached only if the concentration of the second ligand satisfies Eqn. 3. In addition to curve 2, which corresponds to the statistically expected β_{11} , other curves resulting from lower (1) or higher (3 and 4) β_{11} values are presented in Fig. 2. They are all of the same shape, characterized by a plateau at higher concentrations of the constant ligand. On all the curves this flat segment starts at virtually the same value of $[\text{B}]$. It follows that the experimental design of the type given by Fig. 1A (curve 3) and Fig. 2 (curve 2) can help in finding the conditions under which MAB is present at the highest possible relative concentration. Then its contribution to the net experimental response such as the half-wave or peak potential shift in polarography and voltammetry will also be the highest. Generally, the conditions that correspond to the plateau of the curve (Fig. 2) will be chosen for practical work. In such a way the presence or absence of MAB can be detected from a “one-point experiment” because if the mixed-ligand complex cannot be detected under such conditions its “appearance” should not be expected at lower ligand levels, i.e., at lower concentrations of the ternary complex. Sometimes in practice it is not possible to reach the plateau of the curve if the reactants or products are only moderately soluble. Addi-

tionally, the chosen ionic strength can prevent the measurements in concentrated ligand solutions if one or both complexants are charged. In this paper, however, some curves are calculated for unrealistically wide concentration ranges in order to show their trend.

Diagrams similar to those given in Figs. 1A and 2 can be applied not only while trying to confirm the presence of the expected mixed-ligand species but also in work with a previously characterized system whose β_{11} is known. Because a mixed-ligand complex will generally have some specific properties, it may be necessary to convert the maximum fraction of a dissolved metal into this form for analytical or other purposes. From the mentioned diagrams the optimum experimental conditions for such a conversion can easily be found.

Maximum coordination number $N=3$. If the highest coordination number is 3, three mixed-ligand complexes can be formed. The percentage of the total dissolved metal, bound in the ternary species, is then given by

$$P = 100([\text{MAB}] + [\text{MA}_2\text{B}] + [\text{MAB}_2])/[\text{M}]_t \quad (6)$$

The conditions under which this function achieves its maximum value (P_m) can be calculated after expressing the concentrations of all the species in terms of $[\text{M}]$, $[\text{A}]$ and $[\text{B}]$. For a constant value of $[\text{B}]$ the value of $[\text{A}]$ should be found at which the derivative of this function is equal to zero [15]. Such a treatment leads to the following equation:

$$[\text{A}]^4 \beta_{21} \beta_{30} + [\text{A}]^3 (2\beta_{12} \beta_{30} [\text{B}] + 2\beta_{11} \beta_{30}) + [\text{A}]^2 (\beta_{12} \beta_{20} [\text{B}] + \beta_{11} \beta_{20} - \beta_{21} \beta_{10}) - [\text{A}] (2\beta_{21} G - \beta_{11} G - \beta_{12} G [\text{B}]) = 0 \quad (7)$$

where $G = 1 + \beta_{01} [\text{B}] + \beta_{02} [\text{B}]^2 + \beta_{03} [\text{B}]^3$. Again, as for $N=2$, the maximum possible concentration of the dissolved metal bound in the ternary complexes is in a given system governed by the value of $[\text{B}]$ chosen for the experiment.

In order to obtain a $\log [\text{B}]$ vs. $\log [\text{A}]$ or $\log [\text{B}]$ vs. P_m plot, Eqn. 7 can be subjected to an iterative procedure of the Newton type [16], which gives the optimum value of $[\text{A}]$ for each $[\text{B}]$. This

kind of calculation does not cause any difficulty because it can be performed even on a microcomputer, as demonstrated by Scott [17] on a different problem.

For $N = 3$ the $\log [B]$ vs. P_m diagrams are not all of the same shape. If both sets of constants for simple complex formation with A and B are similar, a sigmoidal curve will result as shown in Fig. 3A, in which the Cd(II)–oxalate–malonate system [18] is taken as an example. However, if A is a much stronger complexant than B the resulting plot will be different (Fig. 3B), as in cadmium(II) complexation with oxalate and ethylenediamine [7] where the completely unrealistic value $\log [\text{ox}] = 2$ would be necessary for reaching the plateau at $P_m = 75$. In both instances statistically expected values of β_{ab} constants are assumed.

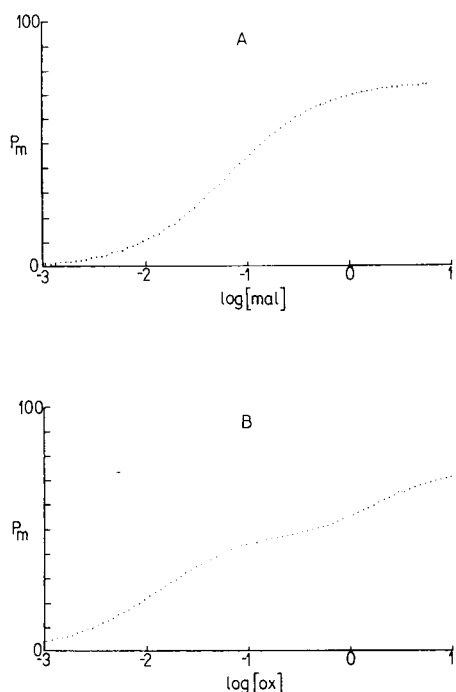


Fig. 3. Highest possible percentage of total dissolved cadmium in the form of mixed-ligand complexes. (A) Cd(II)–malonate–oxalate system ($\log \beta_{10} = 2.65$, $\log \beta_{20} = 4.32$, $\log \beta_{30} = 5.26$, $\log \beta_{01} = 2.0$, $\log \beta_{02} = 3.18$, $\log \beta_{03} = 3.66$, $\log \beta_{11} = 4.04$, $\log \beta_{12} = 4.67$, $\log \beta_{21} = 5.19$ [18]); (B) Cd(II)–oxalate–ethylenediamine system ($\log \beta_{10} = 5.6$, $\log \beta_{20} = 10.6$, $\log \beta_{30} = 12.5$, $\log \beta_{01} = 2.6$, $\log \beta_{02} = 4.1$, $\log \beta_{03} = 5.0$ [7], $\log \beta_{11} = 7.7$, $\log \beta_{12} = 8.0$, $\log \beta_{21} = 10.5$).

An important difference between $N = 2$ and 3 lies in the fact that only in the later instance do optimum ligand concentrations depend on β_{ab} values. During the design of the experiments only statistically expected formation constants can be used, but real values, and so corresponding $\log [B]$ vs. $\log [A]$ and $\log [B]$ vs. P_m diagrams, can differ from the expected ones. Even in such a case the theoretical model can be useful for planning of (preliminary) measurements. This is because the increased values of β_{ab} constants (one, two or three) have a similar effect as previously shown for $N = 2$ (Fig. 2). The curve that gives P_m as a function of $[B]$ is shifted towards lower concentrations of the ligand of constant concentration while its plateau indicates a higher maximum percentage of the total metal in the form of mixed-ligand complexes. At the same time the shape of the curve does not change very much.

It is sometimes useful to work at the maximum possible concentration of one ternary species. The necessary conditions under which each individual MA_aB_b complex reaches its own maximum with respect to the total dissolved metal can be calculated, using expected or known β_{ab} values. By solving the following equations (derived in the way mentioned before):

$$2\beta_{30}[A]^3 + \beta_{20}[A]^2 + \beta_{21}[A]^2[B] - G = 0 \quad (8)$$

$$\beta_{10}[A] - \beta_{30}[A]^3 + \beta_{11}[A][B] + \beta_{12}[A][B]^2 + 2G = 0 \quad (9)$$

$$2\beta_{30}[A]^3 + \beta_{20}[A]^2 + \beta_{21}[A]^2[B] - G = 0 \quad (10)$$

which correspond to the maximum of MAB (Eqn. 8), MA_2B (Eqn. 9) and MAB_2 (Eqn. 10), the optimum $[A]$ for each $[B]$ can be found and both ligand concentrations introduced into the equation for the relative concentration of a given species. Equations 8 and 10 are identical because with the present design (i.e., $[B] = \text{constant}$, $[A] = \text{variable}$) all MA_aB_b complexes with the same value of a should appear together [14], i.e., in the same range of $[A]$. Figure 4 gives an example of how Eqns. 8–10 can be applied in the study of the Cd^{2+} –ox–en system, assuming statistically expected values of mixed-ligand complex formation constants. The $\log [\text{ox}]$ (i.e., $[B]$) vs. P_m diagram

for individual species indicates that mixed-ligand complexes of the same coordination exhibit a similar dependence on the concentration of the constant ligand chosen for the experiment (Fig. 4A). In the $\log [\text{ox}]$ vs. $\log [\text{en}]$ diagram (Fig. 4B), however, all complexes of a given a value reach their maxima at the same ligand concentrations, as already mentioned. Figure 4A is connected with Fig. 3B but they cannot be derived from each other because Fig. 3B indicates the maximum possible concentrations of all the ternary species together at the same value of $[A]$ whereas in Fig. 4A maxima for individual species are reached at different concentrations of A (for the same $[B]$), as follows from Fig. 4B.

Maximum coordination number $N > 3$. In reality, coordination numbers up to $N = 6$ can be found. At $N > 3$ the search for the conditions under which the percentage of a dissolved metal, included in ternary species, reaches its maximum for a chosen $[B]$ leads to more complicated equations than Eqns. 7–10. Taking into account that many practical chemists are more familiar with simpler calculations, it should be said that $\log [B]$

vs. $\log [A]$ or P_m vs. $\log [B]$ diagrams (for all mixed-ligand complexes, single species or groups of them) can be constructed in a mathematically simpler although time-consuming way if corresponding species distributions are calculated for the whole possible range of $[A]$ at 10–15 different values of $[B]$. Maxima obtained in such a way and the concentrations of A at which they appear (at each $[B]$) are the data by means of which curves of the type given in Fig. 4A and B (but more complicated owing to the larger number of possible ternary species) can be produced.

Data presentation

When the formation of mixed-ligand species does not take place in a two-ligand system, the polarographic or voltammetric half-wave or peak potential shift as a function of $[A]$ is given by

$$\Delta E_{1/2} = (2.303RT/nF) \times \log \left(G + \sum_{a=1}^N \beta_{a0} [A]^a \right) \quad (11)$$

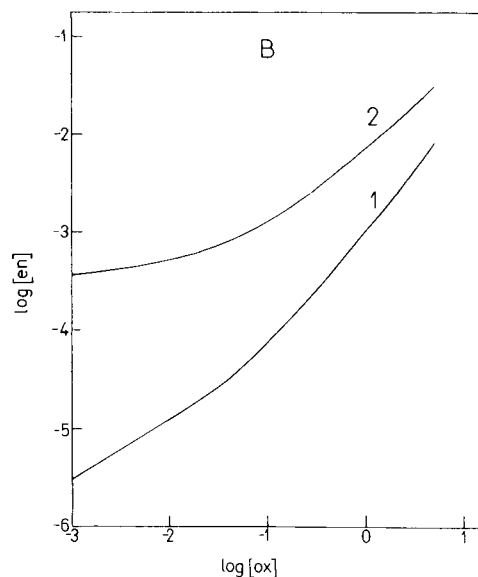
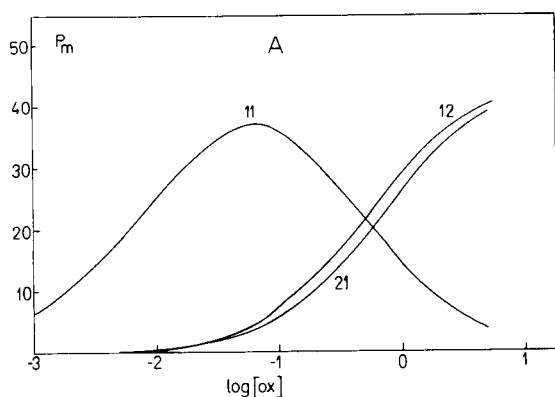


Fig. 4. (A) Predicted highest possible percentages of total dissolved cadmium in the form of individual $\text{Cd}(\text{en})_a(\text{ox})_b$ complexes as a function of oxalate concentrations. Numbers on curves indicate ab values of corresponding ternary species. (B) Optimum pairs of ligand concentrations for obtaining the maximum possible relative concentrations of (1) $\text{Cd}(\text{en})(\text{ox})$ and $\text{Cd}(\text{en})(\text{ox})_2$ and (2) $\text{Cd}(\text{en})_2(\text{ox})$.

where $G = 1 + \sum_{b=1}^N \beta_{0b}[B]^b$. When ternary species are also formed, the expression in parentheses should be extended by the sum $\sum_{a+b=2}^N \beta_{ab}[A]^a[B]^b$ in which a (and b) ≥ 1 . In other words, experimentally obtained half-wave or peak potential shifts will, under the same conditions, be higher in the presence than in the absence of ternary species. Hence, on the basis of such a difference, mixed-ligand complexes can be recognized. (In both instances it is assumed that the complexation does not change the diffusion coefficients significantly. If it does, an additional correction should be introduced [7].)

Wrong statements according to which the increase in $\Delta E_{1/2}$ obtained after addition of the second ligand point to the formation of MA_aB_b species can be found in the literature [19,20]. From Eqn. 11, it follows that in the presence of two complexants $\Delta E_{1/2}$ will always be higher than if only one is present at the same level as in the mixture. However, such an increase is concentration dependent and can be poorly pronounced. There is only evidence for mixed-ligand complex formation if the value of $\Delta E_{1/2}$ (or ΔE_p) exceeds the shift expected in a mixture of simple species. The graphical presentation in Fig. 5 corresponds to cadmium complexation with chloride and bromide ions [21]. The lower curves indicates the hypothetical formation of only simple species while the upper curves give ΔE_p in the presence of all possible ternary complexes, assuming the statistical values of β_{ab} constants. The points were calculated from square-wave voltammetric data [21].

Results obtained with a mixture of ligands are usually presented [7,18,19,22–24] in the form of a table that gives the concentrations of A and the corresponding half-wave or peak potentials (or their shifts), all measured at a constant level of B. Such a presentation is not informative but can be useful after introduction of the results expected with mixtures of simple complexes, i.e., after calculation of the difference between the two values. In comparison with “old” tables, the plots of the type given in Fig. 5 are more illustrative

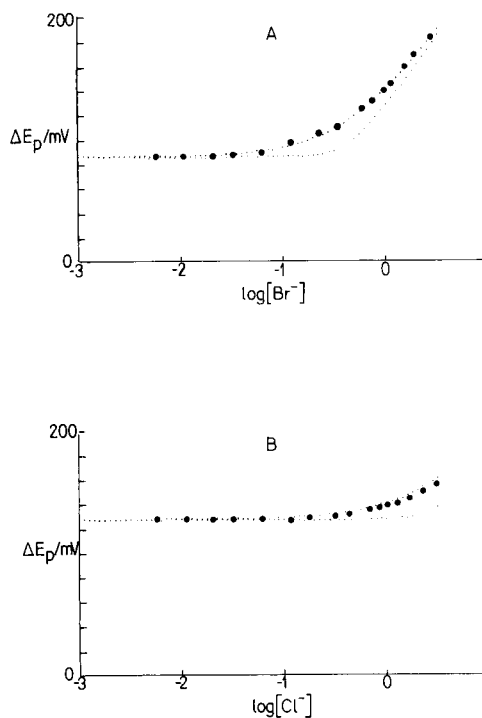


Fig. 5. Expected half-wave or peak potential shifts in the Cd(II)–chloride–bromide system if only simple (lower curves) or simple and mixed complexes (upper curves) are included in the model. Points are based on square-wave voltammetric measurements performed at (A) $[Cl^-] = 1 \text{ mol l}^{-1}$ or (B) $[Br^-] = 1 \text{ mol l}^{-1}$, $I = 4 \text{ mol l}^{-1}$ [21].

because they give an answer regarding the existence of ternary species. However, as the overall potential shift is generally much higher than the “difference” between the two curves (R), this presentation is also not very convenient for quantitative conclusions. Therefore, it is better to prepare a graphical presentation of the difference between the upper and lower curves based on statistically expected β_{ab} constants as a function of $\log [A]$ at a constant $[B]$. When R values obtained from the experimental data are included in such a diagram, their position with respect to the “theoretical” curve indicates if real values of β_{ab} constants are similar to or different from the expected values.

Such a treatment, i.e., reinterpretation of some results published in the literature between early 1960s and late 1980s [7,18,19,22,23], is presented

in Figs. 6–8. For Cu(II)–ox–en, Cd(II)–ox–en, Cd(II)–ox–TMDA (TMDA = trimethylenediamine) and Cd(II)–malonate–DAMP (DAMP = 1,3-diaminopropane) systems, the measured half-wave potential shifts are significantly higher than statistically expected. In agreement with the principle according to which a pair of similar ligands

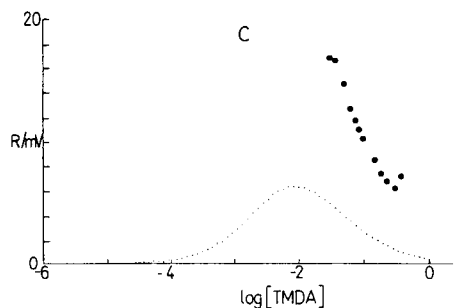
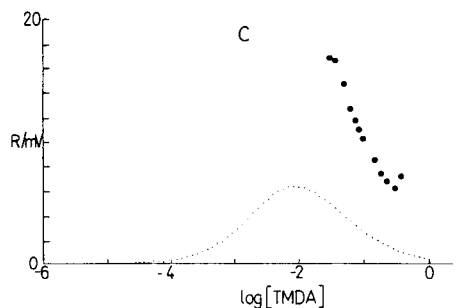
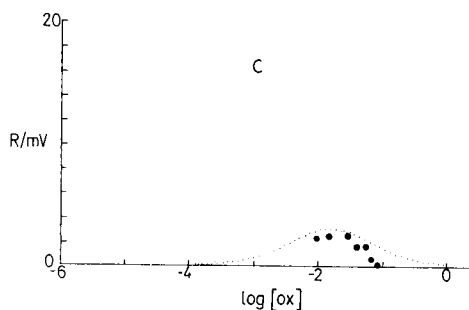
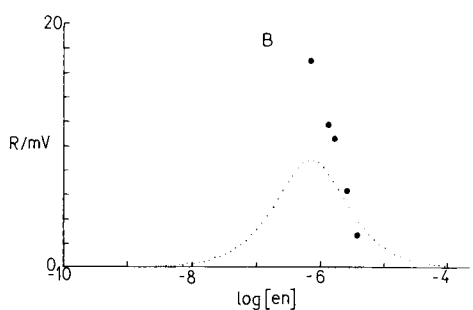
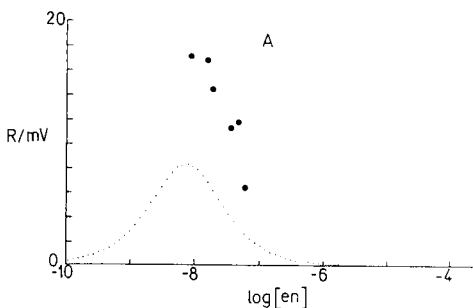
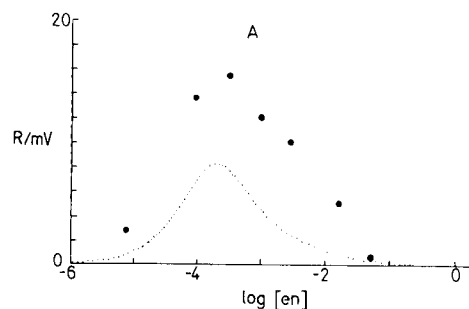


Fig. 6. Expected difference (R) in the half-wave or peak potential shift that corresponds to the presence of all possible and only simple complexes, compared with values that arise from polarographic measurements in the Cu(II)–ox–en system at $[ox] =$ (A) 0.00243 and (B) 0.247 mol l^{-1} [7] or (C) in the Cd(II)–ox–TMDA at $[ox] = 0.2$ mol l^{-1} [19].

Fig. 7. Same as Fig. 6, but for (A) Cd(II)–ox–en ($[ox] = 0.202$ mol l^{-1}) [7], (B) Cd(II)–iodide–bromide ($[I^-] = 0.1317$ mol l^{-1}) [23] and (C) Cd(II)–malonate–oxalate ($[mal] = 0.02$ mol l^{-1}) systems [18].

should produce mixed-ligand complexes with statistical values of formation constants [10], Cd(II)–malonate–ox and Cd(II)–Br $^-$ –I $^-$ systems give half-wave potential shifts very close to the “theoretical” values (in the last case surface effects seem to be successfully reduced).

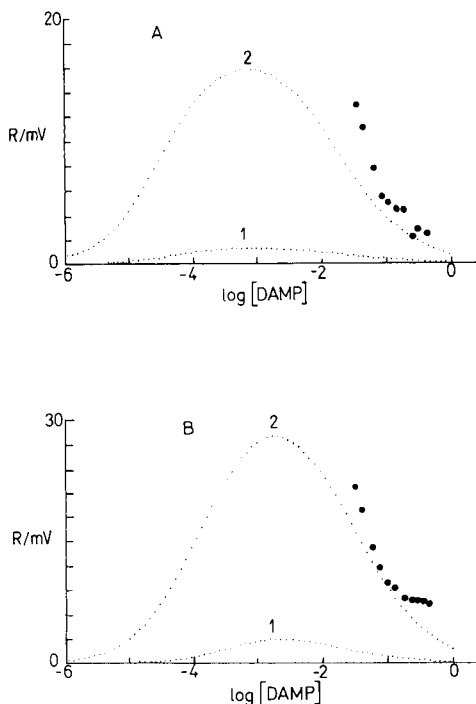


Fig. 8. Same as Fig. 6, but for the Cd(II)-malonate-DAMP system [22]. Curves 1 and 2 are based on statistical and experimental β_{ab} values, respectively. $[mal] = (A) 0.1$ and $(B) 0.25 \text{ mol l}^{-1}$.

Data quality

Closer inspection of the results in Figs. 6–8 leads to the following conclusions: there are relatively small numbers of experimental points, all located in a narrow concentration range of A; only in some instances do the measurements include the optimum level of [A] for a given [B]; and the concentrations of B are not high enough.

In the Cd(II)-malonate-ox system, the chosen malonate concentration could only give R values (expected and measured) lower than 3 mV. In some other instances negative “differences” (up to several millivolts), i.e., half-wave potential shifts lower than expected in a mixture of binary complexes, were obtained at higher concentrations of A where ternary species are less important. Such points, however, were ignored during the preparation of Figs. 6–8.

From all these observations the question of the reliability of stability constants calculated from

the mentioned experimental points arises. In Fig. 8 the curve based on voltammetrically determined β_{ab} values [22] is also included. Unfortunately, the experimental points are not located on the curve that was calculated from them.

The problem of data quality has already been recognized [25] in the study of simple equilibria, but seems to be even more serious after the introduction of ternary species. For really successful determination of β_{ab} values, stability constants of simple complexes should be determined with as low as possible standard deviations. Of course, the same holds for the results measured with mixtures of ligands. Careful preparation of all solutions, a proper titration procedure, a wide concentration range of A and a constant temperature are assumed. Under such conditions, the precision of the half-wave or peak potential reading is the limiting factor. When working with modern polarographic instruments, sampled techniques are generally used, so the applied scan increment (1–2 mV) determines the quality of polarographic and voltammetric results. The importance of accurate measurements becomes obvious when the calculation procedure for the determination of β_{ab} formation constants is discussed. Mathematically, it is the problem of solving the equation

$$\begin{aligned}
 F_{00} &= C_0 + C_1[A] + C_2[A]^2 + \dots + C_N[A]^N \\
 &= (\beta_{00} + \beta_{01} + \beta_{02} + \dots + \beta_{0N}[B]^N)[A]^0 \\
 &\quad + (\beta_{10} + \beta_{11}[B] \\
 &\quad + \beta_{12}[B]^2 + \dots + \beta_{1(N-1)}[B]^{N-1})[A]^1 \\
 &\quad + (\beta_{20} + \beta_{21}[B] + \beta_{22}[B]^2 \\
 &\quad + \dots + \beta_{2(N-2)}[B]^{N-2})[A]^2 \\
 &\quad + \dots + \beta_{N0}[A]^N
 \end{aligned} \tag{12}$$

using the experimental data because

$$F_{00} = \text{antiln}(nF/RT) \Delta E_{1/2} \tag{13}$$

Applying a graphical method [7] or a curve-fitting procedure [26], a set of C coefficients, i.e., the numerical values of the expressions in parentheses (Eqn. 12) for an individual series of measure-

ments (i.e., given [B]) can be obtained. Such values should be further resolved because they include all the terms which depend on [A] in the same way [14]. During such a treatment the contribution of one or more mixed species can be “lost” owing to pronounced experimental errors or poorly chosen ligand concentrations.

Maximum “contribution” of ternary species

It is important to recognize the factors that determine the highest possible R value, i.e., the maximum difference between half-wave or peak potential shifts that correspond to the presence of all possible species and only simple complexes. Generally,

$$\begin{aligned}
 R &= (\Delta E_{1/2})_{\text{all}} - (\Delta E_{1/2})_{\text{simple}} = (2.303RT/nF) \\
 &\times \log \left\{ \left(1 + \sum_{a=1}^N \beta_{a0}[A]^a + \sum_{b=1}^N \beta_{0b}[B]^b \right. \right. \\
 &\left. \left. + \sum_{a+b=2}^N \beta_{ab}[A]^a[B]^b \right) \right. \\
 &\left. \times \left(1 + \sum_{a=1}^N \beta_{a0}[A]^a + \sum_{b=1}^N \beta_{0b}[B]^b \right)^{-1} \right\} \\
 &= (2.303RT/nF) \log \left\{ 1 + \left(\sum_{a+b=2}^N \beta_{ab}[A]^a[B]^b \right) \right. \\
 &\left. \times \left(1 + \sum_{a=1}^N \beta_{a0}[A]^a + \sum_{b=1}^N \beta_{0b}[B]^b \right)^{-1} \right\} \quad (14)
 \end{aligned}$$

Under real conditions, the expression in the last pair of parentheses is much higher than 1. This means that in each system the value of R depends on the concentration ratio between mixed and simple species. As already mentioned [14], the highest percentage (P_m) of the total metal in the form of ternary species is determined by the maximum possible coordination number N . Assuming the statistical values of the constants β_{ab} , P_m tends to 50 ($N = 2$), 75 ($N = 3$) and 87 ($N = 4$). Assuming that the remaining amount of metal is bound in simple species, the needed ratio can be easily calculated. The resulting R values for different N and n are given in Table 1. It can be

TABLE 1

Highest values of the difference (R) between half-wave potential shifts expected in solutions of all possible species and in the mixtures of simple complexes, as a function of the maximum coordination number (N) and the number of electrons (n)

n	R (mV)		
	$N = 2$	$N = 3$	$N = 4$
1	17.8	35.6	52.5
2	8.9	17.8	26.3
3	5.9	11.9	17.5
4	4.5	8.9	13.1

seen that statistically expected formation constants of mixed ligand complexes cannot give $R \geq 2.303RT/nF$ for the usual coordination numbers (2–4). In other words, the experimentally obtained “difference” that significantly exceeds this or other corresponding values given in Table 1 can be taken as evidence that the real β_{ab} constants are higher than expected.

Table 1 also indicates that polarographic and voltammetric techniques will give the highest R values in the systems where $N = 4$ (or more) while the electrode process includes only one electron. In reality, however, n is usually 2 or 3 while the highest possible coordination number equals 3 or 4. Hence, if β_{ab} constants are in agreement with statistically expected values, experimentally obtained R values will only exceptionally be higher than 26 mV.

This work was supported by the Ministry of Science, Technology and Informatics of the Republic of Croatia.

REFERENCES

- 1 H. Sigel (Ed.), *Metal Ions in Biological Systems*, Vol. 2: Mixed-Ligand Complexes, Marcel Dekker, New York, 1973, and references cited therein.
- 2 R.P. Martin and J.P. Scharff, in R.D. Williams (Ed.), *An Introduction to Bioinorganic Chemistry*, Thomas, Springfield, 1976, p. 120.
- 3 L. Newman and D.N. Hume, *J. Am. Chem. Soc.*, 79 (1957) 4581.
- 4 R.H. Byrne and R.W. Young, *J. Solution Chem.*, 11 (1982) 127.

- 5 C.C. Wait and J.A. Munoz Leyva, *Microchem. J.*, 40 (1989) 364.
- 6 J.I. Watters, *J. Am. Chem. Soc.*, 81 (1959) 1560.
- 7 W.B. Schaap and D.L. McMasters, *J. Am. Chem. Soc.*, 83 (1961) 4699.
- 8 E. Casassas, A. Uzquierdo-Ridorsa and R. Tauler, *J. Chem. Soc., Dalton Trans.*, (1990) 2341.
- 9 D. Dyrssen, D. Jagner and F. Wengelin, *Computer Calculation of Ionic Equilibria and Titration Procedures*, Almqvist & Wiksell, Stockholm, 1968.
- 10 V.S. Sharma and J. Schubert, *J. Chem. Educ.*, 46 (1969) 506.
- 11 R.H. Byrne, *Mar. Chem.*, 9 (1980) 75.
- 12 R.H. Byrne, *Mar. Chem.*, 12 (1983) 15.
- 13 R.H. Byrne and W.L. Miller, in M.L. Sohn (Ed.), *Organic Marine Geochemistry* (ACS Symposium Series, Vol. 35), American Chemical Society, Washington, DC, 1986, p. 358.
- 14 M. Zelić and M. Branica, *Anal. Chim. Acta*, 238 (1990) 393.
- 15 A.F. Bermant and I.G. Aramanovich, *Mathematical Analysis*, Mir, Moscow, 1975.
- 16 B. Carnahan, H.A. Luther and J.O. Wilkes, *Applied Numerical Methods*, Wiley, New York, 1969, p. 171.
- 17 P.R. Scott, *Educ. Chem.*, (1985), 40.
- 18 C. Rodriguez-Placeres, G. Ruiz-Cabrera, A. Alloza and A. Arevalo, *Collect. Czech. Chem. Commun.*, 53 (1988) 506.
- 19 H.M. Killa, M.G. Abd El Wahed and H.A. Dessouki, *Polyhedron*, 4 (1985) 1219.
- 20 S.K. Shah, K.M. Suyan and C.M. Gupta, *Talanta*, 27 (1980) 455.
- 21 M. Zelić and M. Branica, *Electroanalysis*, 4 (1992) 701.
- 22 H.M. Killa, *Polyhedron*, 8 (1989) 2299.
- 23 A. Swinarski and A. Grodzicki, *Roczn. Chem.*, 41 (1967) 1205.
- 24 G. Ruiz-Cabrera, J. Rodriguez-Placeres, F. Ramos-Steffens and A. Arevalo, *Polyhedron*, 4 (1985) 221.
- 25 A. Martell and R.J. Motekaitis, *The Determination and Use of Stability Constants*, VCH, New York, 1989.
- 26 D. Pižeta, personal communication.

Expert system for interpretation of x-ray diffraction spectra

B. Adler, P. Schütze and J. Will

BUNA AG, D(O)-4212 Schkopau (Germany)

(Received 6th June 1991)

Abstract

An expert system for the automated qualitative and semi-quantitative interpretation of x-ray diffraction spectra is discussed. The database consists of a reduced spectra file connected with a screen file of the element combinations. The knowledge base contains fuzzy set rules for the interpretation of the signal positions, intensities and so-called forbidden spectra intervals, rules for the similarity and logical rules for necessary or forbidden elements. The latter information is obtained by the interpretation of emission spectral analysis. The semi-quantitative composition of mixtures is determined by a variation calculation of the ten best hits of references.

Keywords: Expert systems; X-ray diffraction; Fuzzy set theory

For the qualitative and quantitative analysis of inorganic mixtures such as fillers and additives in plastics, x-ray diffraction can be employed for concentrations up to about 1–2%. However, impurities of other compounds or different modifications of the same gross composition may be overlooked within this range of concentration. This may have a considerable influence on the structure–property effect of the filler mixture.

This paper does not deal primarily with the identification of pure substances or the quantitative analysis of mixtures of known substances, but rather seeks solutions for the automated interpretation of substance mixtures of a priori unknown composition.

MATHEMATICAL MODEL

X-ray spectra can be illustrated as vectors in formal analogy with the spectra search [1] with

Correspondence to: B. Adler, BUNA AG, D(O)-4212 Schkopau (Germany).

the vector features representing the ordered set of signal positions or intensities:

$$\mathbf{x} = \{x_1, x_2, \dots, x_d\} \quad (1)$$

where x_i is the signal position or intensity in the interval i . This means that the spectrum is divided into d intervals. A signal within the interval i gives a finite x_i value.

$$x_i = \begin{cases} > 0, & \text{signal} \\ 0, & \text{no signal} \end{cases} \quad (2)$$

otherwise the feature is of zero value. A common search strategy related to the classical file search is a comparison between the analytical vector \mathbf{x}^A and the reference \mathbf{x}_j^R of the file in order to select similar references.

$$\mathbf{x}^A \approx \mathbf{x}_j^R \quad (3)$$

Whether a reference \mathbf{x}_j^R corresponds to the analysis \mathbf{x}^A or not can be evaluated from d elementary comparisons between the features:

$$x_{ij}^R \subset x_i^A \quad (4)$$

It has proved to be of benefit to derive the

TABLE 1
Experimental fuzziness in the search intervals

Fuzziness ^a (Å)	Intervals (<i>d</i>) (Å)
0.02	1 < <i>d</i> < 2.5
0.03	2.5 < <i>d</i> < 3.8
0.05	3.8 < <i>d</i> < 5
0.1	5 < <i>d</i> < 10
0.2	<i>d</i> > 10

^a Corresponding to the length of the triangle base.

containment of a reference feature in the analysis by the fuzzy membership [2,3] (Fig. 1):

$$f^R \cap f^A(x_i) = \min[f^R(x_i), f^A(x_i)] \quad (5)$$

where $f^R(x_i)$, $f^A(x_i)$ are memberships within the interval i of analysis and reference.

Usually, the triangle function is recommended as a membership function. The experimental fuzziness of the interval (Table 1) determines the base length of the triangle. As a measure of the correspondence between an analytical spectrum and a reference, the fuzzy set power is used:

$$p_{A,R_j} = \sum_{i=1}^d f(x_i) \quad (6)$$

or its relative measure:

$$P'_{A,R} = \sum_{i=1}^d f(x_i)/n \quad (7)$$

where P = fuzzy set power, P' = relative fuzzy set power and n = maximum signal number of a reference.

From the mathematical viewpoint, it would be more exact to calculate the total fuzziness [4] (Fig. 1b) as a measure of correspondence or similarity. Considering, however, that in this instance a spectrum consists of 243 intervals and the file of more than 5000 spectra, an on-line search is impractical owing to the time required because the number of mathematical operations is immense. The measures of similarity [5,6] from signal positions and signal intensities commonly used for spectral searches of pure substances are suitable only to a limited extent for the task described above to find unexpected impurities because, on the one hand, similarity requires a high degree of correspondence with regard to signal position and intensity. This relationship may be expressed by

$$s = a - \left\{ \sum_{k=1}^a [1 - f(1 - \Delta I)]_k \right\} / i \quad (8)$$

where a = number of the same peak positions in the analysis and reference, ΔI = difference between the signal intensities in the interval k , and i = total number of intervals in the analysis and reference.

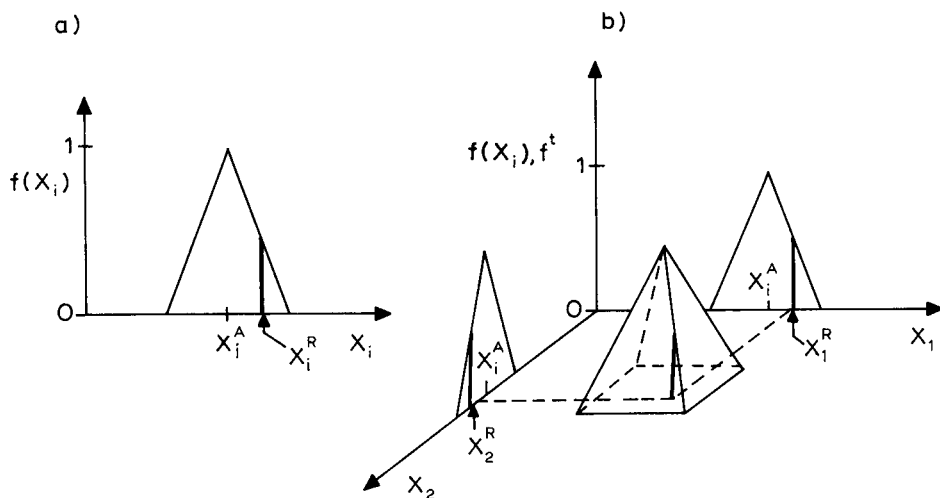


Fig. 1. Fuzziness of the signal positions. (a) Fuzziness of a simple signal; (b) total fuzziness of two-signal diffractogram. f^t = Total fuzziness.

On the other hand, with a multi-component sample, a hit list arranged according to this equation would discriminate the respective by-product due to the non-agreement of the intensities because of the lower concentration. For this reason, only the fuzzy set power according to Eqn. 7 can be considered for a multi-component sample of unexpected composition as a measure of similarity for the hit list arrangement (Fig. 2). As an additional measure (rule), small s values indicate according to Eqn. 8 the existence of a mixture.

Another rule for a multi-component sample results from the so-called forbidden domains. If, for example, spectroscopic signals appear in a reference but not in the analysis, it is assumed for the pure substances search that the reference is not applicable (ballast) (e.g., Fig. 2d). This “strict” rule and its exclusiveness do not apply to multi-component samples. It should rather be considered that the reason why a signal does not appear in the multi-component sample is that the concentration of a component is too low. In order to

characterize non-coincidences, we therefore introduce the term of the fuzzy forbidden domain. Mathematically, according to Eqn. 7, the fuzzy power is multiplied by

$$p' = p \left[\prod_{k=1}^1 (1 - I_i)_k \right] \quad (9)$$

The higher the intensity of a peak within the forbidden domain and the more frequent the appearance of these “forbidden” signals, the more improbable is the reference for highly purified material. For mixtures, such a reference has a relatively lower concentration (by-product).

SEARCH STRATEGIES

It may be assumed that, in a pure material search, the applicable references in the hit list range among the first places, and very often they top the hit list (Table 2, lines 1–3). Sometimes, a repetition of equal structure in higher positions

TABLE 2
Results of search

Components		Proportion (%)	Positions in hit list	Similarity values according to Eqn. 7
Formula	Modification			
CaSO ₄ · 2H ₂ O	Gypsum	100	1–3	0.82 ^a
TiO ₂	Anatase	100	1, 11	0.78 ^a
CaCO ₃	Calcite	100	1	0.67
SiO ₂	α-Quartz	50	1, 3, 4	0.61 ^a
ZnO	Zincite	50	2	0.74
TiO ₂	Rutile	50	1, 2	0.58 ^a
CaCO ₃	Calcite	50	4, 5	0.44
ZnO	Zincite	40	1, 2, 4	0.75 ^a
BaSO ₄	Baryte	40	5	0.46
SiO ₂	Cristobalite	20	3, 6, 8	0.51 ^a
TiO ₂	Rutile	40	1	0.7
TiO ₂	Anatase	30	2	0.61
V ₂ O ₅		30	9	0.29
SiO ₂	α-Quartz	97	4	0.70
ZnO ₃	Zincite	3	1–3	0.74
CaF ₂	Fluorite	95	2	0.62
ZnO	Zincite	5	1	0.65

^a Similarity value of the lowest position in the hit list.

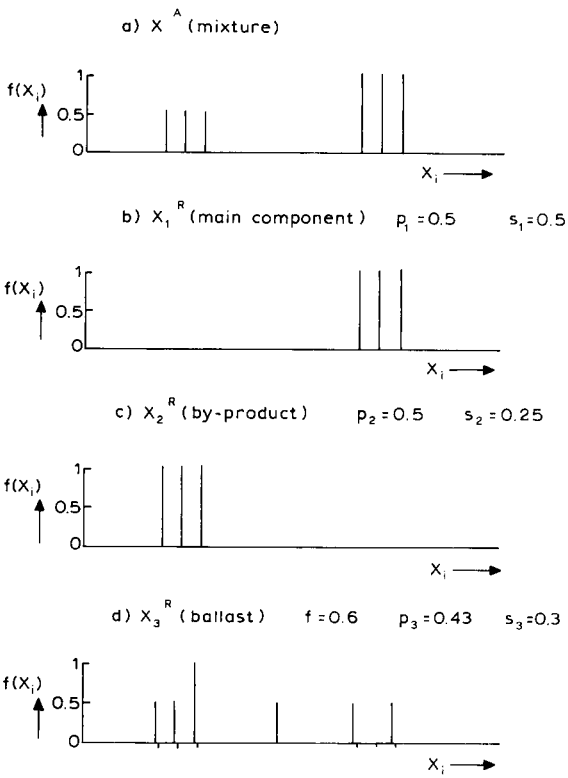


Fig. 2. Comparison of similarity measures by mixtures. Model diffractions.

TABLE 3

Comparison of search regimes

Components of analysis formula	Modification	Positions in hit list		
		Without additional information		Emission spectral data and F.I. (+)
		F.I. (-)	F.I. (+)	
TiO ₂	Rutile	1, 2, 4	1, 5	1, 4
TiO ₂	Anatase	3, 5	2, 3	2, 3, 5
V ₂ O ₅		9	27	6
ZnO	Zincite	1, 4, 6	1	1, 9
SiO ₂	α -Quartz	5, 8, 11	3, 6, 10	2, 4, 5
BaSO ₄	Baryte	7	13	7
ZnO	Zincite	1, 2	12	1, 5, 6
CaF ₂	Fluorite	3, 4, 5	1, 2, 3	2, 3, 4
TiO ₂	Rutile	7	9	2, 10
Sb ₂ O ₃	Senarmonite	1	1	1

^a Forbidden intervals: (-) without, (+) with.

Should be operated with a diagram from the file "ANALYSEN.DAT"? (Yes/no) Yes
 Number of analyses or file:
 Set number: 56
 Fuzzy of intensity: 0
 Lower limit of measuring domain: 1.2
 Upper limit of measuring domain: 8.84
 Inputs all right? (Yes/no)

(a)

Qualitative analysis? (Yes/no) Yes
 Search of a difference spectrum? (Yes/no)

Present hold type: element must be (Ca and Zn)
 Not present ordinary type: forbidden element
 Uncertain faint type: element can be or cannot be

1	2	3	4	5	6	7	8	1	2	3	4	5	6	7	8	He			
1	H															2			
2	Li	Be								3	C	N	O	F	Ne	3			
3	Na	Mg									Al	Si	P	S	Cl	Ar	4		
4	K	Ca	Sc	Ti	U	Cr	Mn	Fe	Co	Ni	Cu	Zn	Ga	Ge	As	Se	Br	4	
5	Rb	Sr	Y	Zr	Nb	Mo	Tc	Ru	Rh	Pd	Ag	Cd	In	Sn	Sb	Te	I	Xe	5
6	Cs	Ba	La	Hf	Ta	W	Re	Os	Ir	Pt	Au	Hg	Tl	Pb	Bi	Po	At	Rn	6
7	Fr	Ra	Ac	Ku															6
8																			7
9																			
10																			
11																			
12																			
13																			
14																			
15																			
16																			
17																			
18																			
19																			
20																			
21																			
22																			
23																			
24																			
25																			
26																			
27																			
28																			
29																			
30																			
31																			
32																			
33																			
34																			
35																			
36																			
37																			
38																			
39																			
40																			
41																			
42																			
43																			
44																			
45																			
46																			
47																			
48																			
49																			
50																			
51																			
52																			
53																			
54																			
55																			
56																			
57																			
58																			
59																			
60																			
61																			
62																			
63																			
64																			
65																			
66																			
67																			
68																			
69																			
70																			
71																			
72																			
73																			
74																			
75																			
76																			
77																			
78																			
79																			
80																			
81																			
82																			
83																			
84																			
85																			
86																			
87																			
88																			
89																			
90																			
91																			
92																			
93																			
94																			
95																			
96																			
97																			
98																			
99																			
100																			

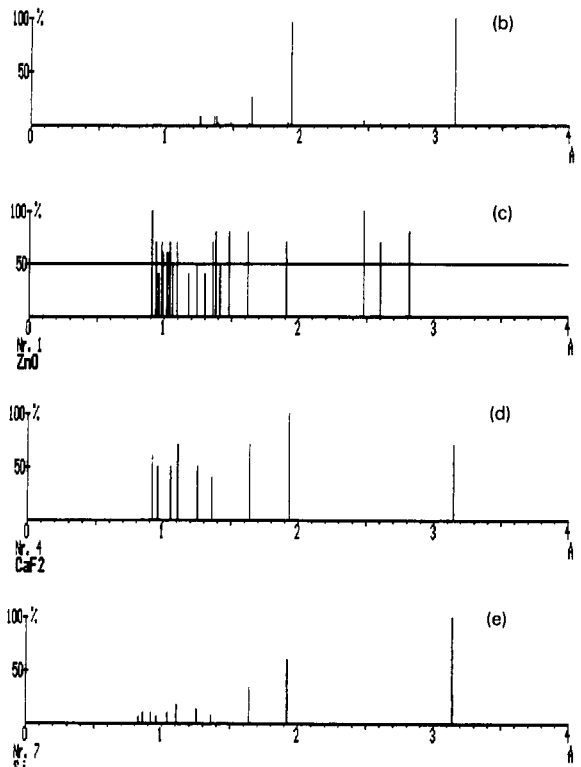


Fig. 3. Analysis of 5% ZnO in 95% CaF₂. (a) Input dialogue; (b) diffractogram of analysis; (c) and (d) ZnO and CaF₂ references; (e) ballast (Si).

indicates a lower quality of the reference or possible contamination of the sample. As expected, spectra of good quality show a high fuzzy set power (Table 2, column 6). Lower concentration pollution < 10% can be identified by the rule of forbidden domains (Eqn. 9). If this rule is applied, such references appear in the higher positions in the hit list (Table 3). However, a spectrum of a mixture must be assumed to be, coincidentally, very similar to a non-relevant reference (Fig. 3b and e). To prevent such misinterpretation, the evaluation of the data from emission spectral analysis and x-ray diffraction should be combined (Table 3, column 4). This seems to be logical because a quantitative analysis can be carried out manually only after a qualitative analysis. In the interactive input dialogue, the element is specified by clicking the element symbols (Fig. 3). The results of the emission spectral analysis are agreed to be necessarily available or impossible/not available. Those elements which are not definitely detectable by emission spectral analysis (C, H, N, O, S, P and the halogens) remain non-agreed and may appear alternatively in the references. This element specification not only validates the search results but also reduces considerably the search time, because at the beginning of every data set a bit screen of the respective element combination is placed as a screen file.

If from the first ten different references of the hit list variations in the concentration ranges of 5% are formed, the composition of the sample can be evaluated in a semi-quantitative manner (Table 4). The quality of the specification of concentration is adequate for routines; it saves experimental expenditure on calibration or specifies the concentration interval where the calibration samples have to be places for more subtle problems.

DISCUSSION

X-ray spectra of unexpected inorganic multi-component samples can be interpreted by applying the rules of the fuzzy set theory by means of search techniques. However, similarity relationships to characterize the references of pure sub-

TABLE 4

Semi-quantitative analysis by data search of x-ray diffractograms

Mixture		Contents (%)		
Formula	Modification	Real	Calculated	Difference
TiO ₂	Rutile	40	41	1
TiO ₂	Anatase	30	29	1
V ₂ O ₅		30	30	0
TiO ₂	Anatase	10	26	16
Sb ₂ O ₃	Senarmontite	90	74	16
TiO ₂	Anatase	50	47	3
Sb ₂ O ₃	Senarmontite	50	53	3
BaSO ₄	Baryte	50	36	14
TiO ₂	Anatase	50	64	14
BaSO ₄	Baryte	20	13	7
TiO ₂	Anatase	80	87	7
α-Al ₂ O ₃		20	21	1
TiO ₂	Anatase	80	79	1
α-Al ₂ O ₃		50	65	15
TiO ₂	Anatase	50	35	15

stances are not applicable to mixtures of unknown structures.

Even by use of a “neural network” [7] it is impossible to solve the above problem more efficiently, as the learning phase requires the nature and number of components for activation of the network. This specification, however, would be a solution of part of the task. The work on fuzzy forbidden domains and the specification of results from emission spectral analysis are an optimum, time-saving strategy of evaluation in semi-quantitative competitive analysis.

REFERENCES

- 1 J. Zupan, *Computer-Supported Spectroscopic Databases*, Wiley, Chichester, 1987.
- 2 T. Blaffert, *Anal. Chim. Acta*, 161 (1984) 135.
- 3 B. Adler, *Computersimulation – eine Einführung*, VG, Leipzig, 2. Auflage, 1991, p. 161.
- 4 S.F. Bocklisch, *Prozessanalysen mit unscharfen Verfahren*, Verlag Technik, Berlin, 1987, p. 73.
- 5 B.A. Knock, J.C. Smith, D.E. Wright and R.G. Ridley, *Anal. Chem.*, 42 (1970) 1516.
- 6 K.S. Lebedev, V.M. Tormyshev, On. N. Sharapova, N.V. Mamaeva, B.G. Derendjaev, V.A. Koptuy, *Izv. Sib. Otd. Akad. Nauk SSR, Ser. Khim. Nauk*, No. 2 (1980) 54.
- 7 J.R. Long, V.G. Gregorion and P.L. Gemperline, *Anal. Chem.*, 62 (1990) 91.

Triacylglycerol determination based on fatty acid composition using chemometrics

Javier García Pulido and Ramón Aparicio López

Instituto de la Grasa y sus Derivados, Avda. Padre García Tejero 4, 41012 Seville (Spain)

(Received 5th June 1992; revised manuscript received 9th September 1992)

Abstract

Multivariate statistics were applied to analyse the relationships between fatty acids and triacylglycerols in virgin olive oil. The chemical significance of factors obtained by applying principal components analysis to both sets of variables was established, and this method is proposed as a useful tool for obtaining information about the biosynthetic route of fatty acids and its regulation. Finally, because both sets of data present the same latent structure, multiple regression analysis is proposed for determining the triacylglycerol composition of an oil according to its fatty acid composition.

Keywords: Gas chromatography; Multivariate calibration; Fatty acids; Olive oil; Triacylglycerols

Over 20 years ago, owing to the lack of a precise analytical technique to determine triacylglycerols, the “1,3-random 2-random distribution” theory was proposed in order to determine them according to the fatty acid composition of an oil [1]. This theory required the determination of total and β -position fatty acids, because it was well known that the β -position in triacylglycerols was mainly esterified by unsaturated fatty acids.

With the later improvements in liquid and gas chromatographic (GC) techniques, it has been possible to test this theory using virgin olive oil [2]. Some of the results for triacylglycerols were verified as being close to the real values, but others were unsatisfactory. This paper proposes a statistical alternative, stepwise regression analy-

sis, for the determination of triacylglycerols based only on the total fatty acid composition.

EXPERIMENTAL

Chemicals and apparatus

Triacylglycerols were determined by GC using a Chrompack CP900 instrument fitted with an flame ionization detector. A fused-silica column (25 m \times 0.25 mm I.D.) coated with TAP phenylmethylsilicone (0.1 μ m thickness) was used. The carrier gas was hydrogen. Samples of 0.2 μ l of a 0.05% solution of Spanish olive oil in hexane were held at a column temperature of 33°C for 1 min, then programmed at 1°C min⁻¹ to the final temperature of 344°C. The following triacylglycerols were measured: O2L, LOP + PoO2, L2O + LnO2, SO2, O3, O2P, POS, L2P + PoLO, P2L + PPoO, OP2, S2O, O2A, O2G and L3 (where O = oleic acid, L = linoleic acid, Ln = linolenic

Correspondence to: R. Aparicio López, Instituto de la Grasa y sus Derivados, Avda. Padre García Tejero 4, 41012 Seville (Spain).

acid, P = palmitic acid, Po = palmitoleic acid, S = stearic acid, A = arachidic acid and G = gadoleic acid); a plus sign signifies that more than one triacylglycerol was quantified in that peak.

Fatty acids were determined by GC following the methods describing in UNE 55037 standards [3].

Data set

One hundred and twenty five olive oil samples were chosen on the premise that the data set represented different majority varieties, zones of production and more than one production season. In addition, the set had to represent oils with different fatty acid and triacylglycerol contents.

Computer systems

A Model 80386 minicomputer was used to run BMDP and SPSS⁺ X statistical procedures.

RESULTS AND DISCUSSION

First, the data matrix was analysed to detect the existence of outliers. A standardized score of ± 3.00 was used as a cut-off for identifying univariate outliers [4]. In this way, ten outlying cases were found, being assigned raw scores on the offending variables that were one unit larger (or smaller) than the next most extreme score in the distribution, preserving the deviancy of the case without allowing it to be so deviant that it perturbs the correlation.

Multivariate outliers were also detected using the ratio CHISQ/DF (ratio of χ^2 to number of degrees of freedom). Six outliers were found among triacylglycerols and two among fatty acids, and it was decided to eliminate them, leaving 117 cases.

Distributions of variables were studied to detect skewness, but no variable transformations were made because they did not improve the results.

Principal components analysis (PCA) of fatty acids

In order to test the factorability of *R* (correlation matrix) various parameters have been used.

TABLE 1

Rotated factor matrix of fatty acids after Varimax rotation

Acid	Factor 1	Factor 2	Factor 3
Oleic	-0.94752	-0.11916	0.11982
Linoleic	0.93170	-0.13874	-0.26641
Linolenic	0.55222	0.53181	0.23702
Palmitol	-0.07572	0.91572	0.03486
Palmitic	0.08840	0.83823	-0.15349
Stearic	-0.18485	-0.06327	0.94101
Explained variance	40.2%	28.8%	14.9%

Although the Kaiser–Meyer–Olkin measure of sampling adequacy (KMO) was not high enough (0.46532), the Bartlett test of sphericity showed that the matrix was suitable to perform factor analysis.

PCA was the extraction method used to analyse the main fatty acids in virgin olive oil, and it showed the existence of three factors, explaining 83.9% of total variance. The criteria to establish the number of significant factors was that the eigenvalues were greater than 0.90 and the rotation method employed was Varimax. These factors, or components, have a clear biochemical significance (Table 1), as they seem to represent the three main branches of the metabolic route generally accepted for the synthesis of fatty acids (Fig. 1). The first factor explains the desaturation of oleic to linolenic acid, through linoleic acid; factor 2 fits palmitic acid synthesis and its desaturation to palmitoleic acid, and factor 3 seems to indicate the path derived from stearic acid elongation.

The fact that the results from PCA fit the biosynthetic route of fatty acids so accurately

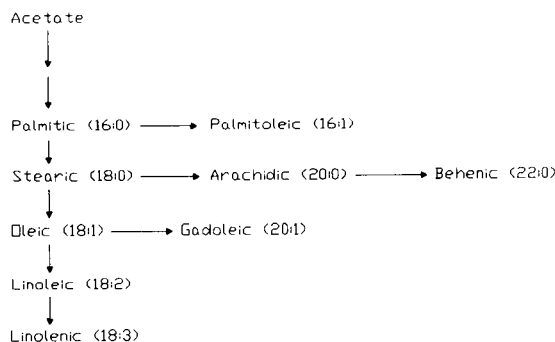


Fig. 1. Biosynthetic route of fatty acids.

suggests the possibility of using this statistical method as a first approach to the study of any route, suggesting general trends of investigation to follow. However, reasonable results are obtained only by working with fatty acids whose average content is higher than 0.5%. This is the reason why arachidic, gadoleic, margaroleic, margaric and behenic acids are not included in the analysis.

On the other hand, oleic acid shows a negative correlation with factor 1, while linoleic and linolenic acids show a positive correlation (Table 1). The same phenomenon is observed in the correlation matrix, where oleic acid shows a highly negative correlation with linoleic acid (−0.91), the negative correlation with linolenic acid being lower (−0.41).

An explanation of the above could be the possible influence of temperature in the regulation of the biosynthetic process [5,6]. Olives from colder zones of production (higher latitude or altitude) tend to produce fatty acids with a higher level of unsaturation. This means that more linoleic would be synthesized to the detriment of oleic acid. This idea agrees with the results of Aparicio and Ferreiro [7], where linoleic acid was one of the variables that entered the discriminant equation distinguishing olive oils from different altitude zones. In fact, a different pattern of fatty acid composition in relation to altitude can be observed in the plot of samples with respect to the first two factors (Fig. 2). Differences among samples from the same altitude are due to regional characteristics (soil, climate, etc.).

Hence PCA also seems to be useful in obtaining general ideas about the regulation of a metabolic process.

Principal components analysis of triacylglycerols

Applying PCA to the triacylglycerols determined in the same oil samples, three factors are obtained again, explaining 92.1% of the total variance, and grouping triacylglycerols according to their fatty acid content (Table 2). The first factor seems to join together those compounds whose main fatty acids are oleic, linoleic and linolenic acids. The second gathers triacylglycerols characterized by their composition of

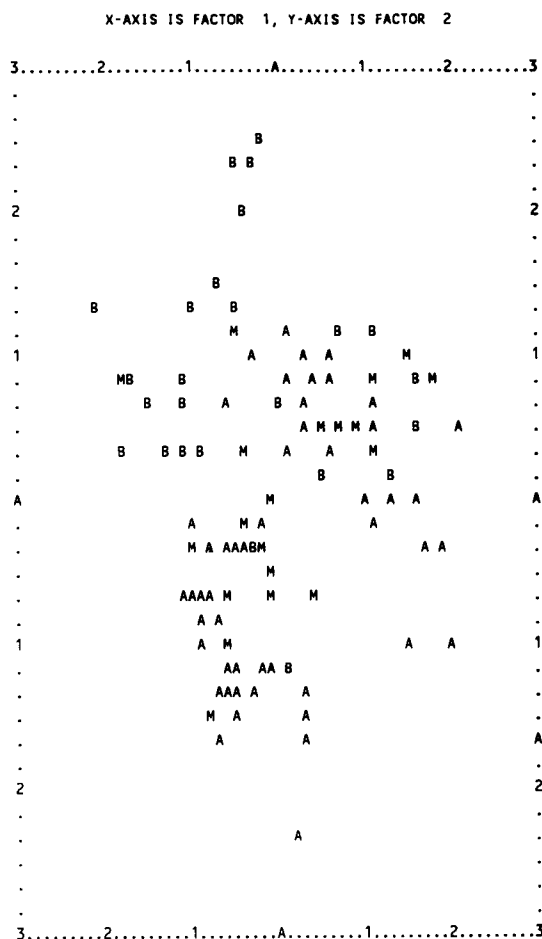


Fig. 2. Plot of samples with respect to the factors obtained from PCA of fatty acids. Samples are labelled as A (600–100 m), M (500–600 m) and B (200–500 m).

TABLE 2

Rotated factor matrix of triacylglycerols after Varimax rotation

Triacylglycerol	Factor 1	Factor 2	Factor 3
O3	−0.92232	0.08697	−0.30466
L2O + LnO2	0.90441	−0.29961	−0.25085
LOP + PoO2	0.90261	−0.28820	0.27207
O2L	0.87256	−0.34477	−0.28846
L2P + PoLO	0.85360	−0.04714	0.24167
S2O	−0.02578	0.94183	−0.01889
POS	−0.20374	0.90971	0.16623
SO2	−0.47536	0.82330	−0.16694
OP2	0.08139	−0.00032	0.95845
P2L + PPoO	0.41924	0.02737	0.84526
O2P	−0.61926	0.03112	0.75704
Explained variance	51.3%	24.3%	16.5%

TABLE 3

Correlation among factor scores: TRIF1 to TRIF3 are the factors obtained for triacylglycerols and FATF1 to FATF3 those for fatty acids

	ACGF1	ACGF2	ACGF3
TRIF1	0.88411	-0.02931	-0.07711
TRIF2	-0.06199	0.79034	-0.17201
TRIF3	-0.07319	0.13754	0.78079

palmitic and palmitoleic acids, and the third those which contain stearic acid. Thus, there seems to be a strong similarity between these factors and those obtained for fatty acids. Again, variables whose average content is lower than 0.5% (O2A, O2G, L3) have not been included in the analysis. The same criterion to establish the number of significant components was used, as well as the same type of rotation. KMO measure of sampling adequacy (0.73271) and Bartlett test of sphericity (2140.5136) had previously confirmed the factorability of R .

A method to test whether two groups of variables have the same latent structure involves correlating factor scores of each group. Table 3 shows the results of this analysis, indicating the existence of a strong positive correlation between each component of fatty acids and its analogue in triacylglycerols. The correlation between non-analogous components no longer exists.

Further, if PCA is performed using all the variables (fatty acids and triacylglycerols) together, and these are represented in a three-dimensional space according to their scores with

respect to the three new factors, it can be seen (Fig. 3) that each factor explains a set of triacylglycerols with their characteristic fatty acids.

The above results support the proposal that the triacylglycerol and fatty acid compositions of an oil are a faithful reflection of each other, as most fatty acids esterify the glycerine moiety in triacylglycerols.

Multiple regression analysis

Owing to the parallelism observed between both sets of variables, the question arises of the extent to which triacylglycerols contents can be statistically predicted from fatty acid composition.

Stepwise regression was the statistical algorithm chosen to test this idea, using as independent variables only those fatty acids involved in the chemical composition of each triacylglycerol. Thereby the equations obtained had a chemical background, thus preventing fatty acids whose relationship with the triacylglycerol was only random from entering the equation.

In addition, it is well known that fatty acids are measured in percentages, and they are not independent of each other because they have to add up to 100. A satisfactory way of dealing with this problem was found by removing those fatty acids which did not relate to any triacylglycerol chemical composition.

On the other hand, some fatty acids may be non-significant for prediction. For example, there are peaks in the chromatogram in which more than one triacylglycerol is quantified (LOP +

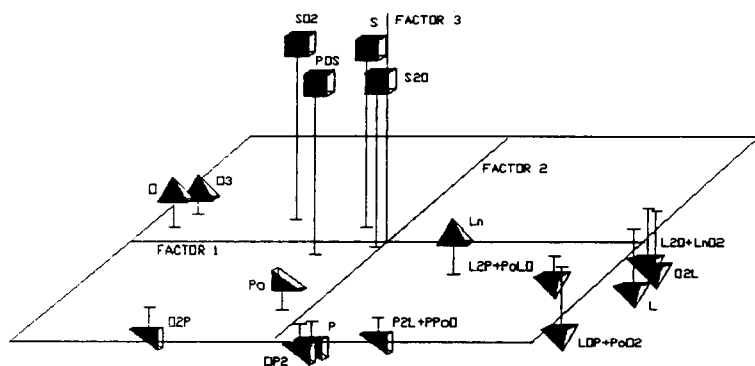


Fig. 3. All the variables in the three-dimensional space formed by factors.

TABLE 4

Stepwise regression among triacylglycerols and fatty acids

Triacylglycerol	Multiple R	Adjusted R^2	Equation
L2O + LnO2	0.94	0.88	$L2O + LnO2 = 0.291L + 0.052O - 4.627$
O2L	0.93	0.87	$O2L = 1.339L + 0.320O - 25.657$
LOP + PoO2	0.90	0.82	$LOP + PoO2 = 0.424L + 0.339P + 0.557Po - 1.906$
SO2	0.88	0.79	$SO2 = 1.375S + 0.154O - 9.452$
O3	0.87	0.75	$O3 = 1.098O - 38.252$
O2P	0.82	0.66	$O2P = 1.578P + 0.405O - 22.102$
P2L + PPoO	0.79	0.62	$P2L + PPoO = 0.593Po - 0.027O + 0.052P + 1.853$
POS	0.79	0.61	$POS = 0.351S + 0.076P + 0.014O - 1.503$
L2P + PoLO	0.76	0.57	$L2P + PoLO = 0.089L + 0.358Po - 0.500$
OP2	0.74	0.55	$OP2 = 0.376P - 0.670$
S2O	0.61	0.36	$S2O = 0.154S + 0.040$

PoO2, L2O + LnO2, etc.), one of them being present in greater amount than the other. In these instances, fatty acids from the minority

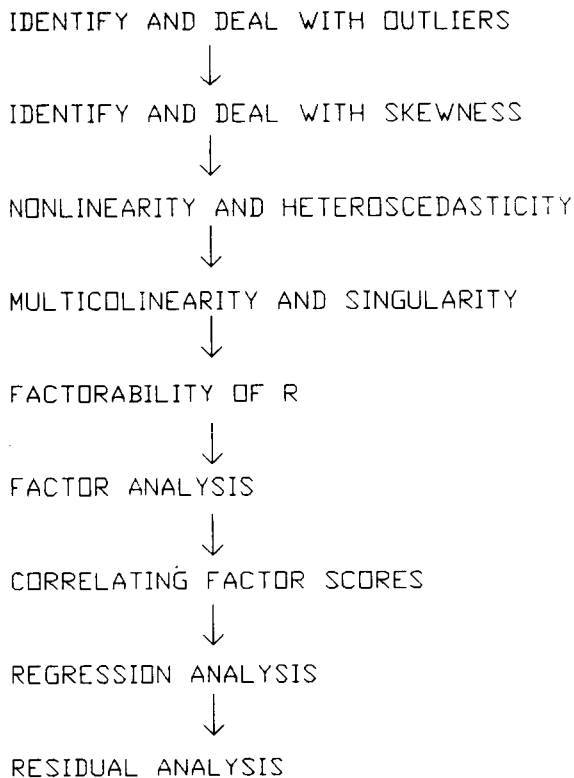


Fig. 4. Procedure followed for determination of triacylglycerols from fatty acid composition.

triacylglycerol must be less important for the prediction of the peak. Hence stepwise regression seems to be the appropriate technique, as at each step it picks up the variable that most adds to the prediction equation, in terms of increasing R^2 , until no more useful information can be obtained.

With respect to the number of samples, Peña [8] suggested that regression works on the basis of a number of samples four or five times the number of independent variables. In this instance, regression was applied to 117 samples, using six fatty acids as the total number of independent variables. In consequence, the data set complies with this suggestion. Residuals scatter plots were analysed in order to test the assumptions of normality, linearity and homoscedasticity.

Table 4 shows the equations obtained, their multiple R and adjusted R^2 , using a probability of F to enter equal to 0.05 (The probability of F to remove was 0.1 and the tolerance was 0.01). These results show that most triacylglycerols can be determined from fatty acid concentrations with multiple R coefficients greater than 0.75. However, the adjusted R^2 coefficients are only good enough for O2L, LOP + PoO2, SO2, O3 and O2P, the most important triacylglycerols in virgin olive oil. The other triacylglycerols obtained by GC represent a very low percentage of the total, so their measurement is more difficult and hence less accurate.

It is concluded that stepwise regression is a good technique for determining the most important triacylglycerols in an oil, given its fatty acid composition. On the other hand, fatty acid determination based on triacylglycerol concentrations as independent variables is not so exact, as the high correlations among the latter cause multicollinearity on the data matrix.

Finally, Fig. 4 shows a possible scheme that could be followed to derive triacylglycerol composition from fatty acids analysis.

REFERENCES

- 1 F.D. Gunstone, *An Introduction to the Chemistry and Biochemistry of Fatty Acids and Their Glycerides*, Chapman and Hall, London, 1967, pp. 168–171.
- 2 R. Aparicio, E. Graciani and L. Ferreiro, *Anal. Chim. Acta*, 259 (1992) 115.
- 3 *Materias Grasas. Determinación de Ácidos Grasos por Cromatografía Gaseosa*, UNE 55037, AENOR, Madrid, 1973.
- 4 B.G. Tabachnick and L.S. Fidell, *Using Multivariate Statistics*, Harper and Row, New York, 1983.
- 5 J.K. Raison, in J.B. St. John, E. Berlin and P.C. Jackson (Eds.), *Frontiers in Membrane Research in Agriculture*, Rowman and Allanheld, Ottawa, 1986, pp. 383–401.
- 6 J. Browse and C. Somerville, *Annu. Rev. Plant Physiol. Plant Mol. Biol.*, 42 (1991) 467.
- 7 R. Aparicio and L. Ferreiro, *Grasas Aceites*, 43 (1992) 149.
- 8 D. Peña, *Estadística. Modelos y Métodos*, Alianza Editorial, Madrid, 1986.

Systematic investigation of multi-element preconcentration from copper alloys by carbamate precipitation before atomic absorption spectrometric analysis

Ch. Frigge and Ewald Jackwerth

Analytical Chemistry, Department of Chemistry, Ruhr University Bochum, P.O. Box 102148, D(W)-4630 Bochum 1 (Germany)

(Received 30th June 1992; revised manuscript received 14th September 1992)

Abstract

Methods for multi-element preconcentration from copper alloys are presented. In systematic investigations the coprecipitation behaviour of traces of Ag, Au, Bi, Cd, Co, Fe, Ga, In, Mn, Ni, Pb, Pd, Sb, Se, Sn, Te and Zn during collector precipitation with hexamethylenammonium hexamethylenedithiocarbamate was tested. Copper and tin as matrix elements have to be separated in preceding steps as CuSCN and SnBr_4 . A quantitative preconcentration of three (Cu–Ni), nine (Cu–Zn), ten (Cu–Sn) or eleven (Cu–Al) elements is achieved. The limits of detection of the combined procedures are, depending on the element, between 0.1 and $2 \mu\text{g g}^{-1}$ for flame atomic absorption spectrometry (AAS) and between 0.01 and $0.1 \mu\text{g g}^{-1}$ for graphite furnace AAS. The relative standard deviations are about 3%.

Keywords: Atomic absorption spectrometry; Copper alloys; Preconcentration; Trace elements

In analytical chemistry, collector precipitations with chelating agents are often used, especially for the separation and enrichment of traces of elements from matrices which usually interfere with a direct instrumental determination. In quality assurance of pure substances, normally the simultaneous determination of many elements is desirable. Until now, such methods for multi-element preconcentration have mostly been developed for either sample materials with a matrix consisting of a single component chemically affecting the analysis (pure metals, metal salts, etc.) or for materials not seriously interfering (water,

glass, etc.) in order to increase the analyte concentration [1,2].

With increasing requirements for materials with complex compositions, such methods will also become necessary for the analysis of multi-component systems, e.g., metal alloys. Although such methods are time consuming, they are important especially for the certification of reference materials. Obviously, the development of such procedures is complicated because they have to perform the separation of groups of elements (trace elements in addition to matrix elements) with components that chemically react very differently. Therefore, such methods up to now have rarely been described [3,4]. If copper is one the matrix components, special problems occur because copper belongs to those elements which

Correspondence to: E. Jackwerth, Analytical Chemistry, Department of Chemistry, Ruhr University Bochum, P.O. Box 102148, D(W)-4630 Bochum 1 (Germany).

form very stable complexes with nearly all common group reagents. This is also true for hexamethylenammonium hexamethylenedithiocarbamate (HMA-HMDTC) used in these investigations. Owing to this reactivity and to the large excess of the matrix copper, the trace complexes necessary for separation are not formed. Based on a procedure for trace enrichment from pure copper described previously [5], in this paper a useful concept for preconcentration from different copper alloys is presented.

EXPERIMENTAL

Reagents

All reagents were of analytical-reagent grade and were used as received. Solutions were prepared with water doubly distilled from a quartz vessel.

HMA-HMDTC solution was prepared by dissolving 1.0 g of HMA-HMDTC and 0.2 g of KOH in water and diluting to 100 ml. Sodium disulphite and potassium thiocyanate solutions were prepared by dissolving 20 g of $\text{Na}_2\text{S}_2\text{O}_5$ and 25 g of KSCN, respectively, in water and diluting to 100 ml.

Apparatus

The atomic absorption spectrometers used for trace element determinations were a Varian Model AA6 with an air-acetylene or a nitrous oxide-acetylene flame and a Perkin-Elmer Model Z3030 with an HGA 600 graphite furnace system.

Preliminary investigations of direct HMDTC precipitation

The number of trace elements that are preconcentrated when a small amount of HMA-HMDTC is added to a metal solution depends on the stability and solubility of the matrix metal-HMDTC complex used as a collector and on the chosen pH [6]. When the sample solution contains copper as a matrix component this element normally dominates the separation and preconcentration behaviour of the whole sample. As examples of the large number of metals that form technically important alloys with copper, the in-

fluence of copper on the recovery of trace elements during preconcentration from Al, Ni and Zn solutions was tested. These three elements form no (Al), only weak (Zn) or relatively strong (Ni) HMDTC complexes.

A 1.0-g amount of a blend of copper powder with Al or Ni or Zn powder is dissolved in 8.0 ml of 37% HCl and 3.5 ml of 30% H_2O_2 or in 4.0 ml of 65% HNO_3 and 1.5 ml of 37% HCl and diluted to ca. 100 ml with water. As aluminium forms no precipitate with HMDTC, 2.0 mg of Mo(VI) are added as a collector element to the pure aluminium samples. After having adjusted the pH with 37% HCl or 25% NH_3 , the collector is precipitated by adding 10 ml of HMDTC solution. After a coagulation time of 20 min, the precipitate is filtered by means of a suction filter device with a membrane filter (cellulose nitrate, pore size 5 μm , diameter 50 mm). During pH adjustment, precipitation of the matrix as hydroxides has to be avoided. The best results are obtained at pH 1 for the Cu-Al and Cu-Zn systems and at pH 4 for the Cu-Ni system. The filter and the precipitate are dissolved together in 2.0 ml of 65% HNO_3 and 0.5 ml of 37% HCl by heating and the solution is diluted to 5.0 ml with water. The resulting trace concentrate is analysed by atomic absorption spectrometry (AAS). For the Cu-Zn system Fig. 1 shows the recovery as a function of sample composition.

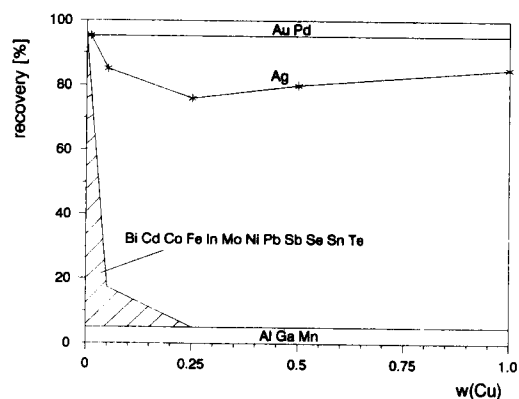


Fig. 1. Dependence of trace element recoveries on the sample composition for the Cu-Zn system during HMDTC precipitation [$w = m_{\text{Cu}} / (m_{\text{Cu}} + m_{\text{Zn}})$].

As observed previously in the analysis of technical zinc alloys [7], there is a strong decrease in the recoveries of nearly all elements tested owing to the stability of the Cu–HMDTC complex even at low copper concentrations. The same is true for the Cu–Al and Cu–Ni systems. Only for samples with low copper contents are some differences between the three systems found. When this small amount of copper is precipitated completely and some excess precipitation reagent is available for the reaction of other elements, the preconcentration behaviour of the trace elements is determined by the complex stability of the second matrix component. According to the decreasing stability, the number of elements that can be preconcentrated from low-copper solutions increases from the Cu–Ni system via Cu–Zn to Cu–Al.

For multi-element preconcentration from solutions with a high copper content it is necessary to separate the copper in a first step. Subsequently, the trace elements can be preconcentrated by HMDTC collector precipitation.

HMDTC precipitation after copper separation by CuSCN precipitation

The selective separation of the matrix copper as CuSCN has already been treated comprehensively in a previous paper [5]. In order to achieve a trace separation from further matrix components in a subsequent step by HMDTC collector precipitation, the pH has to be adjusted appropriately so as to prevent matrix precipitation as hydroxides. The best results are obtained for Cu–Al at pH 1.5, Cu–Zn at pH 1.0 and Cu–Ni at pH 6. As described above, a 1.0-g amount of a blend of metal powders is dissolved in acid and diluted to 80 ml with water. After addition of 30 ml of 37% HCl, the copper is precipitated as CuSCN by adding 5.0 ml of Na₂S₂O₅ solution and 5.0 ml of KSCN solution and is separated by centrifugation. After adjustment of the preselected pH, the trace elements are precipitated in the centrifugate by adding 10 ml of HMDTC solution. After a coagulation time of 20 min, the precipitate is filtered by means of a suction filter device through a membrane filter (cellulose nitrate, pore size 5 μm, diameter 50 mm).

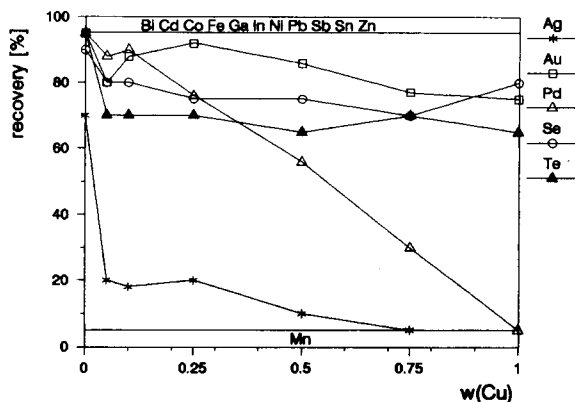


Fig. 2. Dependence of trace element recoveries on the sample composition for the Cu–Al system during HMDTC precipitation including a previous separation of copper [$w = m_{\text{Cu}} / (m_{\text{Cu}} + m_{\text{Al}})$].

The filter and precipitate are dissolved as described above. The trace concentrate is analysed by AAS.

As compared with the results obtained with untreated nickel solutions, an additional enrichment of some elements by coprecipitation as hydroxides that is expected for the Cu–Ni system at pH 6 is hindered by the increased salt content of the solution. In order to achieve optimum recoveries, the amount of reagents used for copper separation (Na₂S₂O₅, KSCN) in this system has to be adapted to the copper content of the sample.

Figures 2–4 show the recoveries as a function of the sample composition for the binary systems Cu–Al, Cu–Ni and Cu–Zn.

The recoveries of most of the trace elements result from a combination of the individual recoveries of the two process steps. The range of elements obtained thereby decreases as expected within the series Cu–Al > Cu–Zn > Cu–Ni.

In contrast to the precipitation results from pure, untreated zinc solutions, where the recoveries of cobalt and antimony are incomplete [2], a quantitative enrichment of these elements is achieved with the Cu–Zn system. Presumably this can be attributed to complexation of both elements by SCN[−], and for antimony additionally to the increased stability of the Sb(III)–HMDTC complex compared with that of Sb(V)–HMDTC.

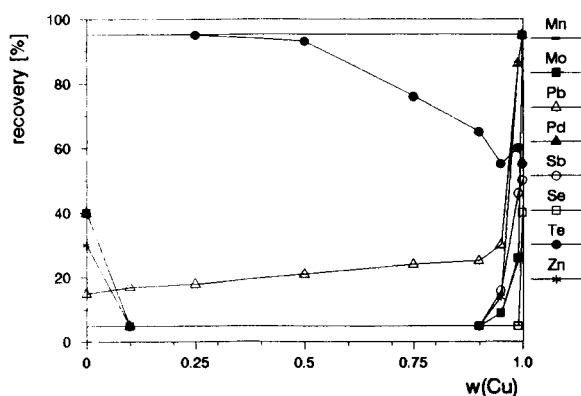
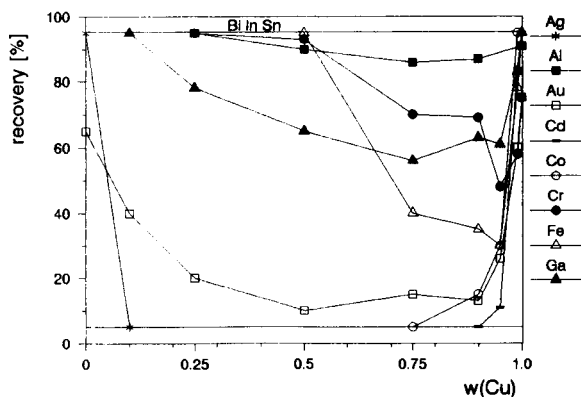


Fig. 3. Dependence of trace element recoveries on the sample composition for the Cu–Ni system during HMDTC precipitation including a previous separation of copper [$w = m_{\text{Cu}} / (m_{\text{Cu}} + m_{\text{Ni}})$].

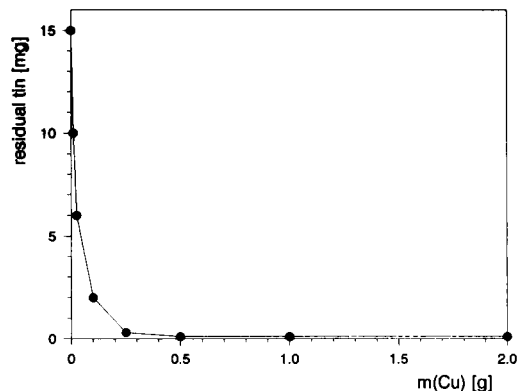
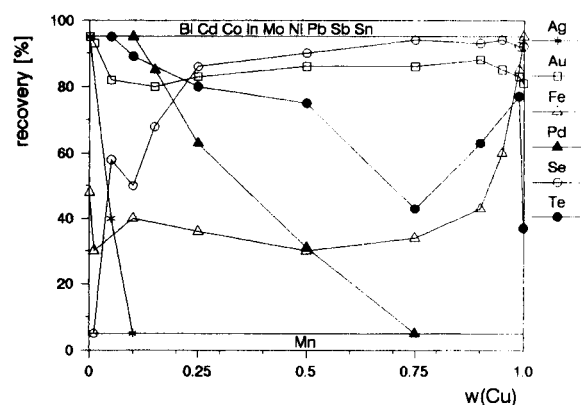


Fig. 5. Residual tin after evaporation of 0.5 g of tin as a function of the amount of copper in the solution.

Trace preconcentration from Cu–Sn bronzes is not successful even after separation of the copper, because tin itself, similarly to copper, forms very stable HMDTC complexes. Moreover, the collector precipitate obtained from tin solutions is very fine grained and not suited for filtration. Nevertheless, the procedure presented here is also applicable to Cu–Sn alloys if, in an additional step, the tin is volatilized selectively as SnBr_4 .

The sample is dissolved in 5.0 ml of 48% HBr and 0.5 ml of Br_2 . After adding 5.0 ml of 48% HBr and 5.0 ml of 96% H_2SO_4 , the tin is evaporated within 60 min (on a heating plate at 250°C). As the copper content of the solution favours the evaporation of tin, this step is effected before the copper is separated. Figure 5 illustrates the amount of residual tin after one evaporation process with 0.5 g of tin as a function of the amount of copper present.

Presumably the improved separation can be explained by partial binding of the bromide, which is necessary for tin volatilization by copper and its release in an equilibrium reaction with tin later. If no copper is present, some of the bromide is volatilized as HBr without any effect. In this instance, good preconcentration coefficients are only obtained by repeated evaporation with fresh HBr added each time. By combining the evaporation of SnBr_4 with the separation of copper as CuSCN , a solution containing the trace elements is obtained. From this solution, traces of Al, Bi,

TABLE 1

Statistical data for CuAl25 and CuZn25 ^a

Metal	Method ^b	Limit of detection ($\mu\text{g g}^{-1}$) (3σ , $n = 20$)		Relative standard deviation (%) ($n = 20$)		Trace element content of the sample ($\mu\text{g g}^{-1}$)
		CuAl25	CuZn25	CuAl25	CuZn25	
Au	A	0.2	0.1	3.5	3.0	2
	B	0.01	0.01	3.7	3.8	0.1
Bi	A	1.0	1.1	1.9	1.9	20
	B	0.04	–	4.1	–	0.5
Cd	A	0.07	0.09	2.0	2.2	2
	B	0.008	–	4.0	–	0.5
Co	A	0.1	0.2	2.2	2.4	10
	B	0.03	–	3.6	–	0.5
Fe	A	1.6 ^c	–	3.5	–	40
Ga	A	0.9 ^c	–	2.6	–	20
	B	0.05 ^c	–	3.0 ^c	–	0.5
In	A	0.2	0.4	1.9	1.5	20
	B	0.09	0.1	4.8	4.3	1.0
Mo	A	–	0.3	–	2.5	20
Ni	A	1.4	1.4	2.3	2.0	10
Pb	A	1.0	1.0	2.2	1.8	20
	B	0.1	–	3.7	–	1.0
Sn	A	1.9	2.3	3.8	3.2	100
	B	0.3	0.4	5.4	4.6	1.0
Zn	A	2.2 ^c	–	3.9	–	10

^a Cu – Al (75 + 25, w/w) and Cu – Zn (75 + 25, w/w) alloys. ^b A = flame AAS; B = graphite furnace AAS. ^c Determined on a sample of pure Cu.

TABLE 2

Recoveries and trace element contents of some technical alloys

Metal	CuZn21Al2		AlCu30		CuSn8	
	Recovery (%)	Concentration ($\mu\text{g g}^{-1}$)	Recovery (%)	Concentration ($\mu\text{g g}^{-1}$)	Recovery (%)	Concentration ($\mu\text{g g}^{-1}$)
Au	90	0.28	85	0.9	–	–
Bi	≥ 95	0.9	≥ 95	2.5	≥ 95	5.0
Cd	≥ 95	0.6	≥ 95	1.2	≥ 95	0.4
Co	≥ 95	0.3	≥ 95	1.9	≥ 95	0.3
Fe	–	–	≥ 95	1500	≥ 95	27
Ga	–	–	≥ 95	110	≥ 95	≤ 0.2
In	≥ 95	≤ 0.3	≥ 95	≤ 0.3	≥ 95	≤ 0.3
Mo	≥ 95	≤ 0.9	–	–	–	–
Ni	≥ 95	95	≥ 95	35	≥ 95	75
Pb	≥ 95	40	≥ 95	70	≥ 95	50
Sb	≥ 95	13	≥ 95	9.3	–	–
Sn	≥ 95	150	≥ 95	1300	–	–
Zn	–	–	≥ 95	500	≥ 95	110

Cd, Co, Fe, Ga, In, Ni, Pb and Zn can be preconcentrated to $\geq 95\%$ as described above using an HMDTC collector precipitation at pH 6 with 2.0 mg of Mo(VI) as an additional collector element.

RESULTS AND DISCUSSION

The procedure presented is generally suited for the analysis of copper alloys of the types tested and works independently of the particular composition of the alloy. The number of trace elements preconcentrated depends on the stability of the HMDTC complexes of the matrix elements that are present apart from copper. In addition to the binary alloy systems described, the procedure should also be suitable for the analysis of samples containing iron and manganese and for some ternary alloys.

The limits of detection and the standard deviations were determined using samples of composition CuAl25 and CuZn25 (Table 1). Because in the technical alloys available most of the trace elements are present in fairly high concentrations, mixtures of the purer metal salts were used vicariously (sample weights corresponding to 1.0 g of metal, $n = 20$). Because of the too high trace contents also in the salts, the limits of detection for Fe, Ga and Zn could not be determined for CuAl25. As an approximation, for these elements the values obtained using pure copper nitrate are given [5].

During matrix separation about 1 mg of copper remains in the centrifugate. The amount of the second matrix element entering the trace concentrate during HMDTC precipitation is about 10 mg for zinc and less than 1 mg for aluminium. Hence the preconcentration coefficients related to the original metal matrix are about 100 for the Cu–Zn system, about 500 for the Cu–Al system and about 1000 for the Cu–Sn system.

The application of the procedure to real sample materials was tested using three technical alloys. The recoveries obtained with these samples and their trace concentrations are given in Table 2.

REFERENCES

- 1 O.G. Koch and G.A. Koch-Dedic, *Handbuch der Spurenanalyse*, Springer, Berlin, 1974.
- 2 R. Eidecker, Doctoral Thesis, Bochum, 1989.
- 3 M. Kohri, O. Kujirai, K. Yamada and H. Okochi, *Anal. Sci.*, 4 (1988) 293.
- 4 H. Yoshikawa, K. Isobe, H. Iwata and N. Benitani, *Fresenius' Z. Anal. Chem.*, 336 (1990) 444.
- 5 Ch. Frigge and E. Jackwerth, *Anal. Chim. Acta*, 242 (1991) 99.
- 6 R. Eidecker and E. Jackwerth, *Fresenius' Z. Anal. Chem.*, 328 (1987) 469.
- 7 H. Mittelstädt, Doctoral Thesis, Bochum, 1987.

Polyfunctionality of resin carboxyl sites in ion exchange with alkali metal ions

Hiroki Tamura, Masashi Kudo and Ryusaburo Furuichi

Faculty of Engineering, Hokkaido University, Sapporo 060 (Japan)

(Received 11th June 1992; revised manuscript received 18th September 1992)

Abstract

The ion-exchange behaviour of a weak acid-type cation-exchange resin with alkali metal ions was obtained as a function of pH by titration. The behaviour was analysed with a model that assumes that the resin has two types of carboxyl sites (I and II) with different reactivities (polyfunctionality) and that the ion exchange at each site is suppressed steadily with progress of ion exchange owing to electrostatic lateral interactions between the species in the solid/solution interphase. The ion-exchange parameters in the model were determined by multi-parametric curve fitting. The values indicate that the type I sites are much more reactive than the type II sites and are more subject to suppression. The polyfunctionality was ascribed to the micropore structure of the resin: the type I sites are distributed in wider pores where hydrated ions can be adsorbed electrostatically with larger lateral interactions and the type II sites in narrower pores where dehydrated ions are adsorbed by forming coordination-type chemical bonds with smaller lateral interactions. The activity coefficients of interphase species are discussed in terms of the electrostatic lateral interactions between these species.

Keywords: Ion exchange; Alkali metal ions; Carboxyl sites; Cation-exchange resin; Polyfunctionality

Ion exchange is important in analytical chemistry, e.g., in the separation of particular ions from other ions, in the preconcentration of ions from very dilute solutions and in chromatography. When performing ion exchange, appropriate exchangers and optimum operating conditions must be chosen for a particular analytical purpose. Equilibrium considerations could provide such information in a more general and less time-consuming way than empirical approaches. However, there is no single theory of ion-exchange equilibria that fully explains or predicts the extent of ion exchange.

Recently, a model was proposed [1] for the exchange of Na^+ ions with the carboxyl protons of a weak acid-type ion-exchange resin. This

model proposes that the resin has two types of carboxyl sites with different reactivities and that the exchange is suppressed with increasing coverage of exchange sites owing to an electrostatic repulsive interaction between adsorbed ions. By fitting the experimental data, equilibrium constants for ion exchange, electrostatic repulsive interaction constants and fractions of each type of sites were determined. These values fitted the experimental data well, showing that the numbers of the two types of sites are about the same and that one has much higher reactivity and repulsive interaction than the other. The polyfunctionality of the carboxyl group sites is interesting, and several possible reasons were considered. However, a satisfactory explanation was not achieved.

In this investigation, the ion exchange of other alkali metal ions was also observed and it was found possible to apply the model to these ions.

Correspondence to: H. Tamura, Faculty of Engineering, Hokkaido University, Sapporo 060 (Japan).

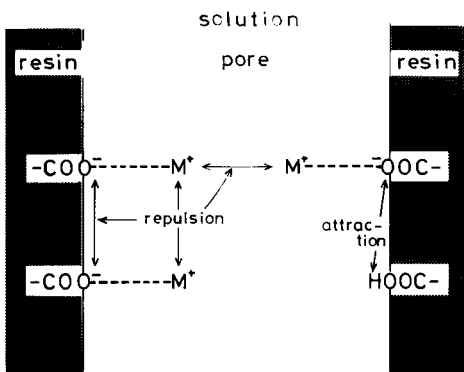


Fig. 1. Species in the resin/solution interphase and their mutual interactions in the resin pore structure.

To elucidate the polyfunctionality, the hydration state of the adsorbed ions and the microenvironment of the carboxyl group sites were considered based on the ion-exchange parameters, and the mechanism of the ion exchange is discussed.

THEORETICAL

As established previously [1], the ion-exchange resin has two types of carboxyl group sites (I and II) with different reactivities. The exchange reactions of alkali metal ions (M^+) with the protons of the type I and II sites are expressed as



The dissociated carboxyl group sites with a negative charge adsorb M^+ ions, and the adsorbed M^+ ions are located in the solution phase, forming an electrical double layer with the charged sites (Fig. 1). The adsorbed M^+ ion and negative charge site pair can be regarded as an ion pair, because the stoichiometry is well defined (the ratio between the amounts of adsorbed M^+ ion and negative charge site is unity) and the location of adsorbed M^+ ions is restricted to the vicinity of the charged sites.

If ϕ is the fraction of site I to the total sites, the mass-balance equations for sites I and II are

$$[-\text{COO}_I\text{H}] + [-\text{COO}_I^- \cdot M^+] = \phi N_s \quad (3)$$

$$[-\text{COO}_{II}\text{H}] + [-\text{COO}_{II}^- \cdot M^+] = (1 - \phi) N_s \quad (4)$$

where the terms in square brackets are the concentrations of the respective sites in the resin (mol g^{-1}) and N_s is the total exchange capacity of the resin (mol g^{-1}).

The mass-action law relationships for reactions 1 and 2 are

$$K_I = \frac{[-\text{COO}_I^- \cdot M^+][H^+]}{[-\text{COO}_I\text{H}][M^+]} \quad (5)$$

$$K_{II} = \frac{[-\text{COO}_{II}^- \cdot M^+][H^+]}{[-\text{COO}_{II}\text{H}][M^+]} \quad (6)$$

The ion-exchange reactions are suppressed with increasing extent of ion exchange, and the concentration ratios, K_I and K_{II} , decrease [1]. It was considered that the Gibbs free energy change in the exchange process contains a further term that increases linearly with coverage owing to lateral interactions between the species in the solid/solution interphase, as in the Frumkin isotherm [2]. The concentration ratios, K_I and K_{II} , are then given by

$$K_I = K_I^\circ \exp(-A_I\theta_I) \quad (7)$$

$$K_{II} = K_{II}^\circ \exp(-A_{II}\theta_{II}) \quad (8)$$

where K_I° and K_{II}° are the intrinsic equilibrium constants, A_I and A_{II} are the lateral interaction constants and θ_I and θ_{II} are the coverages of the I and II sites with adsorbed M^+ ions. The expressions for θ_I and θ_{II} are

$$\theta_I = [-\text{COO}_I^- \cdot M^+] / (\phi N_s) \quad (9)$$

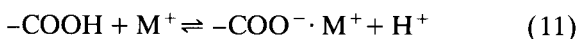
$$\theta_{II} = [-\text{COO}_{II}^- \cdot M^+] / [(1 - \phi) N_s] \quad (10)$$

The coverages are defined with respect to the total concentrations of the respective types of sites. As will be described later, the type I and II sites are distributed over the different regions of the resin, and the definition of the coverage here allows a comparison of the coverages of the different regions and hence a comparison of A_I and A_{II} .

Equations 7 and 8 indicate that the ion-exchange reactions are suppressed with increasing coverage of site I and II, as the concentration ratios decrease exponentially with increasing coverage. The lateral interaction constants, A_I and A_{II} , thus express the extent of suppression of ion exchange by adsorption.

The causes of the suppression may be electrostatic interactions between the species in the solid/solution interphase (Fig. 1). The adsorbed ion and charged site pairs are aligned on the surface of the solid resin and repel each other due to electrostatic repulsion both between the adsorbed ions and between the charged sites. The electrostatic repulsion increases with increasing extent of ion exchange, and results in a progressive suppression of further ion exchange. For the unreacted carboxyl sites, the electrostatic attractive interaction between the carboxyl protons and the neighbouring negative sites can be another cause of the suppression. This attraction inhibits the release of the carboxyl protons and suppresses ion exchange.

The overall or observed exchange reaction is



The measured concentration of adsorbed ions is the sum of the concentrations at the type I and II sites:

$$[-\text{COO}^- \cdot \text{M}^+] = [-\text{COO}_I^- \cdot \text{M}^+] + [-\text{COO}_{II}^- \cdot \text{M}^+] \quad (12)$$

In experiments, the concentrations of adsorbed ions are measured as a function of pH for a given M^+ ion concentration, and the total ion-exchange capacity of the resin, N_s , is known. Then, the concentrations of adsorbed M^+ ions at the respective sites can be calculated with the constants K_I° , K_{II}° , A_I , A_{II} and ϕ as parameters. Calculations and measurements are compared for all the experimental data, and the optimum values of the parameters, giving the smallest deviation, are determined as described previously [1].

EXPERIMENTAL

Materials

The ion-exchange resin was Amberlite IRC-84 with a total exchange capacity, N_s , of 1.0×10^{-2} mol g^{-1} [3]. Analytical-reagent grade lithium, sodium, potassium and caesium nitrate and hydroxide were used as received.

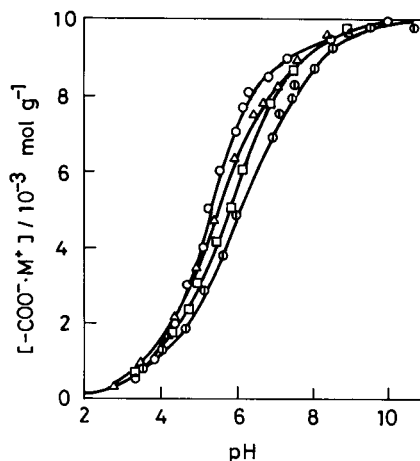


Fig. 2. Amounts of alkali metal ions, M^+ , adsorbed per gram of ion exchanger (Amberlite IRC-84) as a function of pH for an ionic strength of 0.5 M (MNO_3) at 25°C. $\circ = \text{Li}^+$, $\triangle = \text{Na}^+$; $\square = \text{K}^+$; $\diamond = \text{Cs}^+$. Points, experimental; curves, calculated.

Procedure

The ion-exchange resin samples (275–550 mg) were suspended in 200 cm^3 of electrolyte solutions containing 0.5 mol dm^{-3} MNO_3 at 25°C. The suspensions were stirred, various amounts of 1 mol dm^{-3} HNO_3 solution were added and nitrogen was bubbled through for 3 h to remove dissolved carbon dioxide. Then, 4 cm^3 of 1 mol dm^{-3} MOH solution were added, the pH was monitored and the pH values showing no change over 3 h were taken as equilibrium values. Blank titrations were also carried out for solutions without the resin. The amount of H^+ released by the ion exchange was measured with the titrations and the amount of adsorbed M^+ ions was obtained. The details of the procedure have been described previously [1].

RESULTS AND DISCUSSION

Figure 2 shows the amount of alkali metal ions, M^+ , adsorbed per gram of the resin, $[-\text{COO}^- \cdot \text{M}^+]$, as a function of pH. It increases with increasing pH as the functional group for ion exchange is a weak acid. The amount of adsorbed ions increases in the order $\text{Cs}^+ < \text{K}^+ < \text{Na}^+ < \text{Li}^+$ in the pH range 4–8.

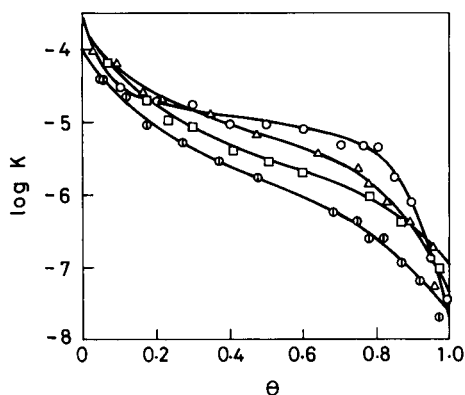


Fig. 3. Logarithm of the concentration ratios, K , as a function of coverage of exchange sites, θ , for an ionic strength of 0.5 M (MNO_3) at 25°C. $\circ = \text{Li}^+$; $\triangle = \text{Na}^+$; $\square = \text{K}^+$; $\diamond = \text{Cs}^+$. Points, experimental; curves, calculated.

The concentration ratio, K , and the coverage, θ , for the overall exchange reaction (Eqn. 11) are

$$K = \frac{[-\text{COO}^- \cdot \text{M}^+][\text{H}^+]}{[-\text{COOH}][\text{M}^+]} \quad (13)$$

$$\theta = [-\text{COO}^- \cdot \text{M}^+]/N_s \quad (14)$$

The values of K and θ corresponding to the experimental data were calculated and $\log K$ was plotted against θ (Fig. 3). It can be seen that K is not constant, and apparently the simple mass-action law does not hold.

The equations developed in the theoretical section were applied to the experimental data, and the relevant constants were determined (Table 1). The curves in Figs. 2 and 3 were calculated with these constants, showing excellent fits with the data points. Calculations with the constants determined here allow an assessment or a prediction of the extent of ion exchange over a wide range of conditions.

TABLE 1

Ion-exchange parameters for Amberlite IRC-84 with alkali metal ions (M^+) at an ionic strength of 0.5 M (MNO_3) and 25°C

M^+	$\text{Log } K_1^\circ$	$\text{Log } K_{\text{II}}^\circ$	$\text{Log } A_1$	$\text{Log } A_{\text{II}}$	ϕ
Li^+	-3.09	-4.75	1.09	0	0.285
Na^+	-3.39	-4.78	0.987	0.103	0.509
K^+	-3.26	-5.16	0.992	0.274	0.497
Cs^+	-3.34	-5.35	1.07	0.306	0.461

Table 1 shows that the values of K_1° are: $\text{Cs}^+ \approx \text{K}^+ \approx \text{Na}^+ < \text{Li}^+$ and the values of K_{II}° increase in the order $\text{Cs}^+ < \text{K}^+ < \text{Na}^+ \approx \text{Li}^+$. These sequences are related to those for the measured amounts of adsorbed ions. The K_1° values are more than one order of magnitude larger than the K_{II}° values. The values of A_1 are about the same for all the alkali metal ions, but A_{II} increases in the order $\text{Li}^+ < \text{Na}^+ < \text{K}^+ < \text{Cs}^+$; A_1 is 5–10 times larger than A_{II} . The experimental data for Na^+ ions are those given previously [1], and the K_1° , K_{II}° and ϕ values are the same as in [1]. The values of A_1 and A_{II} for Na^+ changed according to the new definition of coverage here.

In the previous paper [1], two causes were suggested for the different reactivities of the resin carboxyl sites: the difference in the molecular structure of the carboxyl sites (isomerism) and the effect of cross-linking of the polymer chains surrounding the carboxyl sites (microenvironment). According to the manufacturer, the molecular structure of the carboxyl sites is the same, considering the raw materials and the processes employed in producing the ion exchanger [4]. This indicates the microenvironment to be the cause of the polyfunctionality.

Amberlite IRC-84 used in this investigation is a gel-type microporous ion exchanger. The micropores are the spaces between the polymer chains, which appear when the resin swells in aqueous solution. The pore size depends on the content of cross-linking agent, and with increasing cross-linking less swelling occurs and the pore size decreases [5]. The resin pore structure in turn affects the reactivity of the exchanger; with increasing cross-linking ion exchange becomes more difficult, especially for ions with larger radii [6]. Microscopically, the porosity of a resin bead is not uniform because of a non-random distribution of the cross-linking agent in the resin [7,8], and this may cause the polyfunctionality established in this investigation.

Ions in aqueous solutions are hydrated. It is assumed that the type I sites are in wider pores where hydrated ions can be adsorbed and the type II sites are in narrower pores where dehydration must occur before adsorption can take place. This distinction between the type I and II

sites can explain the differences in the ion-exchange parameters with the types of sites and kinds of ions here (Table 1).

The changes in the ϕ values are explained by the hydrated radii of ions. Ions with smaller crystallographic radii have larger charge densities and bind more dipolar water molecules. The $\text{Li}^+(\text{aq})$ ion in water has the largest hydrated radius among the alkali metal ions [9–11]. The fraction of the type I sites, ϕ , for Li^+ is therefore the smallest. The ϕ values for Na^+ , K^+ and Cs^+ are similar and the hydrated radii of these ions seem to be close. The values of K_i° and A_i are also nearly the same for these ions, suggesting similar hydrated radii.

That K_i° is larger than K_{II}° can be explained by the different hydration states of ions adsorbed on the type I and II sites. For ions adsorbed on the type II sites, dehydration occurs prior to adsorption, and K_{II}° is smaller than K_i° because the equilibrium constant for dehydration is much smaller than unity.

That A_i is larger than A_{II} indicates that electrostatic interaction at the type I sites is larger than at the type II sites. This can also be ascribed to the different hydration states of adsorbed ions on the type I and II sites. On the type I sites, the adsorbed ions are hydrated and the adsorption is due to electrostatic attraction between the hydrated ion and charged site. On the type II sites, however, dehydrated ions are adsorbed, and the adsorption seems similar to complexation with coordination-type chemical bonds, which substitutes hydrated water molecules for ligand carboxyl groups. Less polarization or charge separation of the complexes formed at the type II sites would explain why A_{II} is smaller than A_i .

The increase in K_{II}° and the decrease in A_{II} with decreasing atomic number of the ions also suggests the adsorption on the type II sites to be coordination-type bond formation. Ions with smaller crystallographic radii form more stable complexes with less polarization, as Li^+ ions form more stable EDTA complexes than Na^+ ions [12].

At the type I sites, electrostatic interaction contributes more to the adsorption than at the type II sites, as mentioned above. However, the

Li^+ ion, with the largest hydrated radius and hence the smallest charge density, shows the largest K_i° value and an A_i value similar to those for the other alkali metal ions. There seems to be some contribution of coordination-type bonds to the adsorption of Li^+ ions on the type I sites. The similar A_i values may be due to interaction between ions adsorbed on opposite pore walls. The cross-pore interaction together with the neighbouring-ion interactions are illustrated in Fig. 1. With increasing hydrated radii, the electric charge density of ions decreases, decreasing the repulsion between neighbouring ions, but the inter-ionic distance across the pore becomes shorter, which increases the repulsion between ions across the pore. It is likely that the contribution of the cross-pore repulsion makes the A_i values similar, irrespective of the hydrated radii of ions.

The reported order of affinities of alkali metal ions for the carboxyl group sites [13,14] is the same as that determined here. However, there has been no satisfactory explanation for this order, as only electrostatic attractions have been considered. In this investigation, the hydration states of ions and the micropore structure of the ion-exchange resin were considered, and coordination-type bonds together with electrostatic attractions are suggested to explain the affinity order. A more detailed evaluation of the extent of dehydration of ions and critical pore diameters for the type I and II sites is difficult, because quantitative data on the hydrated radii of alkali metal ions and the size distribution of micropores of ion-exchange resins are lacking.

The intrinsic equilibrium constant, K_i° , established in this investigation is defined by the activities of the species participating in the ion exchange (i represents either the type I or II sites), and the activities are then substituted with the concentrations and the activity coefficients, y , as

$$K_i^\circ = K_i \frac{y(-\text{COO}_i^- \cdot \text{M}^+)y(\text{H}^+)}{y(-\text{COO}_i\text{H})y(\text{M}^+)} \\ = K_i y(-\text{COO}_i^- \cdot \text{M}^+) / y(-\text{COO}_i\text{H}) \quad (15)$$

where K_i is the concentration ratio and $y(\text{H}^+)/y(\text{M}^+) = 1$ or a constant close to 1 for a

fixed ionic strength. Combining the expressions for K_i° in Eqns. 7 and 8 with Eqn. 15 leads to

$$y(-\text{COO}_i^- \cdot \text{M}^+) / y(-\text{COO}_i\text{H}) = \exp(A_i \theta_i) \quad (16)$$

The exponential function expressing the suppression of ion exchange is related to the activity coefficients of interphase species.

Laszlo [15] empirically assigned an exponential function to the activity coefficient of undissociated carboxyl sites and arbitrarily assigned unity to that of dissociated sites with adsorbed ions. However, as discussed above, the activity of dissociated sites with adsorbed ions changes with the mutual electrostatic repulsion and so $y(-\text{COO}_i^- \cdot \text{M}^+)$ cannot be unity.

The following functions are proposed as the activity coefficients of the interphase species by considering the electrostatic lateral interactions (Fig. 1):

$$y(-\text{COO}_i^- \cdot \text{M}^+) = \exp(\alpha_i \theta_i) \quad (17)$$

$$y(-\text{COO}_i\text{H}) = \exp(-\beta_i \theta_i) \quad (18)$$

where α_i is the electrostatic repulsion constant and β_i is the electrostatic attraction constant. For dissociated sites with adsorbed ions, mutual electrostatic repulsion is acting and the activity coefficient increases with increasing coverage to exceed unity (Eqn. 17). For undissociated sites, electrostatic attraction is acting and the activity coefficient decreases to a value less than unity (Eqn. 18). By substituting Eqns. 17 and 18 in Eqn. 16, we obtain the lateral interaction constant A_i as

$$A_i = \alpha_i + \beta_i \quad (19)$$

In the discussion of lateral interactions, the type I and II sites were considered to distribute in different regions of the resin or in physically segregated micropores. The possibility of interactions between different types of sites was tested with a model that assumes a random distribution of the type I and II sites. However, the fit to the data was worse.

The lateral interaction constants may also be derived by considering the potential difference at the solid/solution interface [16]. However, for ion-exchange resins, the potential difference cannot be measured directly or controlled externally,

and a discussion based on the potential is not attempted.

In this investigation, the ion-exchange behaviour of a weak acid-type cation-exchange resin interacting with alkali metal ions was analysed with the model proposed here. The model assumes polyfunctionality of resin carboxyl sites which arises from the heterogeneous micropore structure of the resin and suppression of ion exchange due to electrostatic lateral interactions between solid/solution interphase species. The model applies to any ion-exchange system, and an ion-resin combination is characterized by a unique set of parameter values.

REFERENCES

- 1 H. Tamura, T. Oda and R. Furuichi, *Anal. Chim. Acta*, 244 (1991) 275.
- 2 E. Gileadi, E. Kirowa-Eisner and J. Penciner, *Interfacial Electrochemistry*, Addison-Wesley, Reading, MA, 1975, pp. 82–83.
- 3 Technical Bulletin, Fluid Process Chemicals: Amberlite IRC-84, Rohm & Haas, Philadelphia, PA, 1981, p. 2.
- 4 S. Tamura (Rohm & Haas Japan, Tokyo), personal communication, 1990.
- 5 J. Korkisch, *CRC Handbook of Ion Exchange Resins: Their Application to Inorganic Analytical Chemistry*, Vol. 1, CRC Press, Boca Raton, FL, 1989, p. 8.
- 6 O. Samuelson, *Ion Exchange in Analytical Chemistry*, Wiley, New York, 1953, p. 13.
- 7 J. Korkisch, *CRC Handbook of Ion Exchange Resins: Their Application to Inorganic Analytical Chemistry*, Vol. 1, CRC Press, Boca Raton, FL, 1989, p. 9.
- 8 W. Rieman, III, and H.F. Walton, *Ion Exchange in Analytical Chemistry*, Pergamon, Oxford, 1970, p. 13.
- 9 F.A. Cotton and G. Wilkinson, *Advanced Inorganic Chemistry*, Interscience, New York, 1967, p. 242.
- 10 C.W. Davies, *Ion Association*, Butterworths, London, 1962, p. 150.
- 11 J.O'M. Bockris and A.K.N. Reddy, *Modern Electrochemistry*, Vol. 1, Plenum, New York, 1974, p. 125.
- 12 G. Schwarzenbach and H. Ackerman, *Helv. Chim. Acta*, 30 (1947) 1798.
- 13 J. Korkisch, *CRC Handbook of Ion Exchange Resins: Their Application to Inorganic Analytical Chemistry*, Vol. 1, CRC Press, Boca Raton, FL, 1989, p. 16.
- 14 W. Rieman, III, and H.F. Walton, *Ion Exchange in Analytical Chemistry*, Pergamon, Oxford, 1970, p. 45.
- 15 J.A. Laszlo, *J. Nutr. Biochem.*, 2 (1991) 609.
- 16 R.O. James and G.A. Parks, in E. Matijevic (Ed.) *Surface and Colloid Science*, Vol. 12, Plenum, New York, 1982, pp. 119–216.

Determination of nonionic surfactants by spectrophotometry after extraction with potassium triiodide

Anna A. Boyd-Boland and James M. Eckert

Department of Inorganic Chemistry, University of Sydney, Sydney, NSW 2006 (Australia)

(Received 12th June 1992; revised manuscript received 11th August 1992)

Abstract

A method is described for the determination of nonionic surfactants in the concentration range 0.1–1 mg l⁻¹. The surfactant is extracted into 1,1,1-trichloroethane as an uncharged adduct with potassium triiodide and the determination is completed by measuring the absorbance of the extract at 380 nm. The performance of the method in the presence of anionic surfactants and the major ions of sea water is assessed.

Keywords: Spectrophotometry; Extraction; Sea water; Surfactants; Waters

Reagents containing iodine and potassium iodide in water have been used previously in spectrophotometric studies of nonionic surfactants. Baleux [1], for example, determined ethoxylate nonionics in the concentration range 1–20 mg l⁻¹ by absorbance measurements at 500 nm after addition of an iodine–iodide reagent. Others have studied the interaction of iodine–iodide and nonionic surfactants as a function of the oxyethylene chain lengths of the surfactants [2,3].

This paper describes a method for the determination of nonionic surfactants involving extraction of a neutral adduct of surfactant, iodine and potassium iodide and spectrophotometry of the extract. The new method differs in three ways from previous applications of an iodine–iodide reagent: inclusion of a liquid–liquid extraction step, the choice of wavelength (380 nm) and the

concentration range which can be determined (0.1–1 mg l⁻¹, as Triton X-100).

EXPERIMENTAL

Apparatus and reagents

Standard reference nonionic surfactant solution. The reference nonionic surfactant was Triton X-100 (Merck, gas chromatography grade). Triton X-100 is polyethyleneglycol mono-*p*-(1,1,3,3-tetramethylbutyl)phenyl ether with an average of approximately 10 ethoxy units per molecule. A stock standard solution was prepared containing 1000 mg l⁻¹ and diluted further as required.

Iodine–iodide reagent. Dissolve 124.5 g of potassium iodide and 0.64 g of iodine in water and dilute to 250 ml. Contains 10 mM I₂ and 3 M KI.

1,1,1-Trichloroethane. The commercial solvent (Aldrich, 99%) was used without purification.

Correspondence to: J.M. Eckert, Department of Inorganic Chemistry, University of Sydney, Sydney, NSW 2006 (Australia).

Anionic surfactant. A solution containing 5.93% (w/w) active linear alkylbenzenesulfonic acids (LAS) of mean molecular weight 342 was obtained from the US Environmental Protection Agency and used to prepare a 1000 mg l^{-1} solution which was diluted further as required.

Absorbances were measured with a Hewlett-Packard 8452A diode array spectrophotometer.

Recommended procedure

Place a 200-ml water sample in a 250-ml separating funnel, wrapped in aluminium foil and fitted with a PTFE stopcock. Add 10 ml of iodine-iodide reagent and 10.0 ml of 1,1,1-trichloroethane. Immediately, shake vigorously for 1 min and allow the phases to separate. Run about 9 ml of extract (the bottom layer) into a clean, dry centrifuge tube which has been wrapped in aluminium foil. Cover the tube with a small square of foil and centrifuge, at room temperature and 2500 rpm (ca. 1100 *g*), for 5 min. Measure the absorbance of the clarified extract at 380 nm with 1,1,1-trichloroethane in the reference cell.

Carry out a blank determination with 200 ml of distilled water. The blank absorbance should not be more than 0.010. Calculate the surfactant concentration in the water sample (as mg Triton X-100 l^{-1}) by comparison with standards.

Note: The colour of the extract is stable, away from light, for at least 8 h. If the extract is not measured immediately, it should be stored in a cool, dark place and care taken to minimise evaporation.

RESULTS AND DISCUSSION

Extraction conditions and efficiency

A series of extractions was carried out with reagents containing from 2 to 20 mM I_2 and from 0.5 to 3.0 M KI. The proposed reagent composition gave the lowest blank readings and a linear calibration graph for 0.1–1 mg Triton X-100 l^{-1} . The extraction time was chosen as 1 min after a study to determine the minimum time required to give reproducible absorbances and a linear calibration graph. Varying the pH of the aqueous

phase by including buffers of pH 3.7–9.4 had no significant effect on recovery. The extraction efficiency, obtained from the ratio of the absorbances of successive extracts of the same standard Triton X-100 solution, corrected for the blank, was 97%.

Extracted species

UV-visible spectra of extracts obtained from standard Triton X-100 solutions by following the recommended procedure contain a peak at 510 nm (free iodine) and a second peak at 380 nm which, unlike the peak at 510 nm, is not present in the blank and sensitively reflects the concentrations of surfactant in the standard solutions. Determinations by the proposed method are therefore completed by absorbance measurements at 380 nm.

Nonionic surfactants, with donor oxygen atoms, and iodine, an electron acceptor, together form charge-transfer complexes with λ_{max} in the region 360–390 nm. The dependence of absorption at this wavelength on the concentration and degree of aggregation of the surfactant has provided the basis for methods of measuring critical micelle concentrations [4–7]. Such complexes do not appear to be responsible for the peak at 380 nm in extract spectra. When solutions are prepared containing I_2 and Triton X-100 in 1,1,1-trichloroethane, there is a peak with λ_{max} 390 nm if both solutes are present in mM concentrations. The peak is not evident, however, if the concentration of surfactant is lowered to the μM levels known to be in the extracts.

An alternative explanation of the peak in question is that it is due to triiodide ions, extracted as a neutral adduct with surfactant molecules and K^+ ions as the counter ions. This was tested by an experiment in which extracts from water blanks and standard Triton X-100 solutions were analysed for K^+ and I_3^- ions. I_3^- in the extracts was determined from absorbance measurements at 380 nm, taking ϵ_{max} at this wavelength to be 2.53×10^4 , which is the mid-range of values in the literature (2.50 – 2.55×10^4) for triiodide salts with large cations in various organic solvents [8,9]. To measure K^+ in the extracts, aliquots were evaporated to dryness and

TABLE 1
Composition of extracts

Triton X-100 (mg l ⁻¹)		K ⁺ (μmol) ^b	I ₃ ⁻ (μmol) ^b
(μmol) ^a			
1.00	0.309	0.3 (±0.1)	0.29 (±0.03)
2.00	0.618	0.5 (±0.2)	0.57 (±0.01)

^a Amounts of surfactant in 200-ml aliquots of standard solutions. ^b Amounts of K⁺ and I₃⁻ in 10.0-ml extracts, corrected for blanks. Means of triplicate determinations. Standard deviations are given in parentheses.

water solutions of the residues analysed by flame atomic absorption spectrometry.

The results of the experiment are given in Table 1. Since the extraction of surfactant is virtually quantitative, the mole ratio Triton X-100:K⁺:I₃⁻ in the extracts is, within experimental error, 1:1:1. This observation is consistent with the following extraction mechanism. A K⁺ ion is coordinated by the ether oxygens of a Triton X-100 molecule, after the manner of crown-ether complex formation by alkali metal ions and cyclic polyoxyethylene molecules [10]. The resulting large cation is extracted as a neutral ion pair with I₃⁻ as the counter ion. A similar mechanism has been proposed [11] for the extraction of nonionic surfactant with NH₄⁺ and Co(NCS)₃OH₂⁻ ions in the widely-used Greff method for the determination of nonionic surfactants [12].

The peak at 380 nm is 27 nm to longer wavelength than that of KI₃ in water [13]. This wavelength difference is an example of *metachromasia*, a term originally applied to the colour change that can occur when a dye is adsorbed by a substrate but since applied to any spectral shift caused by ion pairing, micelle formation and/or charge-transfer effects [14].

Calibration, precision and limit of detection

The calibration graph was linear in the concentration range 0.1–1 mg l⁻¹, as Triton X-100. Values of the slope and intercept are given in Table 2, which also shows estimates of precision at the 0.1 and 0.5 mg l⁻¹ levels and the limit of detection, taken to be the surfactant concentration which gave an absorbance, corrected for the

TABLE 2
Slope and intercept of calibration graph, precision and limit of detection

Parameter	Units	Value
Slope ^a	l mg ⁻¹	0.749 (±0.016)
Intercept ^a		0.000 (±0.008)
Precision ^b	R.S.D. (%)	8
	R.S.D. (%)	7
Limit of detection		
	mg l ⁻¹	0.05

^a Slope and intercept of regression line in a typical calibration run; triplicate standards at each of four concentrations in the range 0.1–1.0 mg l⁻¹, as Triton X-100. Standard deviations are given in parentheses. ^b Eight standards were measured at each concentration.

blank, equal to twice the standard deviation of a set of 10 readings at or near blank level.

Interferences

The mean recoveries of Triton X-100 from artificial sea water, prepared as in [15], were 102 and 107% with relative standard deviations ±1–2% (Table 3). In the presence of anionic surfactants, recoveries and precisions were more variable, being 96–119(±1–9)% (Table 4). These results do not point to any obvious systematic interference by anionic surfactants but indicate rather that separating and clarifying the extract is more difficult when the total surfactant concentration is relatively high.

Conclusions

The proposed method has a number of attractive features. It makes use of readily available

TABLE 3
Recovery of Triton X-100 from artificial sea water

Triton X-100 added (mg l ⁻¹)	Mean Triton X-100 found ^a (mg l ⁻¹)	S.D. ^b (mg l ⁻¹)	Recovery (%)
0	< 0.05	0.01	–
0.50	0.51	0.01	102
1.00	1.07	0.01	107

^a Mean of triplicate determinations. ^b Standard deviation.

TABLE 4

Recovery of Triton X-100 from water and sea water in the presence of LAS

LAS present (mg l ⁻¹)	Triton X-100 added (mg l ⁻¹)	Mean Triton X-100 found ^a (mg l ⁻¹)	
		In water	In sea water
0.5	0	ND ^b	ND
0.5	0.50	0.55 (±0.01)	0.48 (±0.04)
1.0	0	ND	ND
1.0	1.00	1.13 (±0.07)	1.19 (±0.01)
2.0	0	ND	ND
2.0	1.00	1.15 (±0.06)	1.08 (±0.04)

^a Mean of triplicate determinations. Standard deviations are given in parentheses. ^b ND = not detected (< 0.05 mg l⁻¹, as Triton X-100).

chemicals, an organic solvent that is less toxic than the solvents used in other methods and a simple spectrophotometric finish. Only one phase-separation step is required and the method is applicable, without modification, to fresh, estuarine and sea-water samples. Anionic surfactants, present in most natural waters containing nonionic surfactants, do not pose a serious interference problem, at least when present in concentrations comparable with that of the nonionic surfactants. It is important, however, to keep the extract out of strong light and care is also needed

to limit loss by evaporation of the potentially ozone-damaging organic solvent.

REFERENCES

- 1 B. Baleux, C.R. Acad. Sci. Paris, 274 (1972) 1617.
- 2 T. Kenjo and T. Matsumoto, J. Jpn. Oil Chem. Soc., 10 (1961) 418.
- 3 J.-H. Chang, M. Ohno, K. Esumi and K. Meguro, J. Am. Oil Chem. Soc., 65 (1988) 1664.
- 4 S. Ross and J.P. Olivier, J. Phys. Chem., 63 (1959) 1671.
- 5 P. Becher, J. Phys. Chem., 63 (1959) 1675.
- 6 J.E. Carless, R.A. Challis and B.A. Mulley, J. Colloid Sci., 19 (1964) 201.
- 7 P.H. Elworthy, J. Pharm. Pharmacol., 12 (1960) 293.
- 8 R.E. Buckles, J.P. Yuk and A.I. Popov, J. Am. Chem. Soc., 74 (1952) 4379.
- 9 A.I. Popov and R.F. Swensen, J. Am. Chem. Soc., 77 (1955) 3724.
- 10 N.N. Greenwood and A. Earnshaw, Chemistry of the Elements, Pergamon, Oxford, 1989, pp. 107, 108.
- 11 P.T. Crisp, in J. Cross (Ed.), Trace Analysis of Nonionic Surfactants in Nonionic Surfactants — Chemical Analysis, Marcel Dekker, New York, 1987, pp. 95–97.
- 12 R.A. Greff, E.A. Setzkorn and W.D. Leslie, J. Am. Oil Chem. Soc., 42 (1965) 180.
- 13 A.D. Awtrey and R.E. Connick, J. Am. Chem. Soc., 73 (1951) 1842.
- 14 G.M. Eckert, F. Gutmann and H. Keyzer in G.M. Eckert, F. Gutmann and H. Keyzer (Eds.), Electropharmacology, CRC Press, Boca Raton, FL, 1990, pp. 231–234.
- 15 J. Lyman and R.H. Fleming, J. Mar. Res., 3 (1940) 134.

Improved spectrophotometric method for the determination of low levels of bromide

David R. Jones

CSIRO Division of Coal and Energy Technology, North Ryde, NSW 2113 (Australia)

(Received 23rd March 1992; revised manuscript received 1st September 1992)

Abstract

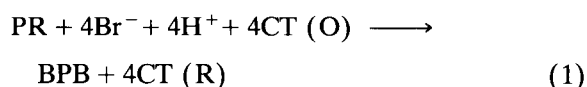
The addition of an excess of NH_4^+ has been found totally to suppress the competing chlorination reactions that have caused problems in all previously published applications of the chloramine-T–Phenol Red method for trace bromide analysis. As a result of this, the dynamic range of the method has been extended four-fold (from 35 to 150 μM , 2.8 to 12 $\mu\text{g ml}^{-1}$ bromide) without sacrificing sensitivity or precision. By adding an ionic strength buffer (1 M NaNO_3) and NH_4^+ (1.5 mM) to both calibration and test samples the concentration of bromide can be accurately measured in solutions containing up to 2 M chloride.

Keywords: Spectrophotometry; Brines; Bromide; Interferences

The determination of low levels of bromide is of importance in many diverse areas of research. These include the metabolism of bromide-containing pharmaceuticals [1], the use of bromide as a conservative tracer to measure the hydrodynamic properties of surface- and ground-waters [2], the effectiveness of brominated compounds as disinfectants and biocides [3,4], and the role of bromide in trihalomethane formation following the chlorination of drinking water [5].

The chloramine-T–Phenol Red spectrophotometric method is a potentially very sensitive and rapid technique for determining low levels of bromide in aqueous solution [6]. In this method Bromophenol Blue (BPB) is generated by the electrophilic substitution of Phenol Red (PR) by oxidised bromide species. Chloramine-T (CT) is used as the oxidising agent. Results obtained by other workers investigating the mechanism of halogenation of *p*-xylene indicate that HOBr ,

H_2OBr^+ , and BrCl are likely to be the active brominating species [7] in the spectrophotometric method. The overall stoichiometry for the production of BPB is



where (O) = oxidised form and (R) = reduced form.

Unfortunately, serious interferences by chloride and ammonium ions have been reported [1,8]. Another, more fundamental, problem is that the hypochlorous acid present in solutions of CT also reacts with PR. This reaction produces Chlorophenol Blue (CPB), which has a very similar visible absorption spectrum to BPB. The major consequence of this competing chlorination reaction is that the reagent blanks produced by application of the published standard method for bromide [6] develop intolerably high colour intensities [9]. The extent of this interference is greatly increased in the presence of chloride. Reduction of the CT to PR ratio from 4 to 1.5 overcame this

Correspondence to: D.R. Jones, CSIRO Division of Coal and Energy Technology, P.O. Box 136, North Ryde NSW 2113 (Australia).

difficulty [9]. Coincidentally, the previously reported interferences by Cl^- and NH_4^+ were effectively eliminated. However, the disadvantage of this approach is that the maximum concentration of bromide in solution that can be measured accurately is $35 \mu\text{M}$.

One group has adapted the spectrophotometric method for use in an automated flow-injection analyser [1]. In this case the problem of high blanks was effectively eliminated by measuring the absorbance of BPB only 20 s after the CT reagent was added. This approach works because CPB is produced more slowly than BPB. There are, however, potential problems with measuring the colour so soon. Since the absorbance of the solution will be increasing rapidly when the measurement is made, any imprecision introduced by slight variations in temperature, sample matrix, or behaviour of the sample introduction valves is likely to be exacerbated. Moreover, this technique for minimising the contribution of the reagent blank cannot be applied to the manual analysis of batches of samples.

In the work reported here the results of a detailed mechanistic study of the colour-producing reactions have been used to develop a method of greatly extended dynamic range that is free from interference by NH_4^+ and Cl^- .

EXPERIMENTAL

Apparatus

A Jasco UVIDEC-610 double-beam spectrophotometer was used to obtain the absorbance data. Glass cells with a path length of 1 cm were used. Measurements of pH were made with an Orion Ross™ combination electrode coupled to an Activon™ Model A-211 portable pH meter. The required volumes of reagents were delivered with Oxford™ volumetric dispensers or a Hamilton™ digital autodiluter. Screw-cap polyethylene scintillation vials of 20 ml capacity were used as reaction vessels.

Reagents

All solutions were prepared in water which had been distilled and deionised and passed

through a $0.2\text{-}\mu\text{m}$ porosity filter. Reagents used were of analytical-reagent grade.

Concentrated stock solutions of the following reagents were prepared: chloramine-T (CT), 3.55 mM; Phenol Red (PR), 0.56 mM; sodium thiosulfate, 2.0 M; KBr, 5 mM. The pH 4.6 buffer stock contained 0.5 M acetic acid and 0.5 M sodium acetate. The preparation of the working reagent solutions required for the standard [6] and modified [9] spectrophotometric methods has been described previously.

The hypochlorite stock was produced by diluting AJAX™ sodium hypochlorite solution (3.5%). This was standardised by iodometric titration with thiosulfate [10]. A stock solution of bromine was prepared by shaking an excess of liquid bromine with water until a saturated solution was obtained. The supernatant was then decanted and stored at 4°C in the dark. This solution was also standardised by titration with thiosulfate. Stock solutions of ammonia were standardised by titration with HCl, using Methyl Orange as the indicator.

Procedures

Mechanism of NH_4^+ action. Vials containing 10 ml of 0 or $44 \mu\text{M}$ NH_3 plus 0.5 ml of acetate buffer were prepared. For the vials containing no NH_3 , 0.5 ml of PR and 0.5 ml of HOBr or HOCl ($[\text{HOBr}]_0 = 25 \mu\text{M}$, $[\text{HOCl}]_0 = 40 \mu\text{M}$) working reagent solutions (see above) were added sequentially. The production of colour was then monitored at 590 nm. The solutions which contained NH_3 were treated differently. HOBr or HOCl solution (0.5 ml) was added and the mixture allowed to react for 5 min prior to the injection of 0.5 ml of PR solution. Colour production was then followed as described above.

The modified CT-PR method. A synthetic matrix containing 3 mM NaCl, 1 mM NaHCO_3 , 1.5 mM MgCl_2 and 0.3 mM MgSO_4 was used to simulate the ionic composition of real samples in this phase of the work. The optimum concentration of $400 \mu\text{M}$ NH_4^+ required to inhibit the CT side reaction with PR was obtained by evaluating blank colour development as a function of $[\text{NH}_4^+]$.

To 10 ml volumes of matrix containing from 0–150 μM of Br^- were added 0.5 ml of NH_4^-

acetate buffer (standard acetic acid–sodium acetate buffer solution containing 8 mM of NH_3) and 0.5 ml of PR solution. The reaction was initiated by injection of 0.5 ml of CT. **It is most important to thoroughly mix the solution immediately after the addition of CT.** The starting concentrations of reagents in the 11.5 ml total volume are as follows: PR = 53 μM , NH_4^+ = 350 μM and CT = 160 μM . After 20 min, 0.13 ml of thiosulfate solution were added. The vials were allowed to stand for a further 15 min, before measuring their absorbances.

Chloride interference. Initial trial experiments showed that commonly available analytical-reagent grade chloride salts (NaCl , KCl , MgCl_2) contained significant trace levels of bromide. Since molar concentrations of the chloride salt were going to be used, the presence of bromide at these levels would have interfered with the experiments to measure the effect of increasing chloride concentration. Accordingly, the salt containing the lowest initial level of bromide contamination (BDH™ NaCl) was further purified. Recrystallisation from water resulted in a two-fold reduction in the amount of bromide. The recrystallised NaCl was dissolved in water, and the resulting solution freed from the residual bromide impurity by purging it with chlorine gas [11].

Colour formation in blank and test solutions as a function of $[\text{Cl}^-]$: A series of vials containing the required amounts of bromide (0 and 37 μM) and chloride (0–2000 mM) in a total volume of 10 ml were prepared. The reagents for the modified spectrophotometric method were then added as described above.

Production of CPB as a function of $[\text{NH}_4^+]$: A procedure identical to that described above was followed for solutions containing 600 or 2000 mM NaCl , and 0–1500 μM of NH_4^+ . The NH_4^+ was produced by adding the required volume of NH_3 stock solution to the pH 4.6 acetate buffer solution. Since the $\text{p}K_a$ of NH_4^+ is 9.25 at 25°C, essentially all of the added NH_3 will be protonated at pH 4.6. The addition of up to 1500 μM NH_3 to the reaction solutions did not significantly alter the pH of the system.

Influence of ionic strength alone: NaNO_3 was substituted for NaCl in the experiment that was

carried out to measure colour formation in blank and test solutions has described above.

RESULTS AND DISCUSSION

Mechanism of action of NH_4^+

The pH dependence of the rate of formation of halamine species shows that they are produced by the reaction between hypohalous acids and ammonia at pH values less than 7 [12,13]:



where $n = 1-3$ and $\text{X} = \text{Cl}, \text{Br}$.

At the pH of 4.6 used in the current work the vast majority of NH_3 will be present as the ammonium ion ($\text{p}K_a$ of NH_4^+ is 9.25). In view of this, the following discussion will refer to the concentration of NH_4^+ rather than that of NH_3 , despite the fact that NH_3 is the actual reactant.

Both hypochlorous (HOCl) and hypobromous (HOBr) acids will be generated at pH 4.6 in a solution containing Br^- and CT. In order to reduce the complexity of the system for the initial mechanistic studies, solutions of HOCl and HOBr were substituted for the mixture of uncertain composition that is produced by the reaction between CT and Br^- . By starting with known concentrations of these reactants, published second order rate constant data for halamine formation could be used to derive the rate constants appropriate for the conditions used in this work.

The concentration of HOCl used was 40 μM . This level was chosen since it corresponded, in oxidising equivalents, to the concentration of CT used in the modified spectrophotometric method [9] discussed in the introduction. A starting concentration of 25 μM was used for Br^- and HOBr . The reactions of the hypohalous acids with PR were carried out in the presence and absence of NH_4^+ .

The broken curves in Fig. 1 show the development of colour in the HOCl and HOBr systems in the absence of NH_4^+ . It is clear from these plots that BPB is produced much more rapidly than CPB. This result is consistent with the findings of Voudrias and Reinhard [7] in their study of the

mechanism of electrophilic substitution of *p*-xylene by solutions of hypochlorous and hypobromous acids [7]. These workers showed that the rate constants for substitution with Br-containing electrophilic species were much higher than for the corresponding Cl-containing species.

The absorbance versus time profiles obtained in the presence of NH_4^+ are also plotted in Fig. 1. An initial concentration of $44 \mu\text{M}$ NH_4^+ was used in order to ensure complete conversion of the hypohalous acids to at least their corresponding monohalamine derivatives. It is clear from Fig. 1 that the generation of CPB is almost completely inhibited by NH_4^+ whereas BPB is produced just as rapidly as when this species is absent. Comparison of the results for HOBr in the presence and absence of NH_4^+ indicates that the bromamines behave almost identically to HOBr in their reaction with PR. This finding is in agreement with the work of Sollo et al. [12] which showed that all three of the brominated amine species are capable of reacting rapidly with PR. In contrast to the reactivity displayed by the bromamines, the chloramine species are orders of magnitude less reactive than HOCl.

Margerum et al. [13] and Galal-Gorchev and Morris [14] have studied the distribution of chloramine and bromamine species ($n = 1-3$ in Eqn. 2), respectively, as a function of pH and halogen

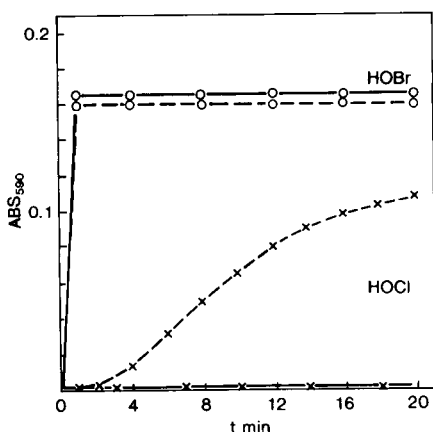


Fig. 1. Effect of NH_4^+ ($44 \mu\text{M}$) on the reaction between $26 \mu\text{M}$ PR and $25 \mu\text{M}$ HOBr or $40 \mu\text{M}$ HOCl. (○—○) HOBr + PR + NH_4^+ ; (×—×) HOCl + PR + NH_4^+ ; (○---○) HOBr + PR; (×---×) HOCl + PR.

TABLE 1

Formation rate constants for halamine species

Product	Rate equation	k	Refer- ence	Derived $t_{1/2}$ (s)
NH_2Cl	$k_1[\text{NH}_3][\text{HOCl}]$	$6.2 \times 10^6 \text{ M}^{-1} \text{ s}^{-1}$	16	16
NHCl_2	$k_2[\text{NH}_2\text{Cl}][\text{HOCl}]$	$150 \text{ M}^{-1} \text{ s}^{-1}$	13	ca. 20
NH_2Br	$k_3[\text{NH}_3][\text{HOBr}]$	$7.5 \times 10^7 \text{ M}^{-1} \text{ s}^{-1}$	17	
		$4 \times 10^7 \text{ M}^{-1} \text{ s}^{-1}$	18	
	Average =	$5.8 \times 10^7 \text{ M}^{-1} \text{ s}^{-1}$		15
NHBBr_2^a	$k_4[\text{H}^+][\text{OBr}_T]^2$	$2.4 \times 10^8 \text{ M}^{-2} \text{ s}^{-1}$	18	ca. 7

^a $[\text{OBr}_T] = \text{Total concentration of hypobromite species, } [\text{HOBr}] + [\text{OBr}^-].$

and ammonia concentration. The results obtained by these workers indicate that, in the case of the current study, the predominant forms should be NH_2Cl and NHCl_2 , and NHBr_2 and NBr_3 . Rate constants for mono- and dihalamine formation, together with reaction half-times calculated for the conditions employed in this work are listed in Table 1. No rate constants were found for the formation of the trihalamines but published data [14,15] suggest that these species are also formed rapidly. The data in Table 1 show that halamine formation would have been complete within the 5 min allowed prior to the addition of PR to the solutions containing NH_4^+ and HOCl or HOBr (Fig. 1).

The above results showed that the reaction of CT with PR to produce CPB can be selectively blocked. This finding indicated that the working range of the method should be able to be extended above a Br^- concentration of $35 \mu\text{M}$, whilst still retaining the stability and low background afforded by the use of a low CT to PR ratio.

Development of improved method

Further development of the method was based on a target value of $155 \mu\text{M}$ for the maximum concentration of Br^- . This value was chosen since complete conversion to BPB would yield an ab-

sorbance of approximately 2.0, which corresponds to the maximum that can be measured with good precision on an average laboratory spectrophotometer. In order to satisfy the stoichiometry specified by Eqn. 1, the concentrations of CT and PR needed for 155 μM Br^- are four and two times higher, respectively, than those required for 35 μM Br^- . Trial experiments showed that 400 μM of NH_4^+ is sufficient to completely suppress CPB formation in the presence of 160 μM CT. The absorbance of the reagent blank under these conditions is only 0.014. This value is in marked contrast to the absorbance of 0.5 produced in the absence of NH_4^+ .

The blank-corrected calibration graph produced by using the reagent concentrations specified above is plotted in Fig. 2. It is seen to consist of two linear segments which define bromide concentration ranges of 0–40 and 40–140 μM .

Precision of determination

In order to evaluate the precision and detection limit of the modified method, five replicates of each of three bromide standard solutions were analysed on two separate days. These determinations were carried out in a synthetic matrix de-

TABLE 2

Precision of modified bromide method

Statistics	[Br ⁻] (μM)					Batch
	0	23.5	78.4	133	154.5	
\bar{x} ^a	0.019	0.268	1.06	–	2.18	1
σ	0.0007	0.001	0.003	–	0.002	
\bar{x}	–	0.271	1.06	1.89	–	2
σ	–	0.002	0.005	0.003	–	

^a Five replicates for each concentration point. \bar{x} = mean, σ = standard deviation.

signed to simulate a slightly brackish freshwater stream. The results are summarised in Table 2. Relative standard deviations ranged from 0.7 for 23.5 μM Br^- down to 0.09 at the maximum concentration of 154.5 μM Br^- that was used. The precision is excellent over a wide range of concentrations both within, and between batches of samples. The detection limit ($\pm 2\sigma$ of the blank) of the method is 0.2 μM .

Application to saline and high ionic strength solutions

The extent of interference by Cl^- in the CT–PR method has previously been shown to depend on the CT concentration used [9]. It has been suggested that this interference may occur via the reaction of HOCl (in equilibrium with CT) with Cl^- to produce Cl_2 which is a stronger chlorinating agent than HOCl [3]. Whatever the precise mechanism of this process, the addition of excess NH_4^+ should eliminate the problem since all active chlorinating species will be rapidly converted to non-reactive chloramines. In this context it should be noted that the addition of NH_3 has been shown to considerably reduce Cl^- interference in a field method for Br^- that uses peroxy-monosulfate (oxone) rather than CT as the oxidising agent [19].

Figure 3 shows the effect of 0–2000 mM Cl^- on the modified spectrophotometric method. The colour intensity in the blank increases steadily with increasing $[\text{Cl}^-]$. This behaviour suggests that there is insufficient NH_4^+ available to react with the increased concentrations of active chlorinating species that are produced at such high Cl^- levels. Accordingly, the absorbance of the blank

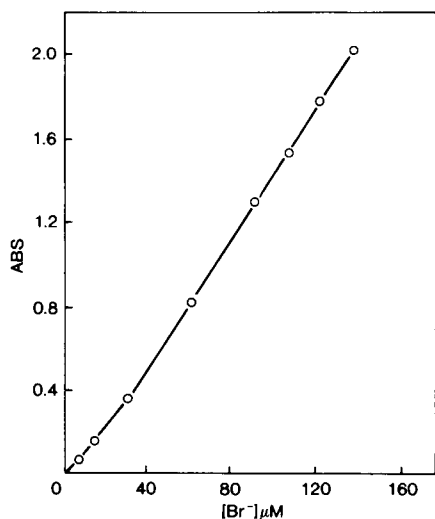


Fig. 2. Blank-corrected (abs. of blank = 0.019) standard curve; [CT] = 160 μM , [PR] = 52 μM , $[\text{NH}_4^+] = 400 \mu\text{M}$. Composition of synthetic matrix: 3 mM NaCl, 1 mM NaHCO_3 , 1.5 mM MgCl_2 and 0.3 mM MgSO_4 .

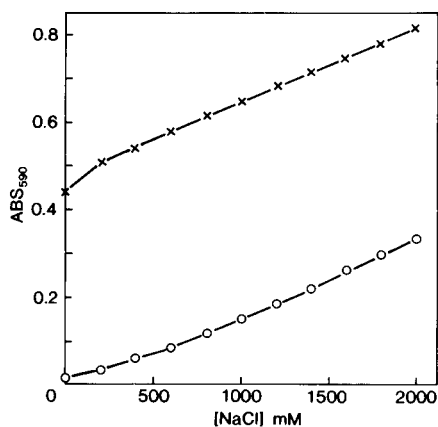


Fig. 3. Production of colour in blank (○—○, [Br⁻] = 0 μM) and test (×—×, [Br⁻] = 37 μM) solutions as a function of [NaCl].

was determined as a function of NH₄⁺ concentration at medium to high levels of Cl⁻ (Fig. 4). The results show that 1500 μM NH₄⁺ will completely suppress CPB formation in solutions containing as much as 2 M Cl⁻. This is a very important result since it means that the spectrophotometric method can be applied directly to brine solutions, without the need to resort to sample dilution to reduce Cl⁻ interference.

The method incorporating 1400 μM NH₄⁺ was applied to a series of Br⁻ standard solutions containing 0–2 M NaCl (Fig. 5, broken lines). The most notable feature in Fig. 5 is that, for most Br⁻ concentrations, there is a small, but significant, dependence of colour yield on Cl⁻. Although the chemical interference by Cl⁻ was

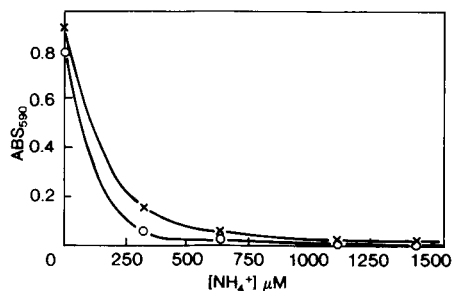


Fig. 4. Effect of [NH₄⁺] on production of CPB in solutions containing (○—○) 600 and (×—×) 2000 mM of bromide-free NaCl.

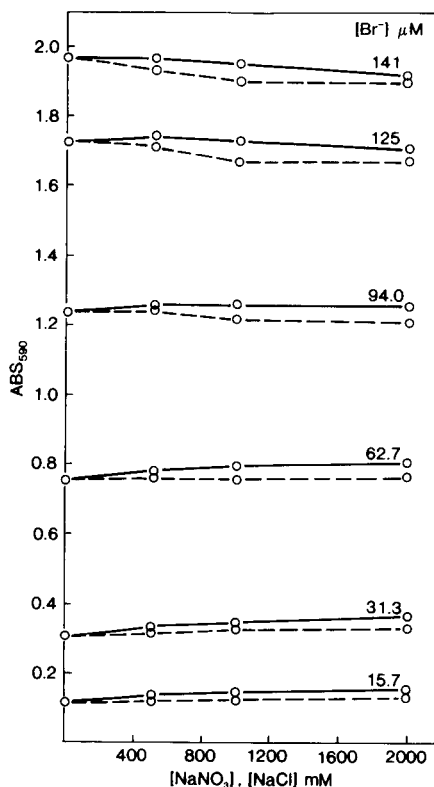


Fig. 5. Dependence of colour production on (○---○) [NaCl] and (○—○) [NaNO₃]. Absorbance values are blank corrected. [CT] = 160 μM, [PR] = 52 μM, [NH₄⁺] = 1500 μM.

completely suppressed by NH₄⁺, the effect of ionic strength at such high salt levels needed to be determined. This was done by substituting NaNO₃ for NaCl in the experiment (Fig. 5, solid lines). The close similarity between the plots for NaCl and NaNO₃ strongly suggests that increasing ionic strength is largely responsible for the variations in colour yield. Both the pK_a of acids (e.g. BPB) and the rate of reaction between species of opposite charge will decrease in response to an increase in ionic strength [20,21].

The above results show that an ionic strength buffer should be used when applying the spectrophotometric method to saline samples. Inspection of Fig. 5 shows that the addition of NaNO₃ to a level of 1 M should be sufficient to overcome ionic strength effects for all but the most saline of solutions.

Conclusions

The addition of excess NH_4^+ has been shown to completely suppress the chlorination side reactions that have caused serious difficulties in all previously published applications of the PR method for the determination of Br^- . This means that it will no longer be necessary to use undesirably short reaction times in automated applications in order to overcome the problem of high blank absorbances. The excellent stability of the colour, coupled with the low absorbances of the reagent blanks, will mean lower detection limits and better precision for both manual and automated applications of the method. Since the same NH_4^+ concentration is added to the standards and samples, there will be no problems with variable levels of NH_4^+ within a batch of samples.

In addition to eliminating the interference by chloride, the addition of NH_4^+ has enabled at least a four-fold increase in the dynamic range of the spectrophotometric method. The maximum Br^- concentration that can be determined without dilution is now governed by the ability of a spectrophotometer to accurately measure high absorbance values.

It is recommended that an ionic strength buffer be used when applying the spectrophotometric method to samples with ionic strengths greater than 50 mM. Figure 5 shows that the use of an ionic strength of 1 M coupled with an NH_4^+ concentration of 1.5 mM should be sufficient to overcome chloride interference and ionic strength effects in all but the most saline of solutions. This condition could be most conveniently achieved in practice by preparing a working sodium acetate-acetic acid buffer solution containing 30 mM NH_4^+ and 10 M NaNO_3 .

It must be noted that, in common with all spectrophotometric methods for Br^- determination that involve electrophilic substitution, the above procedure will be subject to a potential negative interference by natural and man-made organic compounds. Those samples which contain significant levels of dissolved organic carbon should always be checked by standard addition or pre-treated to remove this material.

The author wishes to thank Mr. Stephen Persi for his dedicated assistance in carrying out the experimental work described in this paper.

REFERENCES

- 1 P.I. Anagnostopoulou and M.A. Koupparis, *Anal. Chem.*, 58 (1986) 322.
- 2 D.R. Jones and R.F. Jung, *Water Res.*, 24 (1990) 125.
- 3 A. Bousher, P. Brimblecombe and D. Midgley, *Water Res.*, 23 (1989) 1049.
- 4 J.D. Johnson and R. Overby, *J. Sanit. Eng. Div. Am. Soc. Civ. Eng.*, 97 (1971) 617.
- 5 T.V. Luong, C.J. Peters and R. Perry, *Environ. Sci. Technol.*, 16 (1982) 473.
- 6 American Public Health Association, American Water Works Association, Water Pollution Control Federation, *Standard Methods for the Examination of Water and Wastewater*, American Public Health Association, Washington, DC, 16th edn., 1985, pp. 278, 279.
- 7 E.A. Voudrias and M. Reinhard, *Environ. Sci. Technol.*, 22 (1988) 1049.
- 8 C.L. Basel, J.D. Defreese and D.O. Whittemore, *Anal. Chem.*, 54 (1982) 2090.
- 9 D.R. Jones, *Talanta*, 36 (1989) 1243.
- 10 A.I. Vogel, *A. Textbook of Quantitative Inorganic Analysis*, Longman, London, 3rd edn., 1962, p. 363.
- 11 D.D. Perrin, W.L.F. Armarego and D.R. Perrin, *Purification of Laboratory Chemicals*, Permagon, New York, 2nd edn., 1980, p. 525.
- 12 F.W. Sollo, T.E. Larson and F.F. McGurk, *Environ. Sci. Technol.*, 5 (1971) 240.
- 13 D.W. Margerum, E.T. Gray, Jr. and R.P. Huffman, *Organometals and Organometalloids — Occurrence and Fate in the Environment* (ACS Symposium Series, Vol. 82), American Chemical Society, Washington, DC, 1978, Ch. 17.
- 14 H.A. Galal-Gorchev and J.C. Morris, *Inorg. Chem.*, 4 (1965) 899.
- 15 G.W. Inman, Jr., T.F. La Pointe and J.D. Johnson, *Inorg. Chem.*, 15 (1976) 3037.
- 16 I. Weil and J.C. Morris, *J. Am. Chem. Soc.*, 71 (1949) 1664.
- 17 L.B. Richardson, D.T. Burton, G.R. Helz and J.C. Rhoderick, *Water Res.*, 15 (1981) 1067.
- 18 G.W. Inman and J.D. Johnson, *Environ. Sci. Technol.*, 18 (1984) 219.
- 19 H.F. Dobolyi, *Anal. Chem.*, 56 (1984) 2961.
- 20 R.G. Bates, *Determination of pH. Theory and Practice*, Wiley, New York, 2nd edn., 1973.
- 21 K.J. Laidler, *Chemical Kinetics*, McGraw Hill, New York, 2nd edn., 1965.

Modified acid–base behaviour of resin-bound pH indicators

S. Motellier and P. Toulhoat

Commissariat à l'Energie Atomique, DSD / SCS / LCASH, B.P. 6, 92265 Fontenay-aux-Roses Cedex (France)

(Received 28th May 1992; revised manuscript received 4th September 1992)

Abstract

A fibre-optic device was used to characterize the acid–base properties of pH indicators bound to polymeric resins either by π – π or ionic interactions. The ability of an indicator to give up a proton was found to be significantly modified by the nature of its binding to the resin. When involved in hydrophobic interactions, the increase in its apparent pK_i value accounts for the electron-donating role of the resin. In contrast, when ionically bound to the resin, it displays a higher acidity; in this instance, the resin plays the role of an electron-withdrawing entity. Mixed influences have also been observed.

Keywords: Acid–base indicators; Fibre-optic sensors; pH

Spectrophotometric pH determinations have recently been enhanced by the development of devices using fibre optics [1–8]. These devices are particularly convenient for measurements in locations that are difficult to reach such as *in vivo* or *in situ*. One of the possibilities is based on dye sensors where a chromogenic reagent is immobilized on the tip of an optical fibre. The recorded change in colour is related to the concentration of the compound of interest, i.e. H^+ .

Numerous methods for coupling the pH indicator to the optical fibre have been reported, including embedding and adsorption on polymer supports covalently bound to the fibre [1,2,4,5,8] or covalent binding either to silica [9–11] or to polymer supports [6,7]. Although the latter appears to be the most promising approach, it was

only recently developed owing to inherent difficulties in the polymer chemistry.

Direct immobilization of the chromogenic reagent on polymer supports is convenient and easy to apply, and hence has been extensively studied. Modifications of the acid–base properties of the bound indicators, via either ionic [12] or hydrophobic [2,13,14] binding, have been observed; however the extent of these interactions remain unexplained.

The acid–base behaviour of a series of pH indicators bound to various resins was investigated in this work with the object of gaining a better understanding of the mechanisms involved in the binding.

EXPERIMENTAL

The absorbance spectra of indicators in solution were recorded with a Perkin-Elmer Lambda 5 UV–visible spectrophotometer.

Correspondence to: S. Motellier, Laboratoire de Chimie Analytique en Solution et d'Hydrogéochimie, Commissariat à l'Energie Atomique, D.S.D./S.C.S./L.C.A.S.H., B.P. 6, 92265 Fontenay-aux-Roses Cedex (France).

Amberlite XAD-4 resin was purchased from Prolabo and the AG1-X4, AG1-X8 and AG2-X8 resins purchased from Bio-Rad. All chemicals (analytical-reagent grade) and standard buffer solutions were purchased from Prolabo or Merck. The water used throughout was purified with a Milli-Q system (Millipore).

Determination of indicators pK_i values in solution

For each indicator, a 0.1% solution in ethanol of the desired indicator was diluted (1 + 100) in standard buffer solutions. The visible spectra were recorded in the pH range 3–12. The wavelength of maximum absorbance was selected for the establishment of the sigmoid curves showing the absorbance behaviour of these indicators in solution.

Immobilization procedure

The resins consist of a styrene–divinylbenzene copolymer either as it is (XAD-4) or modified with anion-exchange functional groups [$-N(CH_3)_3^+$ for AG1-type resins and $-N(CH_3)_2C_2H_4OH^+$ for AG2-type resins]. The high hydrophobicity of the former allows direct adsorption of the molecules of indicators. The selected beads of resin (calibrated diameter, roughness of the surface) are successively washed with water and acetone. They are then dried prior to dipping for 1 min into a solution of the desired indicator (0.1% in ethanol). The duration of impregnation is a compromise between the magnitude and the response time of the signal.

The anion-exchange resins are washed with water and then dried prior to dipping for 1 min in the indicator solution (0.1% of the sodium salt of the indicator in ca. 10^{-3} M NaOH).

Determination of the resin-bound indicators pK_i values

A fibre-optic pH sensor [15] was used for the absorbance measurements at given pH values. The indicator-based bead of resin is immobilized at the distal end of a bundle of optical fibres to form a so-called optode. The light source is composed of three diodes of carefully chosen wave-

lengths and the transmitted light is collected on a receiver via a separate optical fibre.

The whole optode is introduced into a standard buffer solution and the signal is recorded until it reaches a steady-state value that corresponds to the resin-bound indicator equilibrated with the medium. The sigmoid curves were established at 590 or 620 nm, whichever was most suitable.

RESULTS AND DISCUSSION

The structures of the selected indicators are characterized by a sulphonphthalein pattern with various substituents. Phenol red can be considered as the reference compound as it bears only two hydroxy groups responsible for its proton-donating ability.

Figure 1 shows the curves of absorbance versus pH for several indicators (see Table 1) in solution, the theory of which was developed by Patrick and Svehla [16]. Their $pK_{i, \text{sol}}$ values derived from Fig. 1 are given in Table 2; they are

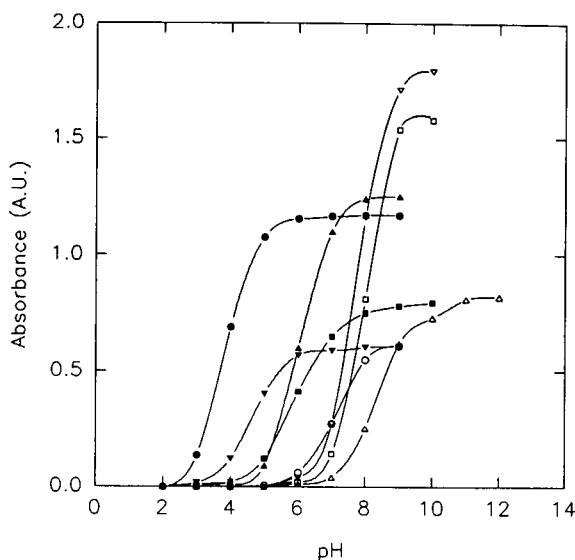


Fig. 1. Sigmoid curves of absorbance versus pH for pH indicators in solution. ● = BPB (592 nm); ▼ = BCG (616 nm); ■ = BPR (576 nm); ▲ = BCP (588 nm); ○ = BTB (620 nm); ▽ = PR (560 nm); □ = CR (572 nm); △ = mCP (580 nm). See Table 1 for names.

TABLE 1
Structures of the indicators

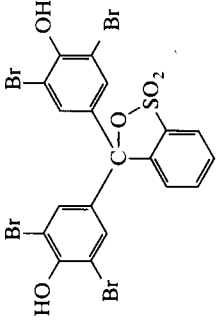
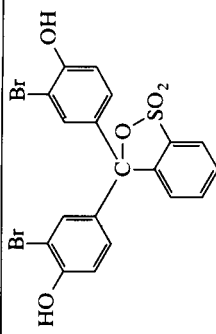
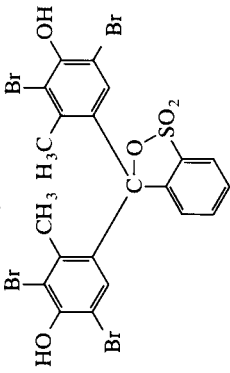
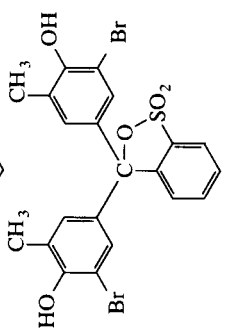
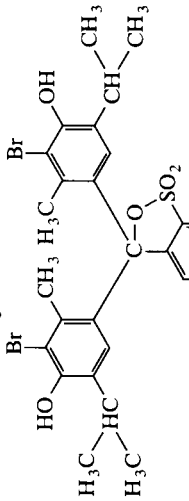
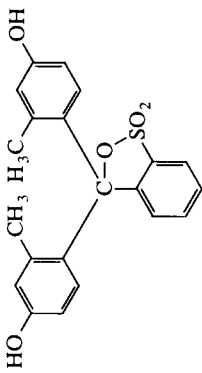
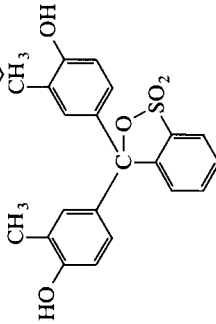
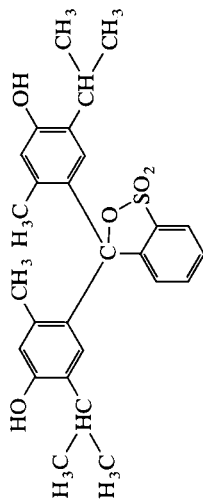
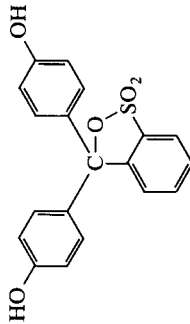
Name	Structure	Name	Structure
Bromophenol Blue (BPP)		Bromophenol Red (BPR)	
Bromocresol Green (BCG)		Bromocresol Purple (BCP)	
Bromothymol Blue (BTB)		<i>meta</i> -Cresol Purple (mCP)	
Cresol Red (CR)		Thymol Blue (TB)	
Phenol Red (PR)			

TABLE 2

Comparison between the apparent pK_i values of indicators in solution and adsorbed on XAD-4, AG1-X4, AG1-X8 and AG2-X8 resins

Parameter	BPB	BCG	BPR	BCP	BTB	PR	CR	mCP	TB
$pK_{i_{\text{H}}}$ ^a	3.85	4.66	–	6.12	7.1	7.81	8.25	8.3	8.90
$pK_{i_{\text{sol}}}$	3.7	4.6	5.9	6.0	7.2	7.8	8.0	8.4	9.1
$pK_{i_{\text{XAD-4}}}$	5.0	7.0	7.3	8.5	11.5	9.2	10.0	11.4	12.8
$pK_{i_{\text{AG1-X4}}}$	1.2	2.3	1.9	1.3	5.9	6.4	6.2	6.2	7.3
$pK_{i_{\text{AG1-X8}}}$	1.5	2.7	3.5	1.5	6.3	6.3	6.3	6.6	8.8
$pK_{i_{\text{AG2-X8}}}$	1.6	2.6	4.3	4.0	6.0	6.4	6.4	6.3	8.7

^a From [17]; $\mu = 0.1$ M.

consistent with the literature data [17] displayed for comparison.

The relative acid strengths of the indicators in solution may be explained with regard to the field effects induced by the either electron-withdrawing or electron-donating substituents located on their phenol rings.

Groups that withdraw (donate) electrons by the field effect increase (decrease) acidity [18]. This phenomenon is mainly due to a stabilizing (destabilizing) effect that spreads (concentrates) the negative charge of the conjugate base (phenolate anion). As a consequence, BPB, BCG, BPR, CPR, BCP and BTB, which all bear at least one electron-withdrawing group, are more acidic than Phenol Red, whereas CR and TB are less acidic. The electron-withdrawing effect of the halide substituent is stronger than the electron-donating effect of the methyl or 2-propyl groups, as the pK_i of BCP (see Table 2), which bears one methyl and one bromide, both in *ortho* positions with respect to the hydroxy group, is shifted towards higher acidity.

TABLE 3

Separate influences of substituents on the phenol rings of the indicators on their pK_i values, calculated as $\Delta pK = pK_0 - pK_i$, where pK_0 is for Phenol Red

Resin	Br (<i>ortho</i>) BPR	Methyl (<i>ortho</i>) CR	Methyl (<i>meta</i>) mCP	2-Propyl (<i>ortho</i>) TB, mCP
Solution	7.8 – 5.9 = 1.9	7.8 – 8.0 = –0.2	7.8 – 8.4 = –0.6	7.8 – 9.1 + 0.6 = –0.7
XAD-4	9.2 – 7.3 = 1.9	9.2 – 10.0 = –0.8	9.2 – 11.4 = –2.2	9.2 – 12.8 + 2.2 = –1.4
AG1-X4	6.4 – 1.9 = 4.5	6.4 – 6.2 = 0.2	6.4 – 6.2 = 0.2	6.4 – 7.3 – 0.2 = –1.1
AG1-X8	6.3 – 3.5 = 2.8	6.3 – 6.3 = 0.0	6.3 – 6.6 = –0.3	6.3 – 8.8 + 0.3 = –2.2
AG2-X8	6.4 – 4.3 = 2.1	6.4 – 6.4 = 0.0	6.4 – 6.3 = 0.1	6.4 – 8.7 – 0.1 = –2.4

A quantitative approach to the effect of structure on reactivity was first attempted by Hammett [19], who measured the influence of X substituents for *m*- and *p*-XC₆H₄Y on the reaction rate or equilibrium constant of a reaction taking place at the Y group. The Hammett equation states that

$$\log(K/K_0) = \sigma\rho = pK_0 - pK$$

where K_0 is the rate or equilibrium constant for X = H, K is the constant for the group X, ρ is a constant for a given reaction under a given set of conditions and σ is a constant characteristic of the group X.

From the above and considering the dissociation reaction of the indicator, it was possible to quantify the influence of each substituent on the pK_i value, depending on its position with respect to the hydroxy group (reference Phenol Red). The calculations are given in Table 3. They confirm the magnitude of the effect of bromide (1.9 units) compared with the influence of alkyl substituents [–0.7 for –CH(CH₃)₂].

The $pK_{i_{\text{sol}}}$ values were compared (Table 2) with those obtained with the same indicators adsorbed on XAD-4 (styrene–divinylbenzene copolymer, 4% cross-linking) and anion-exchange resins [AG1-X4, –N(CH₃)₃⁺ functional groups, 4% cross-linking; AG1-X8, –N(CH₃)₃⁺ functional groups, 8% cross-linking; and AG2-X8, –N(CH₃)₂CH₂OH⁺ functional groups, 8% cross-linking]. An overall comparison between the two sets of $pK_{i_{\text{sol}}}$ and $pK_{i_{\text{XAD-4}}}$ values in Table 2 shows a general tendency towards less acidic behaviour (positive ΔpK_i) for all the indicators immobilized on the resin, with a reference ΔpK_i

value of +1.4 for Phenol Red. The same trend was reported by Narayanaswamy and Sevilla [13] and Bacci et al. [14].

In addition, the same calculations as above, taking Phenol Red as the reference compound, can be completed (Table 3) and indicate that whereas the effect of bromide is not modified, the effects of electron-donating groups such as methyl in *ortho* or *meta* positions and 2-propyl in an *ortho* position are enhanced by the immobilization of the indicators on XAD-4.

The explanation of these phenomena lies in the nature of the binding between the indicator and the resin. The hypothesis put forward states that the aromatic rings of both the resin and the indicator are involved in a charge-transfer bonding to form π - π electron donor-acceptor complexes. Presumably the phenyl ring bearing the sulphonate (electron-attracting by the resonance effect) is the part of the indicator involved.

The general decrease in acidity, i.e., the destabilization of the phenolate anion by concentration of a negative charge on the $-\text{O}^-$, indicates that the aromatic ring is no longer available for the distribution of the electron density. These results support the hypothesis that the resin plays the role of an additional strong electron-donating group that influences the acid-base behaviour of the indicator and emphasizes the effect of electron-donating substituents when present on the indicator.

The anion-exchange resins show an opposite influence on the acid-base behaviour of the indicators with a decrease in $\text{p}K_i$ by ca. 1.4 for the reference compound Phenol Red. The calculations on the separate influence of substituents show an increase in the absolute value for Br and approximately no modification for methyl when the indicator is bound to the resin compared with their values in solution. The magnitude of these effects is greater with the AG1-X4 resin than with the XAD-4 resin, despite their similar physical structures (4% cross-linking). This can be explained by the higher energy of the ionic bonds involved with the AG1-X4, which induces stronger modifications to the electronic configuration of both the indicator and the resin molecules.

These results support the assertion that the

resin (via the ionic binding) acts as an electron-withdrawing entity by attraction of the sulphonate negative charge to stabilize the phenolate anion of the base form.

A comparison within anion-exchange resins shows two different aspects: first, the cross-linking of the resin is an important factor in the acid-base behaviour of the indicators to which it is bound. To be more specific, the greater the cross-linking, the lower is the influence of electron-withdrawing bromide and the higher is the influence of electron-donating methyl and 2-propyl substituents, i.e., the lower is the ionic character of the binding. This suggests a dual character of the binding with anion-exchange resins: ionic bonds involving the strongly basic quaternary functional groups of the resin and the sulphonate group of the indicator on the one hand, and charge-transfer bondings similar to XAD-4 between the aromatic rings of both the indicator and the polymeric matrix of the resin on the other. The share of the latter is logically increased with higher degrees of cross-linking of the resin. Second, the type of anion exchanger of the resin slightly modifies the general tendency: AG2-X8, which differs from AG1-X8 only in its quaternary functional group, seems to behave closer to XAD-4, i.e., smaller negative shifts for electron-withdrawing Br, greater positive shifts for electron-donating 2-propyl and better correlation for indicators bearing additional substituents. This is consistent with the relative basicity of the anion exchangers on both resins. $-\text{N}(\text{CH}_3)_2\text{CH}_2\text{OH}^+$ of AG2-X8 is less basic than $-\text{N}(\text{CH}_3)_3^+$ of AG1-X8, and therefore gives lower energy ionic bonds. This is equivalent to stating that π - π interactions comprise of a larger share with AG2- than with AG1-type resins.

The above indications are summarized in Fig. 2, which illustrates the separate contributions of Br, methyl and 2-propyl groups in *ortho* positions to the dissociation constant of the corresponding indicators (BPR, CR, TB) immobilized on the four resins versus their contribution to the same reaction occurring in solution. $\text{p}K_0$ corresponds to the dissociation constant of PR in each configuration. The contribution of methyl in a *meta* position was not taken into account here as it

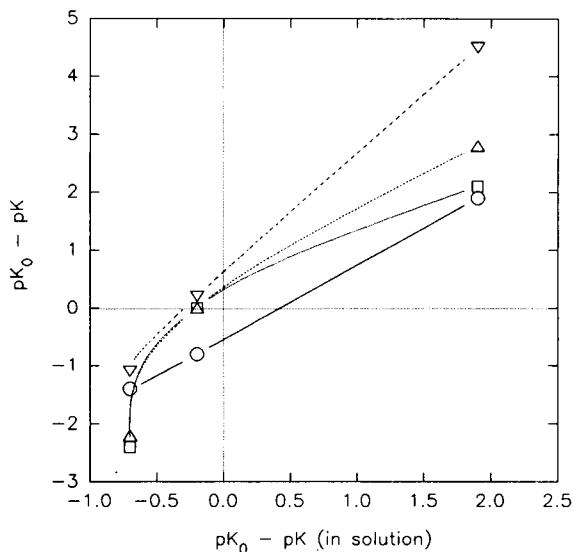


Fig. 2. Comparison between the separate influences of substituents of the phenol rings of immobilized indicators and in solution. \circ = XAD-4; ∇ = AG1-X4; Δ = AG1-X8, \square = AG2-X8.

shows a totally unrelated behaviour. All curves possess a positive slope (positive ρ), which is a characteristic of reactions that are helped by electron-withdrawing groups.

Figure 2 clearly demonstrates that XAD-4 and AG1-X4 resins behave similarly and display a linear relationship with respect to data obtained in solution:

$$pK_0 - pK = a\rho\sigma + b$$

where b represents the influence of the resin, with a negative value for XAD-4 (electron-donating) and a positive value for AG1-X4 (electron-withdrawing). AG1-X8 and AG2-X8 also show a positive intercept which confirms the same tendency to withdraw electrons from the indicator.

The pattern of the curves for these two resins, however, is non-linear. An important deviation for the 2-propyl substituent confirms the dual character of the binding with highly cross-linked resins.

The additivity of the influences of substituents on the dissociation constant of benzoic acids was verified by Stone and Pearson [20]. In this case,

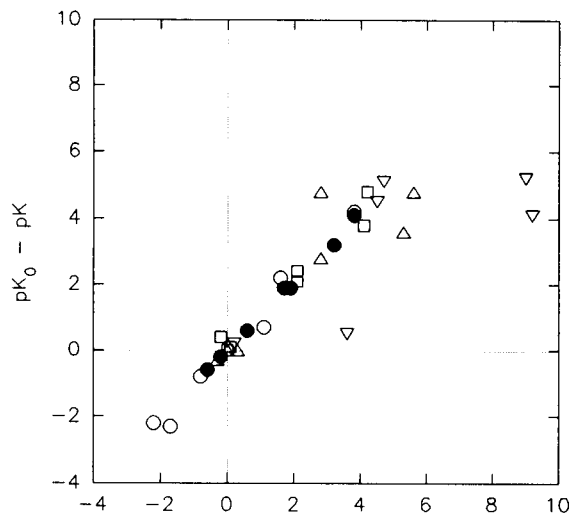


Fig. 3. Additivity of the substituents influences: $pK_0 - pK$ versus $\Sigma\Delta pK$ for each substituent. \bullet = Solution; \circ = XAD-4; ∇ = AG1-X4; Δ = AG1-X8; \square = AG2-X8.

$$pK_0 - pK = \rho\Sigma\sigma$$

For the present work, the values of $pK_0 - pK$ versus $\Sigma\sigma$ are plotted for each indicator in Fig. 3. $\Sigma\sigma$ is calculated for a multi-substituted indicator by addition of the separate contributions (see Table 3).

Additive influences would lead to the location of each point representing an indicator on the first diagonal line. In solution, and also immobilized on XAD-4, AG2-X8 and, to a lesser extent, AG1-X8, such a behaviour for the series of indicators is confirmed, whereas subsequent deviations from the diagonal can be observed for AG1-X4-bound indicators. These observations are further evidence of the different natures of the two bonds with XAD-4 and AG1-X4 and of the existence of $\pi-\pi$ interactions with AG1-X8 and AG2-X8 resins. It is usually assumed that non-additive influences are related to steric inhibition or resonance. Presumably the latter is the most probable explanation for the relatively high-energy ionic binding of the indicators.

Conclusion

The acid-base properties of sulphonphthalein pH indicators have been shown to be influenced by hydrophobic and ionic bindings to various

resins. The acidity constants of all the test indicators were found to be modified consistently with the alteration of the molecular electronic configuration induced by the nature of the binding. The effects can be quantified and even predicted for numbers of indicators with similar chemical structures, which is particularly helpful in the choice of the indicator whose change of colour will match the range of interest.

REFERENCES

- 1 G.F. Kirkbright, R. Narayanaswamy and N.A. Welti, *Analyst*, 109 (1984) 15.
- 2 G.F. Kirkbright, R. Narayanaswamy and N.A. Welti, *Analyst*, 109 (1984) 1025.
- 3 L.A. Saari and W.R. Seitz, *Anal. Chem.*, 54 (1982) 821.
- 4 T.P. Jones and M.D. Porter, *Anal. Chem.*, 60 (1988) 404.
- 5 T.P. Jones, S.J. Coldiron, W.J. Deninger and M.D. Porter, *Appl. Spectrosc.*, 45 (1991) 1271.
- 6 B.S. Rao, J.B. Puschett and K. Matyjaszewsky, *J. Appl. Polym. Sci.*, 43 (1991) 925.
- 7 S.R. Goldstein, J.I. Peterson and R.V. Fitzgerald, *J. Biomech. Eng.*, 102 (1980) 141.
- 8 Z. Zhujun, Y. Zhang, M. Wangbai, R. Russel, Z.M. Shakhsher, C.L. Grant and W.R. Seitz, *Anal. Chem.*, 61 (1989) 202.
- 9 B.G. Harper, *Anal. Chem.*, 47 (1975) 348.
- 10 L.T. Mimms, M.A. McKnight and M.W. Murray, *Anal. Chim. Acta*, 89 (1977) 355.
- 11 M. Bacci, F. Baldini and S. Bracci, *Appl. Spectrosc.*, 45 (1991) 1508.
- 12 M.C. Moreno, A. Martinez, P. Millan and C. Camara, *J. Mol. Struct.*, 143 (1986) 553.
- 13 R. Narayanaswamy and F. Sevilla, *Anal. Chim. Acta*, 189 (1986) 365.
- 14 M. Bacci, F. Baldini and A.M. Scheggi, *Anal. Chim. Acta*, 207 (1988) 343.
- 15 G. Boisdé and J.J. Perez, *Eur. Pat.*, 284 513 (1988).
- 16 R.A. Patrick and G. Svehla, *Anal. Chim. Acta*, 88 (1977) 363.
- 17 E. Bishop, *Indicators*, (International Series of Monographs in Analytical Chemistry, No. 51), Pergamon, Oxford, 1972, p. 99.
- 18 J. March, *Advanced Organic Chemistry – Reactions, Mechanisms, and Structure*, Wiley, New York, 3rd edn., 1985, p. 229.
- 19 H.H. Jaffé, *Chem. Rev.*, 53 (1953) 191.
- 20 R.M. Stone and D.E. Pearson, *J. Org. Chem.*, 26 (1961) 257.

BOOK REVIEWS

D.A.T. Southgate, *Determination of Food Carbohydrates*, 2nd edn., Elsevier Applied Science, London and New York, 1991 (ISBN 1-85166-652-4). ix + 232 pp. Price £65.00/US\$110.50.

This new edition of a book that has been much valued as a working manual for food analysts and technologists is timely, in view of the adoption of newer, especially chromatographic, techniques and renewed interest in food carbohydrates, engendered largely by the “dietary fibre” hypothesis, since the appearance of the First Edition in 1976. The author has, in general, succeeded admirably in his objective of revising the book to take cognizance of these developments.

There are eight, well-organised chapters. A brief introduction is followed by a succinct but comprehensive review of the wide variety of carbohydrates likely to occur in foods, and the physical and chemical properties relevant to their analysis. Four chapters are devoted to the general principles of extraction and analysis of the major classes of food carbohydrates: sugars, starch (including degradation products and modified starches), and the so-called “unavailable carbohydrates”, which are divided into two groups, namely structural components of the plant cell-wall (cellulose, hemi-celluloses and pectic substances) and non-structural polysaccharides, which include those used as additives (exudate and microbial gums, algal polysaccharides and modified celluloses). In Chapter 7 some problems posed by analysis for carbohydrates in specific food groups are discussed before, in the final, long chapter, practical details of the various methods are presented in a form designed to facilitate their application in the laboratory. The book ends with an Appendix, containing tables of data for use in certain classical methods, a useful bibliography and over 200 references.

There are some flaws: a few typographical errors, the author's tendency to use the words “strength” and “concentration” synonymously, which is confusing when applied to acid or alkali, and a glaring error in Table 6.1, which lists the rhamnogalacturonan tragacanth, *Khaya* and *Sterculia* gums as galactomannans, are faults that should be addressed in future editions. The inclusion of more recent references in the section of LC is also desirable; more space should be given to ion chromatography with pulsed amperometric detection, at the expense of the obsolescent ion-exchange separation of sugars as borate complexes. These minor criticisms aside, however, this useful book will surely prove indispensable in any laboratory concerned with analysis of food carbohydrates.

S.C. Churms

Ernest Merian (Ed.), *Metals and their Compounds in the Environment. Occurrence, Analysis and Biological Relevance*, VCH, Weinheim, 1991 (ISBN 3-527-26521-X). xxiii + 1438 pp. Price DM380.

This massive book is a *tour de force*. It contains such a wealth of information on the interaction of most metals (and As and Se) with the environment that it has to be the ultimate source book in this area. The book is essentially in two parts. Eighty six contributors deal with the occurrence, processing and disposal and analytical chemistry of the metals, of their location and speciation in the ‘environment’, be it body fluids and tissues, the chromosphere, waters, the indoor environment, soil or waste materials. There are discussions of the mobility of metals in and between these locations, of their presence in the food chain, and their beneficial and toxic effects

for man and animals. Toxicity is considered in detail, and there are separate chapters on immunotoxicology, mutagenic, carcinogenic and teratogenic effects, and ecogenetics. This first, 711-pp. section concludes with chapters on risk assessment and with Standards and Regulations.

The second section deals with each metal in turn, outlining its physical and chemical properties, sources, production, uses and waste products, distribution in the environment, uptake and metabolism by animals and plants, and with detailed descriptions of its toxicological effects and legal limits. A major strength of each chapter is the extensive bibliography, which provides a tremendous source of further information. Likewise there is a 66-pp. subject index, in keeping with a book of this type. Perhaps the only criticism would be the lack of information on radionuclides, considering their topical importance. Thus, information on Pu, Cs, etc. would have been welcomed. But this is but a minor omission in an otherwise excellent and most welcome text.

Alan Townshend

Helmuth Galster, *pH Measurement. Fundamental Methods, Applications, Instrumentation*, VCH, Weinheim, 1991 (ISBN 3-527-28237-8), x + 340 pp. Price DM155.00/£58.00.

Some of the classic textbooks like *Electrolyte Solutions* by Robinson and Stokes are regrettably out of print with no viable replacement yet. This book excites interest to see if it is a quality replacement for Bates' *Determination of pH. Theory and Practice* (Wiley, 1973) and the earlier 1954 edition with a different title. Alas, the answer is a disappointing, no: this is a translation from the German masquerading as an international book; for, starting on p. 1, we find it is firmly rooted in the DIN standards and citations to German literature and custom and practice, which deviate from IUPAC recommendations.

The author starts with a review of physical chemistry of electrolyte solutions, not all of it relevant, mostly too concise to be digestible and riddled with errors of all descriptions. On p. 41

and Chap. 2, we come again to pH and discussion of pH scales, reaching on p. 52 the extraordinary statement, referring to single and multipoint pH scales (endorsed by IUPAC), that "these add to the difficulty of understanding the already complex basis of pH values which is difficult enough already". One is reminded of motto cards available from bookstalls in the USA: "Don't confuse me with facts, my mind is made up!". Surely in a book of this nature one can reasonably expect a detailed discussion of the arguments with proper citations to the literature, especially since the Preface tells us a "correct understanding is essential to avoid misconceptions" and that the book is intended as a reference text.

The book is stronger, as one might expect from an author who worked for Dr. W. Ingold GmbH., when one comes to practical aspects where Bates' classic was notably weak. Regrettably, this is a parochial book with the translation editor and publishers both very much to blame.

A.K. Covington

K.G. Carr-Brion (Ed.), *Measurement and Control in Bioprocessing*, Elsevier Applied Science, London and New York, 1991 (ISBN 1-85166-620-6). x + 259 pp. Price £70.00.

The aim of the book is to give an introduction to the field of measurement and control for biochemists, biologists and chemists. The book contains eight chapters authored by different specialists in the respective fields.

The first two chapters are very general introductions to control and measurement. In spite of the addition of the term "bioprocessing" hardly any reference is given to the specific aspects of bioprocessing. Chapter 3 gives an overview of the subject of modelling of fermenters. The treatment is very readable but rather qualitative and little attention is paid to new trends in modelling approaches. The next chapter deals with biosensors in process control. This chapter is more general and of interest for all types of control, not only bioprocesses. Chapter 5 discusses the aspects of quality assurance in the biopharmaceu-

tical industry. Although it is an interesting contribution, it does not fit very well with the scope of the other chapters. The last three chapters, dealing with measurement and control in effluent treatment, process scale liquid chromatography and down-stream processing, respectively, fulfill best the aim of this book. They are state-of-the-art discussions of the respective topics and give the reader a flavour of the specific problems encountered in measurement and control in bioprocessing.

In conclusion, the book gives a very readable introduction to the field of control and measurement although in a very qualitative and general way. Only the last few chapters justify the emphasis laid in the title on the aspect of bioprocessing. The editor stresses in his preface the freedom given to the various authors to produce texts that reflect their own interests, but in the reviewer's opinion it is questionable whether such a freedom is an advantage for a book that is aiming to give an introduction to newcomers in the field. More strict guidelines to the authors could have led to a more consistent treatment of the subject.

Willem E. van der Linden

M.R. Smyth (Ed.), *Chemical Analysis in Complex Matrices*, Ellis Horwood, Chichester, 1992 (ISBN 0-13-127671-9). 295 pp. Price US\$90.00.

There are numerous definitions relating to the scope of Analytical Science but a unifying theme is the multidisciplinary nature of the subject. This book outlines the "Analytical Approach" that is common to all analytical problem solving and puts this approach into practice in a number of specific application areas. The definition of Analytical Science upon which the book is loosely based is "that science which deals with the detection, identification and quantification of chemical, biological and microbiological species in matrices of chemical, biological or environmental interest". The book has a distinct Irish flavour, including the chapter on the brewing industry, and is based on an industrial analysis course given at Dublin City University. As such the

target audience is undergraduate and postgraduate students specialising in courses on instrumental analysis.

The "Analytical Approach" is now an integral part of most specialist analytical courses and discusses all aspects of the analytical process, including sampling, sample treatment and data presentation, in an integrated manner. This philosophy is often associated with a matrix based approach to teaching in addition to the more conventional technique based approach.

The matrices discussed here in five easy-to-read chapters are; biological fluids, the brewing industry, the sealants/adhesives industry, air pollution and animal and human feeds. Each chapter contains a brief description of analytical techniques relevant to that particular sample matrix (e.g., chromatographic methods for biological fluids, NIR for the brewing industry), specific sampling and sample treatment procedures relevant to the analyte and the sample matrix (e.g., solid phase extraction) and examples of real problem solving.

The style and presentation are consistent throughout and all of the applications chapters are well referenced (particularly the biological fluids chapter). Some prior knowledge of instrumentation is assumed but the book is written at the right level to stimulate interest in Analytical Science amongst final year undergraduate and postgraduate taught course students. I am also in favour of the problem solving approach to teaching on which this book is based and therefore recommend it as a useful text for students.

Paul J. Worsfold

M. Šaršúnová, O. Hanč and B. Kakáč (Eds.), *HPLC in Pharmacy and Biochemistry*, Hüthig, Heidelberg, 1990 (ISBN 3-7785-1699-X). x + 335 pp. Price DM198.00.

The aim of this book is to provide a working companion for liquid chromatographers working in the fields of drug analysis and clinical biochemistry, covering principles, theoretical and instru-

mental aspects as well as an anthology of applications.

The historical development of chromatography is covered in a brief introduction, and chromatographic separation principles are described in the first chapter which emphasizes the versatility and importance of liquid chromatography (LC). The subject of the next chapter is LC theory. Practical and instrumental considerations are reviewed in Chapter 3, including column types and properties, mobile phase selection, detectors, sample injection, qualitative and quantitative analysis, preparative LC and a detailed section on radiochromatography. An anthology of applications of LC in drug analysis is presented in Chapter 4. The classification covers a broad spectrum of therapeutic areas, such as central nervous system (in particular psychotropic drugs), chemotherapeutics, diuretics, cardiovascular, gastro-intestinal, anti-invasive (in particular antibiotics) and natural products (e.g., vitamins, alkaloids, cardiac glycosides). The usefulness of LC data in structure-activity relationships is considered in Chapter 5, the determination of partition coefficients being one such example. The final chapter describes applications of LC in biochemistry and clinical analysis. Topics include biogenic amines, amino acids, peptides and proteins, saccharides, nucleic acids, lipids and steroids.

The book is useful as a reference text. The lack of chemical structures and the very few chromatographic illustrations are unfortunate, and more recent references in the early chapters on the technique itself would have been helpful.

Richard W. Abbott

Advances in Chromatography, Volume 31: J. Calvin Giddings, E. Grushka and P.R. Brown (Eds.), xix + 393 pp. Marcel Dekker, New York, US\$172.50. Volume 32: J. Calvin Giddings, E. Grushka and P.R. Brown (Eds.), xx + 270 pp. Marcel Dekker, New York, US\$143.75.

The *Advances in Chromatography* series provides a collection of excellent and specialised review articles, and these two new volumes are no

exception. The extensive breadth of chromatographic science does mean, however, that articles collected in any volume have little relationship to each other. As a result most readers are going to be directed to only one or at least a small number of articles in each volume. A coherent unifying theme to each volume, although difficult to achieve in some cases, would make for a significant improvement to the series as a whole. Such themes could be column and thin-layer chromatography, applications of chromatography, gas chromatography, coupled techniques and so on.

Volume 31 includes articles on: non-linear chromatography, aqueous size exclusion chromatography, thin-layer chromatography with organically impregnated stationary phases, counter-current chromatography for peptide purification, boronate affinity chromatography and chromatographic methods for determining carcinogenic benz(c)acridine.

Volume 32 includes articles on: porous graphitic carbon in biomedical applications, tryptic mapping by reversed-phase liquid chromatography, determination of dissolved gases in water, planar and column chromatography for separation of polar lipid classes into their molecular species, chromatography in forensic science and LC of explosives materials.

These volumes will undoubtedly be useful to those whose current application or area of potential interest is covered by articles and they will be of value if available from the reference shelves of libraries.

John D. Green

V.G. Berezkin and Yu.S. Drugov, *Gas Chromatography in Air Pollution Analysis*, Elsevier, Amsterdam, 1991 (ISBN 0-444-98732-0). xii + 211 pp. Price US\$140.00/Dfl.245.00.

This book is Volume 49 in the established and well respected *Journal of Chromatography Library* series. There are eight chapters which broadly cover general aspects of gas chromatography, approaches to the collection and treatment of samples for chromatographic analysis and spe-

cific applications of gas chromatography (GC) to the determination of air pollutants. The treatment of general aspects is relatively brief and includes standard descriptions of a wide range of detectors, including those specifically designed for air pollution studies, such as the thermal energy analyser, which is based on gas phase chemiluminescence.

There is more comprehensive coverage of sample collection and treatment procedures with particular focus on reactive-sorption techniques for the preconcentration of individual gases and groups of gases. This is a crucial step in the quantitation of gaseous pollutants and it is a point that is emphasised by the authors. There is also a useful chapter on the related problem of calibration for the quantitation of gaseous species by GC.

The final chapter describes practical applications of GC and includes 225 references, although many are from Russian language journals and the most recent is from 1987. It contains some good experimental detail but as this material is the focus of the book I would have expected a more comprehensive approach.

The presentation, as with the other contributions in this series, is very good and there is an adequate but not exhaustive index. It is a worthwhile addition to the series and will be of most use for its treatment of theoretical and practical aspects of the sampling and preconcentration of gases from both the global and workplace environments.

Paul J. Worsfold

Sandie Lindsay, *High Performance Liquid Chromatography*, 2nd edn. (*Analytical Chemistry by Open Learning Series*), Wiley, Chichester, 1991 (ISBN 0-471-93115-2). Price (paperback) £17.50.

The second edition of this book shows a considerable improvement over the first edition published some five years ago. The new version is effectively a completely new book rather than an expansion of the old and, as such, now has the

appearance of the good basic text on LC. Of particular note are the chapters on the mobile phase, a large section on the chromatography of ionic solutes, a comprehensive chapter on detectors including post-column reaction and a brief review of newer techniques such as SFC and LC-MS. Although the open learning format remains the same there is a far larger range of self-assessment questions in the second edition.

M. Cooke

Joseph C. Touchstone, *Practice of Thin Layer Chromatography*, 3rd edn., Wiley, New York, 1992 (ISBN 0-471-61222-7). xiv + 377 pp. Price £56.00.

'Touchstone' has been a good friend to thin-layer chromatographers for many years. Thus this third edition is much to be welcomed. The format and content are arranged as previously, but are updated where necessary. In particular, there are major changes in the sections on scanners and on sample preparation, thus giving an up-to-date and comprehensive account of the practice of thin-layer chromatography.

A. Benninghoven, K.T.F. Jansen, J. Tompner and H.W. Werner (Eds.), *Secondary Ion Mass Spectrometry. SIMS VIII*, Wiley, Chichester, 1992 (ISBN 0-471-93064-4). xxv + 917 pp. Price £115.00.

These *Proceedings of the Eighth International Conference on Secondary Ion Mass Spectrometry* held in Amsterdam, September 15-20, 1991, contain more than 200 of the 300 presentations, in camera-ready format. Each article is restricted to 4 pp., except for invited lectures which are allowed a few extra pages. They are grouped under Fundamental (20 papers), Quantification (19), Instrumentation (23), Surface Analysis (8), Depth Profiling (45), Imaging (16), Postionization (6), Combined and/or Related Techniques (15), and Applications - in Biology (12), Isotopic Analysis - Geology (6), Metals and Oxides (13), Polymers

– Organics (12), and Semiconductors (15). The final article is on Ion Microscopy for Biomedical Studies, by S. Chandra – The Morrison Symposium.

L. Cecille, M. Cascari and L. Pietrelli (Eds.), *New Separation Chemistry Techniques for Radioactive Waste and Other Specific Applications*, Elsevier Applied Science, Amsterdam, London, 1991 (ISBN 1-85166-656-7). xiv + 307 pp. Price £58.00.

Thirty four presentations from a seminar held in Rome and jointly sponsored by the Commission of the European Communities and the Italian Commission for Nuclear and Alternative Energy Sources are contained in this book. There is no indication of the date of the seminar but contributions from the European Community, the United States and China are included.

There were six thematic sessions covering amine and amide based extractants, bidentate organophosphorus extractants, calixerenes, crown ethers, other extractants and inorganic ion-exchanger/absorbers.

The contributions are in camera ready format and the general quality of the presentations is good. With modern wordprocessing facilities, however, it should be possible to produce a standard font and format for rapid publications such as this.

The proceedings of the meeting were tightly focussed and this book provides a wide ranging account of ligands available for the selective separation of individual radionuclides and classes of radionuclides from radioactive waste and metal ions from toxic waste. It contains lists of selectivity coefficients, ligand and complex structures and properties and synthetic routes and would be a useful source of information. It also provides some ideas for anyone interested in the use of metal ion selective ligands for other analytical applications.

G.R. Turner and J.M. Askey (Eds.), *Total Quality in the Chemical Industry*, Royal Society of Chemistry, Cambridge, 1992 (ISBN 0-85186-497-X). xix + 102 pp. Price £29.50.

This is an account of the *Proceedings of a Symposium*, organised by the Royal Society of Chemistry and the Society for Chemical Industry, at the University of Salford, 4–5 September, 1991. It includes 11 articles covering various aspects of the Total Quality Philosophy, some relating to experiences in particular industries (not necessary chemical), others dealing with aspects of ISO 9000, and yet others covering certification, tactics and progress. This is a worthwhile document which will provide information and encouragement to those engaged in Total Quality schemes.

ANALYTICA CHIMICA ACTA, VOL. 271 (1993)

AUTHOR INDEX

- Adler, B.
—, Schütze, P. and Will, J.
Expert system for interpretation of x-ray diffraction spectra 287
- Aleixo, L.M.
—, De Fátima B. Souza, M., Godinho, O.E.S., De Oliveira Neto, G., Gushikem, Y. and Moreira, J.C.
Development of a chemically modified electrode based on carbon paste and functionalized silica gel for preconcentration and voltammetric determination of mercury(II) 143
- Andersson, R., see Hämäläinen, M.D. 101
- Aparicio López, R., see García Pulido, J. 293
- Ashurst, P.R., see Koziat, J. 31
- Bakker, T., see Wehrens, R. 11
- Baldwin, J.R., see Rossi, D.T. 59
- Blankenstein, G.
—, Preuschoff, F., Spohn, U., Mohr, K.-H. and Kula, M.-R.
Determination of L-glutamate and L-glutamine by flow-injection analysis and chemiluminescence detection: comparison of an enzyme column and enzyme membrane sensor 231
- Boyd-Boland, A.A.
— and Eckert, J.M.
Determination of nonionic surfactants by spectrophotometry after extraction with potassium triiodide 311
- Broekaert, J.A.C., see Bulska, E. 171
- Buckley, E., see Thompson, R.Q. 223
- Bulska, E.
—, Tschöpel, P., Broekaert, J.A.C. and Tölg, G.
Different sample introduction systems for the simultaneous determination of As, Sb and Se by microwave-induced plasma atomic emission spectrometry 171
- Burns, D.T., see Chimpalee, N. 247
- Buydens, L., see Wehrens, R. 11
- Chen, G.N.
Assessment of environmental water with fuzzy cluster analysis and fuzzy recognition 115
- Chimpalee, D., see Chimpalee, N. 247
- Chimpalee, N.
—, Chimpalee, D., Jarungpattananon, R., Lawratchavee, S. and Burns, D.T.
Spectrofluorimetric flow-injection determination of calcium using Calcein 247
- Dean, J.R., see Kane, M. 83
- De Andrade, J.F.
— and Guimarães, O.M.
Potentiometric study of azide complexes of copper(II) in aqueous medium 149
- De Fátima B. Souza, M., see Aleixo, L.M. 143
- De Oliveira Neto, G., see Aleixo, L.M. 143
- Dowle, C.J., see Kane, M. 83
- Eckert, J.M., see Boyd-Boland, A.A. 311
- Ehrlich, M., see Wienke, D. 253
- El'skaya, A.V., see Korpan, Y.I. 203
- Farias, P.A.M.
—, Ohara, A.K., Takase, I., Ferreira, S.L.C. and Gold, J.S.
Adsorptive preconcentration for voltammetric measurements of trace levels of vanadium in the presence of copper 209
- Ferreira, S.L.C., see Farias, P.A.M. 209
- Frigge, C.
— and Jackwerth, E.
Systematic investigation of multi-element preconcentration from copper alloys by carbamate precipitation before atomic absorption spectrometric analysis 299
- Furuichi, R., see Tamura, H. 305
- Furusawa, M., see Kiba, N. 47
- Galan-Estella, F., see Hernández, P. 217
- García Pulido, J.
— and Aparicio López, R.
Triacylglycerol determination based on fatty acid composition using chemometrics 293
- Godinho, O.E.S., see Aleixo, L.M. 143
- Gold, J.S., see Farias, P.A.M. 209
- Gonchar, M.V., see Korpan, Y.I. 203
- Goto, Y., see Kiba, N. 47
- Guimarães, O.M., see De Andrade, J.F. 149
- Gushikem, Y., see Aleixo, L.M. 143
- Halsall, H.B., see Thompson, R.Q. 223
- Hämäläinen, M.D.
—, Liang, Y.-z., Kvalheim, O.M. and Andersson, R.
Deconvolution in one-dimensional chromatography by heuristic evolving latent projections of whole profiles retention time shifted by simplex optimization of cross-correlation between target peaks 101

- Hasebe, K., see Nakabayashi, S. 25
- Hayashi, Y.
— and Rutan, S.C.
Accuracy, precision and information of the adaptive Kalman filter in chromatography 91
- Heineman, W.R., see Thompson, R.Q. 223
- Hernández, L., see Hernández, P. 217
- Hernández, P.
—, Galan-Estella, F. and Hernández, L.
Determination of 4-nitrobiphenyl by adsorptive stripping square-wave polarography 217
- Higson, S.P.J.
— and Vadgama, P.M.
Diamond-like carbon coated microporous polycarbonate as a composite barrier for a glucose enzyme electrode 125
- Hitchen, S.M., see Kane, M. 83
- Howard, A.G., see Taylor, I. 77
- Irth, H., see Van der Vlis, E. 69
- Jackwerth, E., see Frigge, C. 299
- Jarungpattananon, R., see Chimpalee, N. 247
- Johansson, G., see Skoog, M. 39
- Jones, D.R.
Improved spectrophotometric method for the determination of low levels of bromide 315
- Kane, M.
—, Dean, J.R., Hitchen, S.M., Dowle, C.J. and Tranter, R.L.
Experimental design approach for supercritical fluid extraction 83
- Kateman, G., see Wehrens, R. 11
- Kateman, G., see Wienke, D. 253
- Kiba, N.
—, Ueda, F., Saegusa, K., Goto, Y., Furusawa, M. and Yamane, T.
Flow-injection determination of 1,5-anhydroglucitol in serum with an immobilized pyranose oxidase reactor and chemiluminescence detection 47
- Kojło, A., see Michałowski, J. 239
- Korpan, Y.I.
—, Soldatkin, A.P., Starodub, N.F., El'skaya, A.V., Gonchar, M.V., Sibirny, A.A. and Shul'ga, A.A.
Methylotrophic yeast microbiosensor based on ion-sensitive field effect transistors for methanol and ethanol determination 203
- Koziet, J.
—, Rossmann, A., Martin, G.J. and Ashurst, P.R.
Determination of carbon-13 content of fruit and vegetable juices. A European inter-laboratory comparison 31
- Kudo, I., see Nakabayashi, S. 25
- Kudo, M., see Tamura, H. 305
- Kula, M.-R., see Blankenstein, G. 231
- Kuma, K., see Nakabayashi, S. 25
- Kvalheim, O.M., see Hämäläinen, M.D. 101
- Lakowicz, J.R.
— and Maliwal, B.
Optical sensing of glucose using phase-modulation fluorimetry 155
- Lawratchavee, S., see Chimpalee, N. 247
- Liang, Y.-z., see Hämäläinen, M.D. 101
- Lin, Y., see Wang, J. 53
- Lucasius, C., see Wienke, D. 253
- Maliwal, B., see Lakowicz, J.R. 155
- Martin, G.J., see Koziet, J. 31
- Matsunaga, K., see Nakabayashi, S. 25
- Michałowski, J.
—, Kojło, A., Trojanowicz, M., Szostek, B. and Zagatto, E.A.G.
Simultaneous determination of sucrose and reducing sugars using indirect flow-injection biamperometry 239
- Mohr, K.-H., see Blankenstein, G. 231
- Moreira, J.C., see Aleixo, L.M. 143
- Motellier, S.
— and Toulhoat, P.
Modified acid–base behaviour of resin-bound pH indicators 323
- Mugo, R.K.
— and Orians, K.J.
Seagoing method for the determination of chromium(III) and total chromium in sea water by electron-capture detection gas chromatography 1
- Mulder, W.H., see Wehrens, R. 11
- Nakabayashi, S.
—, Kudo, I., Kuma, K., Matsunaga, K. and Hasebe, K.
Trace determination of sugar acids (gluconic acid) in sea water by liquid chromatography 25
- Narang, P.K., see Rossi, D.T. 59
- Ohara, A.K., see Farias, P.A.M. 209
- Orians, K.J., see Mugo, R.K. 1
- Phillips, B.A., see Rossi, D.T. 59
- Piasecki, D.A.
— and Wirth, M.J.
Internal viscosity of sodium dodecyl sulfate micelles as a function of the chain length of *n*-alcohol modifiers 183
- Porter, M., see Thompson, R.Q. 223
- Powell, H.K.J., see Town, R.M. 195
- Preuschoff, F., see Blankenstein, G. 231
- Rossi, D.T.
—, Phillips, B.A., Baldwin, J.R. and Narang, P.K.
Improved methodology for subnanogram quantitation of doxorubicin and its 13-hydroxy metabolite in biological fluids by liquid chromatography 59
- Rossmann, A., see Koziet, J. 31
- Rothmaier, M.
— and Simon, W.
Chloride-selective electrodes based on mercury organic compounds as neutral carriers 135

- Rutan, S.C., see Hayashi, Y. 91
- Saegusa, K., see Kiba, N. 47
- Sârbu, C.
Application of informational analysis of variance in analytical chemistry 269
- Schütze, P., see Adler, B. 287
- Shul'ga, A.A., see Korpan, Y.I. 203
- Sibirny, A.A., see Korpan, Y.I. 203
- Simon, W., see Rothmaier, M. 135
- Skoog, M.
— and Johansson, G.
Simultaneous enzymatic and tautomeric reactions of D-fructose in a reactor with immobilized hexokinase 39
- Smyth, M.R., see Thompson, R.Q. 223
- Soldatkin, A.P., see Korpan, Y.I. 203
- Spohn, U., see Blankenstein, G. 231
- Starodub, N.F., see Korpan, Y.I. 203
- Stuver, C., see Thompson, R.Q. 223
- Szostek, B., see Michałowski, J. 239
- Takase, I., see Farias, P.A.M. 209
- Tamura, H.
—, Kudo, M. and Furuichi, R.
Polyfunctionality of resin carboxyl sites in ion exchange with alkali metal ions 305
- Tatsu, Y.
—, Yamamura, S., Yamamoto, H. and Yoshikawa, S.
Fluorimetry of haemolysis of red blood cells by catalytic reaction of leaked haemoglobin: application to homogeneous fluorescence immunoassay 165
- Taylor, I.
— and Howard, A.G.
Measurement of primary amine groups on surface-modified silica and their role in metal binding 77
- Thompson, R.Q.
—, Porter, M., Stuver, C., Halsall, H.B., Heineman, W.R., Buckley, E. and Smyth, M.R.
Zeptomole detection limit for alkaline phosphatase using 4-aminophenylphosphate, amperometric detection, and an optimal buffer system 223
- Tjaden, U.R., see Van der Vlis, E. 69
- Tölg, G., see Bulska, E. 171
- Toulhoat, P., see Motellier, S. 323
- Town, R.M.
— and Powell, H.K.J.
Limitations of XAD resins for the isolation of the non-colloidal humic fraction in soil extracts and aquatic samples 195
- Tranter, R.L., see Kane, M. 83
- Trojanowicz, M., see Michałowski, J. 239
- Tschöpel, P., see Bulska, E. 171
- Ueda, F., see Kiba, N. 47
- Vadgama, P.M., see Higson, S.P.J. 125
- Van der Greef, J., see Van der Vlis, E. 69
- Van der Vlis, E.
—, Irth, H., Tjaden, U.R. and Van der Greef, J.
Reversed-phase liquid chromatographic determination of doxorubicin after on-line trace enrichment on iron(III)-loaded 8-hydroxyquinoline-bonded silica 69
- Van Hoof, P., see Wehrens, R. 11
- Vossen, M., see Wehrens, R. 11
- Wang, J.
— and Lin, Y.
On-line organic-phase enzyme detector 53
- Wehrens, R.
—, Van Hoof, P., Buydens, L., Kateman, G., Vossen, M., Mulder, W.H. and Bakker, T.
Sampling of aquatic sediments. Design of a decision-support system and a case study 11
- Wienke, D.
—, Lucasius, C., Ehrlich, M. and Kateman, G.
Multicriteria target vector optimization of analytical procedures using a genetic algorithm. Part II. Polyoptimization of the photometric calibration graph of dry glucose sensors for quantitative clinical analysis 253
- Will, J., see Adler, B. 287
- Wirth, M.J., see Piasecki, D.A. 183
- Yamamoto, H., see Tatsu, Y. 165
- Yamamura, S., see Tatsu, Y. 165
- Yamane, T., see Kiba, N. 47
- Yoshikawa, S., see Tatsu, Y. 165
- Zagatto, E.A.G., see Michałowski, J. 239
- Zelić, M.
Design of experiments and data treatment in the study of mixed-ligand complexes 275

PUBLICATION SCHEDULE FOR 1993

	S'92	O'92	N'92	D'92	J	F	M	A	M
Analytica Chimica Acta	267/1 267/2	268/1 268/2	269/1 269/2	270/1 270/2	271/1 271/2	272/1 272/2 273/1-2	274/1 274/2	275/1 275/2	276/1 276/2
Vibrational Spectroscopy		4/1			4/2		4/3		

INFORMATION FOR AUTHORS

Manuscripts. The language of the journal is English. English linguistic improvement is provided as part of the normal editorial processing. Authors should submit three copies of the manuscript in clear double-spaced typing on one side of the paper only. *Vibrational Spectroscopy* also accepts papers in English only.

Abstract. All papers and reviews begin with an Abstract (50–250 words) which should comprise a factual account of the contents of the paper, with emphasis on new information.

Figures. Figures should be prepared in black waterproof drawing ink on drawing or tracing paper of the same size as that on which the manuscript is typed. One original (or sharp glossy print) and two photostat (or other) copies are required. Attention should be given to line thickness, lettering (which should be kept to a minimum) and spacing on axes of graphs, to ensure suitability for reduction in size on printing. Axes of a graph should be clearly labelled, along the axes, outside the graph itself. All figures should be numbered with Arabic numerals, and require descriptive legends which should be typed on a separate sheet of paper. Simple straight-line graphs are not acceptable, because they can readily be described in the text by means of an equation or a sentence. Claims of linearity should be supported by regression data that include slope, intercept, standard deviations of the slope and intercept, standard error and the number of data points; correlation coefficients are optional. Photographs should be glossy prints and be as rich in contrast as possible; colour photographs cannot be accepted. Line diagrams are generally preferred to photographs of equipment.

Computer outputs for reproduction as figures must be good quality on blank paper, and should preferably be submitted as glossy prints.

Nomenclature, abbreviations and symbols. In general, the recommendations of the International Union of Pure and Applied Chemistry (IUPAC) should be followed, and attention should be given to the recommendations of the Analytical Chemistry Division in the journal *Pure and Applied Chemistry* (see also *IUPAC Compendium of Analytical Nomenclature, Definitive Rules, 1987*).

References. The references should be collected at the end of the paper, numbered in the order of their appearance in the text (not alphabetically) and typed on a separate sheet.

Reprints. Fifty reprints will be supplied free of charge. Additional reprints (minimum 100) can be ordered. An order form containing price quotations will be sent to the authors together with the proofs of their article.

Papers dealing with vibrational spectroscopy should be sent to: Dr J.G. Grasselli, 150 Greentree Road, Chagrin Falls, OH 44022, U.S.A. Telefax: (+ 1-216) 2473360 (Americas, Canada, Australia and New Zealand) or Dr J.H. van der Maas, Department of Analytical Molecule Spectrometry, Faculty of Chemistry, University of Utrecht, P.O. Box 80083, 3508 TB Utrecht, The Netherlands. Telefax: (+ 31-30) 518219 (all other countries).

© 1993, ELSEVIER SCIENCE PUBLISHERS B.V. All rights reserved.

0003-2670/93/\$06.00

No part of this publication may be reproduced, stored in a retrieval system or transmitted in any form or by any means, electronic, mechanical, photocopying, recording or otherwise, without the prior written permission of the publisher, Elsevier Science Publishers B.V., Copyright and Permissions Dept., P.O. Box 521, 1000 AM Amsterdam, The Netherlands.

Upon acceptance of an article by the journal, the author(s) will be asked to transfer copyright of the article to the publisher. The transfer will ensure the widest possible dissemination of information.

Special regulations for readers in the U.S.A.—This journal has been registered with the Copyright Clearance Center, Inc. Consent is given for copying of articles for personal or internal use, or for the personal use of specific clients. This consent is given on the condition that the copier pays through the Center the per-copy fee for copying beyond that permitted by Sections 107 or 108 of the U.S. Copyright Law. The per-copy fee is stated in the code-line at the bottom of the first page of each article. The appropriate fee, together with a copy of the first page of the article, should be forwarded to the Copyright Clearance Center, Inc., 27 Congress Street, Salem, MA 01970, U.S.A. If no code-line appears, broad consent to copy has not been given and permission to copy must be obtained directly from the author(s). All articles published prior to 1980 may be copied for a per-copy fee of US \$2.25, also payable through the Center. This consent does not extend to other kinds of copying, such as for general distribution, resale, advertising and promotion purposes, or for creating new collective works. Special written permission must be obtained from the publisher for such copying.

No responsibility is assumed by the publisher for any injury and/or damage to persons or property as a matter of products liability, negligence or otherwise, or from any use or operation of any methods, products, instructions or ideas contained in the material herein.

Although all advertising material is expected to conform to ethical (medical) standards, inclusion in this publication does not constitute a guarantee or endorsement of the quality or value of such product or of the claims made of it by its manufacturer.

This issue is printed on acid-free paper.

PRINTED IN THE NETHERLANDS

Atomic Absorption Spectrometry

Theory, Design and Applications

edited by S.J. Haswell, School of Chemistry, University of Hull, Hull, UK

Analytical Spectroscopy Library Volume 5

Atomic absorption spectroscopy is now a well-established technique for the determination of trace elements covering a wide range of analyte types. The early theory and instrumentation chapters incorporate recent trends in instrumental design and methodology, in particular those associated with electrothermal techniques and background correction. The major thrust of the book is represented by 14 application chapters which give an extensive well referenced review of the practical use of the technique written by experts drawn from their own speciality areas. These include the determination of trace elements in areas as diverse as environmental, chemical and industrial analysis.

Whilst the book is primarily concerned with atomic absorption spectroscopy, any analyst involved in sample handling prior to trace elemental analysis will find this book a valuable compendium of methodology drawn from a very wide range of applications. For the current user of the technique the well referenced sections critically evaluate the state-of-the-art, while for the newer user the text will form the basis of a good laboratory handbook which offers a comprehensive instruction on the theory and instrumental design in atomic absorption spectroscopy.

Contents:

1. Basic principles (*J.F. Tyson*). 2. Instrumental requirements and optimisation

(*S.J. Haswell*). 3. Practical techniques (*S.J. Haswell*). 4a. Waters, sewage and effluents (*M. Blankley, A. Henson and K.C. Thompson*). 4b. Application of atomic absorption spectrometry to marine analysis (*H. Haraguchi and T. Akagi*). 4c. Analysis of airborne particles in workplace atmospheres (*J.C. Septon*). 4d. Application of atomic absorption spectrometry to the analysis of foods (*T.C. Rains*). 4e. Applications of atomic absorption spectrometry in ferrous metallurgy (*K. Ohls and D. Sommer*). 4f. The analysis of non-ferrous metals by atomic absorption spectrometry (*M.R. North*). 4g. Atomic absorption methods in applied geochemistry (*M. Thompson and E.K. Banerjee*). 4h. Applications of atomic absorption spectrometry in the petroleum industry (*J. Marshall*). 4i. Methods for the analysis of glasses and ceramics by atomic absorption spectrometry (*W.M. Wise, R. A. Burdo and D.E. Goforth*). 4j. Clinical applications of flame techniques (*A. Taylor*). 4k. Elemental analysis of body fluids and tissues by electrothermal atomization and atomic absorption spectrometry (*H.T. Delves and I.L. Shuttler*). 4l. Forensic science (*I.M. Dale*). 4m. Fine, industrial and other chemicals (*L. Ebdon and A.S. Fisher*). 4n. Analysis of polluted soils (*M. Cresser*). Subject Index.

1992 xx + 530 pages

Price: US \$ 177.00 / Dfl. 345.00

ISBN 0-444-88217-0



Elsevier Science Publishers

P.O. Box 211, 1000 AE Amsterdam, The Netherlands

P.O. Box 882, Madison Square Station, New York, NY 10159, USA